

**Tuning, Controlling and Applications of *Cis*-isomer
Stability in Azoheteroarenes and Multiple Azoarenes
Connected Systems**

*A thesis submitted for the partial fulfilment of
the degree of Doctor of Philosophy*

by

SUDHA DEVI



*Department of Chemical Sciences,
Indian Institute of Science Education and Research (IISER) Mohali,
Sector 81, Knowledge City, SAS Nagar, Manauli PO, Mohali, 140306 Punjab,
India*

May, 2018

DEDICATED to
MY BELOVED MOTHER
Late Smt. Savitri Devi

Declaration

I hereby declare that the content included in this thesis entitled “**Tuning, Controlling and Applications of *Cis*-isomer Stability in Azoheteroarenes and Multiple Azoarenes Connected Systems**” is the results of explorations carried out by me under the supervision of **Dr. Sugumar Venkataramani** at the Department of Chemical Sciences, IISER Mohali, SAS Nagar, Mohali, Punjab, India. This work has not been submitted in part or full for the award of any degree, a diploma or a fellowship to any other university or institute. Whenever any contributions of others are involved, every effort is made to indicate it clearly with due acknowledgements. In keeping with general practice in reporting scientific observations, acknowledgements have been made whenever the work was described based on the findings of other investigators. Any omission that might have occurred due to oversight or error in judgment is regretted. A complete bibliography of the books and journals referred to is given at the end of each chapter.

Sudha Devi

Date:

Place:

In my capacity as the supervisor of the student’s thesis work, I certify that the above statements by the student are true to the best of my knowledge.

Dr. Sugumar Venkataramani

Assistant Professor

Department of Chemical Sciences

Indian Institute of Science Education and Research Mohali

Date:

Place:

Acknowledgements

I would like to acknowledge the committee members Prof. K. S. Viswanathan and Dr. R. Vijaya Anand and express my thanks to my supervisor Dr. Sugumar Venkataramani for their guidance, supervision and encouragement made this thesis work possible. I sincerely thank Prof. Debi Prasad Sarkar, Director, IISER Mohali and former Director Prof. N. Sathyamurthy for providing the facilities and infrastructure to carry out my research work. I acknowledge former and current Heads of the Department of Chemical Sciences, IISER Mohali, Prof. K. S. Viswanathan and Dr. S. Arulananda Babu, respectively for providing various research and departmental facilities.

I would also like to thank Physical sciences department for providing advanced training in nuclear magnetic resonance spectroscopy and Chemical sciences department for providing access to the Cary 5000 UV-Vis spectrophotometer, as well as HRMS, Raman Spectrometer instrument training and support. I would like to acknowledge the central facilities of NMR, IR, UV-Vis and HRMS facilities of IISER Mohali for characterizations and studies of my experiments. Along with the aforementioned individuals, I would like to thank Dr. Saonli Roy and current lab members Surbhi Grewal, Ankit Kumar Gaur, Parvesh Kumar, Debapriya Gupta, Anjali Srivastava, Himanshu Kumar, Mayank Saraswat and Chitranjan Shah for their assistance and contributions to experimental and theoretical studies to the work presented herein.

I would like to also thank past lab members Ashish Sharma, Lilit Jacob, Ravi Ranjan, Ravinder, Devender Yadav, Aman Bhosle, Anjali Mahadevan, Athira T John, Rashmi Sinha, and Virender Singh to whose helped me to set up the lab and assistance in lab work.

I am highly thankful to Surbhi Grewal for her help in my work and her patience in during NMR and UV Vis experiments and also thankful to Mayank Saraswat to his contribution in theoretical experiments. I also want to highly thank Debapriya Gupta and Ankit Kumar Gaur for their contributions in NMR and UV Vis based photoswitching experiments.

I wish to thank Dr. Santanu K. Pal and his PhD student Indu Bala and Post-doctoral fellow Dr. Santosh Prasad Gupta for liquid crystal studies which work I have included in my thesis and Dr. Sabyasachi Rakshit to provided his lab instrumentation facilities.

I am thankful to all the faculty members of the Department of Chemical Sciences of IISER Mohali for their cooperation, guidance and encouragement.

A special thanks to my husband Rajeev Kumar Singh supporting me throughout this journey and for always being there through all around of my life.

Thank you to my brother Ansu, my sister Madhu, sister-in-law Kiran Patel and all the family members for their unconditional encouragement, support, wisdom and prayers.

Finally, I would like to very special thanks to my parents; both of you are my inspiration for my success. Mom and Dad, I did it, this thesis is for both of you. I love both of you.

List of Publications from the thesis work

1. **Sudha Devi**, Mayank Saraswat, Surbhi Grewal, Sugumar Venkataramani “Evaluation of Substituent Effect in *Z*-Isomer Stability of Arylazo-1*H*-3,5-dimethylpyrazoles Interplay of Steric, Electronic Effects and Hydrogen Bonding” *J. Org. Chem.*, **2018**, 83 (8), 4307–4322.
2. **Sudha Devi**, Ankit Kumar Gaur, Debapriya Gupta, Mayank Saraswat, Sugumar Venkataramani “Tripodal Arylazo-3,5-dimethylpyrazole-1-tricarboxamides: Photochromic Materials for Rewritable Imaging Applications” *ChemPhotoChem*, **2018**, 2, 806-810.
3. **Sudha Devi**, Indu Bala, Santosh Prasad Gupta, Santanu Kumar Pal, Sugumar Venkataramani “Reversibly photoswitchable alkoxy azobenzenes connected benzenetricarboxamide discotic liquid crystals with perpetual long range columnar assembly”, *Org. Biomol. Chem.*, **2018** (Advance article – DOI: 10.1039/C8OB01579A).

Conferences/Workshop

1. Participated in the 16th National Symposium in Chemistry held at the Indian Institute of Technology Bombay, Pawai, Mumbai, India (07-09 February, 2014).
2. Participated in the International Conference on Nano Science and Technology (ICONST) held at the Institute of Nano Science and Technology Mohali, India (02-05 March, 2014).
3. Participated in the National Seminar on Crystallography 43A held at the Indian Institute of Science Education and Research (IISER) Mohali, S. A. S. Nagar Mohali, India (28-30 March, 2014).
4. Poster presentation entitled “Direct C- Arylation of acetylacetone using substitute anilines under metal-free conditions through *in situ* generation of diazonium salts” **Sudha Devi**; Sugumar Venkataramani* at the 13th Eurasia Conference on Chemical Sciences held at the Indian Institute of Science Bangalore, India (14-18 December, 2014).
5. Poster presentation in the 11th Junior National Organic Symposium (J-NOST) held at the National Institute of Science Education and Research (NISER) Bhubaneswar, India (14-17 December, 2015).
6. Participated in the Workshop on Solid-State and Material Chemistry held at the Institute of Nano Science and Technology Mohali, India (08 February, 2016).
7. Poster presentation in the 18th National Symposium in Chemistry held at the Institute of Nano Science and Technology Mohali and Punjab University India (5th-7th February, 2016).

Index

Table of contents

List of Tables.....	v
List of Figures.....	vii
Abstract.....	1
Chapter 1. General introduction	3
1.1. Photochromism	3
1.2. Important families of organic photochromic molecules	
1.2.1 Spiropyrans	5
1.2.2 Fulgides	6
1.2.3 Stilbenes	6
1.2.4 Diarylethenes	7
1.2.5 Chromenes	7
1.3. Azobenzenes	8
1.3.1 Introduction to azobenzenes	8
1.3.2 Photoisomerization in azobenzene	9
1.3.3 Spectroscopic investigations of the photochemistry in azobenzene	10
1.3.4 Mechanistic aspects in the azobenzene photoisomerization	12
1.3.5 Thermal <i>Z-E</i> reverse isomerization in azobenzene	14
1.4. Multi-state photochromic systems	17
1.5. Solid-phase and liquid crystalline phase photochromism	17
1.6. Motivation and scope of the thesis	18
1.7. References	19
Appendix 1A.....	24
Chapter 2. Evaluation of Substituent Effect in <i>Z</i>-Isomer Stability of Arylazo-1<i>H</i>-3,5-dimethylpyrazoles	27
2.1. Introduction to arylazo-1<i>H</i>-3,5-dimethylpyrazoles	27
2.2. Synthesis	28
2.3. Analysis of photoswitching through UV-Vis and NMR spectroscopic techniques	30
2.4. Effects of substituents and hydrogen bonding in the stability of <i>Z</i>-isomers	38
2.5. Concentration dependency and solvent effects in <i>Z</i>-isomer stability	42
2.6. Conclusions	47
2.7. Experimental section	47
2.8. References	68

Appendix 2A.....	71
Appendix 2B.....	72
Appendix 2C.....	91
Appendix 2D.....	94
Chapter 3. Tripodal <i>N</i>-Functionalized Arylazo-3,5-dimethylpyrazole Derivatives of Trimesic Acid	97
3.1. Introduction	97
3.2. Synthesis	98
3.3. Analysis of Photoswitching studies using UV-Vis spectroscopy	99
3.4. Analysis of photoswitching Studies using NMR spectroscopy	103
3.5. Thermal reverse isomerization kinetics studies using NMR spectroscopy	107
3.6. Solid-state photoisomerisation	108
3.7. Summary	110
3.8. Experimental section	110
3.9. References	116
Appendix 3A.....	118
Appendix 3B.....	127
Appendix 3C.....	136
Chapter 4. Photoswitchable discotic liquid crystals	139
4.1. Introduction	139
4.2. Tripodal alkoxyphenylazopyrazole based derivatives of trimesic acid	140
4.2.1. Synthesis	140
4.2.2. Photoswitching Studies	141
4.2.3. Liquid crystalline studies	141
4.3. Alkoxyphenylazobenzene based tricarboxamide derivatives	142
4.3.1 Synthesis	142
4.3.2 Photoswitching Studies	143
4.3.3 Thermal behaviour	148
4.4. Summary	150
4.5. Experimental section	150
4.6. References	158
Appendix 4A.....	160
Appendix 4B.....	162
Appendix 4C.....	166

Appendix 4D.....	172
Chapter 5. Conclusions and Perspectives.....	181
5.1. Evaluation of substituent effect in <i>Z</i> -isomer stability of arylazo-1 <i>H</i> -3,5-dimethyl pyrazoles.....	181
5.2. Tripodal arylazo-3,5-dimethylpyrazole derivatives of trimesic acid	182
5.3. Photoswitchable discotic liquid crystals.....	183
5.4. Perspectives.....	184
Chapter 6. Materials and Methods.....	187

List of Tables

Table 2.1. Synthesis of substituted phenylazopyrazoles 1-38d and <i>N</i> -methyl phenylazopyrazoles 1e, 3e, 6e, 9e, 15e and 18e	29
Table 2.2. UV-Vis spectroscopic and photoswitching data of (<i>E</i>)- and (<i>Z</i>)- isomers of phenylazopyrazole derivatives 1-38d and <i>N</i> -methyl derivatives 1e, 3e, 6e, 9e, 15e and 18e	34
Table 2.3. NMR spectroscopic data of the selected protons of <i>E</i> - and <i>Z</i> -isomers of different substituted phenylazopyrazoles and <i>N</i> -methyl phenylazopyrazoles.....	37
Table 2.4. Solvent effects in the UV-Vis spectroscopic thermal reverse isomerization (<i>Z</i> - <i>E</i>) of rates phenylazopyrazole 1d and <i>N</i> -methyl phenylazopyrazole 1e	45
Table 3.1. Synthesis of tripodal arylazo-3,5-dimethylpyrazole derivatives of trimesic acid 4a-r	98
Table 3.2. UV-Vis spectroscopic data of the 4a-r in solution phase (CHCl ₃) and solid phase.....	102
Table 3.3. NMR studies of photoisomerization in tripodal arylazo-1 <i>H</i> -3,5-dimethylpyrazole derivatives of trimesic acid 4a-r	105
Table 3.4. Concentration dependency in photoswitching of 4a	106
Table 3.5. Thermal reverse isomerization kinetics data of 4a using NMR spectroscopy.....	107
Table 3.6 Thermal reverse isomerization kinetics data of 4a	108
Table 4.1. Spectral properties of all- <i>trans</i> and - <i>cis</i> isomers using UV-Vis spectroscopy of 7a-c	141
Table 4.2. Spectral properties and solution phase formation rate constants of all- <i>trans</i> isomers using UV-Vis spectroscopy of 13a-c	144
Table 4.3. Thermal properties of the target compounds 13a-c	147

List of Figures

Figure 2.1. Effect of substituents in the absorption properties of <i>E</i> - and <i>Z</i> -isomers of the substituted phenylazopyrazoles	31
Figure 2.2. Representative figures on photoswitching in phenylazopyrazole derivative 1d	32
Figure 2.3. Taft plot for the steric effects in the kinetics of reverse thermal isomerization of phenylazopyrazole derivatives using UV-Vis spectroscopy	39
Figure 2.4. Substituent effects in the kinetics of reverse thermal isomerization of phenylazopyrazole derivatives UV-Vis spectroscopy: Hammett plots.....	40
Figure 2.5. Substituent effects in the kinetics of reverse thermal isomerization of phenylazopyrazole and <i>N</i> -methyl phenylazopyrazole derivatives using NMR spectroscopy: Hammett plots	40
Figure 2.6. Effect of concentration in chemical shift of <i>N</i> -H of 1d	43
Figure 2.7. Screenshot of the results from the estimation of association constant of (<i>Z</i>)- 1d dimer using bindfit program.....	43
Figure 2.8. Solvent effects in the thermal <i>Z</i> - <i>E</i> isomerization rate of 1d	46
Figure 3.1. Photoswitching in 4a	100
Figure 3.2. Long-term photoswitching stability of 4a	101
Figure 3.3. NMR photoswitching studies of 4a	104
Figure 3.4. The composition of photoisomers of compound 4a at different concentration.....	106
Figure 3.5. Thermal reverse isomerization kinetics profile of 4a using ¹ H-NMR.....	108
Figure 3.6. ¹ H-NMR spectrum of 4b	110
Figure 4.1. Photoswitching studies using UV-Vis spectroscopy for 7a-c	141
Figure 4.2. Photoswitching behaviour using UV-Vis spectroscopy for 13a-c	144
Figure 4.3. Photoswitching behaviour in solid state for 13a	147
Figure 4.4. NMR spectra of 13a in CDCl ₃	147
Figure 4.5. NMR spectra of 13a in DMSO- <i>d</i> ₆	145
Figure 4.6. Photomicrographs of compound 13a	146
Figure 4.7. Photomicrographs of compound 13b	147

Tuning, Controlling and Applications of *Cis*-isomer Stability in Azoheteroarenes and Multiple Azoarenes Connected Systems

Abstract

Photoswitchable molecules can exhibit light induced reversible bistability between two different states or isomers. So often it accompanies changes in the molecular properties such as structure, dipole moment, colour etc. Due to this, photoswitchable molecules are attractive candidates in many applications such as optical data storage, sensors, molecular switches, molecular wires, biomedicines etc. Azobenzenes are one of the robust photoswitchable molecules with great efficiency in photoisomerization between *E*- and *Z*-isomers, and also can easily be synthesised and functionalized. For many practical applications, tuning and controlling the photoswitching behaviour, and *Z*-isomer stability of azoarenes are crucial. Due to the increasing popularity of phenylazopyrazoles as photoswitches in recent times, and their improved *Z*-isomer stability, we attempted at understanding the effects of substituents on their photoswitching ability and *Z*-isomer stability. In this regard, 38 aryl substituted arylazo 1*H*-3,5-dimethylpyrazoles have been synthesized. For understanding the steric and electronic effects on their *Z*-isomer stability, Taft and Hammett's relationships have been utilized. Additionally, the *N*-methyl derivatives with *meta* substitutions have been synthesized and their substituent effects have also been studied. Furthermore, the role of hydrogen bonding has been investigated through concentration and solvent effects in the *Z*-isomer stability. Based on these studies, we demonstrated a complex interplay of steric, and electronic effects and also the hydrogen bonding in dictating the stability of *Z*-isomers in phenylazo-1*H*-3,5-dimethylpyrazoles.

In the next part of the work, functionalization of the arylazopyrazoles has been carried out. In this regard, we have connected arylazopyrazole units to a trimesic acid, and using this strategy 18 derivatives have been synthesized. Through UV-Vis and NMR spectroscopic studies, we envisaged the multi-state photochromic properties of these tripodal derivatives. These new class of molecules exhibited many interesting properties such as better solubility, higher photoisomerization conversions towards *ZZZ*-isomers, enhanced stability of *ZZZ*-

isomers, and long-term switching stability etc. Above all, these molecules showed solid-state reversible photoisomerization as well as colour changes that make them excellent candidates for rewritable imaging applications.

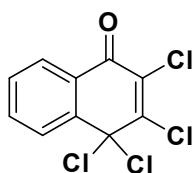
In the last part of the work, we have synthesized long alkoxy chain (viz, C₆, C₈ and C₁₀) containing multiple arylazo-3,5-dimethylpyrazole and azobenzene connected systems for making photoswitchable liquid crystals. This work has been done in collaboration with Dr. Santanu Kumar Pal's group. Despite exhibiting good photoswitching properties, the arylazo-3,5-dimethylpyrazole based systems did not show any liquid crystalline properties. On the other hand, polarized optical microscopic (POM) imaging and small angle X-ray scattering (SAXS) studies revealed the discotic liquid crystal properties of the azobenzene-based tricarboxamide derivatives. All of the three molecules exhibited solution phase as well as solids (thin films) DLC mesophase photoswitching. Interestingly, the compounds with peripheral C₆ alkyl chain exhibits two different mesophases, namely a columnar rectangular (Col_r) phase at low temperature, and a columnar hexagonal (Col_h) phase at a higher temperature. In contrast, the other two higher homologues revealed only Col_h phases at all temperature ranges. Despite the molecules undergoing switching in the LC phase, no changes have been observed with respect to the LC phase. Thus, we were able to develop a new DLC based system that can undergo photoswitching without losing its LC properties.

Chapter 1. General Introduction

1.1 Photochromism

Photochromism [from the Greek words: *photos* (light) and *chroma* (colour)] term was first given by Hirshberg in the early 1950s.¹ Photochromism is a light-driven reversible conversion of a chemical species between two different states or isomers, which demonstrate different physical and chemical properties.²⁻⁴ Historically photochromism is a well-known phenomenon since the era of the Alexander the Great (356–323 BC). Some unknown photochromic compounds were used by his warriors during the wars for attacking the opponents at the right moment. Generally those photochromic compounds were used that can undergo colour changes upon exposing to sunlight.⁵ As far as the scientific reports are concerned, in 1867, Fritzsche for the first time reported the colour changes of tetracene in solution phase. An initial orange coloured solution of tetracene solution faded in colour upon exposure to sunlight, while the solution recovered back to original colour when kept in dark.⁶ Recently photodimerization has been proposed as the reason for such photochromic behaviour.⁷

After that, ter Meer has found that the potassium salt of dinitroethane in the solid-state exhibit photochromism, which appeared as yellow in the dark and red colour in the daylight.⁸ Similarly Phipson was noted that a painted gate post appeared black in the daytime while white colour at night time, which may be due to a zinc pigment, probably lithopone (a white pigment made from zinc sulphide and barium sulphate).⁹ In 1899, Markwald was found the reversible change in the colour of 2,3,4,4-tetrachloronaphthalen-1(4H)-one (β -TCDHN) in the solid-state.¹⁰ Since the 1960s, the interest in photochromism was expanded tremendously, through which the mechanistic and synthetic aspects of many photochromic materials have been explored.



β -TCDHN

Photochromic molecules change their physical as well as chemical properties upon irradiation with an appropriate wavelength of light. For instance, light can typically induce isomerization, which accompanies changes in physical properties such as geometrical structure, planarity, dipole moment, absorption spectra, colour, dielectric constant, chemical

reactivity, solubility, magnetic properties, refractive index, fluorescence emission, π -conjugation, noncovalent interaction, covalent bonding, electron conductivity, electrochemical properties, coordination properties etc. The molecules exhibit such changes in the properties are known as photochromic molecules. Thus, the appropriate wavelength of light can be used for tuning the properties of photochromic molecules.¹¹⁻¹⁴ Due to this fascinating aspect, photochromic molecules have found wide range of applications in various fields such as molecular recognition,¹⁵ photopharmacological applications,¹⁶ artificial ion channels,¹⁷ molecular machines,¹⁸ liquid crystals,¹⁹ sensors,²⁰ logic operations,²¹ data storage, and optical memory devices,²² molecular devices,²³ catalysis,²⁴ etc.

In general, a thermodynamically stable “A-isomer” can be converted into another isomer of it, namely “B” by using the appropriate wavelength of irradiation. The reverse isomerization can occur either thermally or photochemically. Most of the organic photochromic molecules involve unimolecular reactions. The conversion of photochromic molecules, which are colourless in one form e.g. A-isomer, into a coloured isomer e.g. B-isomer, through irradiation are referred to as positive photochromism. The phenomenon involving bimolecular reactions such as photocycloaddition are referred to as negative or inverse photochromism depending on the difference between $\lambda_{\max}(\text{A})$ and $\lambda_{\max}(\text{B})$.

In the case of photochromic molecules, light can induce various chemical processes such as, isomerisation, tautomerisation, bond cleavage, cyclization, coordination changes, redox reactions, electron-hole pair generation, spin crossover etc.²⁵ Through the photochemical processes, the more stable state or the isomeric form of the photochromic molecule can be converted into a less stable state or isomer. The reversal or attainment of the original status of the photochromic molecules can be achieved either thermally or photochemically (by irradiating the sample with a different wavelength of light).

In recent times, several organic photochromic compounds such as azobenzenes, stilbenes, spiropyranes, fulgides, diarylethenes, chromenes etc have been explored. Most of these compounds show excellent photochromic behaviour and reversibility. Based on the mechanism associated with the molecular transformation, these photochromic compounds may belong to one of the following three major classes:

- (i) *E-Z-E* isomerization (C=C bond or N=N bond)
- (ii) Electrocyclic reaction
- (iii) Photoinduced tautomerisation.

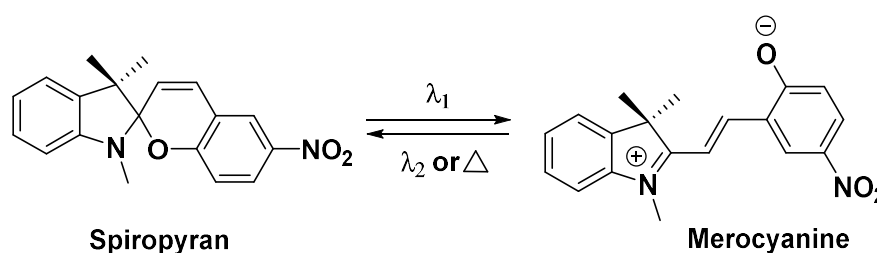
Depending on the energy barrier between the two-isomeric species involved, there can be two possible types of photochromic molecules,²⁵ namely

- (i) T-type (Thermally reversible type): If this barrier is low, the metastable and can be spontaneously converted back to the more stable isomer. Such systems are called T-type referring to the thermally induced reaction. e.g., stilbenes, spiropyranes, chromenes and azobenzenes.
- (ii) P-type (photochemically reversible type): If the barrier is high, only light can be able to induce the isomerization between them. The resulting bistable system is called P-type, which represents photo-induced photochromism. e.g., stilbenes, diarylethenes and fulgides.

1.2 Important families of organic photochromic molecules

1.2.1 Spiropyrans

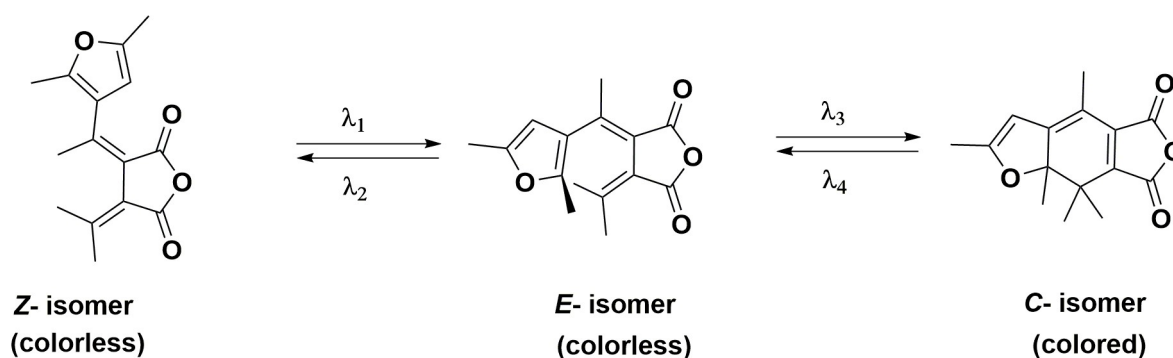
Spiropyran belongs to the oldest families of photochromic molecules. The spiropyran based photochromic molecules consist of two types of heterocyclic groups, an indoline and a chromene moiety which are bound together by a spiro junction at carbon atom while both heterocyclic moieties are orthogonal to each other. These molecules exhibit photochromism between structurally distinct molecules, spiropyran (a closed ring isomer) and merocyanine (an open ring isomer) mainly in solution state with the cleavage of the C_{spiro}-O bond. Merocyanine isomer is the result of the ring-opening reaction, either by heterolytic C-O bond cleavage (Scheme 1.1) or as a 6 π electrocyclic ring opening. Due to C-O bond cleavage this merocyanine isomer has the zwitterionic or the quinoidal resonance forms, respectively.²⁶ There is a large change in polarity of the isomers after isomerization.



Scheme 1.1: Photoisomerization in spiropyran

1.2.2 Fulgides

Fulgides are P-type photochromic molecules, which exhibit light-driven processes through electrocyclic ring closing and ring opening mechanism.²⁷ Typically, these molecules possess a heteroaromatic ring in their structure. It exhibits three thermally stable isomers *E*-, *Z*- and *C*-forms. Among the three, *E*- and *Z*-isomers exist in the ring opened form, which can undergo photoisomerization between them. Indeed, the *E-Z* isomerization channel competes with the ring-closing reaction of the *E*-isomer leading to the *C*-form. During the isomerization, polarity changes occurred to a small extent. Once the *C*-isomer is formed, this reaction is thermally irreversible. However, *C*-isomer can photochemically revert back to the *E*-isomer in an electrocyclic ring-opening reaction. The substituents present around the triene influence the conformations of *E*- and/or *Z*-isomers of the fulgides in the ground state. These substituents also affect the quantum yields in photoisomerization reaction.

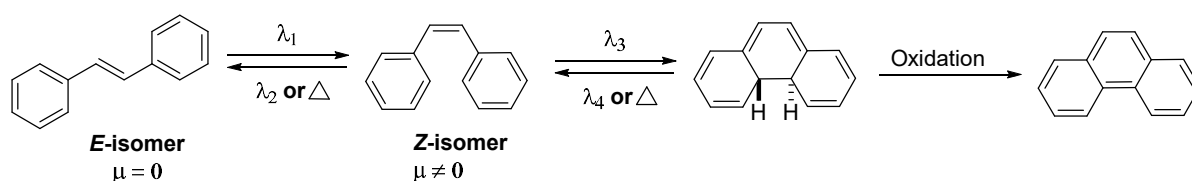


Scheme 1.2: Photoisomerization in fulgides

1.2.3 Stilbenes

The stilbene is a 1,2-diphenylethylene, which exists in the most stable *trans* geometry (*E*-stilbene) in the ground (S_0) state that can isomerize to *cis* structure (*Z*-stilbene) using light.²⁸ The melting point of *E*-isomer is found to be approximately 125 °C, whereas it is 6 °C for the *Z*-isomer. X-ray analysis has determined a nearly planar structure of *E*-stilbene in the solid state. For unsubstituted stilbene, the isomerization can be induced by irradiating at 313 nm UV light that leads to the formation of *Z*-isomer. Interestingly, the *Z*-stilbene attains a propeller-shaped conformation, in which the angle between the planes of phenyl rings is between 30-50°. The photoisomerization mechanistic investigations of stilbene predicted that *E-Z* photoisomerization happens through the rotation around the C=C double bond at the excited

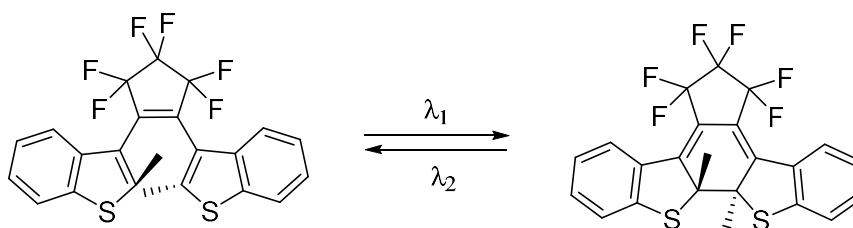
state. The energy barrier for the thermal $Z \rightarrow E$ reverse isomerization is found to be 41-46 kJ/mol and so, the thermal reverse isomerization is negligible at room temperature. One of the limitations in the stilbene photoisomerization process is the formation of dihydrophenanthrene from Z -isomer upon prolonged irradiation that can undergo oxidation to phenanthrene. After the formation of phenanthrene, this system will be no longer reversible.



Scheme 1.3: Photochromic behaviour of stilbene

1.2.4 Diarylethenes

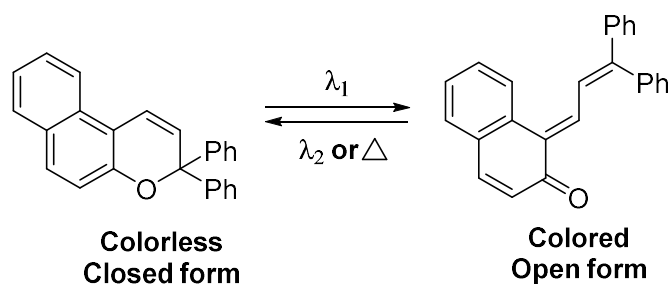
The diarylethenes belong to the thermally irreversible (P-type) photochromic compounds.^{22a} Indeed, diarylethenes are the first examples of P-type photochromic molecules that were reported in the 1960s. Among organic photochromic compounds these diarylethenes have heterocyclic aryl substituents. Electron withdrawing group on these aryl ring decreases the thermal stability of the closed form of diarylethenes. The photochromic behaviour is photochemically driven by the electrocyclic mechanism. These compounds show excellent resistance to fatigue and the switching cycles can be repeated up to ten thousand times. The most striking features of the compounds fatigue resistance and thermal irreversibility are significant for applications to optoelectronic devices, such as memories and switches.



Scheme 1.4: Photoisomerization of diarylethenes.

1.2.5 Chromenes

Chromenes are photochromic compounds with a benzopyran moiety that can reversibly open its ring. Becker and co-workers have studied the photochromic behaviour of chromenes.²⁹ These chromenes show excellent resistance to photodegradation, which is similar to that of spirooxazines. These are T-type photochromic compounds.



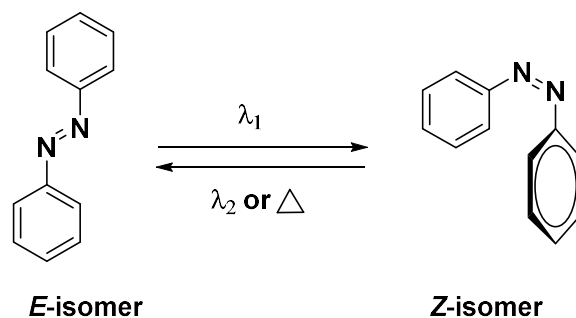
Scheme 1.5: Photoisomerization of chromene

Among all the photochromic compounds, azobenzenes are one of the most widely used organic photochromic molecules, which have very broad applications in numerous fields. Azobenzene is one among the T-type photochromic compounds exhibiting *E-Z-E* geometrical isomerization. Since the heterocyclic and substituted analogues have been extensively used throughout this investigation, a brief introduction related to various properties of azobenzenes have been described based on the literature reports in the following section.

1.3 Azobenzenes

1.3.1 Introduction to azobenzenes

The azo compounds are known since the 19th century. Azobenzene was first time described in 1834 by Eilhard Mitscherlic. Initially these molecules have been utilized in the dye industry owing to the bright colours. Certain azobenzene derivatives such as Prontosil have also been exhibited antibiotic properties and so utilized as drugs in medicinal chemistry. In 1937, Hartley first investigated the *cis* form of azobenzene. The *cis* state was observed through irradiation of the solution of azobenzene in acetone with light. Azobenzene is a derivative of organic diazene (HN=NH), whereas both hydrogens of diazene are replaced by phenyl groups, which have two geometric isomers either *trans* (*E*) or *cis* (*Z*) state around the N=N bond like as a C=C double bond. Azobenzene is an organic photochromic compound, which undergoes reversible photoswitching between two different states or isomers *trans* to *cis* isomerization and *vice versa*. The *E* to *Z* isomerization occurs by using an appropriate wavelength of light on the other hand *Z* to *E* isomerization occurs spontaneously thermally or photochemically into a thermodynamically more stable *E* isomer. (Scheme 1.6) Various chemical methods have been developed for the synthesis of azobenzenes and variety of applications have been explored over the decades in this regard.³⁰



Scheme 1.6: Photoisomerization of azobenzene.

Primarily, numerous derivatives of AB have been investigated. These azobenzenes can be synthesised readily with commonly available cheaper starting materials. This synthetic accessibility led to variation in the structure of azobenzenes including the number of azo units, the nature of aromatic ring such as benzene, naphthalene, pyrrole, thiazole etc., the substitutions at the aromatic rings with the electron donating and electron withdrawing groups and also the position (*ortho*-, *meta*-, and *para*-) of the substituents that can influence the spectroscopic, photophysical and chemical properties of azobenzene derivatives. In general, azobenzene and its derivatives are rigid molecules and anisotropic.

1.3.2 Photoisomerization in azobenzene

The most fascinating properties of all the azo compounds are the efficient and reversible photoisomerization, which occurs upon the irradiation with an appropriate wavelength of light. Typically, *E*-azobenzene exhibit a strong π - π^* (in the UV region) and a weak n - π^* (in the visible region) absorption bands, whereas the *Z*-isomer shows a blue shifted and lower intense π - π^* and strong n - π^* bands. In general, irradiation at a wavelength of light corresponding to π - π^* absorption of the *E*-azobenzene will lead to the forward (*E*-*Z*) isomerization. However, the reverse reaction can be achieved either under irradiation conditions (photochemically) with an appropriate wavelength corresponding to n - π^* absorption of the *Z*-isomer or under thermal conditions. The activation barriers for *E*- to *Z*- and *Z*- to *E*- isomerization is a key parameter for governing the properties of photoswitchable molecules. This activation barrier quantity can be computed by using theoretical methods, but the experimental prediction is not straightforward. The *E*-isomer of azobenzene is around 10-12 kcal/mol more stable than the *Z*-isomer. Furthermore, the interconversion thermal barrier of *Z*- to *E*- isomer is around 18 kcal/mol. When the molecules are in solution, the switching is affected by the aryl substituents, temperature, viscosity and polarity of the solvent and when embedded in polymers, the

conformational change is affected by the polymer matrix. Photoswitchable molecules mainly do not change their conformation in the pure crystalline state.

According to the literature reports, the properties and the investigation of both the thermal and photochemical isomerization of azobenzene have been extensively studied by computational methods, UV-Vis spectroscopy, NMR spectroscopy, X-ray studies, IR spectroscopy studies, Raman spectroscopy etc. other techniques predict the properties and photochemistry of azobenzene. Many mechanisms have been proposed with respect to the forward (photochemical conditions) as well as reverse switching (photochemical and thermal condition) of azobenzenes.³¹

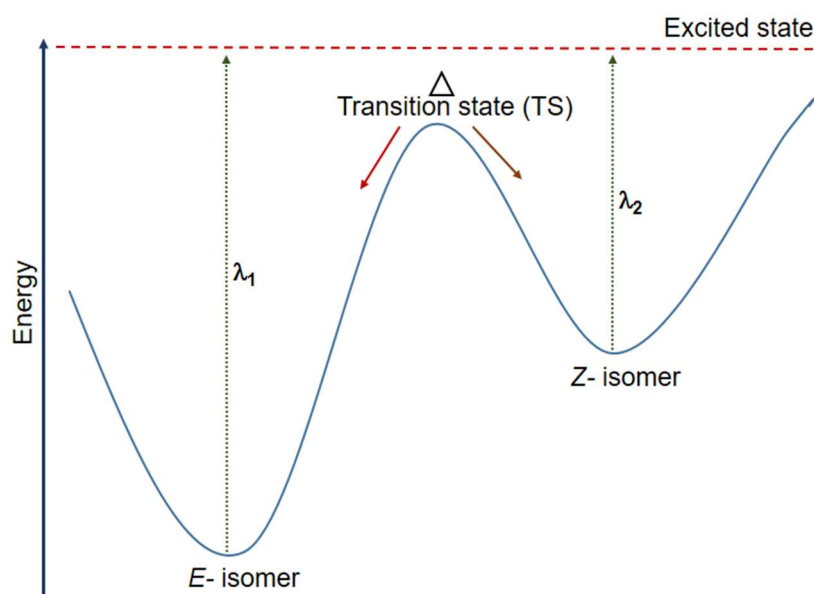


Figure 1.1: Schematic energy profile diagram for the photoswitching process in azobenzene

1.3.3 Spectroscopic investigations of the photochemistry in azobenzene

X-ray of azobenzenes³²

X-ray emission spectroscopy echoes the electronic structure, which is sensitive to the geometry. The isomerization-based photoreactions can be tracked by X-ray emission spectroscopy without considering vibrational effects, as it considers the electronic effects. X-ray emission spectra for *E*- and *Z*-isomers are close interrelation to their electronic configuration. Electronically excited states have been tracked along the dihedral angle (one of the internal coordinates). X-ray studies data indicated that the *E*-azobenzene has a planar structure and C_{2h} symmetry, whereas *Z*-azobenzene adopts a nonplanar and C_2 symmetric structure.

UV-vis spectroscopy of azobenzenes³³

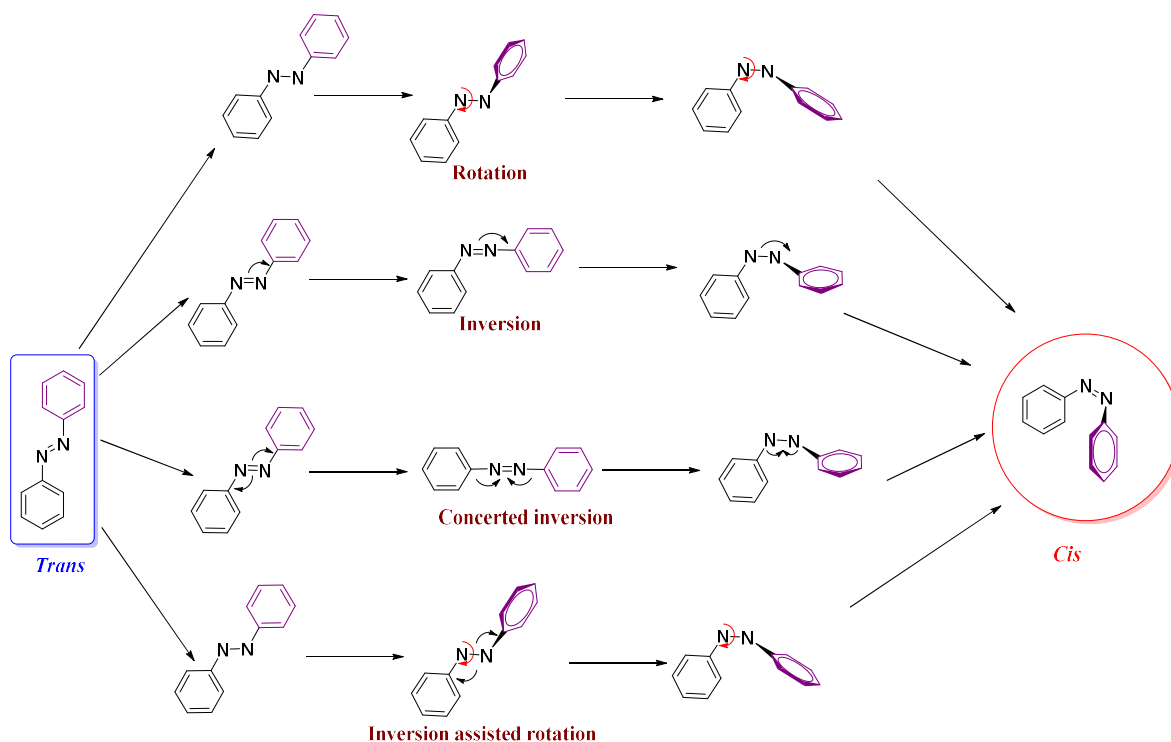
UV-vis absorption spectroscopy has been used as a qualitative analytical technique. In UV-vis spectroscopy, studies the vibrational motions of the nuclei, which affect the electronic transitions in the UV-vis region via fine structure and broadening of the spectrum. UV-vis spectroscopy predicts the intensity shifts of the photoswitchable molecules before and after irradiation. In addition to that, UV-vis absorption spectroscopy has also been applied as a quantitative technique for kinetic studies of the thermal isomerization of (*Z*- to *E*-) azobenzene. Among the four possible transitions in organic molecules (*viz.*, $\sigma\text{-}\sigma^*$, $\pi\text{-}\pi^*$, $n\text{-}\sigma^*$ and $n\text{-}\pi^*$), only $\pi\text{-}\pi^*$ and $n\text{-}\pi^*$ are the lower energy transitions and absorption spectrum can see in UV-vis region, whereas the $n\text{-}\sigma^*$ and $\sigma\text{-}\sigma^*$ are higher energy transitions. UV-Vis spectra of *E*-azobenzene indicates two well-separated bands at 320 nm and 450 nm. In *E*-azobenzene the strong UV band found λ_{max} at 320 nm ($\epsilon \sim 22000 \text{ L mol}^{-1} \text{ cm}^{-1}$), which rises due to a $\pi\text{-}\pi^*$ symmetry allowed transition, and a weaker band λ_{max} at 450 nm ($\epsilon \sim 400 \text{ L mol}^{-1} \text{ cm}^{-1}$) appears due to $n\text{-}\pi^*$ forbidden transitions in the visible region. In case of *Z*-azobenzene, the two $\pi\text{-}\pi^*$ band λ_{max} at 270 nm ($\epsilon \sim 5000 \text{ L mol}^{-1} \text{ cm}^{-1}$) and λ_{max} at 250 nm ($\epsilon \sim 11000 \text{ L mol}^{-1} \text{ cm}^{-1}$) are observed, which are weaker as compared to *E*-isomer, however, in the visible region, the $n\text{-}\pi^*$ transition λ_{max} at 450 nm ($\epsilon \sim 1500 \text{ L mol}^{-1} \text{ cm}^{-1}$) appears as a stronger band than in the case of *E*-azobenzene. During irradiation, the $n\text{-}\pi^*$ and $\pi\text{-}\pi^*$ transitions excite azobenzene from S_0 (ground state) to S_1 ($n\text{-}\pi^*$) and S_2 ($\pi\text{-}\pi^*$) excited states, respectively.

As discussed earlier, the *E* to *Z* isomerization of azobenzene can be achieved by irradiation of appropriate wavelength of light. On the other hand, *Z* to *E* isomerization can occur either thermally or photochemically. The *E* to *Z* isomerisation of azobenzene follows both $S_0 \rightarrow S_1$ ($n\text{-}\pi^*$) and $S_0 \rightarrow S_2$ ($\pi\text{-}\pi^*$) excited states, respectively. Similarly, the photochemical *Z* to *E* reverse isomerization in azobenzene can be achieved by exciting into either S_1 or S_2 state. Indeed, the sum of quantum yields in both isomerization $\Phi_{E \rightarrow Z}$ and $\Phi_{Z \rightarrow E}$ do not show unity indicating that both isomerizations happen through multiple pathways. During the photoisomerization of *E* \rightarrow *Z* azobenzene, S_1 ($n\text{-}\pi^*$) state has the higher quantum yield than S_2 ($\pi\text{-}\pi^*$) state, which violates the Kasha's rule. Typically, azobenzene absorbs radiation of the same wavelength or frequency leading to the establishment of an equilibrium state between the *E* and *Z*-isomer, known as the photostationary state (PSS). Also, the quantum yield depends on the solvent polarity, viscosity and temperature.

NMR Spectroscopy

NMR spectroscopy has been extensively used to investigate the thermal and photoisomerization of azobenzene. Both *E*- and *Z*-isomer of azobenzenes exhibit different NMR spectra. In the ^1H NMR spectra of azobenzene in a deuterated solvent upon UV irradiation at an appropriate wavelength, the signals of the *E*-isomer decrease in intensity and the new signals corresponding to the *Z*-isomer typically appear at shielded regions. The upfield shifts for *Z*-isomer are due to the ring effect or the two phenyl rings of an azobenzene moiety. In this context, the integration ratio of the signals provides the information of conversion between *E*- and *Z*-isomers of the azobenzene by photoirradiation at the given wavelength of light in the PSS.

1.3.4 Mechanistic aspects in the azobenzene photoisomerization



Scheme 1.7: The four proposed mechanisms in photoisomerization of azobenzene

The mechanistic studies of *trans* to *cis* photoisomerization of azobenzene has been investigated through various spectroscopic techniques and computations. The photochemical isomerization has been proposed to be through any one of the channels, *viz.*, rotation, inversion, concerted-inversion, or inversion-assisted rotation with inversion mechanisms. On the other hand, under thermal conditions, the reverse isomerization happens either through the inversion mechanism, or through the rotation mechanism.³¹

The azobenzene photoswitching can be described in terms of the ground and excited state potential energy surface (PES). Among these four isomerization pathways, two pathways rotation and inversion isomerization mechanism are commonly considered to take place. The rotation and inversion mechanism adhere to the diazo bond while both of these mechanisms proceed through relaxation from the excited state. In 1966, Curtin and McCarthy proposed the inversion mechanism,³⁴ which is analogous to the inversion mechanism state of imines. Magee and Eyring have investigated the $Z \rightarrow E$ thermal isomerization and proposed a rotation mechanism with the planar transition state where the N=N bond is broken.³⁵

During photoirradiation, upon electronic excitation from HOMO (π or n orbital) to LUMO (π^* orbital), the molecular geometry attains different positions of the surfaces that will be different in an excited state as compared to the ground state. As a consequence, in the excited state, the molecule experiences a transient force on its external as well as internal coordinates. The transition state formed in inversion, rotation and inversion- assisted rotation pathway possess polar transition state, whereas the transition state formed in concerted inversion mechanism has no net dipole moment. In the inversion pathway mechanism does not involve the rupture of the N=N π -bond. In this mechanism, the C-N=N-C dihedral angle remains fixed at 0° , while one N=N-C angle increases to 180° , which is related to the in-plane inversion. Moreover, in-plane inversion generates a transition state, which results in one sp hybridized azo-nitrogen atom.³⁶ The rotational pathway associated with the cleavage of N=N π -bond, which changes the C-N-N-C dihedral angle although the N-N-C angle remains unchanged at $\sim 120^\circ$. Due to the rupture of N=N π -bond, which allows the free rotation about the N-N bond.³⁷ In the concerted inversion mechanism, both N=N-C bond angles increases to 180° , which generates a linear transition state. In the inversion-assisted rotation mechanism, there are significant (smaller) changes in the N=N-C bond angles while a large change in C-N=N-C dihedral angles occurred simultaneously. All these four isomerization pathways involved the relaxation from transition states that can confer either E or Z isomer. In these mechanisms, we can predict the photostationary states involving both E and Z isomers.

So far, the photoisomerization of Z -azobenzenes has not been investigated experimentally. According to theoretical studies, only one conical intersection found between S_1 and S_0 states along the rotational pathway, on that account both E -azobenzene and Z -azobenzene adopt the same conformation following the $S_0 \rightarrow S_1$ excitation before attaining the ground state. While advance theoretical calculations predict Z -azobenzene undergoes isomerization following both $S_0 \rightarrow S_1$ and $S_0 \rightarrow S_2$ excitation by the rotational pathway.

Resonance Raman intensity analysis and dynamic simulations theoretical studies predicted that rotation dominates $Z \rightarrow E$ isomerization following $S_0 \rightarrow S_1$ excitation.

1.3.5 Thermal Z - E reverse isomerization in azobenzene

Unlike photoisomerization, the Z -isomer can easily be converted into its thermodynamically stable E -isomer even under dark. As indicated before, either inversion or rotation pathway has been proposed for the isomerization mechanism. This thermal isomerization happens through unimolecular reaction and so follows a first order rate. Typically, the isomerization rate can provide information about the half-life of the Z -isomer. Various factors such as irradiation wavelength, the polarity of the solvent, the viscosity of the solvent, temperature, type and position of substituents, acids etc., which affects the quantum yield of the isomerization. Indeed, many of these factors also influence the rate of the thermal reverse isomerization.

Solvent effect:^{38,39} According to the literature reports, as the solvent polarity increases, the rate of thermal isomerisation (Z - to E -isomer) increases with a concomitant decrease in the activation energy. On the other hand, the E to Z isomerization through the $n-\pi^*$ transition, increases with increasing solvent polarity. However, the solvent polarity does not affect the quantum yield of photoisomerisation. Solvent viscosity and polarity also influence the isomerization mechanism of azobenzene. Viscous nonpolar solvents favour the inversion mechanism, whereas non-viscous polar solvents prefer rotation mechanism.

Substituents effects: The effect of aryl substituents at *ortho*, *meta* and *para* positions relative to the azo group influence the photoswitching aspects. The insertion of electron-rich substituents in all four positions of *ortho* to the $N=N$ group exhibit a slight bathochromic and hypochromic shift of the $\pi-\pi^*$ band, whereas the $n-\pi^*$ band exhibit bathochromic and hyperchromic shifts. A red shift in the $n-\pi^*$ band and a blue shift in the first $\pi-\pi^*$ band are expected if the *ortho* positions are increased with steric bulkiness. The red shift is due to the repulsive interaction between the *ortho* substituents and the lone pair on the more distant nitrogen to the azo group. These *ortho* substituents to raise the energy of the nonbonding orbital on nitrogen, with a lowering of the $n-\pi^*$ excitation energy. The blue shift is occurred due to the decrease in the conjugation among the azobenzene molecule, and the result is due to the phenyl ring twisting, an effect caused by the bulky groups at *ortho* position, which lowers the

energy of uppermost filled π -orbital and/or to raise the energy of the lowest empty π^* orbital, thus increasing the π - π^* energy gap i.e. proximal steric effects from *ortho*-substituents. Apart from these shifts, at *ortho* positions, substituents also increases the π - π^* and n - π^* separation. On the other hand, bulky substituents at *ortho* positions increase the rate of thermal isomerization from *Z* to *E* isomer.⁴⁰ When the azobenzene, in which all four of the *ortho* positions are substituted with bulky electron-rich substituents, the isomerization can effectively be induced by visible light.⁴¹ The steric effect in the reverse isomerization rate can be measured through a Taft plot.⁴² For the *ortho*-substituted derivatives, a Taft plot can be plotted between the $\log(k_R/k_{Me})$ vs the steric substituent constant (E_s), where k_R is the isomerization rate of the *ortho*-substituted derivatives and k_{Me} is the rate corresponding to the *ortho*-CH₃ derivative.

Similarly, Hammett relationship can provide the electronic effects of a substituent in an aromatic system. This is a linear free energy relationship (LFER) based on the ratio of the rate constants in the substituted systems relative to the unsubstituted ones and a parameter called substituent constant (σ).⁴³ The Hammett constant (σ) depends on the relative position of the substituent with respect to the reactive group and so, the values for *meta*- and *para*-substituted derivatives are σ_m and σ_p , respectively. Previous investigations on the substituent effects of the thermal reverse isomerization of azobenzene derivatives revealed a non-linear (V-shaped) relationship, which has been explained on the basis of a change in the mechanism from the rotation to inversion.⁴⁴

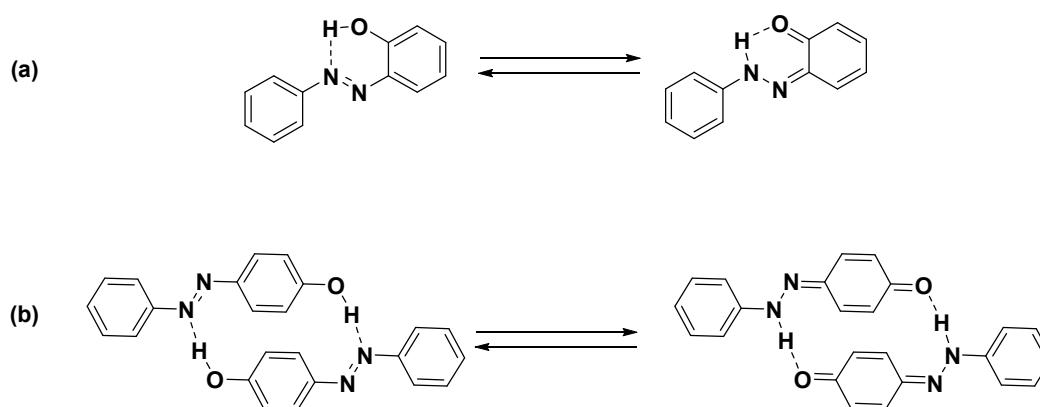
The substituents on the aryl rings of azobenzene produce substantial changes on the absorption, emission and photochemical properties of azobenzene. The azobenzenes are classified into three types based on their electronic states π - π^* and n - π^* absorption bands:⁴⁵

- (a) **Azobenzene type:** These types of compounds have well-separated π - π^* and n - π^* band, where the π - π^* band is very intense and the n - π^* band is weak.
- (b) **Aminoazobenzene type:** These types of compounds have overlapping π - π^* and n - π^* bands in the UV-vis region. These type of compounds have electron donor substituents in the *ortho* or *para* positions to azo bond.
- (c) **Pseudostilbene type:** These types of molecules have nearly degenerate π - π^* and n - π^* band, whereas π - π^* absorption band shifted to bathochromic with respect to n - π^* band. These molecules have electron donating group and electron withdrawing group at the 4 and 4' positions of phenyl rings. In general, these molecules undergo fast reverse switching.

Catalytic effects of acids: Acids accelerate the thermal isomerization of *Z*-azobenzene.⁴⁶ The catalytic mechanism involving the conjugate acid of azobenzene due to the H^+ ions. The H^+ was accepted by $N=N$ bond and forms its conjugate acid, which lowers the activation barrier of *Z* to *E* isomerization.

Temperature effects: Temperature does have a significant effect on the *Z*-*E* isomerization. However, the *Z*-*E* thermal isomerization increases significantly with increases in temperature, because the rate of isomerization increases with increase in the temperature. Although the *E*-*Z* isomerization is possible only through photochemically, the effect of temperature is not pronounced for *E*-*Z* isomerization. However, the thermal reverse isomerization can compete with the photoisomerization channels at a higher temperature that can decrease the efficiency of the light induced isomerization.

Hydrogen-bonding effects: The hydrogen bonding influences both the *E*-*Z* as well as *Z*-*E* isomerization. In general, there are two types of effects, namely, intramolecular and intermolecular hydrogen bonding. For example, the intramolecular and intermolecular hydrogen bonding in 2-hydroxy azobenzene and 4-hydroxyazobenzene, respectively can lead to tautomeric equilibria, due to which both of them undergo fast photoswitching. Similar solvent assisted tautomerization mechanism through hydrogen bonding, particularly in protic solvents has also been proposed for the fast isomerization in aryazoimidazoles⁴⁷ and phenylazoindoles.⁴⁸



Scheme 1.8 Tautomerization in 2-hydroxy and 4-hydroxyazobenzene through intramolecular and intermolecular hydrogen bonding.

1.4 Multi-state photochromic systems:

A single molecule, which has at least two or more photochromic units exhibit multi-state photochromism. However, multiple states containing photochromic systems have been known in few literatures. For example, multi-state photochromic systems such as spiropyrans moieties⁴⁹, diarylethenes moieties⁵⁰, azobenzene⁵¹ are known, which have different photoisomer in a single molecule during the photoisomerisation. In these type of photochromic systems, one photochromic moiety does not affect the properties and photochromic behaviour of the neighbouring photochromic group. We can characterise and examine these multi-state photochromic systems using UV/Vis and NMR spectroscopy. In spite of these reports, the multi-state photochromic systems are still in the exploratory stage with more scope of improvement and applications.

1.5 Solid-phase and liquid crystalline phase photochromism

In recent decades, the efficiency of solution phase photoswitching of azoarenes has been tremendously improved. However, for practical applications, solid-state photoswitching is highly desirable. Lately solid-state bistable compounds showed promising applications in nonlinear optics, molecular machines, information storage, optical switches sensors, displays imaging, in particular reversible writing and erasing part etc.⁵² A wide range of a structurally diverse class of molecules are known for their solid state photochromic properties. However, only some of the photochromic systems are using in these applications in the solid state, which are fulfilling the criteria as a rapid response, better thermal stability, and low fatigue natures of photo isomerised form should be necessary during the photoisomerization process. In the majority of those cases, the light-driven switching has been used for printing, however, thermal conditions are required for erasing. Apart from that, the systems need extensive synthesis or polymeric linkages for enabling the reversible writing and erasing processes.⁵³⁻⁵⁶

Another important challenge in enabling solid-state photoswitching is to design molecular systems with large free-volume that requires control in molecular packing and aggregation. Particularly π -stacking and other supramolecular interactions such as hydrogen bonding needs to be controlled for better efficiency in the light-driven isomerization processes.^{51a}

Photochromic liquid crystals (LC) are very useful as they can change their mesomorphic state upon irradiation.^{57,58} Among the various photochromic groups like

spirooxazines, diarylethenes, azobenzenes etc., azobenzene systems are widely studied owing to the rich photochemistry of azo chromophore and ease of functionalization at aryl groups. Usually, the LC phases of azobenzene incorporated compounds changed to the isotropic phase on irradiation because of the destabilization of the LC phases by *Z*-azobenzene.⁵⁹

1.6 Motivation and scope of the thesis:

In contrast to simple and substituted azobenzenes, heteroazobenzene compounds have been less explored at least in the initial period of this thesis. However, this trend completely changed after the introduction of Fuchter and coworkers report on *N*-methyl pyrazole connected azoarene that showed an enhanced *cis*-isomer stability up to 1000 days.⁴⁰ Since the introduction of phenylazopyrazole, many groups utilized them for various applications. However, there are no systematic studies on tuning or the effect of substitutions in the aryl rings with respect to the photoswitching behaviour, and *cis*-isomer stability. This motivated us to explore the substituent effect of phenylazopyrazole derivatives. The strategy and results are discussed in the second chapter. We utilized a common strategy to synthesize various substituted pyrazole-based azoarenes in good to excellent yields. The influence of position (*ortho*-, *meta*- and *para*-) and nature (electron donating vs electron withdrawing) of the substituents have been investigated. Also, the role of substituents in photoswitching behaviour, thermal reverse isomerization kinetics, and half-lives of the *Z*-isomers has been studied using UV-Vis and NMR spectroscopic techniques. The synthesis of wide range of pyrazole-based substituted azoarenes, their photoswitching properties and thermal reverse isomerization kinetics studies in understanding the effects of electronic, steric and hydrogen bonding are part of chapter 2.

After the understanding of the substituent effects and also the influence of pyrazole NH in the destabilization of *cis*-isomer through hydrogen bonding in arylazopyrazoles, we decide to functionalize them. The amide linkage at NH using trimesic acid provided the access to various substituted tricarboxamide derivatives. The photoswitching, and kinetics of the resulting system provided a highly efficient, multi-state and solvent processible photoswitchable systems. Interestingly, they showed solid state switching, which provided chances for many applications. All of these results are discussed in chapter 3.

In the next part of the work, we explored the possibility of these tricarboxamide derivatives towards the discotic liquid crystalline material, by connecting long alkoxy chain at the aryl rings of the phenylazopyrazole units. However, the presence of the two methyl groups

prevented the supramolecular assembly of these systems, and so we needed to redesign the target systems without the methyl groups. Also, for enhancing the stability of the amide functionality, we utilized the long alkoxy chain containing aminoazobenzene units for making tricarboxamides with the trimesic acid. The resulting derivatives showed promising photoswitching in solution phase and solid phase. The salient feature is that these derivatives showed discotic liquid crystalline phases, and they showed promising switching without affecting the columnar phase. All of these studies are included in chapter 4.

1.7 References

1. Hirshberg, Y.; Fischer, E. *J. Chem. Phys.* **1955**, *23*, 1723-1723.
2. R. P. M. a. S. Guglielmetti, in *Photochromism: Molecules and Systems*, ed. H. Dürr and H. Bouas-Laurent, Elsevier, Amsterdam, 1990 Dürr, H., & Bouas-Laurent, H. (2003). *Photochromism molecules and systems*. Amsterdam: Elsevier.
3. Bouas-Laurent, H.; Dürr, H. *Pure Appl. Chem.* **2001**, *73*(4), 639-665.
4. Hartley, G. S. *Nature* **1937**, *140*, 281-281.
5. Wöhrle, D., Strohrer, W., & Tausch, M. W. (2010) *Photochemie: Konzepte, Methoden, Experimente*. Weinheim: Wiley-VCH.
6. Fritzsche, J. *Comptes Rendus Acad. Sci.* **1867**, *69*, 1035-1037.
7. Olive, A. G. L.; Guerzo, A. D.; Pozzo, J.-L.; Desvergne, J.-P.; Reichwagen, J.; Hopf, H. *J. Phys. Org. Chem.* **2007**, *20*, 838-844.
8. ter Meer, E. *Ann. Chem.* **1876**, 181, 1-22.
9. (a) Phipson, T. L. *Chem. News* **1881**, *43*, 283. (b) Orr, J. B. *Chem. News* **1881**, *44*, 12.
10. Markwald, W. Z. *Phys. Chem.* **1899**, *30*, 140-145.
11. Szacilowski, K. *Chem. Rev.* **2008**, *108*, 3481-3548.
12. Corredor, C. C.; Huang, Z. L.; Belfield, K. D.; Morales, A. R.; Bondar, M. V. *Chem. Mater.* **2017**, *19*, 5165-5173.
13. (a) Toriumi, A.; Kawata, S.; Gu, M. *Opt. Lett.* **1998**, *23*, 1924-1926. (b) Kawata, S.; Kawata, Y. *Chem. Rev.* **2000**, *100*, 1777-1788. (c) Parthenopoulos, D. A.; Rentzepis, P. M. *Science* **1989**, *245*, 843-845. (d) Ogawa, K. *Appl. Sci.* **2014**, *4*(1), 1-18.
14. Lavoie-Cardinal, F.; Jensen, N.A.; Westphal, V.; Stiel, A. C.; Chmyrov, A.; Bierwagen, J.; Testa, I.; Jakobs, S.; Hell, S. W. *ChemPhysChem.* **2014**, *15*, 655-663.
15. For example: (a) Hunter, C. A.; Togrul, M.; Tomas, S. *Chem. Commun.* **2004**, 108-109. (b) Goodman, A.; Breinlinger, E.; Ober, M.; Rotello, V. M. *J. Am. Chem. Soc.* **2001**, *123*, 6213-

6214. (c) Nalluri, S. K. M.; Ravoo, B. J. *Angew. Chem., Int. Ed.* **2010**, *49*, 5371-5374. (d) Yamaguchi, H.; Kobayashi, Y.; Kobayashi, R.; Takashima, Y.; Hashidzume, A.; Harada, A. *Nat. Commun.* **2012**, *3*, 1617/1-1617/5. (e) Gao, Z.; Han, Y.; Chen, S.; Li, Z.; Tong, H.; Wang, F. *ACS Macro Lett.* **2017**, *6*, 541-545. (f) Chen, J.; Serizawa, T.; Komiyama, K. *Angew. Chem., Int. Ed.* **2009**, *48*, 2917-2920.
16. Weston, C. E.; Kramer, A.; Colin, F.; Yildiz, O.; Baud, M. G. J.; Meyer-Almes, F.J.; Fuchter, M. J. *ACS Infect. Dis.* **2017**, *3*, 152-161.
17. For example: (a) Chambers, J. J.; Kramer, R. H. *Methods Cell Biol.* **2008**, *90*, 217-232. (b) Banghart, M.; Borges, K.; Isacoff, E.; Trauner, D.; Kramer, R. H. *Nat. Neurosci.* **2004**, *7*, 1381-1386. (c) Sun, Y.; Ma, J.; Zhang, F.; Zhu, F.; Mei, Y.; Liu, L.; Tian, D.; Li, H. *Nat. Commun.* **2017**, *8*, 1-5. (d) Liu, T.; Bao, C.; Wang, H.; Lin, Y.; Jia, H.; Zhu, L. *Chem. Commun.* **2013**, *49*, 10311-10313. (e) Ying, Y. L.; Zhang, J.; Meng, F. N.; Cao, C.; Yao, X.; Willner, I.; Tian, H.; Long, Y. T. *Sci. Rep.* **2013**, *3*, 1-8.
18. For example: (a) Koumura, N.; Zijlstra, R. W. J.; van Delden, R. A.; Harada, N.; Feringa, B. L. *Nature* **1999**, *401*, 152-155. (b) Eelkema, R.; Pollard, M. M.; Vicario, J.; Katsonis, N.; Ramon, B. S.; Bastiaansen C. W.; Broer, D. J.; Feringa, B. L. *Nature* **2006**, *440*, 163. (c) Feringa, B. L. *Acc. Chem. Res.* **2001**, *34*, 504-513. (d) Haberhauer, G.; Burkhart, C.; Woitschetzki, S.; Woelper, C. *J. Org. Chem.* **2015**, *80*, 1887-1895. (e) Hashim, P. K.; Thomas, R.; Tamaoki, N. *Chem. Eur. J.* **2011**, *17*, 7304-7312.
19. (a) Frigoli, M.; Welch, C.; Mehl, G. H. *J. Am. Chem. Soc.* **2004**, *126*, 15382-15383. (b) Zep, A.; Wojcik, M. M.; Lewandowski, W.; Sitkowska, K.; Prominski, A.; Mieczkowski, J.; Pocięcha, D.; Gorecka, E. *Angew. Chem., Int. Ed.* **2014**, *53*, 13725-13728.
20. For example: (a) Zhang, X.; Hou, L.; Samori, P. *Nat. Commun.* **2016**, *7*, 11118. (b) Do, K.; Boxer, S. G. *J. Am. Chem. Soc.* **2013**, *135*, 10226-10229. (c) Wencel, D.; Abel, T.; McDonagh, C. *Anal. Chem.* **2014**, *86*, 15-29.
21. (a) Venkataramani, S.; Jana, U.; Dommaschk, M.; Soennichsen, F. D.; Tucek, F.; Herges, R. *Science* **2011**, *331*, 445-448. (b) Dommaschk, M.; Schuett, C.; Venkataramani, S.; Jana, U.; Naether, C.; Soennichsen, F. D.; Herges, R. *Dalton Trans.* **2014**, *43*, 17395-17405. (c) de Silva, A. P.; Uchiyama, S. *Nat. Nanotechnol.* **2007**, *2*, 399-410 (d) Jiang, G.; Song, Y.; Guo, X.; Zhang, D.; Zhu, D., *Adv. Mater.* **2008**, *20*, 2888-2898 (e) Pischel, U. *Angew. Chem., Int. Ed.* **2007**, *46*, 4026-4040.
22. For example: (a) Irie, M. *Chem. Rev.* **2000**, *100*, 1685-1716. (b) Sauer, M. *Proc. Natl. Acad. Sci.* **2005**, *102*, 9433-9434. (c) Garcia-Amoros, J.; Velasco, D. *Beilstein J. Org. Chem.* **2012**, *8*, 1003-1017. (d) Li, Z.; Wang, M.; Li, H.; He, J.; Li, N.; Xu, Q.; Lu, J. *J. Mater.*

- Chem. C* **2017**, *5*, 8593-8598. (e) Zhang, J.; Zou, Q.; Tian, H. *Adv. Mater.* **2013**, *25*, 378-399. (f) Dong, H.; Zhu, H.; Meng, Q.; Gong, X.; Hu, W. *Chem. Soc. Rev.* **2012**, *41*, 1754-1808.
23. Merino, E.; Ribagorda, M. *Beilstein J. Org. Chem.* **2012**, *8*, 1071-1090.
24. For example: (a) Stoll, R. S.; Hecht, S. *Angew. Chem., Int. Ed.* **2010**, *49*, 5054-5075. (b) Peter, M. V.; Stoll, R. S.; Kuehn, A.; Hecht, S. *Angew. Chem., Int. Ed.* **2008**, *47*, 5968-5972. (c) Blanco, V.; Leigh, D. A.; Marcos, V. *Chem. Soc. Rev.* **2015**, *44*, 5341-5370. (d) Viehmann, P.; Hecht, S. *Beilstein J. Org. Chem.* **2012**, *8*, 1825-1830. (e) Neri, S.; Martin, S. G.; Pezzato, C.; Prins, L. J. *J. Am. Chem. Soc.* **2017**, *139*, 1794-1797.
25. Zhang, J., & Tian, H. (2016). *Photochromic materials: Preparation, properties and applications*. Weinheim: Wiley-VCH Verlag.
26. (a) Schaudel, B.; Guerneur, C.; Sanchez, C.; Nakatani, K.; Delaire, J.A. *J. Mater. Chem.*, **1997**, *7*, 61-65; (b) Koelsch, C.F.; Workman, W.R. *J. Am. Chem. Soc.*, **1952**, *74*, 24, 6288-6289
27. (a) Cordes, T.; Herzog, T. T.; Malkmus, S.; Draxler, S.; Brust, T.; Digirolamo, J. A.; Lees, W. J.; Braun, M. *Photochem. Photobiol. Sci.* **2009**, *8*, 528-534. (b) Yokoyama, Y. *Chem. Rev.* **2000**, *100*, 1717-1740.
28. Han, W. G.; Lovell, T.; Liu, T. Q.; Noodleman, L. *ChemPhysChem.* **2002**, *3*, 167-178.
29. Ahmed, S. A.; Tanaka, M.; Ando, H.; Iwamoto, H.; Kimura, K. *Eur. J. Org. Chem.* **2003**, *13*, 2437-2442.
30. Merino E. *Chem. Soc. Rev.* **2011**, *40*, 3835-3853.
31. Bandara, H. M. D.; Burdette, S. C. *Chem. Soc. Rev.* **2012**, *41*, 1809-1825.
32. Ebadi, H. *J. Phys. Chem. A* **2014**, *118*, 36, 7832-7837.
33. (a) Lednev, I.; Ye, T.-Q.; Matousek, P.; Towrie, M.; Foggi, P.; Neuwahl, F.; Umaphathy, S.; Hester, R.; Moore, J. *Chemical Physics Letters* **1998**, *290*, 68-74.
34. Curtin, D. Y.; Grubbs, E. J.; McCarthy, C. G. *J. Am. Chem. Soc.* **1966**, *88*, 2775-2786.
35. Magee, J. L.; Shand, W.; Eyring, H. *J. Am. Chem. Soc.* **1941**, *63*, 677-688.
36. Bandara, H. M. D.; Friss, T. R.; Enriquez, M. M.; Isley, W.; Incarvito, C.; Frank, H. A.; Gascon, J.; Burdette, S. C. *J. Org. Chem.* **2010**, *75*, 4817-4827
37. Magee, J. L.; Shand, W.; Eyring, H. *J. Am. Chem. Soc.* **1941**, *63*, 677-688.
38. (a) Lubbe, A. S.; Kistemaker, J. C. M.; Smits, E. J.; Feringa, B. L. *Phys. Chem. Chem. Phys.* **2016**, *18*, 26725-26735. (b) Gille, K.; Knoll, H.; Quitzsch, K. *Int. J. Chem. Kinet.* **1998**, *31*, 337-350. (c) Serra, F.; Terentjev, E. M. *Macromolecules* **2008**, *41*, 981-986.

-
39. *Solvents and Solvent Effects in Organic Chemistry*; Reichardt, C.; Welton, T., 4th Ed.; Wiley-VCH: Weinheim, **2011**.
40. Calbo, J.; Weston, C. E.; White, A. J. P.; Rzepa, H.; Contreras-García, J.; Fuchter, M. J. *J. Am. Chem. Soc.* **2017**, *139*, 1261-1274.
41. For example: (a) Bleger, D.; Schwarz, J.; Brouwer, A. M.; Hecht, S. *J. Am. Chem. Soc.* **2012**, *134*, 20597-20600. (b) Beharry, A.; Sadovski, O.; Woolley, G. A. *J. Am. Chem. Soc.* **2011**, *133*, 19684-19687; (c) Samanta, S.; McCormick, T. M.; Schmidt, S. K.; Seferos, D. S.; Woolley, G. A. *Chem. Commun.* **2013**, *49*, 10314-10316. (d) Bleger, D.; Hecht, S. *Angew. Chem., Int. Ed.* **2015**, *54*, 11338-11349.
42. (a) Taft, R. W. *J. Am. Chem. Soc.* **1952**, *74*, 2729-2732. (b) Fujita, T.; Takayama, C.; Nakajima, M. *J. Org. Chem.* **1973**, *38*, 1623-1630.
43. Hammett, L. P. *J. Am. Chem. Soc.* **1937**, *59*, 96-103.
44. Nishimura, N.; Sueyoshi, T.; Yamanaka, H.; Imai, E.; Yamamoto, S.; Hasegawa, S. *Bull. Chem. Soc. Jpn.* **1976**, *49*, 1381-1387.
45. Brown, E. V.; Granneman, G. R. *J. Am. Chem. Soc.* **1997**, *3*, 621-627.
46. Ciccone, S.; Halpern, J. *Can. J. Chem.* **1959**, *37*, 1903-1910.
47. Otsuki, J.; Suwa, K.; Sarker, K. K.; Sinha, C. *J. Phys. Chem. A* **2007**, *111*, 1403-1409.
48. Simeth, N. A.; Crespi, S.; Fagnoni, M.; König, B. *J. Am. Chem. Soc.* **2018**, *140*, 2940-2946.
49. Schenderlein, H.; Voss, A.; Stark, R. W.; Biesalski, M. *Langmuir* **2013**, *29*, 4525-4534.
50. Jacquemin, D.; Perpète, E. A.; Maurel, F.; Perrier, A. *J. Phys. Chem. C* **2010**, *114*, 9489-9497.
51. (a) Kind, J.; Kaltschnee, L.; Leyendecker, M.; Thiele, C. M. *Chem. Commun.* **2016**, *52*, 12506-12509. (b) Lee, J.; Oh, S.; Pyo, J.; Kim, J.-M.; Je, J. H. *Nanoscale*, **2015**, *7*, 6457-6461. (c) Lee, S.; Oh, S.; Lee, J.; Malpani, Y.; Jung, Y.-S.; Kang, B.; Lee, J. Y.; Ozasa, K.; Isoshima, T.; Lee, S. Y.; Hara, M.; Hashizume, D.; Kim, J.-M., *Langmuir*, **2013**, *29*, 5869-5877. (d) Malpani, Y. R.; Oh, S.; Lee, S.; Jung, Y.-S.; Kim, *Bull. Korean Chem. Soc.*, **2014**, *35*, 2563-2566.
52. a) Harada, J.; Kawazoe, Y.; Ogawa, K., *Chem. Commun.* **2010**, *46*, 2593-2595. (b) Hadjoudis, E.; Mavridis, I. M. *Chem. Soc. Rev.* **2004**, *33*, 579-588. (c) Rao, X.; Huang, Q.; Yang, X.; Cui, Y.; Yang, Y.; Wu, C.; Chen, B.; Qian, G., *J. Mater. Chem.* **2011**, *21*, 3210-3215. (d) Robert, F.; Naik, A. D.; Tinant, B.; Robiette, R.; Garcia, Y. *Chem. Eur. J.* **2009**, *15*, 4327-4342. (e) Moorthy, J. N.; Mal, P.; Natarajan, R.; Venugopalan, P. *Org. Lett.* **2001**, *3*, 1579-1582. (f) Luo, Q.; Cao, F.; Xiong, C.; Dou, Q.; Qu, D.-H. *J. Org. Chem.* **2017**, *82*, 10960-10967.
-

53. Qi, Q.; Li, C.; Liu, X.; Jiang, S.; Xu, Z.; Lee, R.; Zhu, M.; Xu, B.; Tian, W. *J. Am. Chem. Soc.* **2017**, *139*, 16036-16039.
54. Zhou, H.; Xue, C.; Weis, P.; Suzuki, Y.; Huang, S.; Koynov, K.; Auernhammer, G. K.; Berger, R.; Butt, H.-J.; Wu, S. *Nat. Chem.* **2017**, *9*, 145-151.
55. S. Kobatake, I. Yamashita, *Tetrahedron.* **2008**, *64*, 7611-7618.
56. Frolova, L. A.; Rezvanova, A. A.; Lukyanov, B. S.; Sanina, N. A.; Troshin, P. A.; Aldoshin, S. M., *J. Mater. Chem. C* **2015**, *3*, 11675-11680.
57. (a) Burganov, T. I.; Katsyuba, S. A.; Vakhonina, T. A.; Sharipova, A. V.; Fominykh, O. D.; Balakina, M. Y. *J. Phys. Chem. C* **2018**, *122*, 1779-1785. (b) Poutanen, M.; Ikkala, O.; Priimagi, A. *Macromolecules* **2016**, *49*, 4095-4101. (c) Frigoli, M.; Mehl, G. H. *Chem. Commun.* **2004**, *0*, 2040-2041.
58. (a) Chen, Y.; Harrison, W. T. A.; Imrie, C. T.; Ryder, K. S. *J. Mater. Chem.* **2002**, *12*, 579-585. (b) Choi, Y.-J.; Kim, D.-Y.; Park, M.; Yoon, W.-J.; Lee, Y.; Hwang, J.-K.; Chiang, Y.-W.; Kuo, S.-W.; Hsu, C.-H.; Jeong, K.-U. *ACS Appl. Mater. Interfaces.* **2016**, *8*, 9490-9498. (c) Pan, S.; Ni, M.; Mu, B.; Li, Q.; Hu, X.-Y.; Lin, C.; Chen, D.; Wang, L. *Adv. Funct. Mater.* **2015**, *25*, 3571-3580.
59. Pfletscher, M.; Wölper, C.; Gutmann, J. S.; Mezger, M.; Giese, M. *Chem. Commun.* **2016**, *52*, 8549-8552.

Appendix 1A

1.3.5 Kinetic representation for isomerization:²⁵

For the thermal reverse isomerization process of azobenzenes, the representation of the kinetics rates for isomerization processes is relatively straightforward. The thermal reverse isomerization process from *Z* to *E*-state is a simple exponential decay, which follows the first order rate equation. The rate of thermal reaction $Z \rightarrow E$ can be written as:

$$\text{rate} = -\frac{d[Z](t)}{dt} = \frac{d[E](t)}{dt} = k[Z](t) \dots\dots\dots\text{Eqn. 1}$$

where $[E]$ and $[Z]$ are the *trans* and *cis* isomers concentrations, respectively at time t and k is the first order rate constant in the thermal reverse isomerisation process. As we know that the total number of molecules is constant. Assuming that at $t = \infty$ all the molecules are converted back into the *E*-isomer, which gives:

$$[E]_{\infty} = [E] + [Z] \dots\dots\dots\text{Eqn. 2}$$

So that,

$$[Z] = [E]_{\infty} - [E] \dots\dots\dots\text{Eqn. 3}$$

According to the Beer–Lambert’s law, applying on the above equation, the rate of thermal reverse isomerization

$$A_{(t)} = [A_{(0)} - A_{(\infty)}] \exp(-kt) + A_{(\infty)} \dots\dots\dots\text{Eqn. 4}$$

The integrated rate law may be written as

$$\ln(A_{\infty} - A_t) = -kt + \ln(A_{\infty} - A_0) \dots\dots\dots\text{Eqn. 5}$$

where, A_t , A_0 and A_{∞} are the absorbances at time t , t_0 and t_{∞} respectively.

The rate constant depends on the temperature, which can be used to determine the activation energy (E_a) of the reaction and the Arrhenius constant (A). According to the Arrhenius equation, the equation can be:

$$\ln k = -\frac{E_a}{R} \frac{1}{T} + \ln A \dots\dots\dots\text{Eqn. 6}$$

For the calculation of photoisomerisation rate, the above equation (Eqn. 4) is unsatisfactory due to the number of variables and the conditions under which the experiment has been performed. Thus, a complete numerical solution can be obtained by the rate of reaction involved in the three isomerization processes, photoisomerisation from *E* to *Z* and *Z* to *E*-isomer and the thermal reverse isomerization *Z* to *E*-isomer.

The rate of the reaction of these three isomerization processes can be solved with the continuity equation, as indicated in the equation (Eqn. 7).

$$\text{Continuity, } n_{\text{Total}} = n_E + n_Z + n_{\text{TS}} \dots\dots\dots \text{Eqn. 7}$$

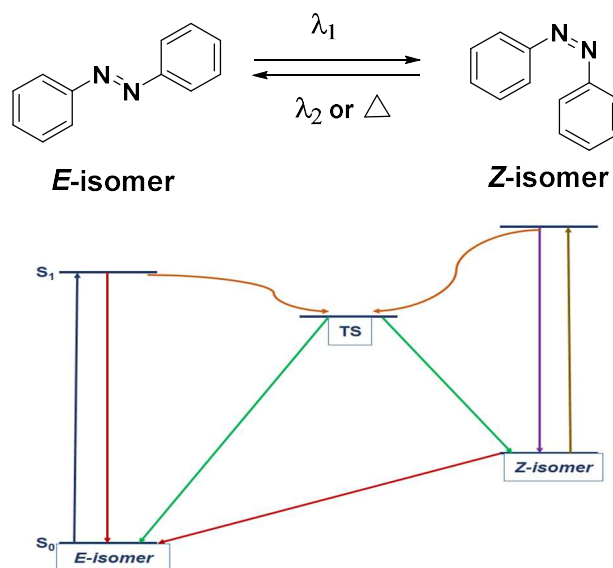


Figure 1.2: Energy level diagram for the photoisomerisation processes of azobenzene.

Excitation of *E* and *Z*- isomers populate a common transition state (TS)

On the other hand, the photostationary state (PSS) can be calculated by the equation

$$\%Z_{PSS} = \frac{[E]_0 - [E]_{PSS}}{[E]_0} \times 100 \dots\dots\dots \text{Eqn. 8}$$

The photoisomerisation kinetics of azobenzene was calculated by monitoring the absorbance of $\pi-\pi^*$ absorbance band. The experimental data can be analysed by according to the equation

$$\ln(A_0 - A_\infty)/(A_t - A_\infty) = k_1 t \dots\dots\dots \text{Eqn. 9}$$

where A_0 , A_t and A_∞ are the trans isomer absorbances corresponding to the time 0, t and at photostationary state respectively and t is the irradiation time. The k_1 is the rate constant has the expression

$$k_1 = k_{E \rightarrow Z} + k_{Z \rightarrow E} = I(\phi_{E \rightarrow Z}\epsilon_E + \phi_{Z \rightarrow E}\epsilon_Z)\ln 10 \dots\dots\dots \text{Eqn. 10}$$

where $k_{E \rightarrow Z}$ and $k_{Z \rightarrow E}$ are the rate constants for the $E \rightarrow Z$ and $Z \rightarrow E$ photoisomerization reactions respectively, while $\phi_{E \rightarrow Z}$ and $\phi_{Z \rightarrow E}$ are the quantum yields of the same processes, ϵ_E and ϵ_Z are the molar extinction coefficients of the *E* and *Z* isomers respectively at the irradiation wavelength light.

On the other hand, thermal $Z \rightarrow E$ isomerization of azobenzene follows the first order kinetics. The kinetic equation should be in this case:

$$\ln(A_\infty - A_0)/(A_\infty - A_t) = k_2 t$$

where k_2 is the rate constant of the $Z \rightarrow E$ isomerization reaction.

The unimolecular thermal *Z* to *E* isomerization process in the dark obeys

$$\Delta A_t = \Delta A_\infty + \Delta A_0 e^{-t/\tau}$$

where ΔA_0 , ΔA_t and ΔA_∞ correspond to the absorbance change at time zero, *t* and infinity, respectively and τ is the half-life (relaxation time) of the *Z*-isomer. The half-life can be derived from the plot of the absorbance, ΔA versus *times* by fitting the above equation to the data.

Chapter 2. Evaluation of Substituent Effect in *Z*-Isomer Stability of Arylazo-1*H*-3,5-dimethylpyrazoles

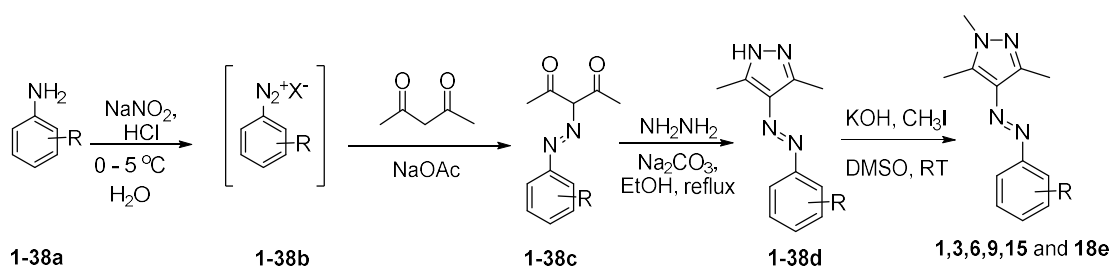
2.1 Introduction to arylazo-1*H*-3,5-dimethylpyrazoles

The salient features of azobenzene as photoswitchable molecules are robustness in switching, the rate of *E-Z* forward switching, the extent of photostationary state (PSS) and thermal half-life of *Z*-isomer. Based on the gap between $\pi-\pi^*$ and $n-\pi^*$ transitions of the azo group, azoarenes have been classified as azobenzenes (well-separated), aminoazobenzenes (overlapping), and pseudo-stilbenes (nearly degenerate).¹ Such classifications are mainly due to the type of substitutions that can dictate the switching ability as well as the stability of *Z*-isomer. Furthermore, the choice and the introduction of specific substituents such as fluoro and alkoxy at all the four *ortho* positions with respect to the azo group can lead to visible light induced isomerization in azoarenes.² Hence, the position of the substituent in the aryl ring is equally important in controlling the photoswitching characteristics. For a variety of applications, all these properties need to be altered. Replacing arenes with heterocycles is an alternative strategy, which is an emerging area in this regard. Pyridine containing heteroazoarenes are one of the well-known photoswitches that have found many interesting applications.³ Despite the presence of many kinds of literature on the analogous five-membered heteroazoarenes, the studies on them have been limited to synthesis and evaluation of medicinal properties in the past.⁴ However, such systems found a considerable attention only after their photoswitching properties have been evaluated. Herges and coworkers have synthesized an imidazole-connected azoarene, which had a long half-life in its *Z*-form.⁵ Fuchter and coworkers enhanced the stability of *Z*-isomer up to 1000 days, when they introduced *N*-methyl pyrazole moiety.⁶ After these findings, many groups started utilizing them for various light-driven processes and as photoswitches.⁷

Fuchter's group has explored the effects of *N*-methyl five-membered heterocycles towards tuning the photoswitching behaviour.⁸ Using experimental rate constants and computational data, they investigated the influence of heterocycles on the stability of *Z*-isomer. Recently, König and coworkers have tuned the lifetimes of *Z*-

isomer of phenylazoindoles from nanoseconds to days by controlling the hydrazone tautomerization.⁹ Despite the presence of enormous literature on azoarenes and their derivatives, including their mechanistic studies, the general role of substituents in the photoswitching is not explored in a systematic way. Few issues like the choice of substituents in enhancing the *Z*-isomer stability and the role of electronic effects in photoswitching behavior and reverse isomerization can be vital in the design and development of azoarene based molecular switches. In order to address these issues, we have chosen phenylazopyrazole **1d** as our target, which structurally lacks the *N*-methyl group (**1e**) that was previously reported by Fuchter and co-workers.⁶ The advantages of this choice are the ease of synthetic access to a variety of substituted derivatives, and also the possibility of post-functionalization at pyrazole N-H. Apart from that, the kinetic studies on such NH phenylazopyrazole **1d** showed almost three order of magnitude higher rate constant than that of **1e**, which provide a better opportunity to study the enormous insights into the role of substituents. In this regard, the *modus operandi* of substituents, particularly with respect to the photoswitching behavior, stability of *Z*-isomer, and their influence in the thermal reverse switching of the *Z*-isomer, which are the primary focus of this investigation. The influence of position (*ortho*-, *meta*- and *para*-) and nature (electron donating vs electron withdrawing) of the substituents have been investigated. Also, the role of substituents in photoswitching behavior, thermal reverse isomerization kinetics, and half-lives of the *Z*-isomers has been studied using UV-Vis and NMR spectroscopic techniques. The synthesis of a wide range of pyrazole based substituted azoarenes, their photoswitching properties and *Z*-isomer stability in understanding the effects of electronic, steric and hydrogen bonding are described in this chapter in detail.

2.2 Synthesis



Scheme 2.1. Synthesis of N-H [**1-38d**] and selected *N*-methyl phenylazopyrazoles [R = H(**1e**); 3-F(**3e**); 3-Cl(**6e**); 3-Br(**9e**); 3-OCH₃(**15e**); 3-CF₃(**18e**)]

Table 2.1. Synthesis of substituted phenylazopyrazoles **1-38d** and *N*-methyl phenylazopyrazoles **1e, 3e, 6e, 9e, 15e** and **18e**.

S. No.	Substituent	Step-2 ^a			Step-3			
		Product	Time (h)	Yield (%)	Product	Condition	Time (h)	Yield (%)
1	Nil	1c	5	97	1d	A	6	85
2	2-F	2c	10	99	2d	A	10	96
3	3-F	3c	6	97	3d	A	8	82
4	4-F	4c	13	99	4d	A	12	93
5	2-Cl	5c	3	98	5d	A	17	61
6	3-Cl	6c	3	98	6d	A	10	70
7	4-Cl	7c	5	95	7d	A	6	93
8	2-Br	8c	7	96	8d	A	6	70
9	3-Br	9c	7	95	9d	A	6	90
10	4-Br	10c	6	73	10d	A	6	72
11	2-OH	11c	5	98	11d	A	10	93
12	3-OH	12c	10	60	12d	A	5	92
13	4-OH	13c	12	94	13d	A	8	79
14	2-CF ₃	14c	4	97	14d	A	10	72
15	3-CF ₃	15c	5	91	15d	A	14	74
16	4-CF ₃	16c	5	91	16d	A	23	83
17	2-OMe	17c	8	82	17d	A	10	70
18	3-OMe	18c	8	87	18d	A	12	98
19	4-OMe	19c	10	95	19d	A	8	87
20	2-NO ₂	20c	13	76	20d	A	24	81
21	3-NO ₂	21c	13	69	21d	A	13	83
22	4-NO ₂	22c	8	82	22d	A	8	97
23	2-CH ₃	23c	7	98	23d	A	8	95
24	3-CH ₃	24c	3	67	24d	A	6	96
25	4-CH ₃	25c	3	63	25d	A	8	92
26	3-COOH	26c	8	75	26d	A	11	56
27	4-COOH	27c	2	98	27d	A	12	81
28	3-NHAc	28c	3	85	28d	A	10	57
29	4-NHAc	29c	5	89	29d	B	5	93
30	2-Et	30c	8	98	30d	A	3	99
31	2,4,6-triMe	31c	18	85	31d	A	6	99
32	Ar = α -Np	32c	3	66	32d	A	22	63
33	2,5-diCl	33c	14	54	33d	A	18	45
34	2,6-diCl	34c	3	62	34d	A	12	89
35	2,4-diF	35c	3	99	35d	A	9	78
36	2,5-diF	36c	5	99	36d	A	8	54
37	2,6-diF	37c	10	98	37d	A	10	53
38	3,5-diF	38c	4	99	38d	A	11	87
Step-4								
		Product	Time (h)	Yield (%)	Condition			
39	Nil	1e	4	88	C			
40	3-F	3e	3	82	C			
41	3-Cl	6e	4	90	C			
42	3-Br	9e	3	94	C			
43	3-CF ₃	15e	3	90	C			
44	3-OMe	18e	3	85	C			

^aTemperature = RT; Ar = α -Np (α -Naphthyl), Condition-A: Na₂CO₃ (3.0 eq.), NH₂NH₂.2HCl (1.5 eq.), EtOH, reflux; Condition-B: NH₂NH₂.H₂O (1.0 eq.), EtOH, 40 °C; Condition-C: CH₃I (1.2 eq.), KOH (3.0 eq.), DMSO, RT.

A two-step strategy has been adopted to prepare the desired 1*H*-3,5-dimethylpyrazole connected azoarene derivatives. The first step is to synthesize the arylazoacetylacetone derivatives (**1c-38c**).¹⁰ These derivatives can be accessible

through the diazotization of readily available aryl amines, followed by the treatment with acetylacetone (**Scheme 2.1** and **Table 2.1**). The yields are particularly high when aqueous sodium acetate has been used along with acetylacetone. On reacting the isolated **1c-38c** with hydrazine led to the target pyrazole-based substituted heteroazoarene derivatives (**1d-38d**). Additionally, *N*-methylation has been performed at the pyrazole NH using KOH as a base and CH₃I on a set of pyrazole derivatives **1d**, **3d**, **6d**, **9d**, **15d** and **18d**. This led to the synthesis of the corresponding *N*-methylated pyrazole connected azoarenes **1e**, **3e**, **6e**, **9e**, **15e** and **18e**.

2.3 Analysis of photoswitching through UV-Vis and NMR spectroscopic techniques

Traditionally UV-Vis spectroscopic studies play a very important role in understanding the *E-Z* isomerization of azobenzenes. This is because of the distinguishable spectral features for *E*- and *Z*-isomers, arising due to drastic changes in the electronic structure. In order to understand the effects of substituents on their electronic spectra, the spectral data of the *E*- and *Z*-isomers of phenylazopyrazole derivatives **1-38d** have been compared. For comparison, all the photoswitching and kinetics experiments have been carried out in acetonitrile, and at a temperature of 25 ± 1 °C in order to minimize the errors due to external parameters. Electronic spectroscopic parameters such as λ_{\max} and molar extinction coefficient (ϵ) have been obtained for all the *E*- and *Z*- isomers in this regard (**Figure 2.1** and **2.2**). Upon irradiation at a wavelength of 365 nm, almost all of the derivatives exhibited *E* to *Z* isomerization. The data on the shifts in the λ_{\max} corresponding to $\pi-\pi^*$ and $n-\pi^*$ absorptions of *Z*-isomers have been included in table 2.2. The ϵ values of $\pi-\pi^*$ and $n-\pi^*$ transitions of *Z*-isomers have been estimated based on the PSS composition and its corresponding absorption values.¹¹ The plots on the absorption maxima vs ϵ of the individual $\pi-\pi^*$ transitions of *E*- and *Z*-isomers show that only the former is sensitive to the electronic effects (**Figure 2.1a** and **2.1b**). Due to the breaking of conjugation, the azo group in *Z*-isomers is less sensitive to the electronic influence, and so the majority of the substituted *Z*-arylazopyrazoles exhibit similar $\pi-\pi^*$ absorption properties. However, there is a reasonable steric influence, which can be understood from the deviation for those derivatives having *ortho* substituents in the phenyl ring with respect to the parent **1d**.

behaviour. This can be attributed to varied contributions of electronic effects majorly through resonance and inductive effects.

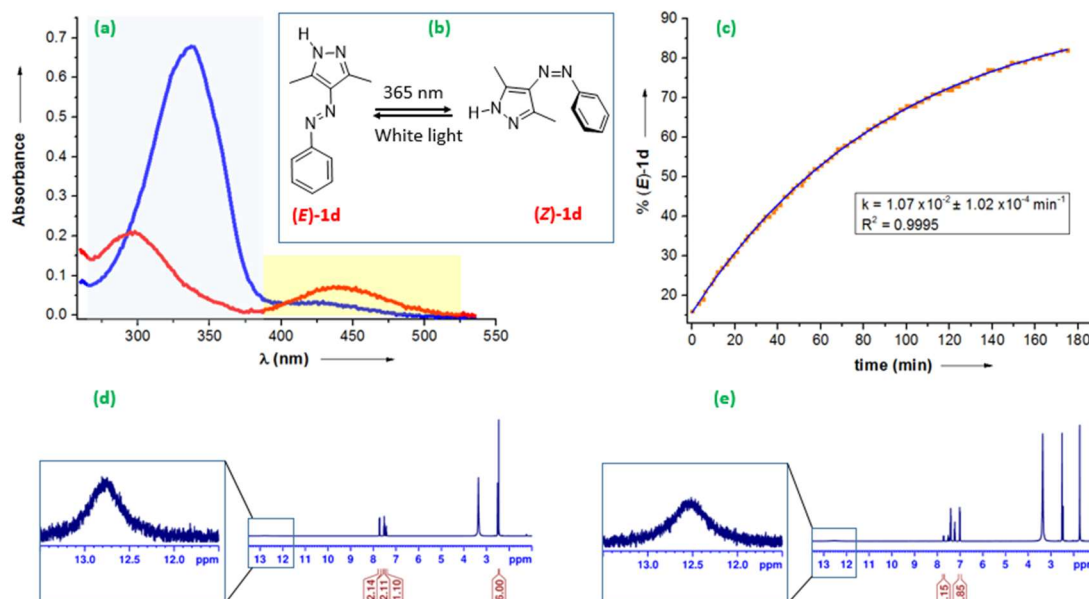


Figure 2.2 Representative figures on photoswitching in phenylazopyrazole derivative **1d**: (a) Analysis of photoswitching of **1d** in DMSO using UV-Vis spectroscopy (Spectral trace in blue – (**E**)-**1d**; red – after 365 nm irradiation to attain PSS); (b) Reversible photoisomerization of **1d**; (c) First order kinetics trace corresponding to the thermal reverse *Z-E* isomerization of **1d** (using NMR spectroscopy); NMR spectrum of (**E**)-**1d** in DMSO- d_6 (d) before irradiation, and (e) after irradiation at 365 nm for 30 minutes.

For the *E*-isomers of many derivatives, the $n-\pi^*$ absorption bands have been observed as a shoulder to $\pi-\pi^*$ absorptions, hence, the identification of exact λ_{max} corresponding to such transitions are cumbersome. In this regard, we adopted a Gaussian fitting to obtain the λ_{max} values in such cases. Upon comparison of the $n-\pi^*$ absorptions of all those substituted *E*-isomers of phenylazopyrazoles, we observed a resemblance in the spread of the λ_{max} and ϵ values of *meta*-substituted ones as in the case of $\pi-\pi^*$ absorptions. Similarly, the *ortho*-substituted derivatives also showed a narrow deviation with respect to the substituent effect. The only difference between them is the observation of red shifts in the case of *ortho*, whereas, *meta* substitutions led to blue shifts in the λ_{max} values relative to the parent **1d**. In contrast, the behaviour of $n-\pi^*$ absorptions of *para*-substituted systems did not show any trend at all.

On comparing the λ_{max} values, (**Figure 2.1c** and **2.1d**) the *meta*-derivatives showed a very similar trend as in the case of *E*-isomers. Similarly, the *ortho*-

substituents showed little variation in the λ_{\max} of both $n-\pi^*$ and $\pi-\pi^*$ absorptions of *Z*-isomers. Once again, the *para*-substitution showed a larger variation upon changing the substitutions. The difference between the $\pi-\pi^*$ transitions of *E*- and *Z*-isomers have been calculated and the results are tabulated as $\Delta\lambda_{\text{conjugation}}$ in **Table 2.2**. The values are indicative of the extent of breaking of conjugation upon isomerization from *E* to *Z*. Conversely, the larger the value of $\Delta\lambda_{\text{conjugation}}$, the attainment of non-planarity is the dominant feature. On comparison of these values for various substituents, we found out that the majority of substitution at *ortho* position provided a larger deviation from planarity or conjugation breaking upon isomerization, followed by *meta* and then *para*. The steric reason might provide a necessary condition to alter its geometry to attain non-planarity upon isomerization, which could be a plausible reason for this behaviour.

Few derivatives such as 2-hydroxy **11d** and 4-hydroxy phenylazopyrazole **13d** derivatives exhibit minimal spectral changes albeit a small to a substantial decrease in their intensities. Interestingly, the spectral features of **11d** with two split-up bands in the $\pi-\pi^*$ region resemble that of 2-hydroxyazobenzene. The intramolecular hydrogen bonding and/or solvent assisted tautomerization leading to the hydrazone form may be the plausible reason for this behaviour.¹ Similarly 2-nitro **20d** and 4-nitro phenylazopyrazole **22d** also showed a little change in the spectra after irradiation. Presumably, both of them behave like a push-pull type azobenzene, for which the switching rates are expected to be fast. Furthermore, the 3-nitro phenylazopyrazole **21d** also showed a very high reverse isomerization (*Z-E*) rate. The reasons for this non-switching nature of **20d** and **22d** can be attributed to resonance, whereas inductive effects of the nitro group influence a fast reverse switching in **21d** that renders a push-pull type mechanism. The plausible tautomers and resonance structures of **11d**, **13d**, **20d** and **22d** are indicated. (**Scheme 2.1**)

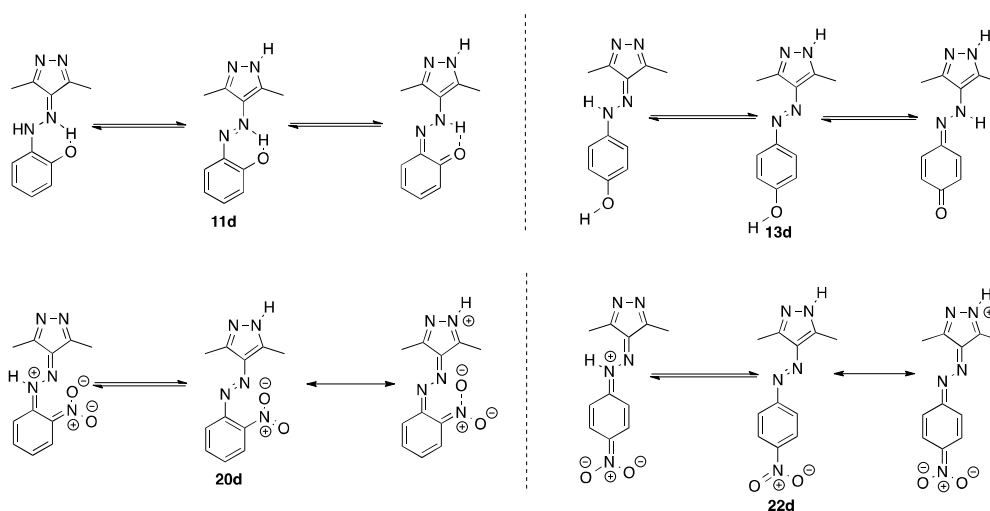
Table 2.2. UV-Vis spectroscopic and photoswitching data of (*E*)- and (*Z*)- isomers of phenylazopyrazole derivatives **1-38d** and *N*-methyl derivatives **1e, 3e, 6e, 9e, 15e** and **18e**.

S. No.	Compound	R=	<i>E</i> -isomer ^a				<i>Z</i> -isomer ^a				$\Delta\lambda_{conf}$	k^g, min^{-1}	[μM] $\mu\text{mol.L}^{-1}$
			$\pi-\pi^*$ λ_{max} (e)	$\pi-\pi^*$ λ_{max} (e)	$\Delta\lambda_{\text{trans}}^b$	<i>E-Z</i> PSS ^c (% <i>Z</i>)	$\pi-\pi^*$ λ_{max}	$\pi-\pi^*$ λ_{max}	$\Delta\lambda_{\text{cis}}^d$	<i>Z-E</i> PSS ^e (% <i>E</i>)			
1	1d	H	330 (19369 ± 278)	421 (1199 ± 57)	91	85	293 (7186)	436 (2251)	143	77	37	$1.31 \times 10^{-3} \pm 5.99 \times 10^{-6}$	37
2	2d	2-F	334 (23807 ± 862)	418 (910 ± 108)	84	90	294 (7701)	442 (2716)	155	75	47	$2.73 \times 10^{-3} \pm 9.48 \times 10^{-6}$	29
3	3d	3-F	334 (25338 ± 2314)	417 (1129 ± 116)	83	87	292 (8957)	437 (2853)	145	74	42	$3.35 \times 10^{-4} \pm 2.22 \times 10^{-5}$	29
4	4d	4-F	330 (19853 ± 278)	426 (1532 ± 26)	96	85	293 (9542)	436 (3137)	143	96	37	$6.13 \times 10^{-5} \pm 1.85 \times 10^{-5}$	27
5	5d	2-Cl	339 (34674 ± 681)	426 (1641 ± 125)	87	84	292 (20294)	432 (7482)	140	86	47	$1.53 \times 10^{-5} \pm 1.33 \times 10^{-5}$	21
6	6d	3-Cl	336 (32797 ± 278)	418 (3694 ± 185)	82	80	290 (15263)	418 (5328)	128	77	46	$1.14 \times 10^{-2} \pm 7.89 \times 10^{-5}$	19
7	7d	4-Cl	336 (29398 ± 1823)	430 (2397 ± 106)	94	90	295 (12801)	439 (4347)	144	94	41	$3.59 \times 10^{-4} \pm 1.28 \times 10^{-5}$	23
8	8d	2-Br	340 (23530 ± 1509)	424 (1383 ± 83)	84	88	289 (12758)	431 (2944)	142	72	51	$4.29 \times 10^{-3} \pm 1.13 \times 10^{-5}$	22
9	9d	3-Br	335 (20818 ± 1147)	416 (1293 ± 34)	81	86	296 (10174)	437 (3406)	141	73	39	$5.87 \times 10^{-2} \pm 4.82 \times 10^{-4}$	24
10	10d	4-Br	337 (21721 ± 1530)	416 (1355 ± 52)	79	92	293 (7924)	440 (2464)	147	72	44	$1.79 \times 10^{-3} \pm 5.39 \times 10^{-6}$	31
11	11d	2-OH**	332 (17638) 366 (16042)	-	-	-	-	-	-	-	-	-	39
12	12d	3-OH	330 (16678 ± 1556)	412 (1179 ± 52)	82	86	292 (6211)	437 (2187)	145	69	38	$4.97 \times 10^{-4} \pm 1.37 \times 10^{-5}$	38
13	13d	4-OH***	342 (16786)	400 (1433)	58	-	-	-	-	-	-	-	39
14	14d	2-CF ₃	335 (19703 ± 1221)	428 (1122 ± 26)	93	41	327 (29819)	437 (3957)	110	87	8	$3.28 \times 10^{-1} \pm 7.12 \times 10^{-3}$	31
15	15d	3-CF ₃	332 (22045 ± 392)	419 (1320 ± 84)	87	83	294 (9002)	436 (2953)	142	86	38	$2.65 \times 10^{-3} \pm 9.46 \times 10^{-6}$	24
16	16d	4-CF ₃	334 (22010 ± 858)	392 (1578 ± 53)	58	79	297 (8459)	436 (2728)	139	80	37	$2.96 \times 10^{-2} \pm 1.15 \times 10^{-4}$	29
17	17d	2-OMe	350 (13044 ± 338)	421 (1483 ± 42)	71	92	294 (6434)	430 (2427)	136	56	56	$1.04 \times 10^{-3} \pm 1.71 \times 10^{-5}$	45
18	18d	3-OMe	330 (21893 ± 364)	419 (1605 ± 3)	89	85	292 (9039)	437 (3313)	145	65	38	$2.97 \times 10^{-3} \pm 2.00 \times 10^{-5}$	24
19	19d	4-OMe	342 (33110 ± 1817)	403 (2293 ± 68)	61	92	301 (15000)	441 (4463)	140	68	41	$5.72 \times 10^{-4} \pm 1.53 \times 10^{-5}$	16
20	20d	2-NO ₂ ***	339 (32724)	-	-	-	-	-	-	-	-	-	41
21	21d ^h	3-NO ₂ **	332 (17420 ± 630)	421 (897)	89	24	277 (36509)	426 (4009)	-	91	-	$3.54 \times 10^{-1} \pm 1.01 \times 10^{-5}$	37
22	22d	4-NO ₂ ***	360 (29247)	-	-	-	-	-	-	-	-	-	33

Chapter 2. Evaluation of Substituent Effect...

23	23d	2-CH ₃	336 (34578 ± 3434)	423 (2914 ± 197)	87	92	292 (15881)	435 (4752)	143	80	44	6.92 x 10 ⁻³ ± 1.16 x 10 ⁻⁵	18
24	24d	3-CH ₃	331 (18375 ± 1608)	419 (1046 ± 35)	88	88	292 (6575)	441 (2060)	149	61	39	1.99 x 10 ⁻³ ± 1.15 x 10 ⁻⁵	30
25	25d	4-CH ₃	335 (16747 ± 2099)	416 (1262 ± 18)	81	90	295 (6531)	437 (2011)	142	73	40	1.45 x 10 ⁻³ ± 3.24 x 10 ⁻⁶	31
26	26d	3-CO ₂ H	332 (19329 ± 235)	419 (1045 ± 15)	87	81	295 (7846)	435 (2395)	140	65	37	3.04 x 10 ⁻² ± 6.50 x 10 ⁻⁵	27
27	27d	4-CO ₂ H	342 (15675 ± 967)	410 (1002 ± 66)	68	83	268 (8002)	441 (2159)	141	81	42	4.41 x 10 ⁻² ± 1.22 x 10 ⁻⁴	38
28	28d	3-NHAc	329 (16296 ± 858)	423 (1024 ± 72)	94	86	285 (7088)	438 (2335)	153	78	44	5.44 x 10 ⁻² ± 1.43 x 10 ⁻⁴	34
29	29d	4-NHAc	350 (19166 ± 886)	410 (2382 ± 46)	60	91	291 (9896)	445 (2983)	142	68	47	1.44 x 10 ⁻³ ± 4.99 x 10 ⁻⁶	36
30	30d	2-Et	337 (20424 ± 1608)	425 (1096 ± 57)	88	92	293 (8455)	436 (2425)	143	74	44	1.30 x 10 ⁻² ± 1.08 x 10 ⁻⁵	29
31	31d	2,4,6-triMe	324 (18479 ± 881)	431 (950 ± 125)	107	79	288 (12596)	429 (2823)	141	77	36	3.62 x 10 ⁻³ ± 5.46 x 10 ⁻⁶	26
32	32d	Ar = α-Np	366 (18852 ± 882)	-	-	89	307 (11028)	446 (3944)	139	72	59	4.35 x 10 ⁻³ ± 3.69 x 10 ⁻⁶	32
33	33d	2,5-diCl	346 (19153 ± 419)	425 (1140 ± 43)	79	92	294 (8030)	432 (2437)	138	68	52	4.45 x 10 ⁻² ± 3.23 x 10 ⁻⁵	30
34	34d	2,6-diCl	307 (12943 ± 732)	423 (609 ± 38)	116	33	298 (27684)	421 (3755)	123	92	9	1.89 x 10 ⁻³ ± 2.52 x 10 ⁻⁵	44
35	35d	2,4-diF	336 (14567 ± 635)	418 (1442 ± 34)	82	85	292 (5908)	427 (2094)	135	69	44	3.26 x 10 ⁻³ ± 9.69 x 10 ⁻⁶	36
36	36d	2,5-diF	343 (21844 ± 1048)	428 (1653 ± 35)	85	66	300 (18741)	429 (5798)	129	77	43	2.83 x 10 ⁻¹ ± 2.31 x 10 ⁻³	26
37	37d	2,6-diF	321 (20491 ± 559)	418 (1482 ± 37)	97	62	299 (14838)	421 (4100)	122	81	22	6.46 x 10 ⁻³ ± 1.21 x 10 ⁻⁵	26
38	38d	3,5-diF	334 (22857 ± 1168)	426 (1069 ± 63)	92	56	294	433 (3260)	139	84	40	8.27 x 10 ⁻² ± 3.77 x 10 ⁻⁴	23
39	1eⁱ	Nil	334 (19252 ± 435)	423 (1055 ± 57)	89	87	296 (8373)	429 (3513)	133	73	38	1.86 x 10 ⁻³ ± 1.42 x 10 ⁻⁴	34
40	3eⁱ	3-F	338 (18843 ± 536)	426 (1058 ± 46)	88	89	298 (6452)	441 (2414)	143	89	40	1.06 x 10 ⁻³ ± 5.28 x 10 ⁻⁵	47
41	6eⁱ	3-Cl	339 (19171 ± 511)	421 (1153 ± 15)	82	93	299 (6129)	441 (2358)	142	79	40	7.43 x 10 ⁻⁴ ± 1.34 x 10 ⁻⁴	37
42	9eⁱ	3-Br	339 (22171 ± 465)	427 (1661 ± 98)	88	89	299 (7654)	430 (3443)	131	86	40	9.29 x 10 ⁻⁴ ± 1.80 x 10 ⁻⁴	32
43	15eⁱ	3-CF ₃	337 (21283 ± 358)	423 (1240 ± 72)	86	91	299 (7460)	441 (2689)	142	89	38	2.09 x 10 ⁻³ ± 3.70 x 10 ⁻⁴	36
44	18eⁱ	3-OMe	335 (17123 ± 244)	421 (1143 ± 25)	86	87	295 (7040)	442 (2580)	147	81	40	1.44 x 10 ⁻³ ± 2.77 x 10 ⁻⁴	51

^aThe values of λ_{\max} are given in nm and ϵ in L.mol⁻¹.cm⁻¹; ^b $\Delta\lambda_{\text{trans}}$ is the difference between $\pi-\pi^*$ and $n-\pi^*$ absorption maxima of *E*-isomer; ^cPSS at 365 nm for *E-Z* isomerization has been estimated; ^d $\Delta\lambda_{\text{cis}}$ is the difference between $\pi-\pi^*$ and $n-\pi^*$ absorption maxima of *Z*-isomer; ^ePSS at white light (CFL lamp) for *Z-E* isomerization has been estimated using UV-Vis spectroscopy with an uncertainty 2-5%; (as indicated in the literature reference 21); ^f $\Delta\lambda_{\text{conjugation}}$ is the difference between $\pi-\pi^*$ absorption maxima of *E*- and *Z*-isomers; ^gKinetics have been performed in CH₃CN at 25 ± 1 °C; ^hKinetics has been measured in DMSO at 23 ± 1 °C; ⁱKinetics have been performed in CH₃CN at 40 ± 1 °C. (**Upon 365 nm irradiation, the absorptions showed a decrease with the isosbestic points. ***For 4-OH derivative, photoirradiation did not lead to any spectral change.)



Scheme 2.1. Possible intramolecular or solvent assisted tautomerism in hydroxyphenylazopyrazole derivatives **11d**, and **13d**; Influence of resonance and solvent assisted tautomerism in nitro- derivatives **20d** and **22d** leading to push-pull type azoarenes with fast switching.

The photoswitching studies have also been carried out using NMR spectroscopy. Both photoswitching and reverse thermal isomerization kinetics have been studied in CD_3CN at 25°C . In order to understand the influence of the substituents in the structural features of the *E*- and *Z*-isomers, a closer inspection at the NMR spectral analysis was carried out. Upon switching from *E*- to *Z*-isomer, the *ortho*-protons of the aryl group, the two methyl groups of the pyrazoles and also the N-H protons exhibited major shifts towards shielding regions. In spite of showing shifts upon isomerization from *E* to *Z*, the *meta*- and *para*-protons of the aryl group are not considered in this analysis due to the overlapping nature of the signals. The changes in the chemical shift values ($\Delta\delta$) for all the substituents that we studied are included (**Table 2.3**). The results showed that the *ortho* proton showed a larger upfield shift when the electron-withdrawing substituent is present either at the *ortho* or *meta* position. Also, the same effect is observed, when electron-donating power increases for the substituent at the *para* position. Upon isomerization, the two methyl groups showed upfield shifts in the range between 0.67 and 0.72, except for 3,5-difluoro-substituted system that showed a shift of 0.62. This clearly indicates that the methyl groups of the pyrazoles showed less perturbation upon isomerization due to the remote distance from the position of substituents at the aryl ring. Also, their shifts further confirm that the role of a steric factor, which is nearly equal in all the cases irrespective of the position of the substituents. Similarly, N-H protons also showed only a negligible effect in the

chemical shift values upon varying the substituents. The same trend was observed in the case of *N*-methylated derivatives as well. For all these molecules, *Z-E* reverse isomerization kinetics have been followed and the rates have been tabulated (**Appendix 2A**). However, we found that the rates are quite different from the UV-Vis kinetics experiments, which can be attributed to electronic and steric effects apart from the difference in the concentration and the reasons are explained in section 2.4 and 2.5.

Table 2.3. NMR spectroscopic data of the selected protons of *E*- and *Z*-isomers of different substituted phenylazopyrazoles and *N*-methyl phenylazopyrazoles.

S. No.	Compound	Substituent	Conversion ^a	N – H region ^b			CH ₃ region ^b			Aromatic region ^b (<i>ortho</i> -H)		
				(<i>E</i> -)	(<i>Z</i> -)	$\Delta\delta$	(<i>E</i> -)	(<i>Z</i> -)	$\Delta\delta$	(<i>E</i> -)	(<i>Z</i> -)	$\Delta\delta$
1	1d	H	89	10.83	10.66	0.17	2.49	1.77	0.72	7.77	7.00	0.77
2	2d	2-F	85	10.88	10.71	0.17	2.49	1.81	0.68	7.72	6.94	0.78
3	5d	2-Cl	81	10.88	10.72	0.16	2.51	1.83	0.68	7.69	6.66	1.03
4	14d	2-CF ₃	69	10.93	10.85	0.08	2.49	1.79	0.70	7.83	6.70	1.13
5	3d	3-F	85	10.88	10.69	0.19	2.49	1.81	0.68	7.63	6.84	0.79
6	6d	3-Cl	89	10.88	10.70	0.18	2.49	1.81	0.68	7.72	6.95	0.77
7	9d	3-Br	77	10.89	10.73	0.16	2.49	1.81	0.68	7.76	6.99	0.77
8	15d	3-CF ₃	92	10.90	10.71	0.19	2.50	1.78	0.72	8.02	7.21	0.81
9	18d	3-OCH ₃	63	10.76	10.63	0.13	3.85^c	3.72^c	0.13^c	7.39^d	6.55^d	0.84^d
10	4d	4-F	85	10.83	10.65	0.18	2.48	1.80	0.68	7.81	7.08	0.73
11	7d	4-Cl	86	10.85	10.67	0.18	2.48	1.80	0.68	7.76	7.02	0.74
12	10d	4-Br	86	10.83	10.67	0.16	2.48	1.80	0.68	7.67	6.95	0.72
13	16d	4-CF ₃	88	10.92	10.72	0.20	2.50	1.79	0.71	7.91	7.17	0.74
14	19d	4-OCH ₃	62	10.71	10.59	0.12	2.47	1.80	0.67	7.76	6.89	0.87
							3.85^c	3.78^c	0.07^c			
15	36d	2,5-diF	89	10.94	10.77	0.17	2.49	1.80	0.69	7.47	6.82	0.65
16	38d	3,5-diF	80	10.94	10.78	0.16	2.48	1.86	0.62	7.40	6.67	0.73

				N – H region ^b			CH ₃ region ^b			Aromatic region ^b (<i>ortho</i> -H)		
17	1e	H	26	3.73	3.60	0.13	2.41	1.47	0.94	7.76	7.02	0.74
							2.55	2.15	0.40			
18	3e	3-F	35	3.73	3.61	0.12	2.41	1.50	0.91	7.63	6.86	0.77
							2.55	2.10	0.40			
19	6e	3-Cl	45	3.73	3.62	0.11	2.40	1.49	0.91	7.72	6.96	0.76
							2.55	2.11	0.44			
20	9e	3-Br	51	3.73	3.62	0.11	2.40	1.49	0.91	7.76	6.99	0.77
							2.55	2.11	0.44			
21	15e	3-CF ₃	62	3.74	3.61	0.13	2.42	1.46	0.96	8.05	7.41	0.64
							2.57	2.08	0.47			
22	18e	3-OCH ₃	76	3.73	3.60	0.13	2.41	1.51	0.90	7.38	6.60	0.78
							2.55	2.08	0.47			

^a*E-Z* conversion during photoisomerization using 365 nm at PSS; ^bChemical shift values are in ppm; ^cBold = OMe protons; ^dTwo distinct *ortho* protons have been observed (All the spectra have been recorded in CD₃CN at 298 K in 400 MHz NMR).

2.4. Effects of substituents and hydrogen bonding in the stability of *Z*-isomers

The effects of substituents on the stability of *Z*-isomer have been studied through thermal reverse isomerization kinetics using UV-Vis spectroscopy in CH₃CN at 25 ± 1 °C **Appendix 2B**. All of the substituted phenylazopyrazole derivatives have been switched from *E*- to *Z*-isomer using a light of wavelength 365 nm, followed by the thermal reverse isomerization kinetics have been measured. The photoisomerization has been performed in such a way that maximum *Z*-isomer conversion is observed or the irradiation is done until the establishment of the photostationary state (PSS). Upon the thermal reverse isomerization, the exponential rate of formation of the *E*-isomer has been plotted at an absorbance λ_{\max} corresponding to the π - π^* transition of the *E*-isomer. Using the first order rate constant, the half-life of the *Z*-isomer has also been deduced. For comparison, the kinetics experiments have been studied for the selected substituents using NMR spectroscopy and also computations (**Table 2A1.1 in Appendix 2A**). For minimizing the solvent effects, the kinetics experiments have been done in CD₃CN (for NMR) experiments and using acetonitrile as a solvent model (for computations). In the case of NMR studies, a CD₃CN solution of *E*-isomer in a quartz NMR tube has been irradiated at 365 nm to reach a PSS, subsequently the formation of *E*-isomer has been followed. Using the integral ratios of identical protons of both the isomers (often aromatic *ortho* protons, which are non-overlapping), the growth rate of *E*-isomer has been estimated (**Appendix 2C**).

For understanding the effects and influence of the substituents in the stability of *Z*-isomer, a quantitative relationship of the involvement of steric and electronic effects comprising resonance, field and inductive effects, respectively in the reverse isomerization kinetics is necessary. In this regard, we have considered the Taft¹² (for *ortho*-substitution) and Hammett¹³ (for *meta* and *para*-substitution) relationships. For the *ortho*-substituted derivatives, a Taft plot has been plotted between the $\log(k_R/k_{Me})$ vs the steric substituent constant (E_s), where k_R is the isomerization rate of the *ortho*-substituted phenylazopyrazole derivatives and k_{Me} is the rate corresponding to the 2-CH₃ derivative **23d** (**Figure 2.3**). The resulting plot showed a good correlation with a negative slope indicating the influence of steric factors (arising from the *ortho*-substitutions at the phenyl ring) in the thermal reverse isomerization processes. This

indicates that the transition state possesses less steric repulsion relative to the corresponding *Z*-isomer. Indeed, these results show consistency with the earlier reports on azoheteroarenes possessing *ortho* substituents, whose rates of thermal isomerization were high.⁸ Due to this reason, for the NMR and computational kinetics studies, we have considered only the electronic effects and so focused on the *meta* and *para* substituents.

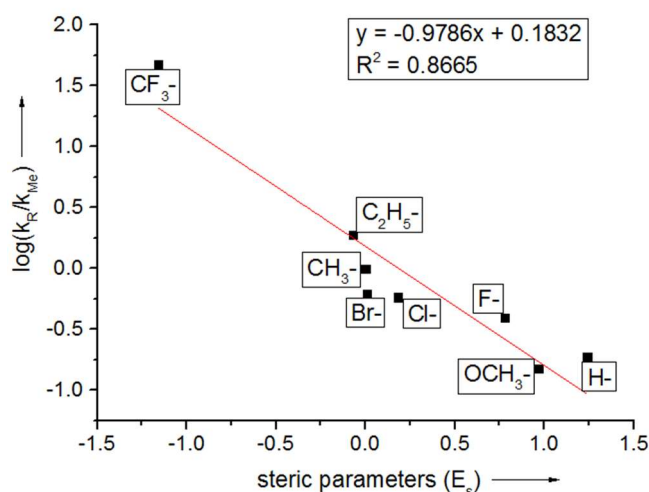


Figure 2.3. Taft plot for the steric effects in the kinetics of reverse thermal isomerization of phenylazopyrazole **1d** and their *ortho*-substituted derivatives using UV-Vis spectroscopy in CH₃CN at 25 ± 1 °C.

For *meta* and *para* substituents, we have considered the Hammett relationship by plotting $\log(k_R/k_H)$ vs substituent constants. On utilizing the kinetics rate constants derived from UV-Vis spectroscopic data, we observed a non-linear correlation, however, it showed a reasonable positive trend in both the cases (**Figure 2.4**). Based on the linear free energy relationships, it is very clear that electronic factors strongly influence the reaction rates. Either change in the mechanism (rotation vs inversion) upon changing the substituents or the combined perturbations due to solvents (solvent assisted tautomerism) and steric factors (due to the two methyl groups) along with the electronic effects could be the reason for the non-linearity.¹⁴ To understand this behaviour, Mayank Saraswat has plotted the Hammett relationship using computed rate constants (**Figure 2.5d, e**). Not only those plots showed a very good correlation with positive slopes for both *meta*- and *para*- substituted arylazopyrazoles, but also confirmed the presence of substantial electronic effects in the rate of isomerization. Apparently, accumulation of negative charges has been observed at the two azo nitrogens for both the transition states.

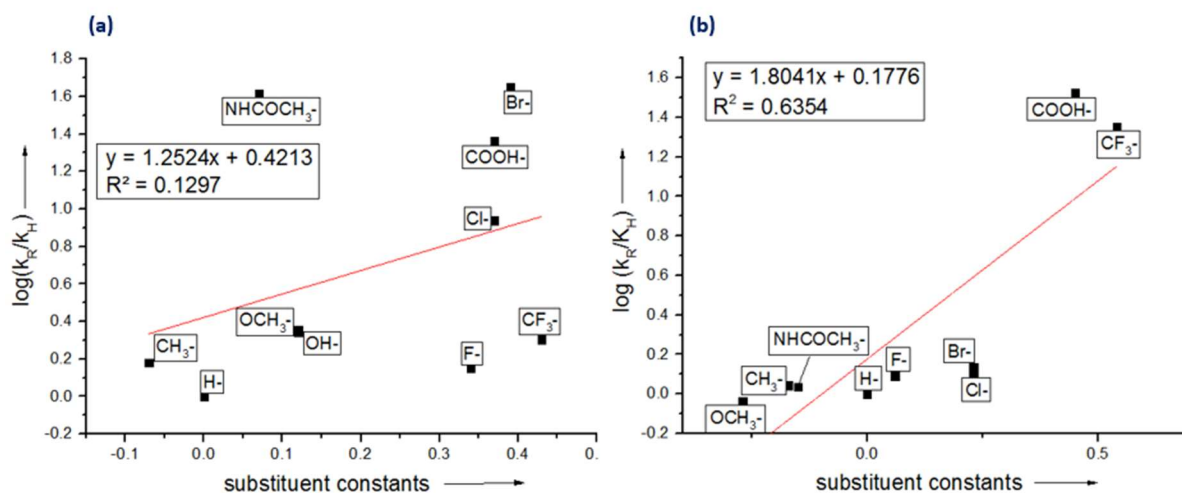


Figure 2.4. Substituent effects in the kinetics of reverse thermal isomerization of phenylazopyrazole derivatives using UV-Vis spectroscopy in CH_3CN at 25 ± 1 °C: Hammett plots for (a) *meta*-substitutions; (b) *para*-substitutions.

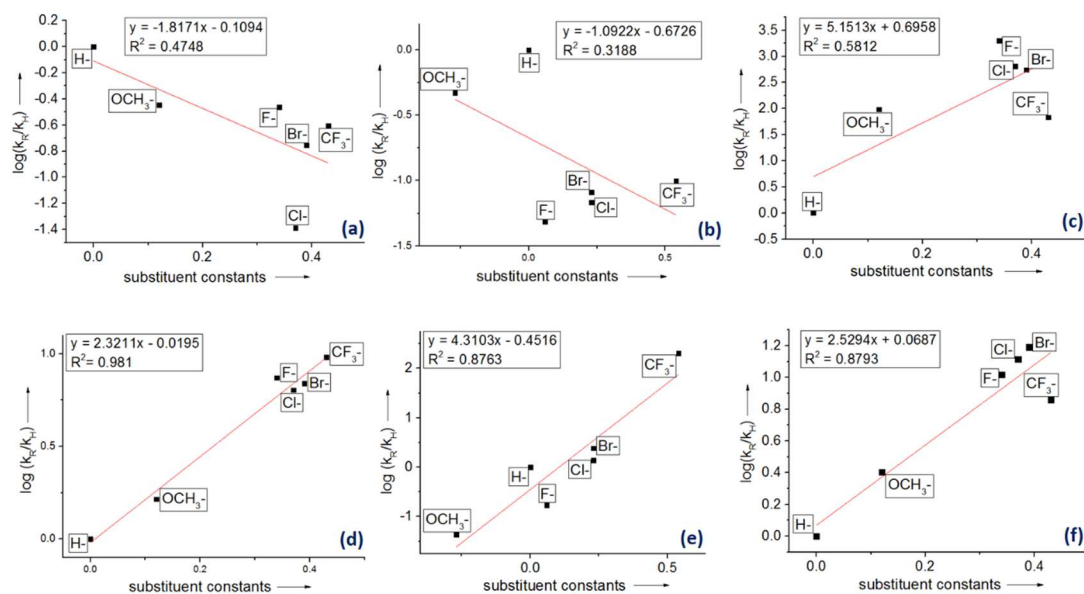


Figure 2.5. Substituent effects in kinetics of reverse thermal isomerization of phenylazopyrazole and *N*-methyl phenylazopyrazole derivatives using NMR spectroscopy in CD_3CN at 298 K: Hammett plots for (a) *meta*-substitutions; (b) *para*-substitutions; (c) *N*-methylated *meta*-substitutions; using computations at B3LYP/6-311G(d,p) level of theory: Hammett plot for (d) *meta*-substitutions; (e) *para*-substitutions; (f) *N*-methylated *meta*-substitutions.

In contrast, the Hammett relationships for *meta* and *para*-substituted phenylazopyrazoles using rate constants derived from NMR revealed a trend with a negative slope (**Figure 2.5a, b**). This trend is completely opposite to the computational

(in the gas phase) and UV-Vis (in acetonitrile) based relationships. The major difference between the rate of the reverse isomerization kinetics in NMR and UV-Vis spectroscopic experiments can be the concentration. For UV-Vis spectroscopy, the experiments have been performed at μM concentration, whereas, for NMR studies, we have utilized a concentration range of mM. The higher concentration, in principle can influence the rates in the following ways namely, supramolecular interactions through π -stacking or through hydrogen bonding. Due to the presence of two methyl groups, the π -stacking interactions can be unfavourable. However, the presence of a free N-H in phenylazopyrazole derivatives can potentially form hydrogen bonding at various sites that include azo nitrogens, pyrazole nitrogen and the hydrogen bond acceptor substituents, if any. Also, due to the steric reasons only the azo nitrogens of *Z*-isomer can accept intermolecular hydrogen bonding. This assumption is particularly fitting very well with the change in the slope for Hammett plots, upon increasing the concentration. Under such circumstances, the charge at the inverting azo nitrogen center is expected to gain more positive values or less negative charge, which is in perfect corroboration with the computed charges at azo nitrogen centers. The hydrogen bonding at one of the azo nitrogen's led to lowering of negative charges at the adjacent nitrogen atom, which undergoes inversion. Apart from the substantial electronic effects, the hydrogen bonding is expected to play a crucial role in the reverse switching of phenylazopyrazole derivatives.

In order to downplay the hydrogen bonding, six *meta*-substituted *N*-methyl phenylazopyrazole derivatives (**1e**, **3e**, **6e**, **9e**, **15e** and **18e**) have been chosen and Hammett relationship has been studied. Since the unsubstituted *N*-methyl derivative **1e**, has been extensively studied by Fuchter and coworkers, the rate constant for its thermal isomerization has been taken from their studies.^{6,8} For the rest of the derivatives, the *Z*-*E* isomerization kinetics have been performed in CD_3CN at 298 K and the Hammett relationship has been plotted (**Figure 2.5c**). The results for *N*-methylated derivatives revealed that the plot once again reverted back to a positive slope, which is similar to their corresponding computational plot in figure 2.5f. This clearly demonstrates the role of pyrazole NH in hydrogen bonding.

2.5 Concentration dependency and solvent effects in *Z*-isomer stability

During our investigations on photoswitching and reverse isomerization behaviour of substituted phenylazopyrazoles, we realized the importance of the effects of concentration. Apart from the reverse isomerization rate, photoswitching efficiency also strongly depend on the concentration. In this regard, we did the concentration-dependent kinetics for the compound **1d**. The results suggested that the half-life of the (*Z*)-**1d** decreases by three times (21.6 min to 8.2 min) when the concentration increases by approximately 14 times (0.004 M to 0.055 M). The results clearly confirm that at the higher concentration, the *Z*-*E* isomerization rate constant increases and the half-life of *Z*-isomer decreases. Besides, we observed a marginal downfield shift in the N-H proton of **1d**, whereas other protons showed no significant shifts upon increasing the concentration. On the other hand, the rest of signals did not show any appreciable shifts. These observations clearly confirm the possibility of hydrogen bonding involving pyrazole N-H. To understand the mode of hydrogen bonding in concentration dependency, we estimated the association constant of the hydrogen bonding dimer of the (*E*)-**1d**. Using NMR spectroscopy in CD₃CN at 298 K, the spectral shifts of the pyrazole NH protons accompanying the concentration changes (relative to the residual protons of the solvent) have been considered. Using the open access web-based bindfit program, a non-linear fitting process has been executed in this regard.¹⁵



The resulting binding constant for the 1:1 (*E*)-**1d** dimer was found to be $1.47 \times 10^{-3} \pm 1.69 \times 10^{-4} \text{ L mol}^{-1}$. (See the details in **Figure 2.6** and **2.7**).

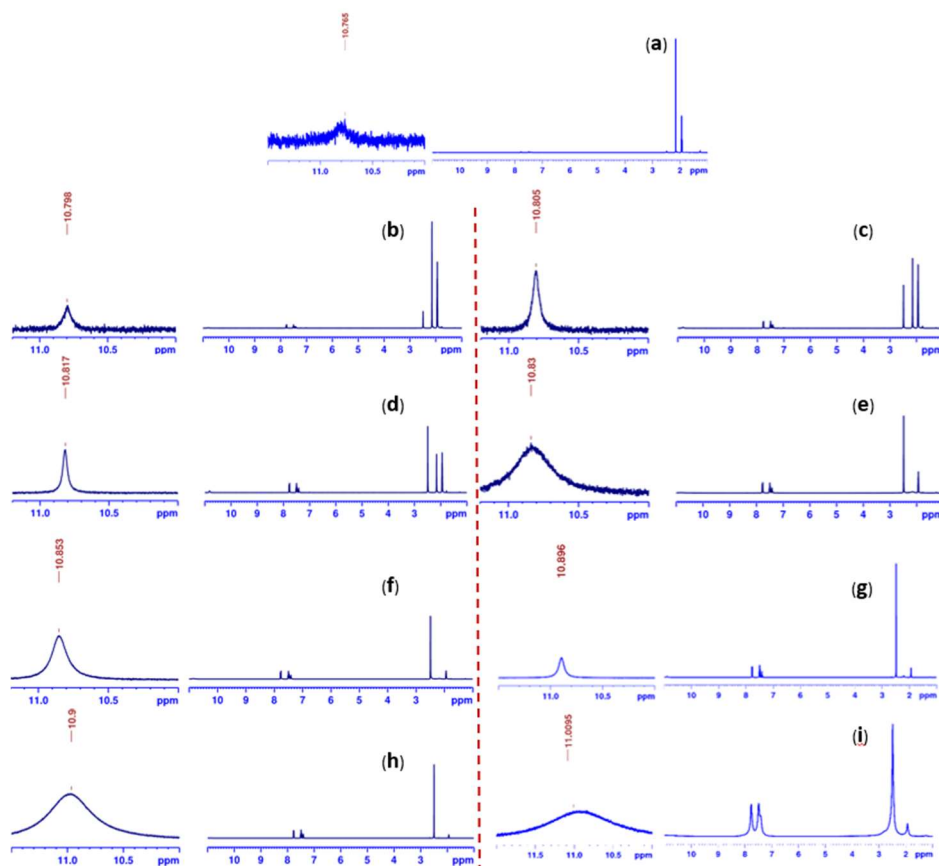


Figure 2.6. Effect of concentration in chemical shift of *N*-H of **1d** in acetonitrile (a) 0.00150 (b) 0.003121 M (c) 0.006243 M (d) 0.012480 M (e) 0.024970 M (f) 0.049940 M (g) 0.099880 M (h) 0.199750 M (i) 0.329600 M.

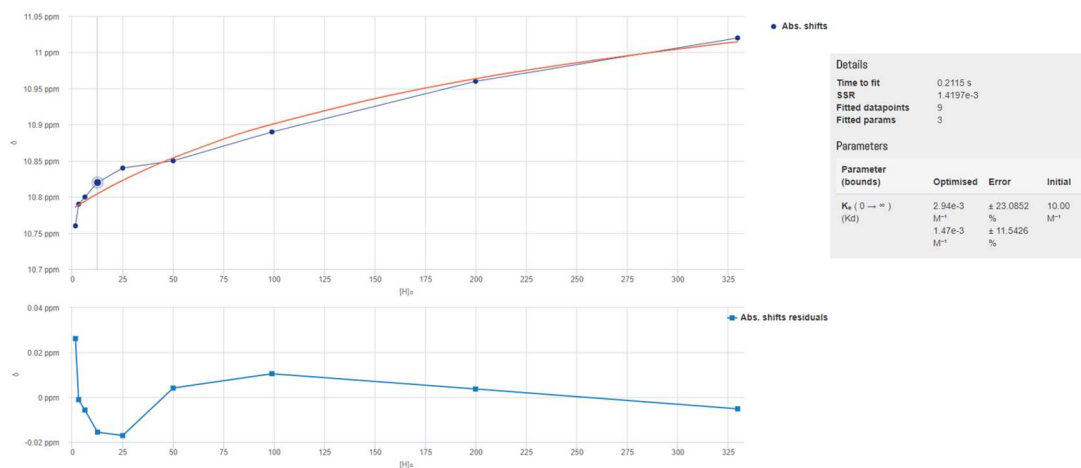


Figure 2.7. Screenshot of the results from the estimation of the association constant of (*Z*)-**1d** dimer using bindfit program available as open access in the website supramolecular.org (Method: Nelder-Mead/NMR dimer aggregation) The data can be archived from the unique URL: <http://app.supramolecular.org/bindfit/view/29d630ea-1bfd-40cc-a5dc-1375f5308416>

In order to differentiate the solute-solute and solute-solvent interactions, the phenylazopyrazole **1d** has been subjected to NMR kinetics in DMSO-*d*₆, which is known for the breaking of intermolecular hydrogen bonding (**Figure 2.2**). As a result, the half-life of the *Z*-isomer has increased and the rate of reverse isomerization has been decreased.

To emulate such hydrogen bonding possibilities and also to understand the effects of it in the thermal reverse isomerization, computations are highly desired. In this regard, we explored the barriers for the thermal isomerization step using simple pyrazole as a model compound, with and without hydrogen bonding. From those calculations, we inferred that the thermal isomerization barriers indeed showed a lowering of Gibbs free energy of activation upon hydrogen bonding. Although the changes in the barrier energies are found to be very small, it indeed significantly influenced the rate constants and half-lives. A similar trend has also been observed when actual dimeric phenylazopyrazole dimers are invoked in the computations.

In the same context, we have also studied the effects of solvents in the thermal reverse *Z-E* isomerization rate by varying the polarity of the solvents at the identical concentration. The results are tabulated (**Table 2.4**). Based on the results, the polar protic solvents such as ethanol and methanol showed a maximum influence such that **1d** underwent fast thermal *Z-E* isomerization. Indeed in methanol the rate could not be determined. On the other hand, rate constants are estimated to be smaller in the case of non-polar solvents such as toluene, whereas the polar aprotic solvents still influence the rate from moderate to high.

To relate the effects of solvents in the reverse isomerization,¹⁶ various properties of the solvents such as Kamlet-Taft parameters for hydrogen bonding ability (α) and hydrogen donating ability (β) and the solvatochromism scales π^* ¹⁷⁻¹⁹ and E_T ^{N20} have been considered. Previous studies on a limited number of azobenzenes revealed that the solvent polarity rather than the viscosity of the solvents is vital for the thermal isomerization kinetics.^{16b,c} The correlation between the individual parameters with the rate constants, (plots of $\ln k$ vs solvent parameters) have been clearly showed a remarkable influence of hydrogen bonding effects (**Figure 2.8**). Particularly the solvents with a higher proton donating abilities strongly influence the reverse isomerization rates. The exceptions in the case of DMSO and THF can be rationalized on the basis of their hydrogen bond breaking abilities. All these observations show

consistency with the results related to the arylazoimidazoles²¹ and phenylazoindoles⁹, where the involvement of protic molecules has been proposed for fast isomerization through tautomerization mechanism.

Table 2.4. Solvent effects in the UV-Vis spectroscopic thermal reverse isomerization (*Z-E*) rates of phenylazopyrazole **1d** and *N*-methyl phenylazopyrazole **1e**.

S. No.	Solvent ^a	Solvent Parameters ^b				k^a (min ⁻¹)	k^c (min ⁻¹)
		α	β	π^*	E_T^N		
1.	Acetonitrile	0.19	0.40	0.66	0.460	$7.27 \times 10^{-3} \pm 2.50 \times 10^{-5}$	-
2.	Chloroform	0.20	0.10	0.69	0.259	$2.67 \times 10^{-3} \pm 1.26 \times 10^{-5}$	-
3.	Dichloromethane	0.13	0.10	0.73	0.309	$2.20 \times 10^{-3} \pm 1.18 \times 10^{-5}$	-
4.	DMF	0.00	0.69	0.88	0.386	$6.72 \times 10^{-2} \pm 1.20 \times 10^{-3}$	$4.29 \times 10^{-3} \pm 6.83 \times 10^{-5}$
5.	Ethyl acetate	0.00	0.45	0.45	0.228	$1.00 \times 10^{-2} \pm 1.35 \times 10^{-5}$	-
6.	Ethanol	0.86	0.75	0.54	0.654	$8.37 \times 10^{-2} \pm 2.55 \times 10^{-5}$	$2.32 \times 10^{-3} \pm 1.77 \times 10^{-4}$
7.	Methanol	0.98	0.66	0.60	0.762	-	-
8.	Toluene	0.00	0.11	0.49	0.099	$3.00 \times 10^{-3} \pm 1.31 \times 10^{-5}$	$5.42 \times 10^{-3} \pm 1.16 \times 10^{-4}$
9.	THF	0.00	0.55	0.55	0.207	$1.20 \times 10^{-3} \pm 1.84 \times 10^{-5}$	-
10.	DMSO	0.00	0.76	1.00	0.444	$9.73 \times 10^{-3} \pm 4.21 \times 10^{-4}$	$4.12 \times 10^{-3} \pm 1.10 \times 10^{-4}$

^aAll the solutions of **1d** have been studied in different solvents at an identical concentration (29 μ M) and the rates have been measured at 25 ± 1 °C; ^bSolvent parameters are the Kamlet–Taft parameters for hydrogen bonding ability (α) and hydrogen donating ability (β) and the solvatochromism scales π^* and E_T^N ; ^cAll the solutions of **1e** have been studied in different solvents at an identical concentration (34 μ M) and the rates have been measured at 60 ± 1 °C.

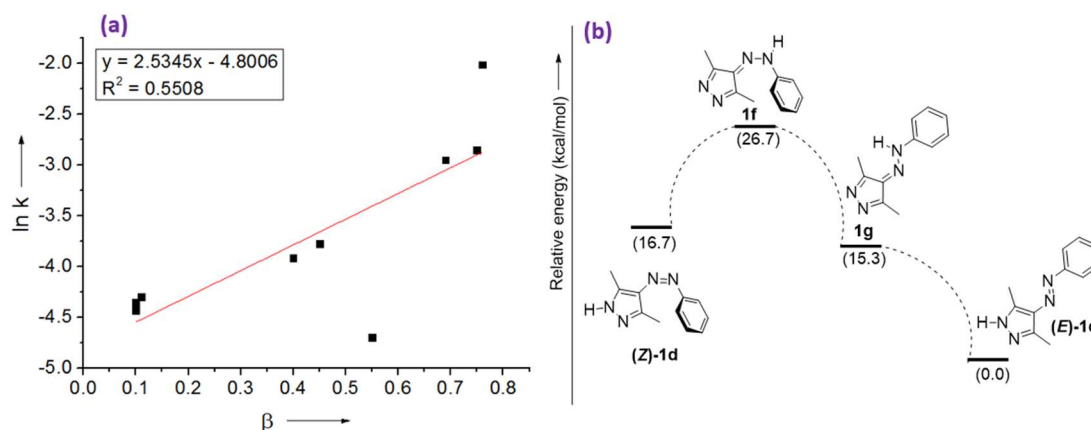


Figure 2.8. Solvent effects in the thermal *Z-E* isomerization rate of **1d**. (a) Graphical plots showing the relation between $\ln k$ and the Kamlet–Taft parameters for hydrogen donating ability, β ; (b) Possible mechanism for the solvent assisted thermal *Z-E* isomerization through tautomerization (Relative energies in kcal/mol are computed at B3LYP/6-311G(d,p) level of theory).

In a similar way, solvent effects have been studied for the *N*-methylated derivative **1e**. Due to the very slow rate of *Z-E* isomerization, the studies have been performed at 60 °C (**Figure Appendix D**). Hence, the experiments have been performed only in low volatile solvents such as DMSO, DMF, toluene and ethanol. Remarkably, the isomerization rates in all these solvents have been estimated to be in the same order (**Table 2.4**). All these data clearly demonstrate that the hydrogen bonding and proton donation are the most influential factors for the faster *Z-E* isomerization kinetics. Particularly when the azo groups are forming hydrogen bonding, the rates are very high, whereas, the non-covalent interactions involving the solvents and the pyrazole-NH decrease the thermal isomerization rates.

Based on all these studies, we obtained the following general trends: (1) Hydrogen bonding either increases the rate of reverse isomerization and/or inhibits the photoswitching efficiency; (2) Any solvent that can protonate azo nitrogen or forming hydrogen bonding with them increases the rate of the thermal reverse isomerization through tautomerization mechanism; (3) At higher concentration, the hydrogen bonding interactions competitively play important roles in deciding the photoswitching behaviour. For designing new photoswitches, the intermolecular hydrogen bonding possibilities may also need to be taken care, in particular, for controlling the *Z*-isomer stability.

2.6 Conclusions

In summary, we have synthesized 38 substituted phenylazopyrazole derivatives and six *N*-methylated phenylazopyrazole derivatives using a two/three-step synthetic method with good to excellent yields. The UV-Vis spectroscopic investigations on those molecules revealed the importance of steric factor in attaining highly strained *Z*-isomer geometries that favour a faster reverse switching. Taft plot clearly proved the release of a steric factor during reverse isomerization in *ortho* substituted phenylazopyrazoles. In contrast, the *meta* and *para* substituted azopyrazoles undergo reverse isomerization with electronic influence, however, Hammett plot exhibited a deviation from linear correlation. Substantial influences of electronic effects have been further confirmed by Hammett plots using computed rate constants for the selected *meta* and *para*-substituted derivatives. The NMR spectroscopic studies also revealed the influence of electronic effects in thermal reverse isomerization, however, the slopes are completely opposite to that of UV-Vis spectroscopic and computational studies. The similar studies on the *N*-methylated derivatives with *meta* substitution reverted back to the positive slope in the Hammett plot. Concentration dependency in the half-life of the *Z*-isomer, NMR shifts in the pyrazole NH, solvent effects and also the computations clearly demonstrate the decisive role of hydrogen bonding. The solvent or any proton donor can influence the isomerization rate through assisting in the protonation leading to tautomerization. Thus, the non-linear behaviour in the substituent effects of isomerization rate and *Z*-isomer stability can be due to a combined effect of steric, electronic effects and the hydrogen bonding. At higher concentrations, hydrogen bonding dominates and at lower concentrations, apart from the electronic and steric factors, solvent assisted tautomerization also prevail in deciding the rate of thermal reverse isomerization, in turn, the stability of *Z*-isomers.

2.7 Experimental section

General procedure for the synthesis of arylazoacetylacetone derivatives (1-38c):

A mixture of aniline or substituted anilines (20.0 mmol) and deionized water in a two neck round bottom flask was cooled to 0 °C. To this 37% conc. HCl (6.5 mL) was added and stirred to get a clear solution. Then a cold aqueous solution of sodium nitrite (1.52 g, 22.0 mmol in 20 mL of water) was added dropwise into the reaction

mixture slowly. After the addition, the diazonium salt started forming. The reaction mixture was allowed to stir for half an hour for completion. Afterwards, at 0 °C a cold aqueous solution of sodium acetate (5.90 g, 70.0 mmol) and acetylacetone (2.00 g, 20.0 mmol in 100 mL of water and 10 ml of ethanol) was added. The reaction was continued at room temperature and was monitored by TLC. After completion of the reaction, the reaction mixture was filtered off to obtain a yellow-orange solid product, which was dried under vacuum to yield the desired product.

General procedure for the synthesis of arylazopyrazole derivatives (1-38d):

A mixture of arylazoacetylacetone derivative (1.0 mmol), hydrazine dihydrochloride (2.0 mmol) and Na₂CO₃ (4.0 mmol) in 10 mL absolute ethanol was refluxed. The reaction was followed using TLC upto the completion of the reaction. After completion of the reaction, the product was purified by column chromatography. (Eluent: 1:1 ethylacetate/n-hexane)

Arylazoacetylacetone Derivatives

3-(2-Phenylhydrazono)pentane-2,4-dione (1c):

Yellow solid, mp = 81-83 °C, 198.1 mg, 97% yield. ¹H NMR (400 MHz, CDCl₃) δ 2.52 (s, 3H), 2.63 (s, 3H), 7.22–7.25 (m, 1H), 7.43–7.44 (d, *J* = 4.3 Hz, 4H), 14.76 (s, 1H); ¹³C NMR (100 MHz, CDCl₃) δ 26.65, 31.69, 116.26, 125.91, 129.66, 133.21, 141.52, 197.13, 197.95; HRMS (ESI-TOF): calcd. for C₁₁H₁₂N₂O₂[M-H]⁺: 203.0821, experimental found: 203.0810.

3-(2-(2-Fluorophenyl)hydrazono)pentane-2,4-dione (2c):

Yellow solid, mp = 117-120 °C, 219.9 mg, 99% yield. ¹H NMR (400 MHz, CDCl₃) δ 2.52 (s, 3H), 2.64 (s, 3H), 7.16–7.17 (td, *J* = 7.8, 5.5, 4.5 Hz, 2H), 7.18–7.19 (m, 1H), 7.16–7.17 (t, *J* = 8.4 Hz, 2H), 14.75 (s, 1H); ¹³C NMR (100 MHz, CDCl₃) δ 26.65, 31.72, 115.97 (*J* = 18 Hz), 166.42, 125.15, (*J* = 3.63 Hz), 125.89 (*J* = 7.24 Hz), 130.08, (*J* = 9 Hz), 134.35, 152.05 (*J* = 246 Hz), 197.09, 197.95; HRMS (ESI-TOF): calcd. for C₁₁H₁₁FN₂O₂[M-H]⁺: 221.0726, found: 221.0716.

3-(2-(3-Fluorophenyl)hydrazono)pentane-2,4-dione (3c):

Yellow solid, mp = 115-118 °C, 215.6 mg, 97% yield. ¹H NMR (400 MHz, CDCl₃) δ 2.51 (s, 3H), 2.62 (s, 3H), 6.88–6.92 (td, *J* = 8.3, 2.1 Hz 1H), 7.10–7.12 (dd, *J* = 8.1,

1.3 Hz, 1H), 7.20–7.23 (dt, $J = 7.9, 2.1$ Hz, 1H), 7.34–7.40 (ddd, $J = 8.1, 6.1$ Hz, 1H), 14.63 (s, 1H); ^{13}C NMR (100 MHz, CDCl_3) δ 26.65, 31.76, 103.27 ($J = 20.3$ Hz), 112.09 ($J = 2.89$ Hz), 112.49 ($J = 21.56$ Hz), 130.98 ($J = 9.25$ Hz), 133.55, 143.23, 163.97 ($J = 245.29$ Hz), 196.99, 198.24; HRMS (ESI-TOF): calcd. for $\text{C}_{11}\text{H}_{11}\text{FN}_2\text{O}_2[\text{M-H}]^+$: 221.0726, found: 221.0713.

3-(2-(4-Fluorophenyl)hydrazono)pentane-2,4-dione (**4c**):

Yellow solid, mp = 127–129 °C, 220.0 mg, 99% yield. ^1H NMR (400 MHz, CDCl_3) δ 2.50 (s, 3H), 2.62 (s, 3H), 7.11–7.16 (m, 2H), 7.39–7.43 (m, 2H), 14.83 (s, 1H); ^{13}C NMR (100 MHz, CDCl_3) δ 26.64, 31.68, 116.48, 116.71, 117.66 ($J = 8.14$ Hz),, , 133.20, 137.81 ($J = 2.77$ Hz), 160.60 ($J = 244.36$ Hz), 196.98, 198.04; ^{13}C NMR (100 MHz, CDCl_3): δ 26.64, 31.68, 116.48, 116.71, 117.62, 117.70, 133.20, 137.80, 159.38, 161.83, 196.98, 198.04; HRMS (ESI-TOF): calcd. for $\text{C}_{11}\text{H}_{11}\text{FN}_2\text{O}_2[\text{M-H}]^+$: 221.0726, found: 221.0715.

3-(2-(2-Chlorophenyl)hydrazono)pentane-2,4-dione (**5c**):

Yellow solid, mp = 137–139 °C, 233.9 mg, 98% yield. ^1H NMR (400 MHz, CDCl_3) δ 2.52 (s, 3H), 2.64 (s, 3H), 7.12–7.16 (td, $J = 1.5, 8.0$ Hz, 1H), 7.34–7.38 (t, $J = 8.2$ Hz 1H), 7.40–7.43 (d, $J = 1.3, 8.0$ Hz 1H), 7.80–7.83 (d, $J = 1.5, 8.2$ Hz 1H), 14.89 (s, 1H); ^{13}C NMR (100 MHz, CDCl_3) δ 26.69, 31.73, 116.27, 122.06, 125.91, 127.68, 128.10, 129.86, 130.09, 134.34, 138.35, 196.99, 198.05; HRMS (ESI-TOF): calcd. for $\text{C}_{11}\text{H}_{11}\text{ClN}_2\text{O}_2[\text{M-H}]^+$: 237.0431, found: 237.0427.

3-(2-(3-Chlorophenyl)hydrazono)pentane-2,4-dione (**6c**):

Yellow solid, mp = 135–138 °C, 233.9 mg, 98% yield. ^1H NMR (400 MHz, CDCl_3) δ 2.52 (s, 3H), 2.63 (s, 3H), 7.17–7.19 (dq, $J = 7.9, 0.9$ Hz 1H), 7.23–7.26 (dq, $J = 8.1$ Hz 1H), 7.32–7.36 (t, $J = 8.0$ Hz 1H), 7.46–7.47 (t, $J = 2.0$ Hz 1H), 14.62 (s, 1H); ^{13}C NMR (100 MHz, CDCl_3) δ 26.69, 31.76, 114.49, 116.11, 125.65, 130.68, 133.67, 135.67, 142.73, 197.03, 198.27; HRMS (ESI-TOF): calcd. for $\text{C}_{11}\text{H}_{11}\text{ClN}_2\text{O}_2[\text{M-H}]^+$: 237.0431, found: 237.0421.

3-(2-(4-Chlorophenyl)hydrazono)pentane-2,4-dione (7c):

Yellow solid, mp = 112-115 °C, 226.7 mg, 95% yield. ¹H NMR (400 MHz, CDCl₃) δ 2.49(s, 3H), 2.61 (s, 3H), 7.34– 7.39, (m, 4H), 14.62 (s, 1H); ¹³C NMR (100 MHz, CDCl₃) δ 26.64, 31.73, 117.33, 129.37, 129.76, 130.98, 133.42, 140.15, 196.94, 198.16; HRMS (ESI-TOF): calcd. for C₁₁H₁₁ClN₂O₂[M-H]⁺: 237.0431, found: 237.0418.

4-(2-(2-Bromophenyl)hydrazono)pentane-2,4-dione (8c):

Yellow solid, mp = 121-123 °C, 271.8 mg, 96% yield. ¹H NMR (400 MHz, CDCl₃) δ 2.53 (s, 3H), 2.65 (s, 3H), 7.06–7.09 (t, *J* = 8.0 Hz, 1H), 7.39– 7.43, (t, *J* = 7.7 Hz, 1H), 7.58–7.60 (d, *J* = 8.0 Hz, 1H), 7.79–7.82 (d, *J* = 8.2 Hz, 1H), 14.89 (s, 1H); ¹³C NMR (100 MHz, CDCl₃) δ 26.70, 31.72, 111.16, 116.64, 126.33, 128.71, 133.04, 134.27, 139.57, 197.09, 197.71; HRMS (ESI-TOF): calcd. for C₁₁H₁₁BrN₂O₂[M-H]⁺: 283.0082, 285.0062, found: 283.0118, 285.0096.

3-(2-(3-Bromophenyl)hydrazono)pentane-2,4-dione (9c):

Yellow solid, mp = 129-131 °C, 268.9 mg, 95% yield. ¹H NMR (400 MHz, CDCl₃) δ 2.50 (s, 3H), 2.61 (s, 3H), 7.26–7.33 (m, 4H), 7.58–7.59 (t, *J* = 1.8 Hz, 1H), 14.60 (s, 1H); ¹³C NMR (100 MHz, CDCl₃) δ 26.71, 31.78, 114.92, 119.01, 123.55, 128.55, 130.92, 133.67, 142.80, 196.99, 198.24; HRMS (ESI-TOF): calcd. for C₁₁H₁₁BrN₂O₂[M-H]⁺: 280.9926, 282.9905, found: 280.9913, 282.9884.

3-(2-(4-Bromophenyl)hydrazono)pentane-2,4-dione (10c):

Yellow solid, mp = 136-139 °C, 206.7 mg, 73% yield. ¹H NMR (400 MHz, CDCl₃) δ 2.51(s, 3H), 2.63 (s, 3H), 7.30–7.32 (d, *J* = 8.9 Hz, 2H), 7.53– 7.55, (d, *J* = 8.8 Hz, 2H), 14.70 (s, 1H); ¹³C NMR (100 MHz, CDCl₃) δ 26.67, 31.76, 117.67, 118.66, 132.70, 133.48, 140.15, 196.98, 198.23; HRMS (ESI-TOF): calcd. for C₁₁H₁₁BrN₂O₂[M-H]⁺: 280.9926, 282.9905, found: 280.9913, 282.9891.

3-(2-(2-Hydroxyphenyl)hydrazono)pentane-2,4-dione (11c):

Yellow solid, mp = 167-169 °C, 215.8 mg, 98% yield. ¹H NMR (400 MHz, DMSO-*d*₆) δ 2.42 (s, 3H), 2.49 (s, 3H), 6.92–6.97 (m, 2H), 7.04–7.09 (m, 1H), 7.65–7.67 (dd, *J* = 8.0, 1.5 Hz, 1H), 10.54 (s, 1H), 14.60 (s, 1H); ¹³C NMR (100 MHz, DMSO-*d*₆) δ 29.94,

31.68, 115.36, 116.22, 120.67, 126.64, 129.73, 133.63, 146.81, 196.66, 196.83; HRMS (ESI-TOF): calcd. for $C_{11}H_{12}N_2O_3[M-H]^+$: 219.0770, found: 219.0758.

3-(2-(3-Hydroxyphenyl)hydrazono)pentane-2,4-dione (**12c**):

Yellow solid, mp = 187-189 °C, 132.1 mg, 60% yield. 1H NMR (400 MHz, CD_3OD) δ 2.48 (s, 3H), 2.54 (s, 3H), 6.65–6.67 (d, J = 8.1, 1.8 Hz, 1H), 6.89-6.91 (d, J = 7.9 Hz, 1H), 7.01 (t, J = 2.0 Hz, 1H), 7.21-7.25(t, J = 8.1 Hz, 1H); ^{13}C NMR (100 MHz, CD_3OD) δ 25.16, 30.21, 102.35, 107.42, 112.81, 126.90, 130.17, 142.81, 158.68, 197.15, 197.60; HRMS (ESI-TOF): calcd. for $C_{11}H_{12}N_2O_3[M-H]^+$: 219.0770, found: 219.0761.

3-(2-(4-Hydroxyphenyl)hydrazono)pentane-2,4-dione (**13c**):

Yellow solid, mp = 174-176 °C, 207.0 mg, 94% yield. 1H NMR (400 MHz, $DMSO-d_6$) δ 2.37 (s, 3H), 2.46 (s, 3H), 6.83–6.85 (d, J = 8.8 Hz, 2H), 7.42–7.44 (d, J = 8.8 Hz, 2H), 9.67 (s, 1H, OH), 14.51 (s, 1H); ^{13}C NMR (100 MHz, $DMSO-d_6$) δ 29.89, 31.56, 116.53, 116.60, 118.50, 132.51, 134.14, 156.35, 196.38; HRMS (ESI-TOF): calcd. for $C_{11}H_{12}N_2O_3[M-H]^+$: 219.0770, found: 219.0758.

3-(2-(2-(Trifluoromethyl)phenyl)hydrazono)pentane-2,4-dione (**14c**):

Yellow solid, mp = 107-109 °C, 264.1 mg, 97% yield. 1H NMR (400 MHz, $CDCl_3$) δ 2.53 (s, 3H), 2.64 (s, 3H), 7.26–7.30 (tt, J = 8.6, 0.9 Hz, 1H), 7.62–7.66 (m, 2H), 7.97–7.99 (d, J = 7.9 Hz, 1H), 15.09 (s, 1H); ^{13}C NMR (100 MHz, $CDCl_3$) δ 26.68, 31.62, 116.73, 117.80, 122.39, 124.76, 125.10, 126.43, 126.53, 126.58, 133.39, 134.76, 139.39, 197.01, 198.05; HRMS (ESI-TOF) calcd. for $C_{11}H_{11}F_3N_2O_2[M-H]^+$: 271.0694, found: 271.0681.

3-(2-(3-(Trifluoromethyl)phenyl)hydrazono)pentane-2,4-dione (**15c**):

Yellow solid, mp = 110-113 °C, 247.7 mg, 91% yield. 1H NMR (400 MHz, $CDCl_3$) δ 2.53 (s, 3H), 2.64 (s, 3H), 7.45–7.47 (d, J = 7.2 Hz, 1H), 7.55–7.58 (m, 2H), 7.68 (s, 1H), 14.70 (s, 1H); ^{13}C NMR (100 MHz, $CDCl_3$) δ 26.67, 31.78, 112.82, 112.86, 119.19, 121.03, 122.01, 122.05, 122.26, 124.97, 129.93, 130.29, 132.10, 132.43, 133.87, 142.11, 196.97, 198.42; HRMS (ESI-TOF) calcd. for $C_{11}H_{11}F_3N_2O_2[M-H]^+$: 271.0694, found: 271.0693.

3-(2-(4-(Trifluoromethyl)phenyl)hydrazono)pentane-2,4-dione (16c):

Yellow solid, mp = 105-108 °C, 247.7 mg, 91% yield. ¹H NMR (400 MHz, CDCl₃) δ 2.53 (s, 3H), 2.64 (s, 3H), 7.49–7.59 (d, *J* = 8.3 Hz, 2H), 7.67–7.69 (d, *J* = 8.0 Hz, 2H), 14.61 (s, 1H); ¹³C NMR (100 MHz, CDCl₃) δ 26.60, 31.81, 115.99, 118.01, 126.61, 126.95, 126.98, 127.12, 134.11, 114.28, 196.97, 198.45; HRMS (ESI-TOF) calcd. for C₁₁H₁₁F₃N₂O₂[M-H]⁺: 271.0694, found: 271.0689.

3-(2-(2-Methoxyphenyl)hydrazono)pentane-2,4-dione (17c):

Yellow solid, mp = 112-115 °C, 192.1 mg, 82% yield. ¹H NMR (400 MHz, CDCl₃) δ 2.51 (s, 3H), 2.63 (s, 3H), 3.98 (s, 3H), 6.96–6.98 (d, *J* = 8.2, Hz, 1H), 7.03–7.07 (t, *J* = 7.9 Hz, 1H), 7.16–7.20 (td, *J* = 7.6, 1.6 Hz, 1H), 7.74–7.76 (d, *J* = 8.0 Hz, 1H), 14.82 (s, 1H); ¹³C NMR (100 MHz, CDCl₃) δ 26.71, 31.67, 55.92, 111.09, 115.18, 121.47, 126.09, 130.79, 133.66, 148.57, 197.26, 197.32; HRMS (ESI-TOF) calcd. for C₁₁H₁₄N₂O₃[M-H]⁺: 233.0926, found: 233.0913.

3-(2-(3-Methoxyphenyl)hydrazono)pentane-2,4-dione (18c):

Yellow solid, mp = 123-126 °C, 203.8 mg, 87% yield. ¹H NMR (400 MHz, CDCl₃) δ 2.47 (s, 3H), 2.59 (s, 3H), 3.83 (s, 3H), 6.72–6.75 (dd, *J* = 8.3, 2.4 Hz, 1H), 6.92–6.95 (dd, *J* = 8.0, 1.8 Hz, 1H), 6.97–6.98 (t, *J* = 2.2 Hz, 1H), 7.26–7.31 (t, *J* = 8.0 Hz, 1H), 14.65 (s, 1H); ¹³C NMR (100 MHz, CDCl₃) δ 26.61, 31.69, 55.36, 101.76, 108.89, 111.38, 130.47, 133.09, 142.74, 160.76, 197.01, 197.88; HRMS (ESI-TOF) calcd. for C₁₁H₁₄N₂O₃[M-H]⁺: 233.0926, found: 233.0915.

3-(2-(4-Methoxyphenyl)hydrazono)pentane-2,4-dione (19c):

Yellow solid, mp = 118-120 °C, 222.5 mg, 95% yield. ¹H NMR (400 MHz, CDCl₃) δ 2.50 (s, 3H), 2.62 (s, 3H),), 3.86 (s, 3H), 6.96–6.98 (d, *J* = 9.0, Hz, 2H), 7.39–7.40 (d, *J* = 9.0 Hz, 2H), 15.00 (s, 1H); ¹³C NMR (100 MHz, CDCl₃) δ 26.65, 31.60, 55.62, 114.94, 117.69, 132.68, 135.09, 158.07, 197.16, 197.65; HRMS (ESI-TOF) calcd. for C₁₁H₁₄N₂O₃[M-H]⁺: 233.0926, found: 233.0913.

3-(2-(2-Nitrophenyl)hydrazono)pentane-2,4-dione (20c):

Yellow-orange solid, mp = 177-179 °C, 189.4 mg, 76% yield. ¹H NMR (400 MHz, CDCl₃) δ 2.57 (s, 3H), 2.67 (s, 3H), 7.26–7.30 (td, *J* = 7.2, 1.3 Hz, 1H), 7.72–7.76 (t, *J* = 8.4 Hz, 1H), 8.14–8.17 (dd, *J* = 8.5, 1.1 Hz, 1H), 8.29–8.31 (dd, *J* = 8.5, 1.4 Hz, 1H), 15.51 (s, 1H); ¹³C NMR (100 MHz, CDCl₃) δ 26.80, 31.78, 117.24, 124.04, 126.16, 135.85, 136.22, 138.40, 197.10, 197.19; HRMS (ESI-TOF) calcd. for C₁₁H₁₁N₃O₄[M-H]⁺: 248.0671, found: 248.0662.

3-(2-(3-Nitrophenyl)hydrazono)pentane-2,4-dione (21c):

Yellow-orange solid, mp = 182-184 °C, 171.9 mg, 69% yield. ¹H NMR (400 MHz, CDCl₃) δ 2.55 (s, 3H), 2.65 (s, 3H), 7.58–7.63 (t, *J* = 8.1 Hz, 1H), 7.69–7.72 (dq *J* = 8.1, 1.0 Hz, 1H), 8.03–8.06 (dq, *J* = 8.1, 1.0, Hz, 1H), 8.27–8.28 (t, *J* = 2.1 Hz, 1H), 14.66 (s, 1H); ¹³C NMR (100 MHz, CDCl₃) δ 26.68, 31.79, 110.78, 119.75, 121.53, 130.58, 134.34, 142.87, 149.35, 196.83, 198.63; HRMS (ESI-TOF) calcd. for C₁₁H₁₁N₃O₄[M-H]⁺: 248.0671, found: 248.0660.

3-(2-(4-Nitrophenyl)hydrazono)pentane-2,4-dione (22c):

Orange-red solid, mp = 173-176 °C, 204.4 mg, 82% yield. ¹H NMR (400 MHz, CDCl₃) δ 2.55 (s, 3H), 2.66 (s, 3H), 7.51–7.53 (d, *J* = 9.1 Hz, 2H), 8.34–8.32 (d, *J* = 9.1 Hz, 2H), 14.56 (s, 1H); ¹³C NMR (100 MHz, CDCl₃) δ 26.71, 31.91, 115.83, 125.82, 134.98, 146.60, 148.54, 196.87, 198.78; HRMS (ESI-TOF) calcd. for C₁₁H₁₁N₃O₄[M-H]⁺: 248.0671, found: 248.0659.

3-(2-(*o*-Tolyl)hydrazono)pentane-2,4-dione (23c):

Yellow solid, mp = 139-141 °C, 213.9 mg, 98% yield. ¹H NMR (400 MHz, CDCl₃) δ 2.41 (s, 3H), 2.53 (s, 3H), 2.65 (s, 3H), 7.12–7.16 (t, *J* = 7.5, Hz, 1H), 7.22–7.24 (d, *J* = 7.4 Hz, 1H), 7.30–7.34 (t, *J* = 7.8 Hz, 1H), 7.76–7.78 (d, *J* = 8.2 Hz, 1H), 15.01 (s, 1H); ¹³C NMR (100 MHz, CDCl₃) δ 17.02, 26.72, 31.66, 114.96, 125.59, 125.72, 127.49, 131.08, 133.72, 139.69, 197.33, 197.85; HRMS (ESI-TOF) calcd. for C₁₁H₁₄N₂O₂[M-H]⁺: 217.0977, found: 217.0969.

3-(2-(*m*-Tolyl)hydrazono)pentane-2,4-dione (24c):

Yellow solid, mp = 132-135 °C, 146.2 mg, 67% yield. ¹H NMR (400 MHz, CDCl₃) δ 2.42 (s, 3H), 2.52 (s, 3H), 2.63 (s, 3H), 7.03–7.05 (d, *J* = 7.4 Hz, 1H), 7.24–7.33 (m, 3H), 14.75 (s, 1H); ¹³C NMR (100 MHz, CDCl₃) δ 21.55, 26.69, 31.69, 113.50, 116.85, 126.83, 129.50, 133.11, 139.76, 141.49, 197.17, 197.86; HRMS (ESI-TOF) calcd. for C₁₁H₁₄N₂O₂[M-H]⁺: 217.0977, found: 217.0970.

3-(2-(*p*-Tolyl)hydrazono)pentane-2,4-dione (25c):

Yellow solid, mp = 131-133 °C, 137.5 mg, 63% yield. ¹H NMR (400 MHz, CDCl₃) δ 2.38 (s, 3H), 2.50 (s, 3H), 2.62 (s, 3H), 7.21–7.23 (d, *J* = 8.1 Hz, 2H), 7.324–7.34 (d, *J* = 8.3 Hz, 2H), 14.75 (s, 1H); ¹³C NMR (100 MHz, CDCl₃) δ 21.04, 26.68, 31.67, 116.24, 130.21, 132.87, 135.97, 139.21, 197.11, 197.77; HRMS (ESI-TOF) calcd. for C₁₁H₁₄N₂O₂[M-H]⁺: 217.0977, found: 217.0967.

3-(2-(2,4-Dioxopentan-3-ylidene)hydrazinyl)benzoic acid (26c):

Yellow solid, mp = 193-196 °C, 186.2 mg, 75% yield. ¹H NMR (400 MHz, DMSO-*d*₆) δ 2.41 (s, 3H), 2.48 (s, 3H), 7.51–7.55 (t, *J* = 7.7 Hz, 1H), 7.72–7.80 (d, *J* = 7.4 Hz, 2H), 8.09 (s, 1H), 13.18(s, 1H), 13.88 (s, 1H); ¹³C NMR (100 MHz, DMSO-*d*₆) δ 26.71, 31.69, 117.12, 120.85, 126.14, 130.28, 132.58, 134.33, 142.66, 167.22, 196.65, 197.28; HRMS (ESI-TOF) calcd. for C₁₂H₁₂N₂O₄[M-H]⁺: 247.0719, found: 247.0707.

4-(2-(2,4-Dioxopentan-3-ylidene)hydrazinyl)benzoic acid (27c):

Yellow solid, mp = 197-199 °C, 243.27 mg, 98% yield. ¹H NMR (400 MHz, DMSO-*d*₆) δ 2.39 (s, 3H), 2.46 (s, 3H), 7.55–7.56 (d, *J* = 8.5 Hz, 2H), 7.93–7.96 (d, *J* = 8.5 Hz, 2H), 13.79 (s, 1H); ¹³C NMR (100 MHz, DMSO-*d*₆) δ 26.78, 31.71, 116.06, 120.08, 131.30, 134.99, 145.29, 167.73, 172.60, 196.81, 197.66; HRMS (ESI-TOF) calc. for C₁₁H₁₄N₂O₂[M-H]⁺: 247.0719, found: 247.0710.

***N*-(3-(2-(2,4-Dioxopentan-3-ylidene)hydrazinyl)phenyl)acetamide (28c):**

Yellow-orange solid, mp = 187-189 °C, 222.1 mg, 85% yield. ¹H NMR (400 MHz, CD₃OD) δ 2.15 (s, 3H), 2.44 (s, 3H), 2.51 (s, 3H), 7.01–7.11 (d, *J* = 7.3 Hz, 1H), 7.27–7.33 (m, 2H), 7.91 (s, 1H); ¹³C NMR (100 MHz, CD₃OD) δ 22.6, 25.3, 30.3, 106.8, 111.4, 116.4, 129.6, 132.8, 140.1, 142.0, 170.4, 197.2, 197.5; HRMS (ESI-TOF)

calcd for $C_{13}H_{15}N_3O_3[M-H]^+$: 260.1035; found: 260.1026; IR (ATR, cm^{-1}) 3292, 3078, 1666, 1624, 1596, 876.

N-(4-(2-(2,4-Dioxopentan-3-ylidene)hydrazinyl)phenyl)acetamide (**29c**):

Yellow solid, mp = 181-183 °C, 232.5 mg, 89% yield. 1H NMR (400 MHz, $CDCl_3$) δ 2.22 (s, 3H), 2.50 (s, 3H), 2.62 (s, 3H), 7.38–7.40 (d, $J = 8.9$ Hz, 2H), 7.50 (b, 1H), 7.58–7.61 (d, $J = 8.9$ Hz, 2H), 14.86 (s, 1H); ^{13}C NMR (100 MHz, $CDCl_3$) δ 24.64, 26.70, 31.70, 116.89, 121.02, 133.04, 135.87, 137.79, 168.30, 197.11, 197.89; HRMS (ESI-TOF) calcd. for $C_{13}H_{15}N_3O_3[M-H]^+$: 260.1035, found: 260.1023.

3-(2-(2-Ethylphenyl)hydrazono)pentane-2,4-dione (**30c**):

Yellow solid, mp = 103-106 °C, 227.47 mg, 98% yield. 1H NMR (400 MHz, $CDCl_3$) δ 1.33-1.36 (t, $J = 7.6$ Hz, 3H), 2.53 (s, 3H), 2.65 (s, 3H), 2.75–2.80 (q, $J = 7.6$ Hz, 1H), 7.17–7.21 (m, 1H), 7.25–7.27 (m, 1H), 7.31–7.35 (td, $J = 8.2, 1.0$ Hz, 1H), 7.79–7.81 (d, $J = 8.1$ Hz, 1H), 15.14 (s, 1H); ^{13}C NMR (100 MHz, $CDCl_3$) δ 13.88, 24.05, 26.74, 31.64, 115.26, 125.99, 127.47, 129.30, 131.68, 133.72, 139.05, 197.24, 197.89; HRMS (ESI-TOF) calcd. for $C_{11}H_{14}N_2O_2[M+H]^+$: 233.1290, found: 233.1280.

3-(2-Mesitylhydrazono)pentane-2,4-dione (**31c**):

Yellow solid, mp = 110-111 °C, 209.4 mg, 85% yield. 1H NMR (400 MHz, $CDCl_3$) δ 2.32 (s, 3H), 2.42 (s, 3H), 2.43 (s, 3H), 2.64 (s, 3H), 6.94 (s, 2H), 15.03 (s, 1H); ^{13}C NMR (100 MHz, $CDCl_3$) δ 19.3, 20.9, 27.0, 31.6, 129.8, 130.3, 133.4, 135.7, 136.3, 197.3, 197.5; HRMS (ESI-TOF) calcd for $C_{14}H_{18}N_2O_2[M-H]^+$: 245.1290, found: 245.1278; IR (ATR, cm^{-1}) 2790, 2918, 1714, 1656, 1611.

3-(2-(Naphthalen-1-yl)hydrazono)pentane-2,4-dione (**32c**):

Yellow solid, mp = 153-155 °C, 167.89 mg, 66% yield. 1H NMR (400 MHz, $CDCl_3$) δ 2.59 (s, 3H), 2.72 (s, 3H), 7.56–7.66 (m, 3H), 7.75–7.77 (d, $J = 8.2$ Hz, 1H), 7.93–7.95 (d, $J = 7.9$ Hz, 1H), 8.05–8.07 (d, $J = 8.1$ Hz, 1H), 15.78 (s, 1H); ^{13}C NMR (100 MHz, $CDCl_3$) δ 26.8, 31.8, 112.0, 119.6, 123.4, 126.1, 126.1, 126.6, 127.1, 128.8, 134.1, 134.3, 136.5, 197.3, 198.2; HRMS (ESI-TOF) calcd for $C_{15}H_{14}N_2O_2[M-H]^+$: 253.0977, found: 253.0965; IR (ATR, cm^{-1}) 3057, 2987, 2921, 1661, 1621, 1494.

3-(2-(2,5-Dichlorophenyl)hydrazono)pentane-2,4-dione (33c):

Yellow-orange solid, mp = 151-153 °C, 147.5 mg, 54% yield. ¹H NMR (400 MHz, CDCl₃) δ 2.55 (s, 3H), 2.66 (s, 3H), 7.10–7.12 (dd, *J* = 8.6, 2.4 Hz, 1H), 7.35–7.37 (d, *J* = 8.5 Hz, 1H), 7.77 (s, 1H), 14.78 (s, 1H); ¹³C NMR (100 MHz, CDCl₃) δ 26.77, 31.78, 116.21, 121.51, 125.55, 126.24, 130.78, 198.11; HRMS (ESI-TOF) calcd. for C₁₁H₁₀Cl₂N₂O₂[M-H]⁺: 271.0041, found: 271.0029.

3-(2-(2,6-Dichlorophenyl)hydrazono)pentane-2,4-dione (34c):

Yellow-orange solid, mp = 149-152 °C, 169.3 mg, 62% yield. ¹H NMR (400 MHz, CDCl₃) δ 2.45 (s, 3H), 2.65 (s, 3H), 7.11–7.16 (t, *J* = 8.3 Hz, 1H), 7.41–7.43 (d, *J* = 8.1 Hz, 2H), 14.58 (s, 1H); ¹³C NMR (100 MHz, CDCl₃) δ 26.83, 31.75, 126.76, 127.48, 128.30, 129.66, 134.49, 135.35, 197.52, 198.20; HRMS (ESI-TOF) calcd. for C₁₁H₁₀Cl₂N₂O₂[M-H]⁺: 271.0041, found: 271.0027.

3-(2-(2,4-Difluorophenyl)hydrazono)pentane-2,4-dione (35c):

Yellow solid, mp = 126-129 °C, 237.8 mg, 99% yield. ¹H NMR (400 MHz, CDCl₃) δ 2.51 (s, 3H), 2.64 (s, 3H), 6.94–7.01 (m, 2H), 7.73–7.78 (m, 1H), 14.76 (s, 1H); ¹³C NMR (100 MHz, CDCl₃) δ 26.62, 31.67, 104.52, 104.79, 112.23, 112.27, 112.46, 112.49, 117.16, 117.25, 134.39, 158.49, 160.96, 161.06, 196.89, 198.01; HRMS (ESI-TOF) calcd. for C₁₁H₁₀F₂N₂O₂[M-H]⁺: 239.0632, found: 239.0620.

3-(2-(2,5-Difluorophenyl)hydrazono)pentane-2,4-dione (36c):

Yellow solid, mp = 129-131 °C, 237.8 mg, 99% yield. ¹H NMR (400 MHz, CDCl₃) δ 2.52 (s, 3H), 2.63 (s, 3H), 6.80–6.85 (m, 1H), 7.09–7.16 (m, 1H), 7.43–7.48 (m, 1H), 14.59 (s, 1H); ¹³C NMR (100 MHz, CDCl₃) δ 26.63, 31.74, 103.29, 103.58, 111.56, 111.63, 111.80, 111.88, 116.72, 116.81, 116.92, 117.02, 131.04, 131.14, 134.77, 146.77, 149.18, 158.24, 160.66, 160.68, 196.92, 198.20; HRMS (ESI-TOF) calc. for calcd. for C₁₁H₁₀F₂N₂O₂[M-H]⁺: 239.0632, found: 239.0621.

3-(2-(2,6-Difluorophenyl)hydrazono)pentane-2,4-dione (37c):

Yellow solid, mp = 114-117 °C, 235.4 mg, 98% yield. ¹H NMR (400 MHz, CDCl₃) δ 2.45 (s, 3H), 2.64 (s, 3H), 7.00–7.05 (m, 2H), 7.10–7.16 (m, 1H), 14.46 (s, 1H); ¹³C NMR (100 MHz, CDCl₃) δ 26.45, 31.71, 112.42, 112.47, 112.59, 112.64, 135.03,

152.86, 152.89, 155.36, 197.45, 198.15; HRMS (ESI-TOF) calcd for $C_{11}H_{10}F_2N_2O_2[M-H]^+$: 239.0632, found: 239.0663.

3-(2-(3,5-Difluorophenyl)hydrazono)pentane-2,4-dione (**38c**):

Yellow solid, mp = 151-153 °C, 237.8 mg, 99% yield. 1H NMR (400 MHz, $CDCl_3$) δ 2.51 (s, 3H), 2.63 (s, 3H), 6.62–6.67 (tt, $J = 9.1, 2.2$ Hz, 1H), 6.93–6.96 (d, $J = 8.0, 1.9$ Hz, 1H), 14.49 (s, 1H); ^{13}C NMR (100 MHz, $CDCl_3$) δ 26.6, 31.8, 99.5 ($J = 20.3, 9.0$ Hz), 100.6 ($J = 25.7$ Hz), 133.9, 144.0, 163.8 ($J = 247.0, 14.2$ Hz), 196.9, 198.5 HRMS (ESI-TOF) calcd for $C_{11}H_{10}F_2N_2O_2[M-H]^+$: 239.0632, found: 239.0620; IR (ATR, cm^{-1}) 3059, 1675, 1602, 1524, 1471, 1407.

Arylazopyrazole Derivatives

(*E*)-3,5-Dimethyl-4-(phenyldiazenyl)-1*H*-pyrazole (**1d**):

Yellow solid, mp = 141-143 °C, 170.2 mg, 85% yield. 1H NMR (400 MHz, $CDCl_3$) δ 2.64 (s, 6H), 7.41-7.43 (m, 1H), 7.78-7.52 (t, $J = 7.2$ Hz, 2H), 7.82-7.84 (m, 2H); ^{13}C NMR (100 MHz, $CDCl_3$) δ 12.2, 121.9, 128.9, 129.5, 134.7, 141.5, 153.6; HRMS (ESI-TOF) calcd for $C_{11}H_{12}N_4[M+H]^+$: 201.1140, found: 201.1132; IR (ATR, cm^{-1}) 3114, 3042, 2968, 2887, 1411, 1322, 1118, 829.

(*E*)-4-((2-Fluorophenyl)diazenyl)-3,5-dimethyl-1*H*-pyrazole (**2d**):

Yellow solid, mp = 158-160 °C, 209.5 mg, 96% yield. 1H NMR (400 MHz, $CDCl_3$) δ 2.63 (s, 6H), 7.35-7.43 (m, 2H), 7.69-7.72 (dt, $J = 7.7, 1.7$ Hz, 1H), 7.78-7.79 (t, $J = 1.7$ Hz, 1H); ^{13}C NMR (100 MHz, $CDCl_3$) δ 12.3, 120.9, 121.3, 129.2, 130.0, 134.7, 134.9, 141.8, 154.4; HRMS (ESI-TOF) calcd for $C_{11}H_{11}FN_4[M+H]^+$: 219.1046, found: 219.1038; IR (ATR, cm^{-1}) 3173, 3110, 2966, 2883, 1400, 1315, 1184, 776.

(*E*)-4-((3-Fluorophenyl)diazenyl)-3,5-dimethyl-1*H*-pyrazole (**3d**):

Yellow solid, mp = 128-131 °C, 178.9 mg, 82% yield. 1H NMR (400 MHz, $CDCl_3$) δ 2.64 (s, 6H), 7.09-7.13 (tdd, $J = 8.2, 2.6, 0.7$ Hz, 1H), 7.42-7.51 (m, 2H), 7.63-7.65 (dt, $J = 6.8, 1.4$ Hz, 1H); ^{13}C NMR (100 MHz, $CDCl_3$) δ 12.2, 107.0 (d, $J = 22.7$ Hz), 116.2 (d, $J = 22.1$ Hz), 119.5 (d, $J = 2.8$ Hz), 130.1 (d, $J = 8.6$ Hz), 134.6, 141.9, 155.1 (d, $J = 6.8$ Hz), 163.4 (d, $J = 245.1$ Hz); HRMS (ESI-TOF) calcd for $C_{11}H_{11}FN_4[M+H]^+$:

219.1046, found: 219.1035; IR (ATR, cm^{-1}) 3198, 3115, 3051, 2965, 2896, 1666, 1408, 1324, 1108, 867.

(*E*)-4-((4-Fluorophenyl)diazenyl)-3,5-dimethyl-1*H*-pyrazole (**4d**):

Yellow solid, mp = 166-168 °C, 202.9 mg, 93% yield. ^1H NMR (400 MHz, CDCl_3) δ 2.63 (s, 6H), 7.15-7.19 (t, $J = 8.6$ Hz, 2H), 7.80-7.84 (dd, $J = 8.6, 5.2$ Hz, 2H); ^{13}C NMR (100 MHz, CDCl_3) δ 12.2, 115.8 (d, $J = 22.8$ Hz), 123.6 (d, $J = 8.7$ Hz), 134.5, 141.5, 150.0 (d, $J = 2.9$ Hz), 163.5 (d, $J = 247.9$ Hz); HRMS (ESI-TOF) calcd for $\text{C}_{11}\text{H}_{11}\text{FN}_4$ $[\text{M}+\text{H}]^+$: 219.1046, found: 219.1057; IR (ATR, cm^{-1}) 3605, 2385, 2308, 1421, 1218, 831.

(*E*)-4-((2-Chlorophenyl)diazenyl)-3,5-dimethyl-1*H*-pyrazole (**5d**):

Yellow solid, mp = 170-172 °C, 143.2 mg, 61% yield. ^1H NMR (400 MHz, CDCl_3) δ 2.67 (s, 6H), 7.31-7.34 (m, 2H), 7.53-7.55 (m, 1H), 7.69-7.72 (m, 1H); ^{13}C NMR (100 MHz, CDCl_3) δ 12.3, 116.8, 127.1, 130.2, 130.4, 134.3, 135.6, 142.1, 149.4; HRMS (ESI-TOF) calcd for $\text{C}_{11}\text{H}_{11}\text{ClN}_4$ $[\text{M}+\text{H}]^+$: 235.0750, found: 235.0741; IR (ATR, cm^{-1}) 3192, 3113, 3052, 2914, 1491, 1395, 1194, 889.

(*E*)-4-((3-Chlorophenyl)diazenyl)-3,5-dimethyl-1*H*-pyrazole (**6d**):

Yellow solid, mp = 170-172 °C, 164.3 mg, 70% yield. ^1H NMR (400 MHz, CDCl_3) δ 2.65 (s, 6H), 7.18-7.26 (m, 2H), 7.34-7.40 (m, 1H), 7.69-7.73 (td, $J = 1.8, 7.9$ Hz, 1H); ^{13}C NMR (100 MHz, CDCl_3) δ 12.2, 116.8 (d, $J = 19.7$ Hz), 117.1, 124.1 (d, $J = 3.8$ Hz), 130.7 (d, $J = 8.0$ Hz), 135.5, 141.4 (d, $J = 7.0$ Hz), 141.9, 159.4 (d, $J = 25.4$ Hz); HRMS (ESI-TOF) calcd for $\text{C}_{11}\text{H}_{11}\text{ClN}_4$ $[\text{M}+\text{H}]^+$: 235.0750, found: 235.0741; IR (ATR, cm^{-1}) 2984, 1502, 1359, 1303, 1177, 1063, 922, 767, 680.

(*E*)-4-((4-Chlorophenyl)diazenyl)-3,5-dimethyl-1*H*-pyrazole (**7d**):

Yellow solid, mp = 167-169 °C, 218.3 mg, 93% yield. ^1H NMR (400 MHz, CDCl_3) δ 2.62 (s, 6H), 7.43-7.46 (d, $J = 8.7$ Hz, 2H), 7.73-7.77 (d, $J = 8.7$ Hz, 2H); ^{13}C NMR (100 MHz, CDCl_3) δ 12.22, 123.10, 129.12, 134.67, 135.18, 141.73, 151.88; HRMS (ESI-TOF) calcd for $\text{C}_{11}\text{H}_{11}\text{ClN}_4$ $[\text{M}+\text{H}]^+$: 235.0750, found: 235.0759; IR (ATR, cm^{-1}) 3192, 2957, 2875, 2820, 1506, 1412, 829.

(E)-4-((2-Bromophenyl)diazenyl)-3,5-dimethyl-1*H*-pyrazole (**8d**):

Yellow solid, mp = 165-168 °C, 195.4 mg, 70% yield. ¹H NMR (400 MHz, CDCl₃) δ 2.68 (s, 6H), 7.23-7.27 (t, *J* = 7.2 Hz, 1H), 7.36-7.40 (t, *J* = 7.5 Hz, 1H), 7.68-7.70 (d, *J* = 7.4 Hz, 1H), 7.73-7.75 (d, *J* = 7.9 Hz, 1H); ¹³C NMR (100 MHz, CDCl₃) δ 12.4, 117.1, 124.8, 127.8, 130.5, 133.5, 135.5, 142.1, 150.4; HRMS (ESI-TOF) calcd for C₁₁H₁₁BrN₄[M+H]⁺: 279.0245, 281.0225, found: 279.0236, 281.0209; IR (ATR, cm⁻¹) 3194, 3105, 3051, 2966, 2915, 1498, 1405, 854.

(E)-4-((3-Bromophenyl)diazenyl)-3,5-dimethyl-1*H*-pyrazole (**9d**):

Yellow solid, mp = 168-170 °C, 251.2 mg, 90% yield. ¹H NMR (400 MHz, CDCl₃) δ 2.63 (s, 6H), 7.34-7.38 (t, *J* = 7.9 Hz, 1H), 7.51-7.53 (ddd, *J* = 7.9, 1.9, 0.9 Hz, 1H), 7.74-7.76 (ddd, *J* = 7.5, 1.7, 0.7 Hz, 1H), 7.93-7.94 (t, *J* = 1.8 Hz, 1H); ¹³C NMR (100 MHz, CDCl₃) δ 12.3, 121.8, 123.0, 123.8, 130.3, 132.1, 135.0, 142.1, 154.5; HRMS (ESI-TOF) calcd for C₁₁H₁₁BrN₄ [M+H]⁺: 279.0245, 281.0225, found: 279.0232, 281.0208; IR (ATR, cm⁻¹) 3176, 3114, 2965, 2921, 1495, 1393, 1312, 901, 773.

(E)-4-((4-Bromophenyl)diazenyl)-3,5-dimethyl-1*H*-pyrazole (**10d**):

Yellow solid, mp = 166-168 °C, 201.1 mg, 72% yield. ¹H NMR (400 MHz, CDCl₃) δ 2.61 (s, 6H), 7.60-7.62 (d, *J* = 8.8 Hz, 2H), 7.68-7.71 (d, *J* = 8.8 Hz, 2H); ¹³C NMR (100 MHz, CDCl₃) δ 12.2, 123.4, 123.6, 132.1, 134.7, 141.7, 152.2; HRMS (ESI-TOF) calcd for C₁₁H₁₁BrN₄ [M+H]⁺: 279.0245, 281.0225, found: 279.0235, 281.0211; IR (ATR, cm⁻¹) 3194, 3103, 2961, 2879, 1415, 827, 774.

(E)-2-((3,5-Dimethyl-1*H*-pyrazol-4-yl)diazenyl)phenol (**11d**):

Yellow solid, mp = 164-166 °C, 201.1 mg, 93% yield. ¹H NMR (400 MHz, CDCl₃) δ 2.60 (s, 6H), 6.99-7.06 (m, 2H), 7.27-7.31 (td, *J* = 6.0, 1.5 Hz, 1H), 7.80-7.83 (dd, *J* = 7.9, 1.6 Hz, 1H); ¹³C NMR (100 MHz, CDCl₃) δ 12.3, 117.9, 119.8, 131.5, 131.6, 132.5, 137.6, 140.9, 152.1; HRMS (ESI-TOF) calcd for C₁₁H₁₂N₄O [M+H]⁺: 217.1089, found: 217.1077; IR (ATR, cm⁻¹) 3281, 3116, 2914, 2807, 1418, 1221, 820.

(E)-3-((3,5-Dimethyl-1*H*-pyrazol-4-yl)diazenyl)phenol (**12d**):

Yellow solid, mp = 199-203 °C, 198.9 mg, 92% yield. ¹H NMR (400 MHz, DMSO-*d*₆) δ 2.39 (s, 3H), 2.50 (s, 3H), 6.82-6.84 (dd, *J* = 8.0, 1.3 Hz, 1H), 7.13 (1H), 7.19-7.21

(d, $J = 7.8$ Hz, 1H), 7.28-7.32 (t, $J = 7.9$ Hz, 1H), 9.68 (s, 1H, OH), 12.85 (s, 1H, NH); ^{13}C NMR (100 MHz, DMSO- d_6) δ 10.5, 14.2, 106.8, 114.5, 117.1, 130.3, 134.5, 138.8, 143.0, 154.8, 158.5; HRMS (ESI-TOF) calcd for $\text{C}_{11}\text{H}_{12}\text{N}_4\text{O} [\text{M}+\text{H}]^+$: 217.1089, found: 217.1080; IR (ATR, cm^{-1}) 3335, 3246, 3060, 2922, 1590, 1470, 1411, 1128, 1114, 857.

(*E*)-4-((3,5-Dimethyl-1*H*-pyrazol-4-yl)diazenyl)phenol (**13d**):

Yellow solid, mp = 198-205 °C, 170.8 mg, 79% yield. ^1H NMR (400 MHz, DMSO- d_6) δ 2.40 (s, 3H), 2.46 (s, 3H), 6.86-6.89 (d, $J = 8.9$ Hz, 2H), 7.61-7.63 (d, $J = 8.9$ Hz, 2H), 9.97 (s, 1H, OH), 12.72 (s, 1H, NH); ^{13}C NMR (100 MHz, DMSO- d_6) δ 10.4, 14.1, 116.1, 123.6, 134.2, 137.7, 142.9, 146.6, 159.5; HRMS (ESI-TOF) calcd for $\text{C}_{11}\text{H}_{12}\text{N}_4\text{O} [\text{M}+\text{H}]^+$: 217.1089, found: 217.1081; IR (ATR, cm^{-1}) 3291, 3190, 3119, 2917, 1482, 1420, 1134, 1061, 825.

(*E*)-3,5-Dimethyl-4-((2-(trifluoromethyl)phenyl)diazenyl)-1*H*-pyrazole (**14d**):

Yellow solid, mp = 170-172 °C, 193.1 mg, 72% yield. ^1H NMR (400 MHz, CDCl_3) δ 2.65 (s, 6H), 7.46-7.50 (t, $J = 7.8$ Hz, 1H), 7.60-7.64 (t, $J = 7.9$ Hz, 1H), 7.79-7.81 (d, $J = 8.0$ Hz, 2H); ^{13}C NMR (100 MHz, CDCl_3) δ 12.1, 115.8, 124.2 (q, $J = 273.7$ Hz), 126.3 (q, $J = 5.5$ Hz), 127.3 (q, $J = 30.7$ Hz), 128.9, 132.4, 135.5, 142.4, 150.4; HRMS (ESI-TOF) calcd for $\text{C}_{12}\text{H}_{11}\text{F}_3\text{N}_4 [\text{M}+\text{H}]^+$: 269.1014, found: 269.1002; IR (ATR, cm^{-1}) 3196, 3107, 3049, 2883, 2308, 1497, 1408, 1122, 1035, 762.

(*E*)-3,5-Dimethyl-4-((3-(trifluoromethyl)phenyl)diazenyl)-1*H*-pyrazole (**15d**):

Yellow solid, mp = 153-155 °C, 198.5 mg, 74% yield. ^1H NMR (400 MHz, CDCl_3) δ 2.66 (s, 6H), 7.55-7.59 (t, $J = 7.8$ Hz, 1H), 7.63-7.65 (d, $J = 7.7$ Hz, 1H), 7.95-7.97 (d, $J = 7.9$ Hz, 1H), 8.05 (s, 1H); ^{13}C NMR (100 MHz, CDCl_3) δ 12.2, 118.8 (q, $J = 3.8$ Hz), 124.0 (q, $J = 272.04$ Hz), 124.9, 125.71 (q, $J = 3.7$ Hz), 129.5, 131.42 (q, $J = 32.6$ Hz), 134.7, 142.0, 153.5; HRMS (ESI-TOF) calcd for $\text{C}_{12}\text{H}_{11}\text{F}_3\text{N}_4 [\text{M}+\text{H}]^+$: 269.1014, found: 269.1004; IR (ATR, cm^{-1}) 3201, 3126, 2958, 2916, 1488, 1319, 1106, 787, 689.

(*E*)-3,5-Dimethyl-4-((4-(trifluoromethyl)phenyl)diazenyl)-1*H*-pyrazole (**16d**):

Yellow solid, mp = 138-140 °C, 222.6 mg, 83% yield. ^1H NMR (400 MHz, CDCl_3) δ 2.65 (s, 6H), 7.70-7.72 (d, $J = 8.3$ Hz, 2H), 7.84-7.86 (d, $J = 8.2$ Hz, 2H); ^{13}C NMR

(100 MHz, CDCl₃) δ 12.2, 122.0, 124.1 (q, $J = 272$ Hz), 126.1 (q, $J = 3.4$ Hz), 130.8 (q, $J = 32.4$ Hz), 134.9, 142.1, 155.4, 155.4; HRMS (ESI-TOF) calcd for C₁₂H₁₁F₃N₄ [M+H]⁺: 269.1014, found: 269.1001; IR (ATR, cm⁻¹) 3197, 3109, 2973, 2890, 1673, 1416, 1317, 1113, 895, 840.

(*E*)-4-((2-Methoxyphenyl)diazenyl)-3,5-dimethyl-1*H*-pyrazole (**17d**):

Yellow solid, mp = 156-159 °C, 161.2 mg, 70% yield. ¹H NMR (400 MHz, CDCl₃) δ 2.66 (s, 6H), 4.01 (s, 3H, OCH₃), 7.01-7.05 (td, $J = 7.6, 1.1$ Hz, 1H), 7.07-7.09 (dd, $J = 8.3, 0.7$ Hz, 1H), 7.36-7.40 (td, $J = 8.5, 1.7$ Hz, 1H), 7.62-7.64 (dd, $J = 7.9, 1.6$ Hz, 1H); ¹³C NMR (100 MHz, CDCl₃) δ 12.1, 56.47, 112.8, 116.3, 120.9, 130.8, 135.7, 141.3, 143.2, 156.2; HRMS (ESI-TOF) calcd for C₁₂H₁₄N₄O [M+H]⁺: 231.1246, found: 231.1235; IR (ATR, cm⁻¹) 3193, 3109, 3042, 2877, 2826, 2308, 1586, 1408, 1110, 892.

(*E*)-4-((3-Methoxyphenyl)diazenyl)-3,5-dimethyl-1*H*-pyrazole (**18d**):

Yellow solid, mp = 144-145 °C, 225.7 mg, 98% yield. ¹H NMR (400 MHz, CDCl₃) δ 2.66 (s, 6H), 3.91 (s, 3H, OCH₃), 6.97-7.00 (ddd, $J = 8.0, 2.6, 1.1$ Hz, 1H), 7.37-7.47 (m, 3H); ¹³C NMR (100 MHz, CDCl₃) δ 12.2, 55.4, 105.5, 115.7, 115.8, 129.7, 134.6, 141.5, 154.8, 160.2; HRMS (ESI-TOF) calcd for C₁₂H₁₄N₄O [M+H]⁺: 231.1246, found: 231.1235; IR (ATR, cm⁻¹) 3120, 3045, 2957, 2897, 1737, 1475, 1404, 1133, 834, 675.

(*E*)-4-((4-Methoxyphenyl)diazenyl)-3,5-dimethyl-1*H*-pyrazole (**19d**):

Yellow solid, mp = 174-177 °C, 200.3 mg, 87% yield. ¹H NMR (400 MHz, CDCl₃) δ 2.62 (s, 6H), 3.90 (s, 3H, OCH₃), 6.99-7.01 (d, $J = 9.0$ Hz, 2H), 7.80-7.82 (d, $J = 9.0$ Hz, 2H); ¹³C NMR (100 MHz, CDCl₃) δ 12.2, 55.5, 114.0, 123.4, 134.5, 141.0, 147.9, 160.8; HRMS (ESI-TOF) calcd for C₁₂H₁₄N₄O [M+H]⁺: 231.1246, found: 231.1250; IR (ATR, cm⁻¹) 3740, 2921, 2544, 1494, 1412, 1144, 1016, 832, 770.

(*E*)-3,5-Dimethyl-4-((2-nitrophenyl)diazenyl)-1*H*-pyrazole (**20d**):

Orange solid, mp = 170-172 °C, 198.6 mg, 81% yield. ¹H NMR (400 MHz, CDCl₃) δ 2.60 (s, 6H), 7.47-7.51 (td, $J = 7.6, 1.3$ Hz, 1H), 7.61-7.66 (td, $J = 7.2, 1.3$ Hz, 1H), 7.70-7.73 (dd, $J = 8.1, 1.2$ Hz, 1H), 7.82-7.84 (dd, $J = 8.0, 1.1$ Hz, 1H), 11.87 (br, 1H, NH); ¹³C NMR (100 MHz, CDCl₃) δ 12.2, 118.0, 123.7, 129.1, 132.6, 135.5, 142.8,

145.9, 147.4; HRMS (ESI-TOF) calcd for $C_{11}H_{11}N_5O_2$ $[M+H]^+$: 246.0991, found: 246.0994; IR (ATR, cm^{-1}) 3192, 2886, 1588, 1519, 1406, 1110, 848, 757.

(*E*)-3,5-Dimethyl-4-((3-nitrophenyl)diazenyl)-1*H*-pyrazole (**21d**):

Orange solid, mp = 227-229 °C, 203.5 mg, 83% yield. 1H NMR (400 MHz, $CDCl_3$) δ 2.64 (s, 6H), 7.65-7.69 (t, J = 8.0 Hz, 1H), 8.14-8.16 (d, J = 7.9 Hz, 1H), 8.25-8.27 (d, J = 8.0 Hz, 1H), 8.62 (s, 1H); ^{13}C NMR (100 MHz, $CDCl_3$) δ 12.4, 116.2, 123.5, 128.24, 129.7, 134.9, 143.2, 149.0, 154.0; HRMS (ESI-TOF) calcd for $C_{11}H_{11}N_5O_2$ $[M+H]^+$: 246.0991, found: 246.0979; IR (ATR, cm^{-1}) 3185, 3096, 2967, 2881, 2823, 1412, 1340, 865, 803.

(*E*)-3,5-Dimethyl-4-((4-nitrophenyl)diazenyl)-1*H*-pyrazole (**22d**):

Orange solid, mp = 198-200 °C, 237.8 mg, 97% yield. 1H NMR (400 MHz, $CDCl_3$) δ 2.65 (s, 6H), 7.90-7.93 (d, J = 8.8 Hz, 2H), 8.34-8.37 (d, J = 8.8 Hz, 2H); ^{13}C NMR (100 MHz, $CDCl_3$) δ 12.3, 122.4, 124.7, 135.4, 143.0, 147.7, 156.9; HRMS (ESI-TOF) calcd for $C_{11}H_{11}N_5O_2$ $[M+H]^+$: 246.0991, found: 246.0980; IR (ATR, cm^{-1}) 3195, 3101, 2969, 2886, 1507, 1400, 898, 849.

(*E*)-3,5-Dimethyl-4-(*o*-tolyl diazenyl)-1*H*-pyrazole (**23d**):

Yellow solid, mp = 163-165 °C, 207.5 mg, 95% yield. 1H NMR (400 MHz, $CDCl_3$) δ 2.67 (s, 6H), 2.68 (s, 3H), 7.26-7.36 (m, 3H), 7.64-7.67 (dd, J = 7.3, 1.4 Hz, 1H); ^{13}C NMR (100 MHz, $CDCl_3$) δ 12.3, 17.9, 114.7, 126.3, 129.5, 131.1, 135.4, 136.8, 141.4, 151.5; HRMS (ESI-TOF) calcd for $C_{12}H_{14}N_4$ $[M+H]^+$: 215.1297, found: 215.1290; IR (ATR, cm^{-1}) 3193, 3109, 3042, 2877, 2826, 2308, 1586, 1494, 1408, 892, 820, 763.

(*E*)-3,5-Dimethyl-4-(*m*-tolyl diazenyl)-1*H*-pyrazole (**24d**):

Yellow solid, mp = 148-152 °C, 205.7 mg, 96% yield. 1H NMR (400 MHz, $CDCl_3$) δ 2.47 (s, 3H), 2.65 (s, 6H), 7.22-7.24 (d, J = 7.5 Hz, 1H), 7.36-7.40 (t, J = 8.4 Hz, 1H), 7.62-7.64 (m, 2H); ^{13}C NMR (100 MHz, $CDCl_3$) δ 12.2, 21.4, 119.1, 122.4, 128.7, 130.3, 134.8, 138.8, 141.5, 153.6; HRMS (ESI-TOF) calcd for $C_{12}H_{14}N_4$ $[M+H]^+$: 215.1297, found: 215.1310; IR (ATR, cm^{-1}) 3193, 3102, 3043, 2954, 2918, 1595, 1497, 1480, 1404, 842, 782.

(E)-3,5-Dimethyl-4-(*p*-tolyl diazenyl)-1*H*-pyrazole (**25d**):

Yellow solid, mp = 153-155 °C, 197.1 mg, 92% yield. ¹H NMR (400 MHz, CDCl₃) δ 2.44 (s, 3H), 2.63 (s, 6H), 7.28-7.30 (d, *J* = 8.2 Hz, 2H), 7.72-7.74 (d, *J* = 8.2 Hz, 2H); ¹³C NMR (100 MHz, CDCl₃) δ 12.2, 21.4, 121.8, 129.6, 134.6, 139.8, 141.6, 151.6; HRMS (ESI-TOF) calcd for C₁₂H₁₄N₄ [M+H]⁺: 215.1297, found: 215.1288; IR (ATR, cm⁻¹) 3195, 3113, 3041, 2874, 2820, 2310, 1591, 1409, 816, 770.

(E)-3-((3,5-Dimethyl-1*H*-pyrazol-4-yl) diazenyl) benzoic acid (**26d**):

Yellow solid, mp = 230-233 °C, 136.8 mg, 56% yield. ¹H NMR (400 MHz, CD₃OD) δ 2.55 (s, 6H), 7.47-7.50 (t, *J* = 7.7 Hz, 1H), 7.82-7.84 (d, *J* = 7.8 Hz, 1H), 8.00-8.02 (d, *J* = 7.5 Hz, 1H), 8.39 (s, 1H); ¹³C NMR (100 MHz, CD₃OD) δ 10.6, 122.3, 122.9, 128.0, 129.9, 134.2, 138.9, 141.2, 153.3, 173.5; HRMS (ESI-TOF) calcd for C₁₂H₁₂N₄O₂ [M+H]⁺: 245.1039, found: 245.1030; IR (ATR, cm⁻¹) 3736, 3207, 2918, 2388, 1677, 1368, 1269, 1164, 1062, 864, 764.

(E)-4-((3,5-Dimethyl-1*H*-pyrazol-4-yl) diazenyl) benzoic acid (**27d**):

Yellow solid, mp = 219-223 °C, 197.8 mg, 81% yield. ¹H NMR (400 MHz, DMSO-*d*₆) δ 2.47 (s, 6H), 7.78-7.81 (d, *J* = 8.4 Hz, 2H), 8.06-8.08 (d, *J* = 8.4 Hz, 2H), 13.00 (br, 1H); ¹³C NMR (100 MHz, DMSO-*d*₆) δ 12.5, 121.8, 131.0, 131.4, 135.1, 141.6, 156.0, 167.4; HRMS (ESI-TOF) calcd for C₁₂H₁₂N₄O₂ [M+H]⁺: 245.1039, found: 245.1030; IR (ATR, cm⁻¹) 3737, 3199, 2923, 2314, 1407, 1292, 1061, 996, 767.

(E)-*N*-(3-((3,5-Dimethyl-1*H*-pyrazol-4-yl) diazenyl) phenyl) acetamide (**28d**):

Yellow solid, mp = 209-212 °C, 146.7 mg, 57% yield. ¹H NMR (400 MHz, DMSO-*d*₆) δ 2.07 (s, 3H, NHCOCH₃), 2.40 (s, 3H), 2.51 (s, 3H), 7.41-7.43 (m, 2H), 7.62-7.65 (m, 1H), 7.98 (s, 1H), 10.12 (br, 1H), 12.87 (br, 1H); ¹³C NMR (100 MHz, DMSO-*d*₆) δ 10.5, 14.2, 24.5, 111.9, 117.1, 120.3, 129.8, 134.5, 139.0, 140.6, 143.0, 153.8, 169.0; HRMS (ESI-TOF) calcd for C₁₃H₁₅N₅O [M+H]⁺: 258.1355, found: 258.1367; IR (ATR, cm⁻¹) 3390, 3307, 3198, 3138, 2918, 1659, 1548, 1493, 1428, 885.

(E)-*N*-(4-((3,5-Dimethyl-1*H*-pyrazol-4-yl) diazenyl) phenyl) acetamide (**29d**):

Yellow solid, mp = 222-225 °C, 239.2 mg, 93% yield. ¹H NMR (400 MHz, DMSO-*d*₆) δ 2.08 (s, 3H), 2.42 (s, 3H), 2.47 (s, 3H), 7.68-7.74 (dd, *J* = 8.9, 7.9 Hz, 4H), 10.18 (s,

1H), 12.78 (s, 1H); ¹³C NMR (100 MHz, DMSO-*d*₆) δ 24.6, 119.6, 122.6, 134.4, 141.0, 149.0, 169.0; HRMS (ESI-TOF) calcd for C₁₃H₁₅N₅O [M+H]⁺: 258.1355, found: 258.1343; IR (ATR, cm⁻¹) 3266, 3176, 3088, 3039, 2958, 2871, 2310, 1659, 1598, 1531, 1419, 836.

(*E*)-4-((2-Ethylphenyl)diazenyl)-3,5-dimethyl-1*H*-pyrazole (**30d**):

Yellow solid, mp = 154-156 °C, 226.0 mg, 99% yield. ¹H NMR (400 MHz, CDCl₃) δ 1.30-1.34(t, *J* = 7.5 Hz, 3H), 2.65 (s, 6H), 3.08-3.14 (q, *J* = 7.5 Hz, 2H), 7.26-7.30 (m, 1H), 7.35-7.36 (m, 2H), 7.64-7.66 (d, *J* = 7.8 Hz, 1H); ¹³C NMR (100 MHz, CDCl₃) δ 12.26, 16.21, 24.95, 114.70, 126.40, 129.60, 129.78, 135.37, 141.42, 142.80, 150.93; HRMS (ESI-TOF) calcd for C₁₃H₁₆N₄ [M+H]⁺: 229.1453, found: 229.1444; IR (ATR, cm⁻¹) 3199, 3116, 3047, 2873, 2311, 1406, 1322, 1113, 839, 762.

(*E*)-4-(Mesityldiazenyl)-3,5-dimethyl-1*H*-pyrazole (**31d**):

Yellow solid, mp = 168-170 °C, 239.8 mg, 99% yield. ¹H NMR (400 MHz, CDCl₃) δ 2.34 (s, 3H), 2.39 (s, 6H), 2.58 (s, 6H), 6.95 (s, 2H); ¹³C NMR (100 MHz, CDCl₃) δ 12.2, 19.6, 21.0, 129.9, 130.9, 135.3, 137.3, 149.4; HRMS (ESI-TOF) calcd for C₁₄H₁₈N₄ [M+H]⁺: 243.1610, found: 243.1599; IR (ATR, cm⁻¹) 3194, 3110, 3043, 2955, 2879, 2312, 1419, 846.

(*E*)-3,5-Dimethyl-4-(naphthalen-1-yl)diazenyl)-1*H*-pyrazole (**32d**):

Yellow solid, mp = 180-182 °C, 157.7 mg, 63% yield. ¹H NMR (400 MHz, CDCl₃) δ 2.77 (s, 6H), 7.55-7.67 (m, 3H), 7.80-7.82 (dd, *J* = 7.5, 0.8 Hz, 1H), 7.92-7.95 (dd, *J* = 7.9, 3.5 Hz, 2H), 8.82-8.84 (d, *J* = 8.4 Hz, 1H); ¹³C NMR (100 MHz, CDCl₃) δ 12.6, 110.8, 123.5, 125.7, 126.2, 126.5, 127.9, 129.8, 131.0, 134.3, 135.9, 141.6, 148.7; HRMS (ESI-TOF) calcd for C₁₅H₁₄N₄ [M+H]⁺: 251.1297, found: 251.1307; IR (ATR, cm⁻¹) 3177, 3112, 3042, 2964, 2923, 2877, 2309, 1412, 965, 765.

(*E*)-4-((2,5-Dichlorophenyl)diazenyl)-3,5-dimethyl-1*H*-pyrazole (**33d**):

Yellow solid, mp = 238-242 °C, 121.1 mg, 45% yield. ¹H NMR (400 MHz, DMSO-*d*₆) δ 2.42 (s, 3H), 2.53 (s, 3H), 7.47-7.49 (dd, *J* = 8.6, 1.8 Hz, 1H), 7.62 (d, *J* = 0.4 Hz, 1H), 7.65-7.68 (d, *J* = 8.6 Hz, 1H), 13.06 (s, 1H); ¹³C NMR (100 MHz, DMSO-*d*₆) δ 10.55, 14.30, 116.84, 130.30, 131.60, 132.34, 133.10, 135.66, 140.86, 143.60, 149.83;

HRMS (ESI-TOF) calcd for $C_{11}H_{10}Cl_2N_4 [M+H]^+$: 269.0361, found: 269.0351; IR (ATR, cm^{-1}) 3201, 3112, 3044, 2957, 2870, 1415, 1367, 1335, 882, 836, 768, 708.

(*E*)-4-((2,6-Dichlorophenyl)diazenyl)-3,5-dimethyl-1H-pyrazole (**34d**):

Yellow solid, mp = 178-181 °C, 239.5 mg, 89% yield. 1H NMR (400 MHz, $CDCl_3$) δ 2.64 (s, 6H), 7.13-7.18 (dd, $J = 8.4, 7.8$ Hz, 1H), 7.40-7.42 (d, $J = 8.0$ Hz, 2H); ^{13}C NMR (100 MHz, $CDCl_3$) δ 12.2, 127.2, 127.6, 129.1, 135.4, 142.4, 148.7; HRMS (ESI-TOF) calcd for $C_{11}H_{10}Cl_2N_4 [M+H]^+$: 269.0361, found: 269.0353; IR (ATR, cm^{-1}) 3188, 3089, 2958, 2881, 2821, 2310, 1405, 1327, 1256, 893, 771.

(*E*)-4-((2,4-Difluorophenyl)diazenyl)-3,5-dimethyl-1H-pyrazole (**35d**):

Yellow solid, mp = 185-187 °C, 184.3 mg, 78% yield. 1H NMR (400 MHz, $CDCl_3$) δ 2.63 (s, 6H), 6.91-7.00 (m, 2H), 7.70-7.76 (m, 1H); ^{13}C NMR (100 MHz, $CDCl_3$) δ 12.2, 104.5 ($J = 25.5$ Hz), 111.5 ($J = 22.4$ Hz), 118.1 ($J = 9.8$ Hz), 138.3 ($J = 4.0$ Hz), 141.9, 159.6 ($J = 216.8, 4.6$ Hz), 163.4 ($J = 246.1, 11.4$ Hz); HRMS (ESI-TOF) calcd for $C_{11}H_{10}F_2N_4 [M+H]^+$: 237.0952, found: 237.0941; IR (ATR, cm^{-1}) 3430, 3198, 3108, 2882, 2312, 1404, 1261, 961, 848.

(*E*)-4-((2,5-Difluorophenyl)diazenyl)-3,5-dimethyl-1H-pyrazole (**36d**):

Yellow solid, mp = 196 -198 °C, 127.6 mg, 54% yield. 1H NMR (400 MHz, $CDCl_3$) δ 2.63 (s, 6H), 7.04-7.10 (m, 1H), 7.17-7.23 (td, $J = 9.3, 4.6$ Hz, 1H), 7.41-7.46 (m, 1H); ^{13}C NMR (100 MHz, $CDCl_3$) δ 12.2, 103.4 ($J = 24.9$ Hz), 116.9 ($J = 25.0, 8.1$ Hz), 117.6 ($J = 22.5, 8.5$ Hz), 135.4, 141.9 ($J = 5.9, 2.8$ Hz), 142.3, 155.7 ($J = 250.3, 2.4$ Hz), 158.9 ($J = 242.3, 2.3$ Hz); HRMS (ESI-TOF) calcd for $C_{11}H_{10}F_2N_4 [M+H]^+$: 237.0952, found: 237.0944; IR (ATR, cm^{-1}) 3192, 3113, 2876, 2819, 2310, 1388, 1240, 869, 725.

(*E*)-4-((2,6-Difluorophenyl)diazenyl)-3,5-dimethyl-1H-pyrazole (**37d**):

Yellow solid, mp = 145-148 °C, 125.2 mg, 53% yield. 1H NMR (400 MHz, $CDCl_3$) δ 2.61 (s, 6H), 7.00-7.04 (m, 2H), 7.22-7.28 (m, 1H); ^{13}C NMR (100 MHz, $CDCl_3$) δ 12.2, 112.3 ($J = 18.2, 5.6$ Hz), 128.5 ($J = 10.1$ Hz), 132.0, 136.2, 142.1, 155.7 ($J = 255.2, 4.8$ Hz); HRMS (ESI-TOF) calcd for $C_{11}H_{10}F_2N_4 [M+H]^+$: 237.0952, found: 237.0941; IR (ATR, cm^{-1}) 3204, 2971, 2913, 2301, 1405, 1233, 1014, 774.

(E)-4-((3,5-Difluorophenyl)diazenyl)-3,5-dimethyl-1H-pyrazole (38d):

Yellow solid, mp = 185-190 °C, 205.5 mg, 87% yield. ¹H NMR (400 MHz, CDCl₃) δ 2.62 (s, 6H), 6.83-6.87 (tt, *J* = 8.5, 2.4 Hz, 1H), 7.33-7.35 (m, 2H); ¹³C NMR (100 MHz, CDCl₃) δ 12.3, 104.3 (*J* = 26.0 Hz), 105.0 (*J* = 19.3, 7.0 Hz), 134.5, 142.4, 155.6 (*J* = 9.0 Hz), 163.3 (*J* = 246.1, 13.2 Hz); HRMS (ESI-TOF) calcd for C₁₁H₁₀F₂N₄ [M+H]⁺: 237.0952, found: 237.0942; IR (ATR, cm⁻¹) 3193, 3098, 3046, 2878, 2822, 1406, 1256, 856, 770, 657.

The general procedure of synthesis of (E)-1,3,5-trimethyl-4-(phenyldiazenyl)-1H-pyrazole Derivatives:

A mixture of arylazopyrazole (1.0 mmol) and 1 ml of DMSO was taken in a round bottom flask. To this solution, pulverized potassium hydroxide (3.0 mmol) was added and the resulting suspension was stirred for 1 h at 80 °C. Then cooled to room temperature, and then methyl iodide (1.2 mmol) in 1 ml of DMSO was added over a period of 1 h at 20 °C. The mixture was then allowed to stir for 3 h and monitored by TLC. After completion of the reaction, the product was extracted with chloroform and water, evaporated and column purification. (Eluent: 1:9 ethylacetate/n-hexane).

(E)-1,3,5-Trimethyl-4-(phenyldiazenyl)-1H-pyrazole (1e):

Orange solid, mp = 60-63 °C, 189 mg, 88% yield. ¹H NMR (400MHz, CDCl₃) δ 2.50 (s, 3H), 2.57 (s, 3H), 3.77 (s, 3H), 7.35-7.38 (t, *J* = 7.0 Hz, 1H), 7.44-7.48 (t, *J* = 7.9 Hz, 2H), 7.77-7.79 (d, *J* = 8.1 Hz, 2H); ¹³C NMR (100 MHz, CDCl₃) δ 10.1, 14.0, 36.1, 121.9, 129.0, 129.4, 135.2, 138.9, 142.5, 153.7; HRMS (ESI-TOF) calcd for C₁₂H₁₄N₄ [M+H]⁺: 215.1297, found: 215.1291; IR (ATR, cm⁻¹) 1556, 1513, 1408, 766.

(E)-4-((3-Fluorophenyl)diazenyl)-1,3,5-trimethyl-1H-pyrazole (3e):

Yellow solid, mp = 45-48 °C, 191 mg, 82% yield. ¹H NMR (400MHz, CDCl₃) δ 2.48 (s, 3H), 2.56 (s, 3H), 3.77 (s, 3H), 7.03-7.07 (t, *J* = 7.2 Hz, 1H), 7.38-7.47 (m, 2H), 7.58-7.60 (d, *J* = 7.9 Hz, 1H); ¹³C NMR (100 MHz, CDCl₃) δ 10.0, 14.0, 36.1, 106.9 (d, *J* = 22.5 Hz), 116.0 (d, *J* = 22.0 Hz), 119.5 (d, *J* = 2.7 Hz), 130.1 (d, *J* = 8.6 Hz), 135.1, 139.6, 142.6, 155.3 (d, *J* = 6.8 Hz), 155.3 (d, *J* = 6.8 Hz), 163.4 (d, *J* = 244.9 Hz); HRMS (ESI-TOF) calcd for C₁₂H₁₃FN₄ [M+H]⁺: 233.1202, found: 233.1191; IR (ATR, cm⁻¹) 1556, 1514, 1406, 1112, 784.

(E)-4-((3-Chlorophenyl)diazenyl)-1,3,5-trimethyl-1H-pyrazole (6e):

Yellow solid, mp = 90-93 °C, 225 mg, 90% yield. ¹H NMR (400MHz, CDCl₃) δ 2.48 (s, 3H), 2.57 (s, 3H), 3.78 (s, 3H), 7.31-7.40 (m, 2H), 7.66-7.68 (d, *J* = 7.8 Hz, 1H), 7.75 (br, 1H); ¹³C NMR (100 MHz, CDCl₃) δ 10.1, 14.1, 36.2, 120.8, 121.4, 129.1, 130.0, 135.0, 135.2, 139.7, 142.6, 154.6; HRMS (ESI-TOF) calcd for C₁₂H₁₃ClN₄ [M+H]⁺: 249.0907, found: 249.0897; IR (ATR, cm⁻¹) 1556, 1514, 1403, 693, 784.

(E)-4-((3-Bromophenyl)diazenyl)-1,3,5-trimethyl-1H-pyrazole (9e):

Yellow solid, mp = 99-102 °C, 275 mg, 94% yield. ¹H NMR (400MHz, CDCl₃) δ 2.48 (s, 3H), 2.58 (s, 3H), 3.79 (s, 3H), 7.31-7.35 (t, *J* = 7.9 Hz, 1H), 7.47-7.49 (d, *J* = 7.6 Hz, 1H), 7.71-7.73 (d, *J* = 7.8 Hz, 1H), 7.90 (s, 1H); ¹³C NMR (100 MHz, CDCl₃) δ 10.1, 14.1, 36.2, 121.9, 123.1, 123.8, 130.4, 132.0, 135.2, 139.7, 142.7, 154.7; HRMS (ESI-TOF) calcd for C₁₂H₁₃BrN₄ [M+H]⁺: 293.0402, 295.0381 found: 293.0392, 295.0371; IR (ATR, cm⁻¹) 1514, 1555. 1401, 783, 703.

(E)-1,3,5-Trimethyl-4-((3-(trifluoromethyl)phenyl)diazenyl)-1H-pyrazole (15e):

Yellow solid, mp = 100-103 °C, 255 mg, 90% yield. ¹H NMR (400MHz, CDCl₃) δ 2.51 (s, 3H), 2.61 (s, 3H), 3.81 (s, 3H), 7.56-7.64 (m, 2H), 7.95-7.97 (d, *J* = 7.6 Hz, 1H), 8.03 (s, 1H); ¹³C NMR (100 MHz, CDCl₃) δ 10.1, 14.1, 36.1, 118.7 (q, *J* = 3.8 Hz), 122.8, 125.1, 125.6 (q, *J* = 2.4 Hz), 129.5, 131.5 (q, *J* = 32.3 Hz), 135.3, 139.8, 142.7, 153.7; HRMS (ESI-TOF) calcd for C₁₃H₁₃F₃N₄ [M+H]⁺: 283.1171, found: 283.1163; IR (ATR, cm⁻¹) 1554, 1433, 1323, 1111, 801.

(E)-4-((3-Methoxyphenyl)diazenyl)-1,3,5-trimethyl-1H-pyrazole (18e):

Yellow solid, mp = 70-74 °C, 275 mg, 85% yield. ¹H NMR (400MHz, CDCl₃) δ 2.50 (s, 3H), 2.57 (s, 3H), 3.78 (s, 3H), 3.88 (s, 3H), 6.93-6.95 (d, *J* = 6.9 Hz, 1H), 7.33-7.42 (m, 3H); ¹³C NMR (100 MHz, CDCl₃) δ 10.1, 14.0, 36.1, 55.5, 105.6, 115.66, 115.69, 129.7, 135.2, 139.0, 142.6, 155.0, 160.3; HRMS (ESI-TOF) calcd for C₁₃H₁₆N₄O [M+H]⁺: 245.1402, found: 245.1390; IR (ATR, cm⁻¹) 1556, 1514, 1407, 1130, 785.

2.8 References:

1. Bandara, H. M. D.; Burdette, S. C. *Chem. Soc. Rev.* **2012**, *41*, 1809-1825.
2. For example: (a) Bleger, D.; Schwarz, J.; Brouwer, A. M.; Hecht, S. *J. Am. Chem. Soc.* **2012**, *134*, 20597-20600. (b) Beharry, A.; Sadowski, O.; Woolley, G. A. *J. Am. Chem. Soc.* **2011**, *133*, 19684-19687. (c) Samanta, S.; McCormick, T. M.; Schmidt, S. K.; Seferos, D. S.; Woolley, G. A. *Chem. Commun.* **2013**, *49*, 10314-10316. (d) Bleger, D.; Hecht, S. *Angew. Chem., Int. Ed.* **2015**, *54*, 11338-11349.
3. For example: (a) Huang, Y. G.; Shiota, Y.; Su, S. Q.; Wu, S. Q.; Yao, Z. S.; Li, G. L.; Kanegawa, S.; Kang, S.; Kamachi, T.; Yoshizawa, K.; Ariga, K.; Sato, O. *Angew. Chem., Int. Ed.* **2016**, *55*, 14628-14632. (b) Venkataramani, S.; Jana, U.; Dommaschk, M.; Soennichsen, F. D.; Tucek, F.; Herges, R. *Science* **2011**, *331*, 445-448. (c) Dommaschk, M.; Peters, M.; Gutzeit, F.; Schuett, C.; Naether, C.; Soennichsen, F. D.; Tiwari, S.; Riedel, C.; Boretius, S.; Herges, R. *J. Am. Chem. Soc.* **2015**, *137*, 7552-7555. (d) Wang, Y.; Ge, X.; Schull, G.; Berndt, R.; Tang, H.; Bornholdt, C.; Koehler, F.; Herges, R. *J. Am. Chem. Soc.* **2010**, *132*, 1196-1197. (e) Iranpoor, N.; Firouzabadi, H.; Khalili, D.; Motevalli, S. *J. Org. Chem.* **2008**, *73*, 4882-4887.
4. For example: (a) Byabartta, P. *Int. J. Curr. Res. Chem. Pharm. Sci.* **2015**, *2*, 75-81. (b) Pandey, P.; Maheshwari, N.; Dave, A. *J. Liq. Chromatogr.* **1991**, *14*, 3311-3315. (c) Jain, R.; Agarwal, D. D.; Goyal, R. N.; Fresenius, Z. *Anal. Chem.* **1979**, *298*, 44. (d) Pradhan, S.; Mondal, S.; Sinha, C. *J. Indian Chem. Soc.* **2015**, *93*, 1067-1084. (e) Al-Saleh, B.; El-Asasery, M. A.; Elnagdi, M. H. *J. Chem. Res.* **2004**, 578-580. (f) Al-Shiekh, M. A.; Salah El-Din, A. M.; Hafez, E. A.; Elnagdi, M. H. *J. Heterocycl. Chem.* **2004**, *41*, 647-654. (g) Khound, S.; Das, P. *J. Indian J. Chem., Sect. B* **1998**, *37B*, 155-157.
5. Wendler, T.; Schuett, C.; Naether, C.; Herges, R. *J. Org. Chem.* **2012**, *77*, 3284-3287.
6. Weston, C. E.; Richardson, R. D.; Haycock, P. R.; White, A. J. P.; Fuchter, M. J. *J. Am. Chem. Soc.* **2014**, *136*, 11878-11881.
7. For example: (a) Weston, C. E.; Kramer, A.; Colin, F.; Yildiz, O.; Baud, M. G. J.; Meyer-Almes, F.J.; Fuchter, M. J. *ACS Infect. Dis.* **2017**, *3*, 152-161. (b) Stricker, L.; Fritz, E. C.; Peterlechner, M.; Doltsinis, N. L.; Ravoo, B. J. *J. Am. Chem. Soc.*

- 2016**, *138*, 4547-4554. (c) Ghebreyessus, K.; Cooper, S. M. Jr. *Organometallics* **2017**, *36*, 3360-3370.
8. Calbo, J.; Weston, C. E.; White, A. J. P.; Rzepa, H.; Contreras-García, J.; Fuchter, M. J. *J. Am. Chem. Soc.* **2017**, *139*, 1261-1274.
9. Simeth, N. A.; Crespi, S.; Fagnoni, M.; König, B. *J. Am. Chem. Soc.* **2018**, *140*, 2940-2946.
10. (a) Sharma, P.; Kumar, A.; Upadhyay, S.; Singh, J.; Sahu, V. *Med. Chem. Res.* **2010**, *19*, 589-602. (b) Marten, J.; Seichter, W.; Weber, E. *Z. Anorg. Allg. Chem.* **2005**, *631*, 869-877. (c) Burra, V. R.; Reddy, N. B.; Ravidranath, L. K. *Pharma Chem.* **2015**, *7*, 43-48. (d) Han, X.; Zhu, X.; Hong, Z.; Wei, L.; Ren, Y.; Wan, F.; Zhu, S.; Peng, H.; Guo, L.; Rao, L.; Feng, L.; Wan, J. *J. Chem. Inf. Model.* **2017**, *57*, 1426-1438. (e) Kunitomo, J.; Yoshikawa, M.; Fushimi, M.; Kawada, A.; Quinn, J. F.; Oki, H.; Kokubo, H.; Kondo, M.; Nakashima, K.; Kamiguchi, N.; Suzuki, K.; Kimura, H.; Taniguchi, T. *J. Med. Chem.* **2014**, *57*, 9627-9643. (f) Kale, P. D. *J. Chem. Pharm. Res.* **2013**, *5*, 130-134.
11. Cho, E. N.; Zhitomirsky, D.; Han, G. G. D.; Liu, Y.; Grossman, J. C. *ACS Appl. Mater. Interfaces* **2017**, *9*, 8679-8687.
12. (a) Taft, R. W. *J. Am. Chem. Soc.* **1952**, *74*, 2729-2732. (b) Fujita, T.; Takayama, C.; Nakajima, M. *J. Org. Chem.* **1973**, *38*, 1623-1630.
13. Hammett, L. P. *J. Am. Chem. Soc.* **1937**, *59*, 96-103.
14. Nishimura, N.; Sueyoshi, T.; Yamanaka, H.; Imai, E.; Yamamoto, S.; Hasegawa, S. *Bull. Chem. Soc. Jpn.* **1976**, *49*, 1381-1387.
15. (a) Thordarson, P. *Chem. Soc. Rev.* **2011**, *40*, 1305-1323. (b) Hibbert, D. B.; Thordarson, P. *Chem. Commun.* **2016**, *52*, 12792-12805. (c) The non-linear fitting has been performed using the web-based bindfit program available as open access in the website: www.supramolecular.org
16. (a) Lubbe, A. S.; Kistemaker, J. C. M.; Smits, E. J.; Feringa, B. L. *Phys. Chem. Chem. Phys.* **2016**, *18*, 26725-26735. (b) Gille, K.; Knoll, H.; Quitzsch, K. *Int. J. Chem. Kinet.* **1998**, *31*, 337-350. (c) Serra, F.; Terentjev, E. M. *Macromolecules* **2008**, *41*, 981-986.
17. *Solvents and Solvent Effects in Organic Chemistry*; Reichardt, C.; Welton, T., 4th Ed.; Wiley-VCH: Weinheim, 2011.
18. Kamlet, M. J.; Abboud, J. L. M.; Abraham, M. H.; Taft, R. W. *J. Org. Chem.* **1983**, *48*, 2877-2887.

19. Marcus, Y. *Chem. Soc. Rev.* **1993**, 22, 409-416.
20. Cerón-Carrasco, J. P.; Jacquemin, D.; Laurence, C.; Planchat, A.; Reichardt, C.; Sraïdi, K. *J. Phys. Org. Chem.* **2014**, 27, 512-518.
21. Otsuki, J.; Suwa, K.; Sarker, K. K.; Sinha, C. *J. Phys. Chem. A* **2007**, 111, 1403-1409.

Appendix 2A:

Table 2A.1. Comparison of rate constants of selected substituted phenylazopyrazoles obtained from UV-Vis, NMR spectroscopies and computations^a

S. No	Compound No	Substitution	UV-Vis Data			NMR Data			Computational Data (Weight Averaged)	
			[μM] mol.L ⁻¹	k/min ⁻¹	t _{1/2} (min)	[mM] mol. L ⁻¹	k/min ⁻¹	t _{1/2} (min)	k/s ⁻¹	t _{1/2} (min)
1.	1d	Nil	37.2	1.31 x 10 ⁻³ ± 5.99 x 10 ⁻⁶	527.4 ± 2.4	21.0	7.50 x 10 ⁻² ± 1.85 x 10 ⁻²	9.2 ± 2.3	2.87 x 10 ⁻⁴ (1.53 x 10 ⁻⁴)	40.2 (75.2)
2.	3d	3-F	29.5	3.35 x 10 ⁻⁴ ± 2.22 x 10 ⁻⁵	2068.5 ± 137.3	10.1	2.58 x 10 ⁻² ± 2.20 x 10 ⁻³	26.8 ± 2.3	2.13 x 10 ⁻³ (2.56 x 10 ⁻³)	5.4 (4.5)
3.	6d	3-Cl	19.9	1.14 x 10 ⁻² ± 7.89 x 10 ⁻⁵	60.6 ± 0.4	12.8	3.08 x 10 ⁻³ ± 4.65 x 10 ⁻⁴	224.8 ± 33.9	1.83 x 10 ⁻³ (3.30 x 10 ⁻³)	6.3 (3.5)
4.	9d	3-Br	24.4	5.87 x 10 ⁻² ± 4.82 x 10 ⁻⁴	11.8 ± 0.1	22.2	1.32 x 10 ⁻² ± 4.54 x 10 ⁻⁴	52.2 ± 1.8	1.99 x 10 ⁻³ (2.81 x 10 ⁻³)	5.8 (4.1)
5.	15d	3-CF ₃	24.7	2.65 x 10 ⁻³ ± 9.46 x 10 ⁻⁶	261.9 ± 0.9	8.2	1.87 x 10 ⁻² ± 7.10 x 10 ⁻⁴	37.0 ± 1.4	2.75 x 10 ⁻³ (1.08 x 10 ⁻³)	4.2 (10.6)
6.	18d	3-OCH ₃	24.7	2.97 x 10 ⁻³ ± 2.00 x 10 ⁻⁵	233.6 ± 1.6	14.8	2.68 x 10 ⁻² ± 1.02 x 10 ⁻³	25.8 ± 0.9	4.71 x 10 ⁻⁴ (1.44 x 10 ⁻⁴)	24.5 (80.0)
7.	4d	4-F	27.5	6.13 x 10 ⁻⁵ ± 1.85 x 10 ⁻⁵	11301.9 ± 3410.6	9.2	3.63 x 10 ⁻³ ± 1.02 x 10 ⁻³	190.9 ± 53.6	4.84 x 10 ⁻⁵ (3.35 x 10 ⁻⁵)	238.5 (343.9)
8.	7d	4-Cl	23.0	3.59 x 10 ⁻⁴ ± 1.28 x 10 ⁻⁵	1929.6 ± 68.8	16.2	5.11 x 10 ⁻³ ± 6.95 x 10 ⁻⁴	135.7 ± 18.5	3.98 x 10 ⁻⁴ (7.00 x 10 ⁻⁴)	29.0 (16.5)
9.	10d	4-Br	31.1	1.79 x 10 ⁻³ ± 5.39 x 10 ⁻⁶	386.8 ± 1.1	7.9	6.17 x 10 ⁻³ ± 5.28 x 10 ⁻⁴	112.4 ± 9.6	6.95 x 10 ⁻⁴ (1.07 x 10 ⁻³)	16.6 (10.7)
10.	16d	4-CF ₃	29.3	2.96 x 10 ⁻² ± 1.15 x 10 ⁻⁴	23.4 ± 0.1	12.7			5.77 x 10 ⁻² (1.92 x 10 ⁻¹)	0.2 (0.06)
11.	19d	4-OCH ₃	16.6	5.72 x 10 ⁻⁴ ± 1.53 x 10 ⁻⁵	1211.8 ± 32.5	13.0	3.52 x 10 ⁻² ± 5.68 x 10 ⁻⁴	19.6 ± 0.3	1.25 x 10 ⁻⁵ (5.77 x 10 ⁻⁶)	920.3 (2001.5)
12.	1e	Nil	34.0	1.86 x 10 ⁻³ ± 1.42 x 10 ⁻⁴	372.1 ± 28.6	-	-	-	1.279 x 10 ⁻³	9.0
13.	3e	3-F	47.0	1.06 x 10 ⁻³ ± 5.28 x 10 ⁻⁵	655.1 ± 32.7	11.0	9.28 x 10 ⁻² ± 7.82 x 10 ⁻³	7.5 ± 0.6	1.330 x 10 ⁻²	0.9
14.	6e	3-Cl	37.0	1.41 x 10 ⁻³ ± 2.28 x 10 ⁻⁴	491.2 ± 79.6	8.9	2.96 x 10 ⁻² ± 8.57 x 10 ⁻⁴	23.4 ± 0.7	1.668 x 10 ⁻²	0.7
15.	9e	3-Br	32.0	9.29 x 10 ⁻⁴ ± 1.80 x 10 ⁻⁴	745.5 ± 144.9	9.3	2.57 x 10 ⁻² ± 7.12 x 10 ⁻⁴	26.9 ± 0.7	1.983 x 10 ⁻²	0.6
16.	15e	3-CF ₃	36.0	2.09 x 10 ⁻³ ± 3.70 x 10 ⁻⁴	331.4 ± 58.8	9.7	3.15 x 10 ⁻³ ± 8.06 x 10 ⁻⁴	219.7 ± 56.2	9.267 x 10 ⁻³	1.2
17.	18e	3-OCH ₃	51.0	1.44 x 10 ⁻³ ± 2.77 x 10 ⁻⁴	480.7 ± 92.5	17.0	4.47 x 10 ⁻³ ± 1.25 x 10 ⁻³	155.0 ± 43.4	3.235 x 10 ⁻³	3.6

^aComputations have been performed at B3LYP/6-311G(d,p) at 298 K; Rate constant in s⁻¹ and half-life in min; Normal font - gas phase, and italics inside parentheses – in CH₃CN (solvent model).

Appendix 2B:

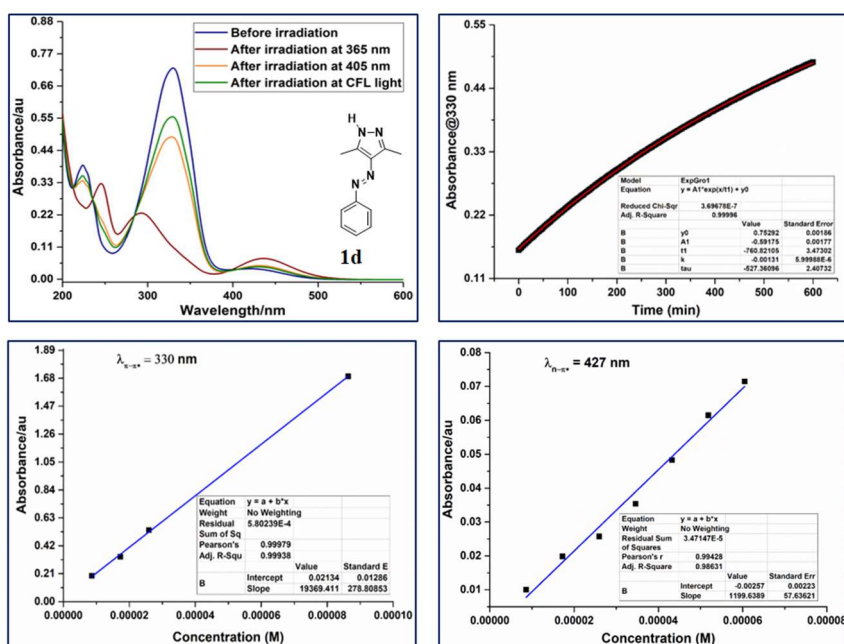


Figure 2B.1: UV-Vis photoswitching studies of **1d** (a) in CH_3CN solvent; (b) first-order kinetics plots; Estimation of molar extinction coefficient (in CH_3CN) for the (c) $\pi-\pi^*$ absorption and (d) $n-\pi^*$ absorption.

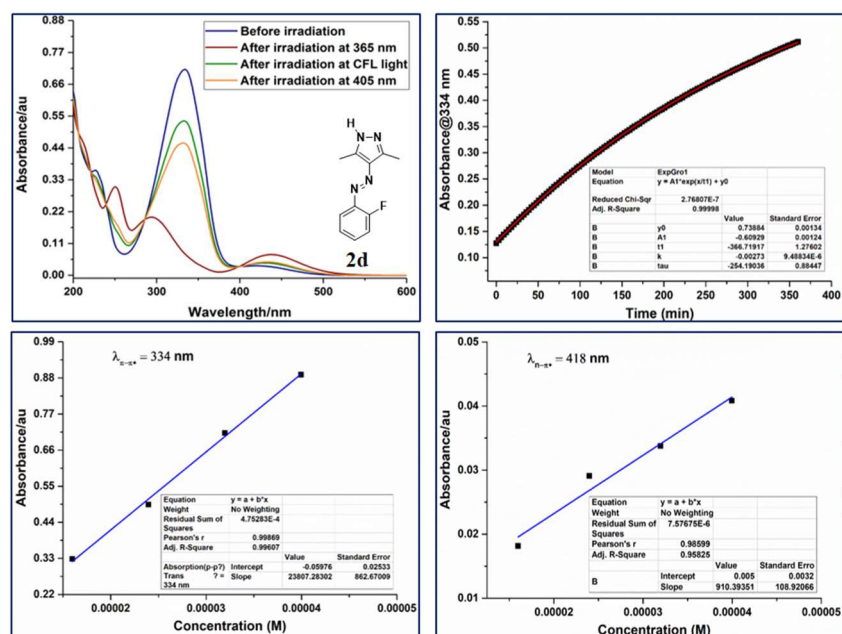


Figure 2B.2: UV-Vis photoswitching studies of **2d** (a) in CH_3CN solvent; (b) first-order kinetics plots; Estimation of molar extinction coefficient (in CH_3CN) for the (c) $\pi-\pi^*$ absorption and (d) $n-\pi^*$ absorption.

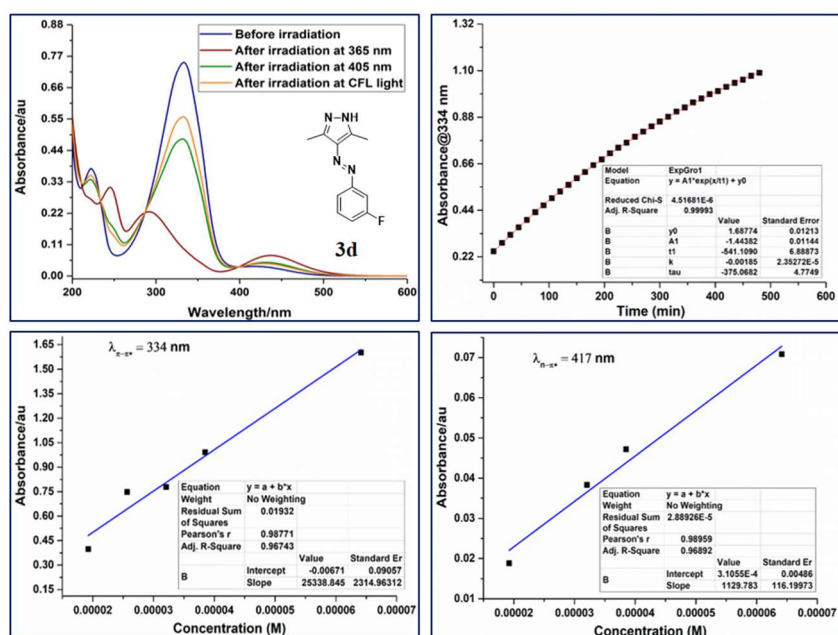


Figure 2B.3: UV-Vis photoswitching studies of **3d** (a) in CH_3CN solvent; (b) first-order kinetics plots; Estimation of molar extinction coefficient (in CH_3CN) for the (c) $\pi-\pi^*$ absorption and (d) $n-\pi^*$ absorption.

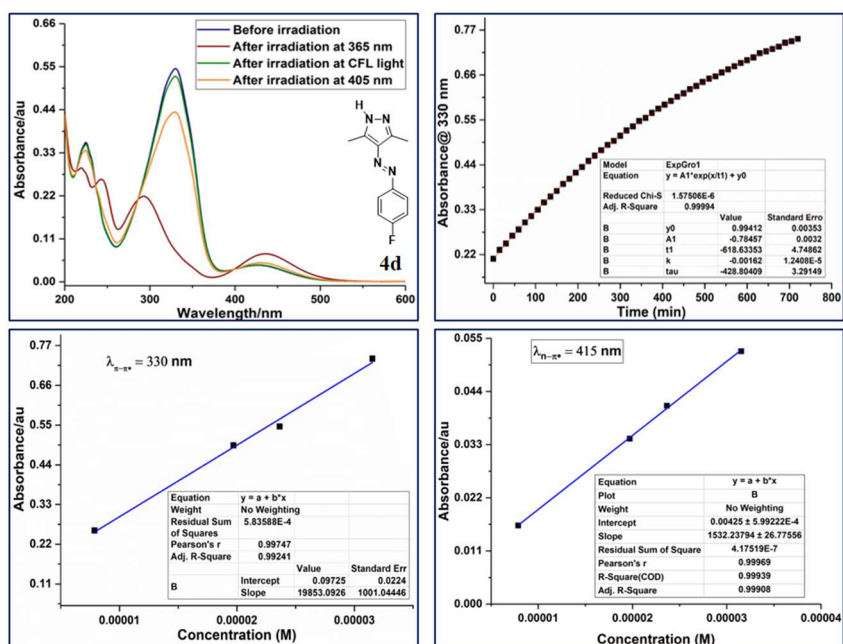


Figure 2B.4: UV-Vis photoswitching studies of **4d** (a) in CH_3CN solvent; (b) first-order kinetics plots; Estimation of molar extinction coefficient (in CH_3CN) for the (c) $\pi-\pi^*$ absorption and (d) $n-\pi^*$ absorption.

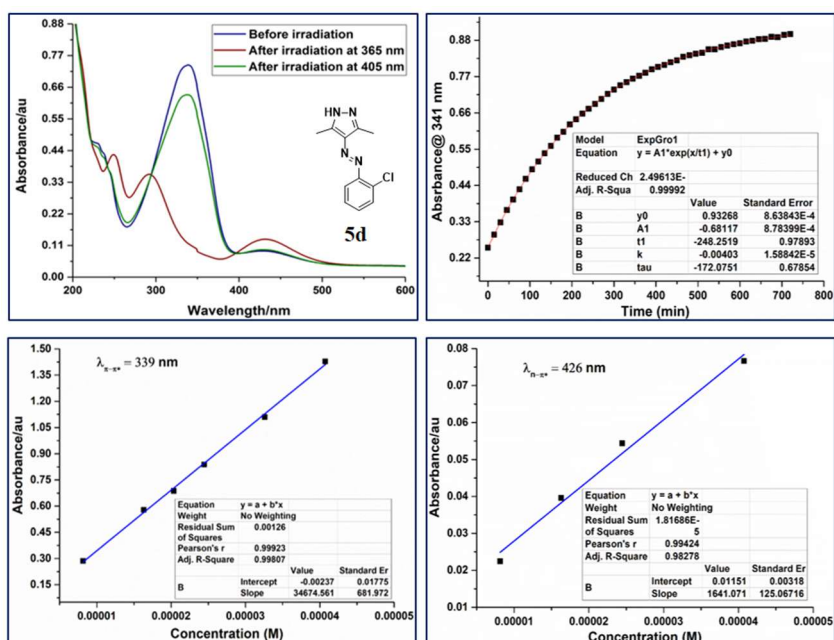


Figure 2B.5: UV-Vis photoswitching studies of **5d** (a) in CH₃CN solvent; (b) first-order kinetics plots; Estimation of molar extinction coefficient (in CH₃CN) for the (c) $\pi-\pi^*$ absorption and (d) $n-\pi^*$ absorption.

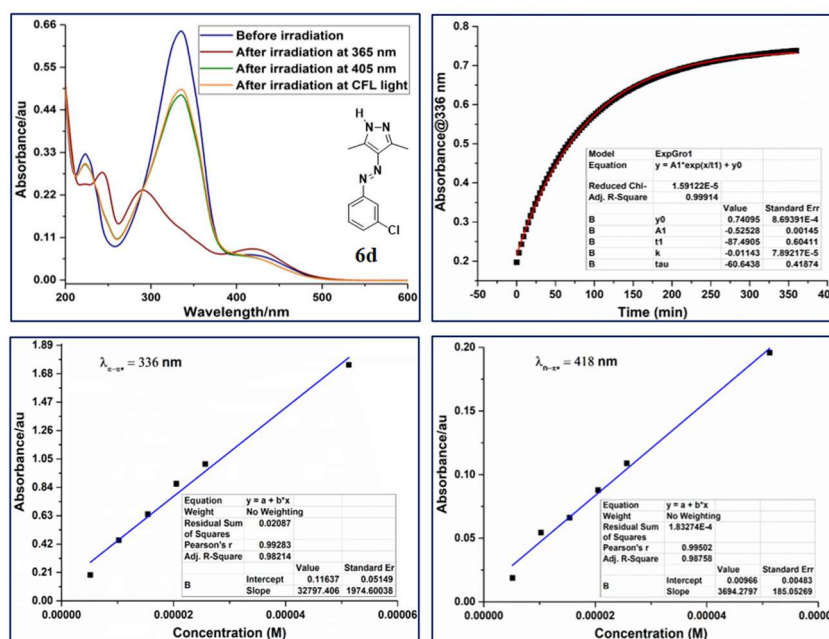


Figure 2B.6: UV-Vis photoswitching studies of **6d** (a) in CH₃CN solvent; (b) first-order kinetics plots; Estimation of molar extinction coefficient (in CH₃CN) for the (c) $\pi-\pi^*$ absorption and (d) $n-\pi^*$ absorption.

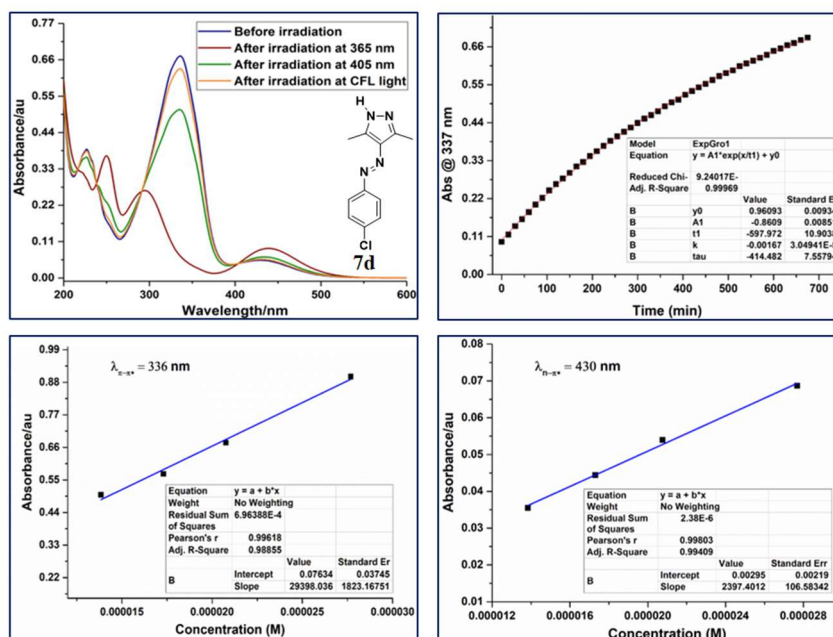


Figure 2B.7: UV-Vis photoswitching studies of **7d** (a) in CH₃CN solvent; (b) first-order kinetics plots; Estimation of molar extinction coefficient (in CH₃CN) for the (c) $\pi-\pi^*$ absorption and (d) $n-\pi^*$ absorption.

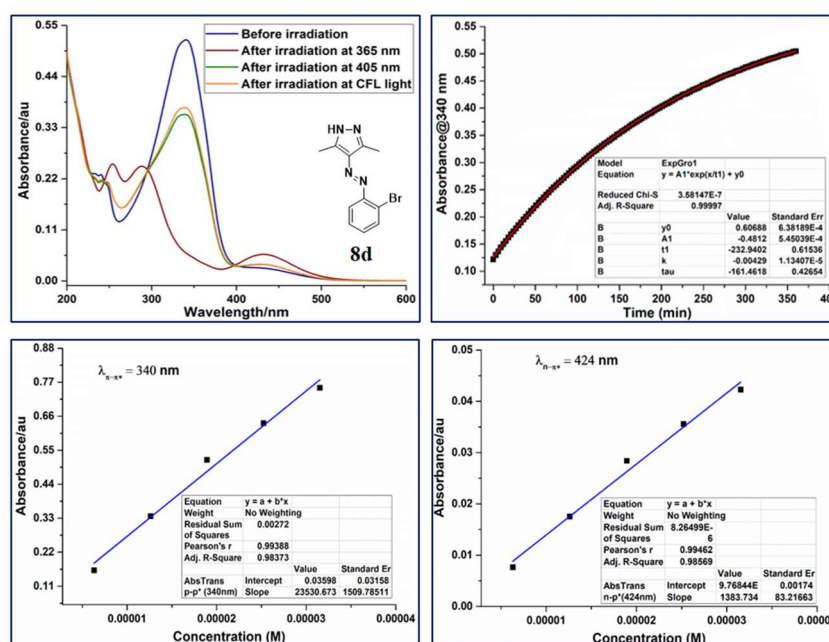


Figure 2B.8: UV-Vis photoswitching studies of **8d** (a) in CH₃CN solvent; (b) first-order kinetics plots; Estimation of molar extinction coefficient (in CH₃CN) for the (c) $\pi-\pi^*$ absorption and (d) $n-\pi^*$ absorption.

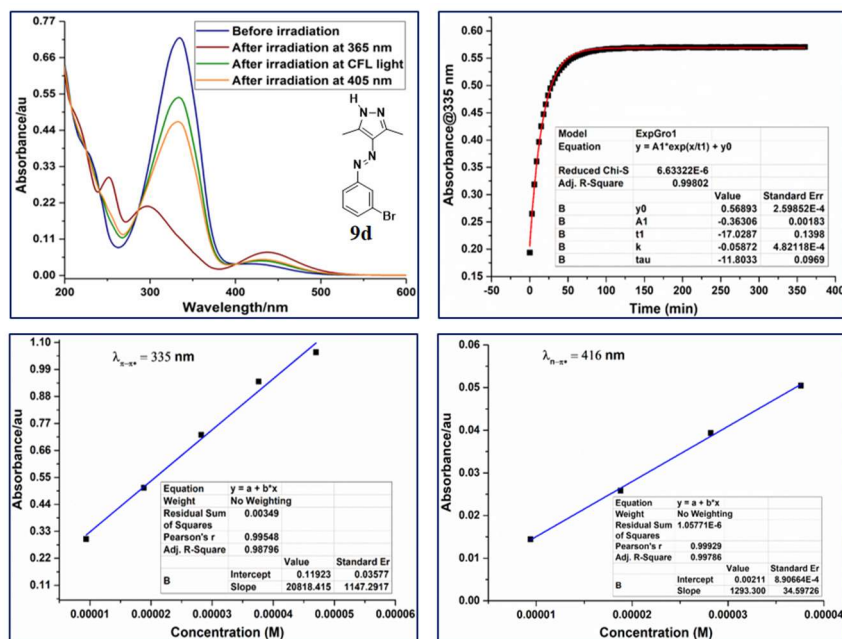


Figure 2B.9: UV-Vis photoswitching studies of **9d** (a) in CH₃CN solvent; (b) first-order kinetics plots; Estimation of molar extinction coefficient (in CH₃CN) for the (c) $\pi-\pi^*$ absorption and (d) $n-\pi^*$ absorption.

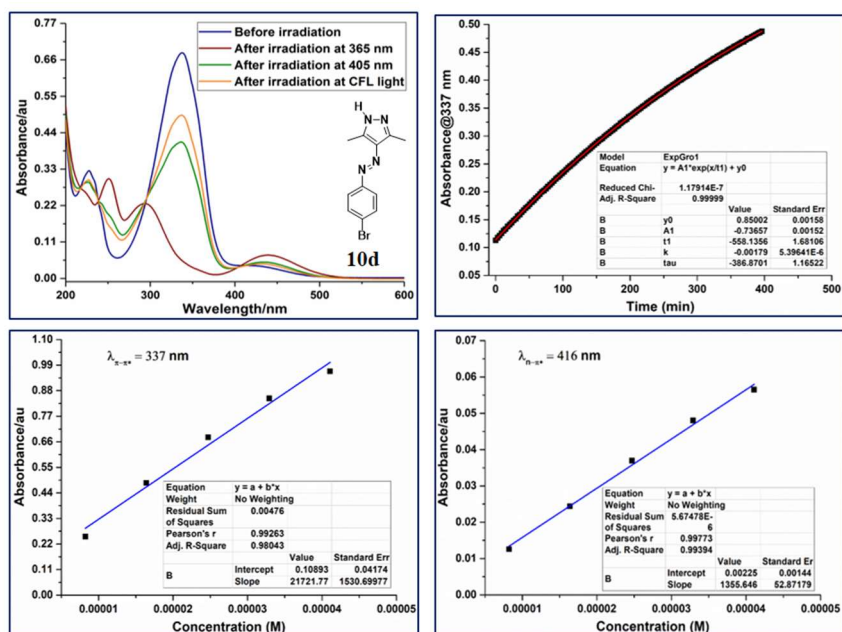


Figure 2B.10: UV-Vis photoswitching studies of **10d** (a) in CH₃CN solvent; (b) first-order kinetics plots; Estimation of molar extinction coefficient (in CH₃CN) for the (c) $\pi-\pi^*$ absorption and (d) $n-\pi^*$ absorption.

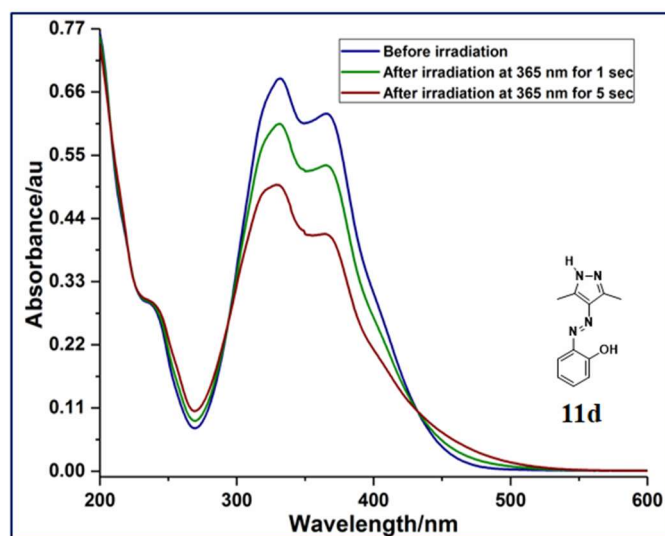


Figure 2B.11: UV-Vis photoswitching studies of **11d** (a) in CH_3CN solvent; (b) first-order kinetics plots; Estimation of molar extinction coefficient (in CH_3CN) for the (c) $\pi-\pi^*$ absorption and (d) $n-\pi^*$ absorption.

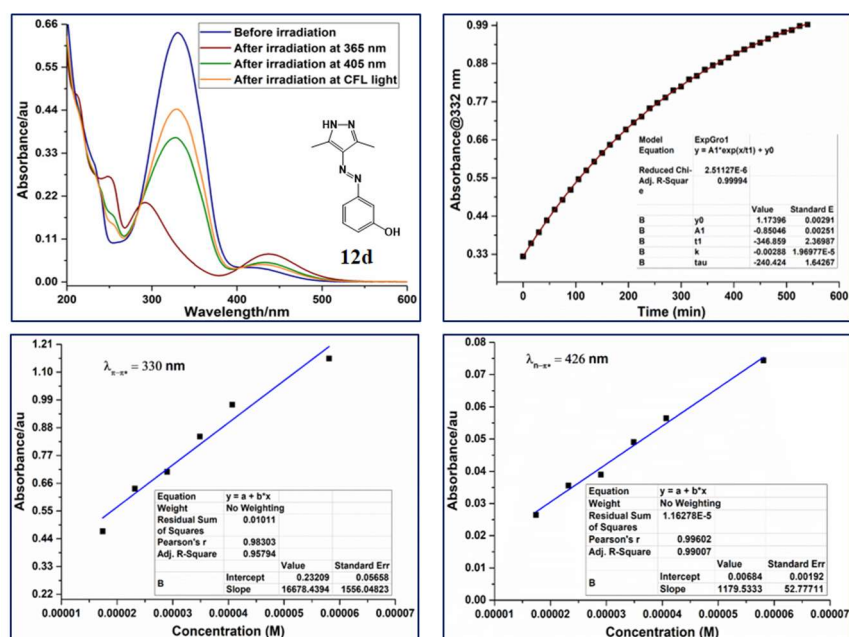


Figure 2B.12: UV-Vis photoswitching studies of **12d** (a) in CH_3CN solvent; (b) first-order kinetics plots; Estimation of molar extinction coefficient (in CH_3CN) for the (c) $\pi-\pi^*$ absorption and (d) $n-\pi^*$ absorption.

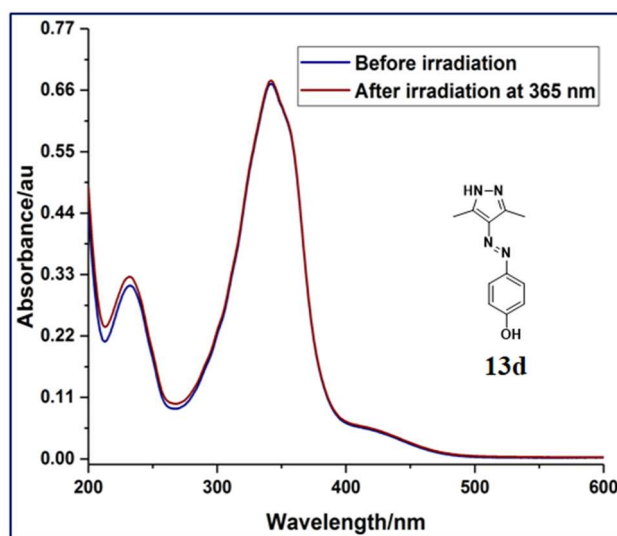


Figure 2B.13: UV-Vis photoswitching studies of **13d** (a) in CH_3CN solvent; (b) first-order kinetics plots; Estimation of molar extinction coefficient (in CH_3CN) for the (c) $\pi-\pi^*$ absorption and (d) $n-\pi^*$ absorption.

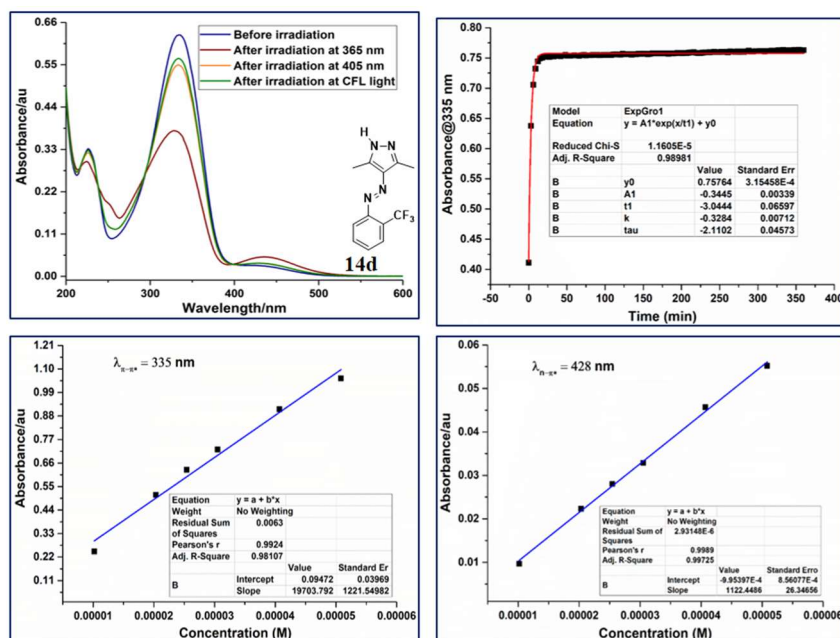


Figure 2B.14: UV-Vis photoswitching studies of **14d** (a) in CH_3CN solvent; (b) first-order kinetics plots; Estimation of molar extinction coefficient (in CH_3CN) for the (c) $\pi-\pi^*$ absorption and (d) $n-\pi^*$ absorption.

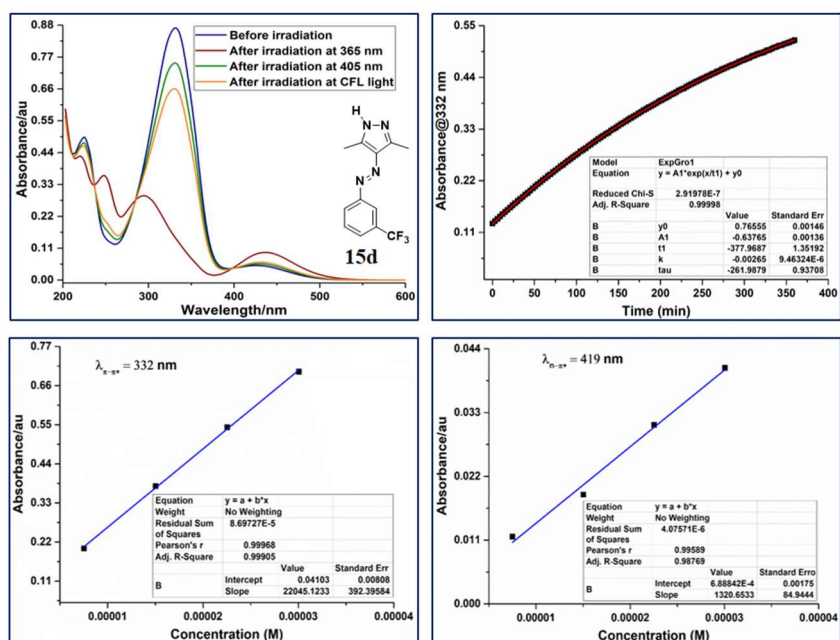


Figure 2B.15: UV-Vis photoswitching studies of **15d** (a) in CH_3CN solvent; (b) first-order kinetics plots; Estimation of molar extinction coefficient (in CH_3CN) for the (c) $\pi-\pi^*$ absorption and (d) $n-\pi^*$ absorption.

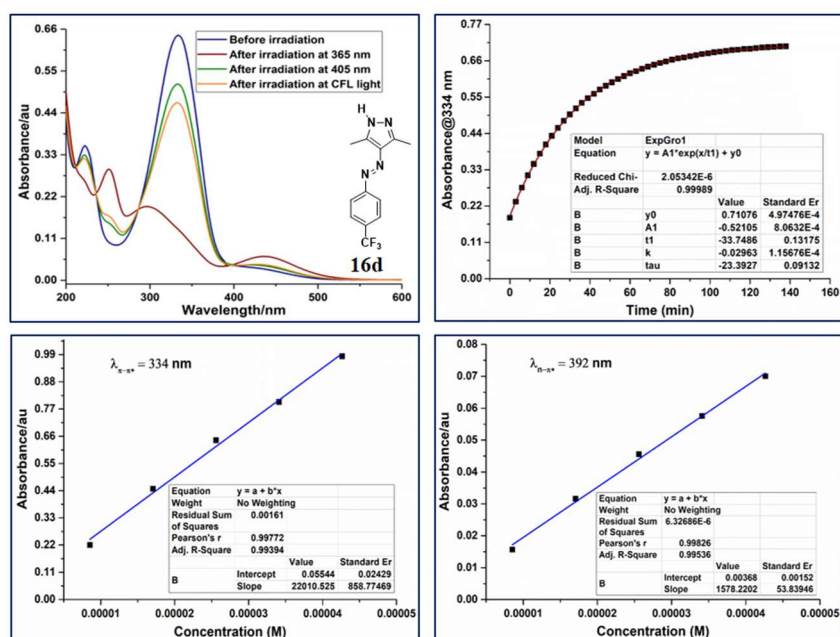


Figure 2B.16: UV-Vis photoswitching studies of **16d** (a) in CH_3CN solvent; (b) first-order kinetics plots; Estimation of molar extinction coefficient (in CH_3CN) for the (c) $\pi-\pi^*$ absorption and (d) $n-\pi^*$ absorption.

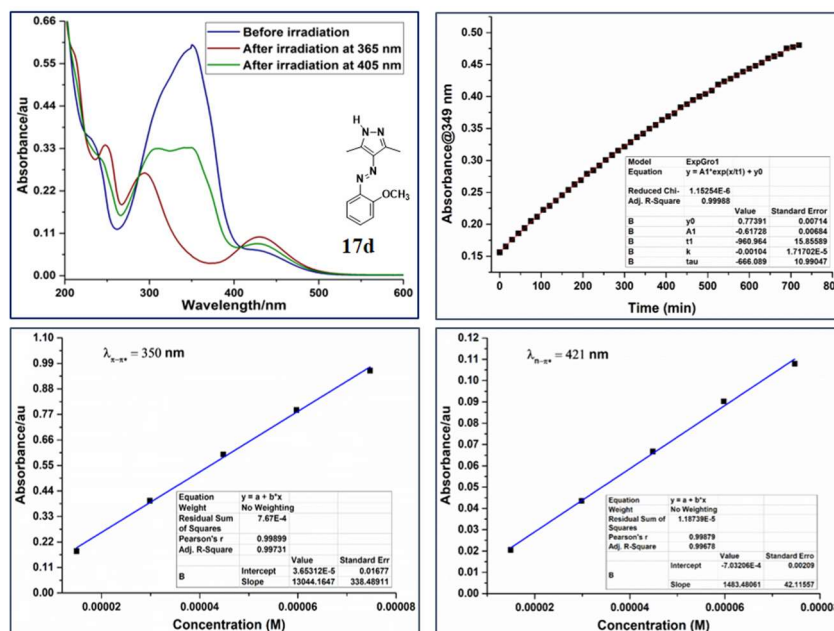


Figure 2B.17: UV-Vis photoswitching studies of **17d** (a) in CH₃CN solvent; (b) first-order kinetics plots; Estimation of molar extinction coefficient (in CH₃CN) for the (c) $\pi-\pi^*$ absorption and (d) $n-\pi^*$ absorption.

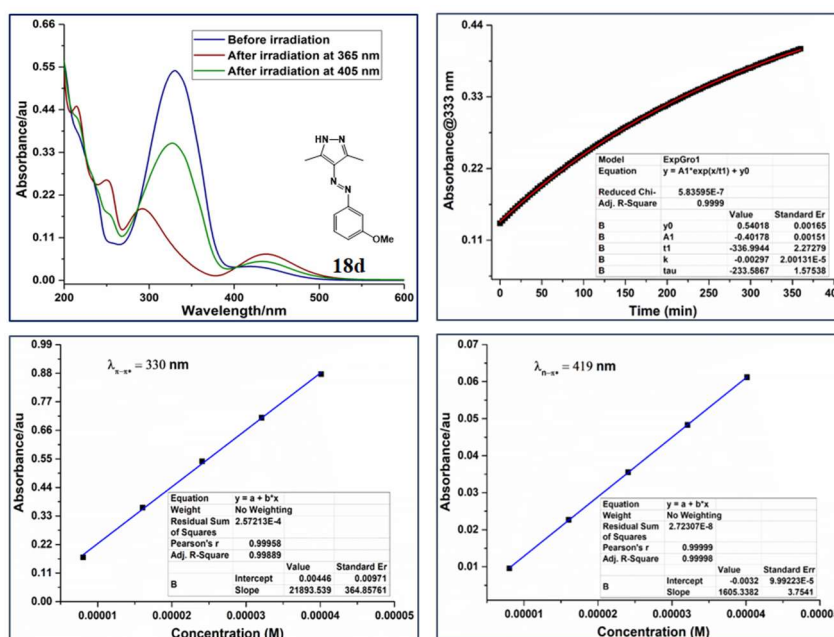


Figure 2B.18: UV-Vis photoswitching studies of **18d** (a) in CH₃CN solvent; (b) first-order kinetics plots; Estimation of molar extinction coefficient (in CH₃CN) for the (c) $\pi-\pi^*$ absorption and (d) $n-\pi^*$ absorption.

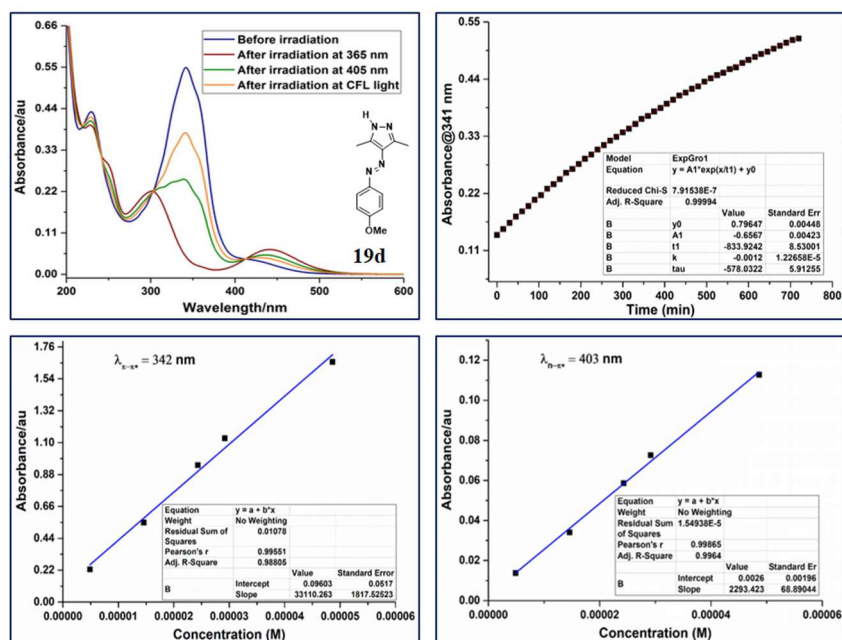


Figure 2B.19: UV-Vis photoswitching studies of **19d** (a) in CH₃CN solvent; (b) first-order kinetics plots; Estimation of molar extinction coefficient (in CH₃CN) for the (c) $\pi-\pi^*$ absorption and (d) $n-\pi^*$ absorption.

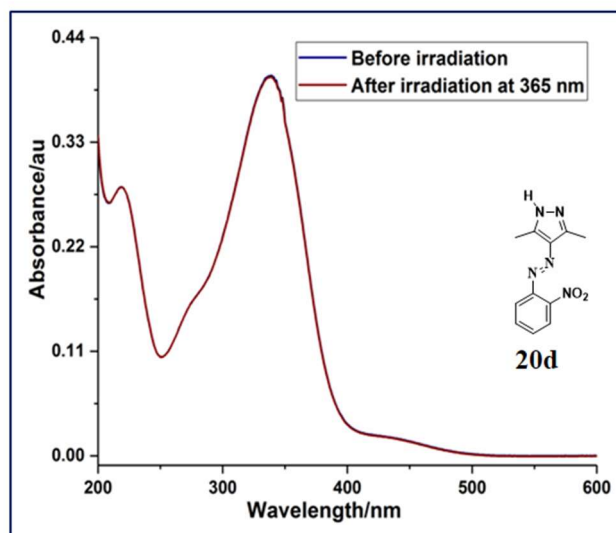


Figure 2B.20: UV-Vis photoswitching studies of **20d** (a) in CH₃CN solvent; (b) first-order kinetics plots; Estimation of molar extinction coefficient (in CH₃CN) for the (c) $\pi-\pi^*$ absorption and (d) $n-\pi^*$ absorption.

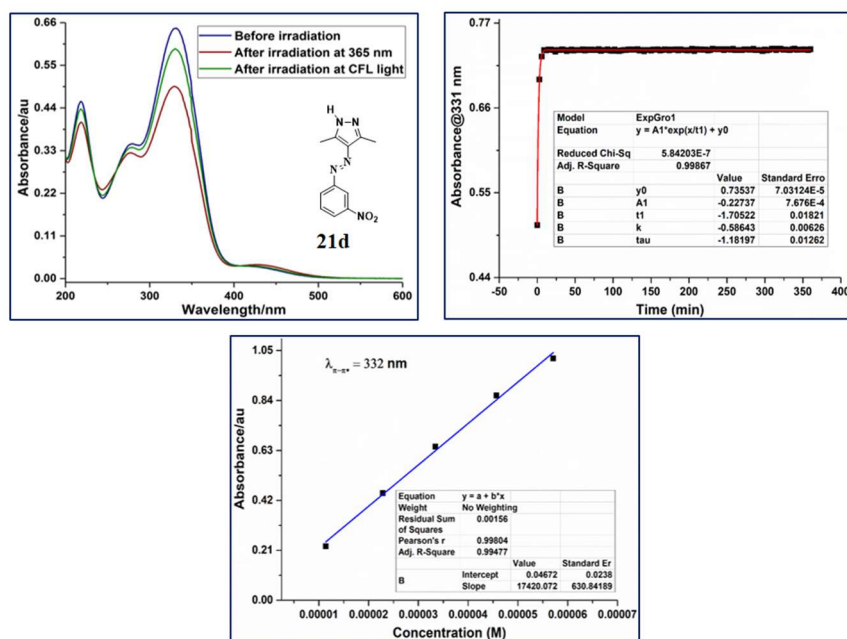


Figure 2B.21: UV-Vis photoswitching studies of **21d** (a) in CH_3CN solvent; (b) first-order kinetics plots; Estimation of molar extinction coefficient (in CH_3CN) for the (c) $\pi-\pi^*$ absorption and (d) $n-\pi^*$ absorption.

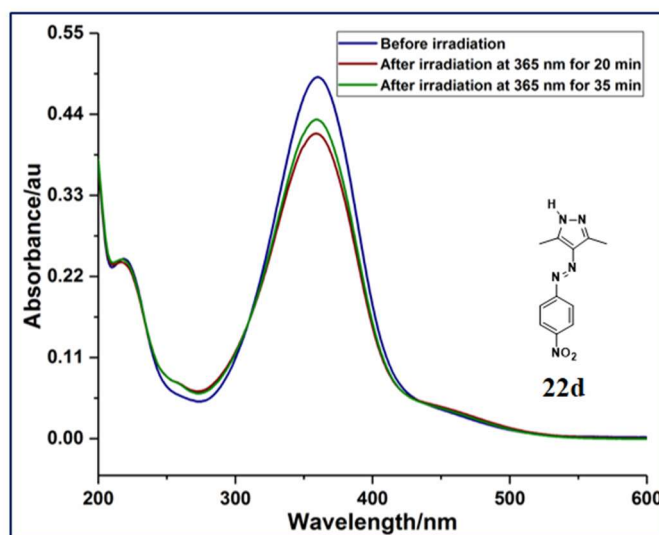


Figure 2B.22: UV-Vis photoswitching studies of **22d** (a) in CH_3CN solvent; (b) first-order kinetics plots; Estimation of molar extinction coefficient (in CH_3CN) for the (c) $\pi-\pi^*$ absorption and (d) $n-\pi^*$ absorption.

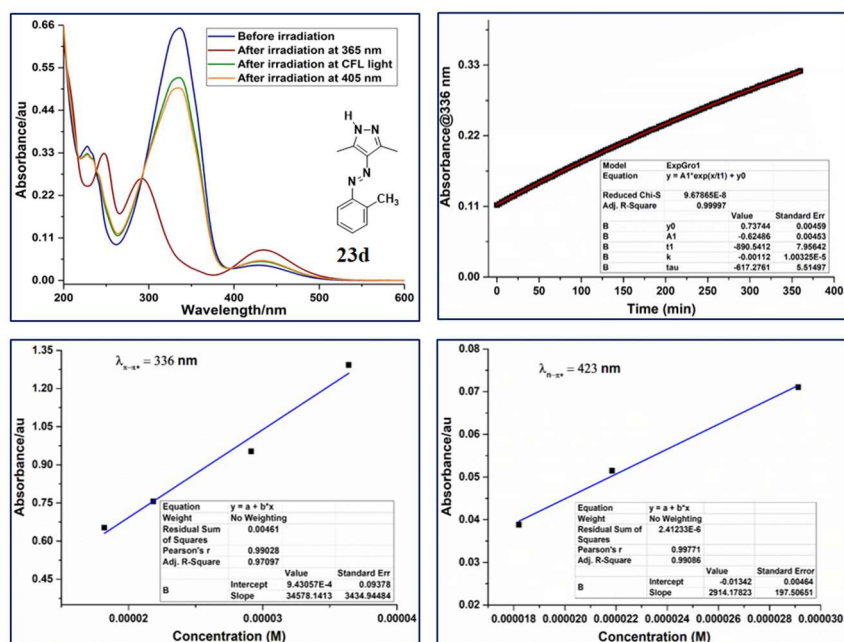


Figure 2B.23: UV-Vis photoswitching studies of **23d** (a) in CH₃CN solvent; (b) first-order kinetics plots; Estimation of molar extinction coefficient (in CH₃CN) for the (c) $\pi-\pi^*$ absorption and (d) $n-\pi^*$ absorption.

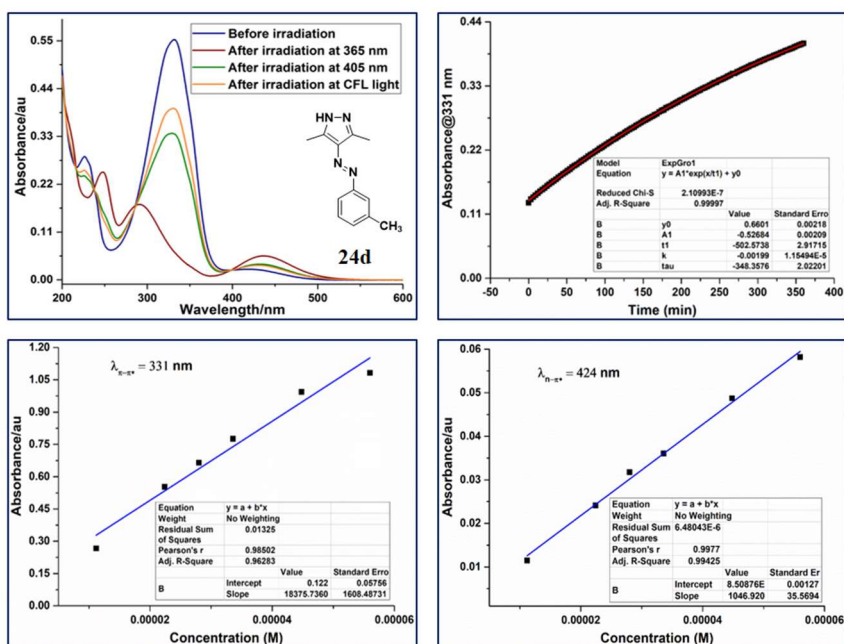


Figure 2B.24: UV-Vis photoswitching studies of **24d** (a) in CH₃CN solvent; (b) first-order kinetics plots; Estimation of molar extinction coefficient (in CH₃CN) for the (c) $\pi-\pi^*$ absorption and (d) $n-\pi^*$ absorption.

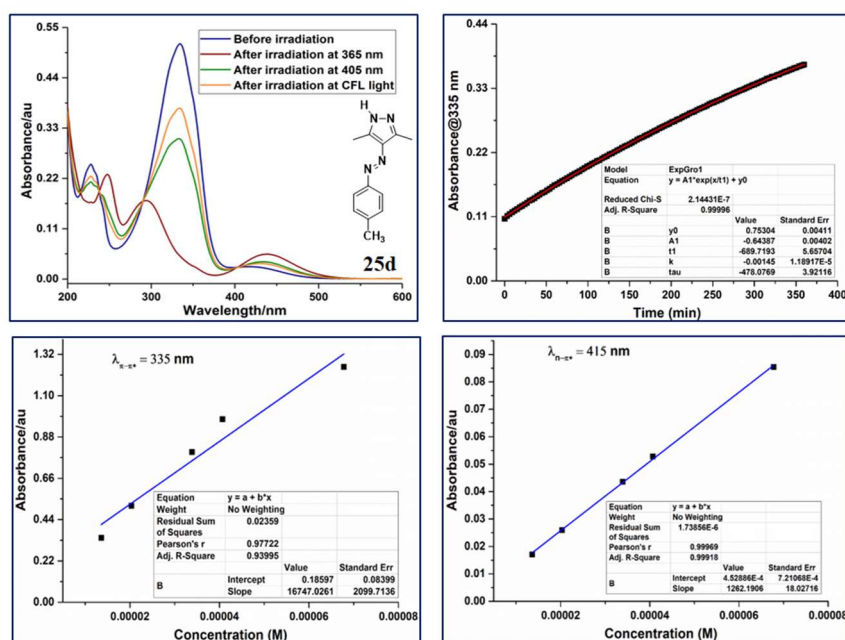


Figure 2B.25: UV-Vis photoswitching studies of **25d** (a) in CH_3CN solvent; (b) first-order kinetics plots; Estimation of molar extinction coefficient (in CH_3CN) for the (c) $\pi-\pi^*$ absorption and (d) $n-\pi^*$ absorption.

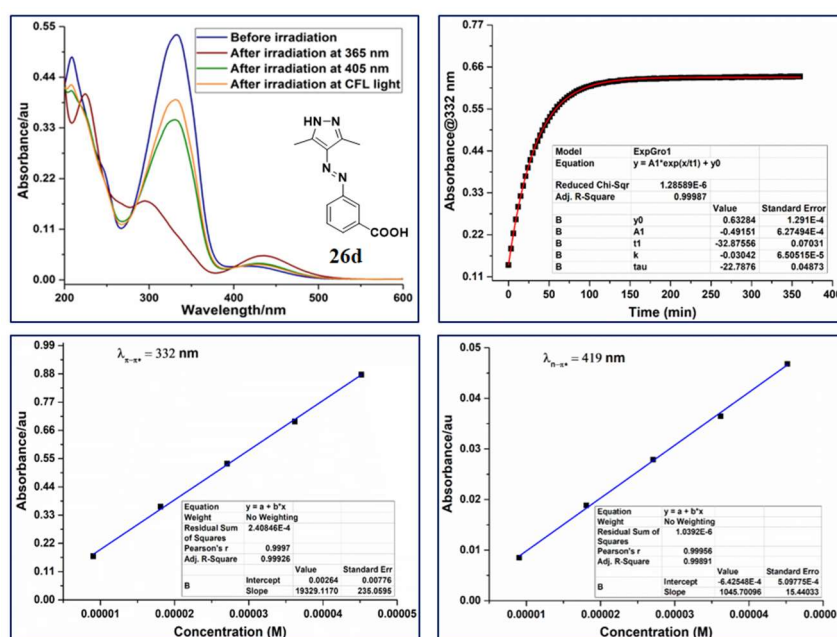


Figure 2B.26: UV-Vis photoswitching studies of **26d** (a) in CH_3CN solvent; (b) first-order kinetics plots; Estimation of molar extinction coefficient (in CH_3CN) for the (c) $\pi-\pi^*$ absorption and (d) $n-\pi^*$ absorption.

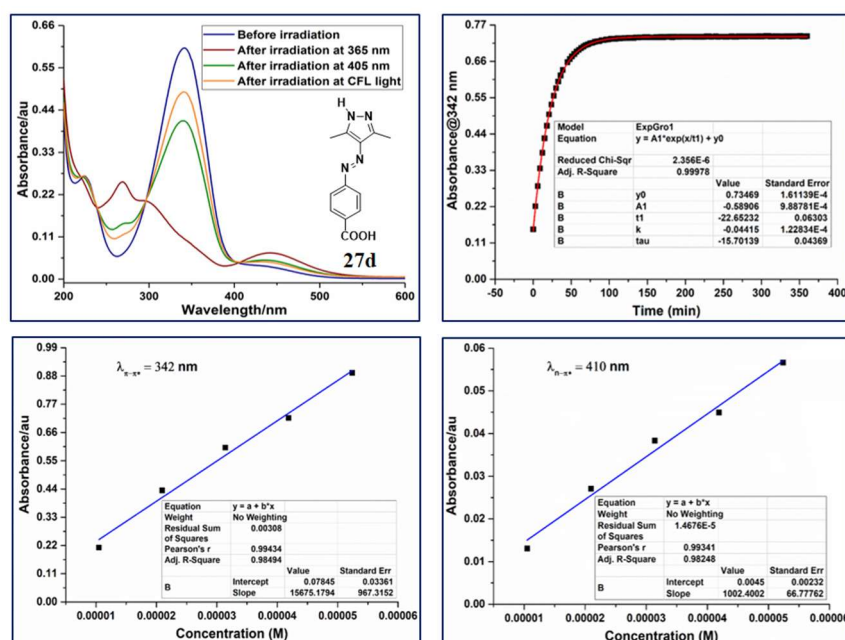


Figure 2B.27: UV-Vis photoswitching studies of **27d** (a) in CH₃CN solvent; (b) first-order kinetics plots; Estimation of molar extinction coefficient (in CH₃CN) for the (c) $\pi-\pi^*$ absorption and (d) $n-\pi^*$ absorption.

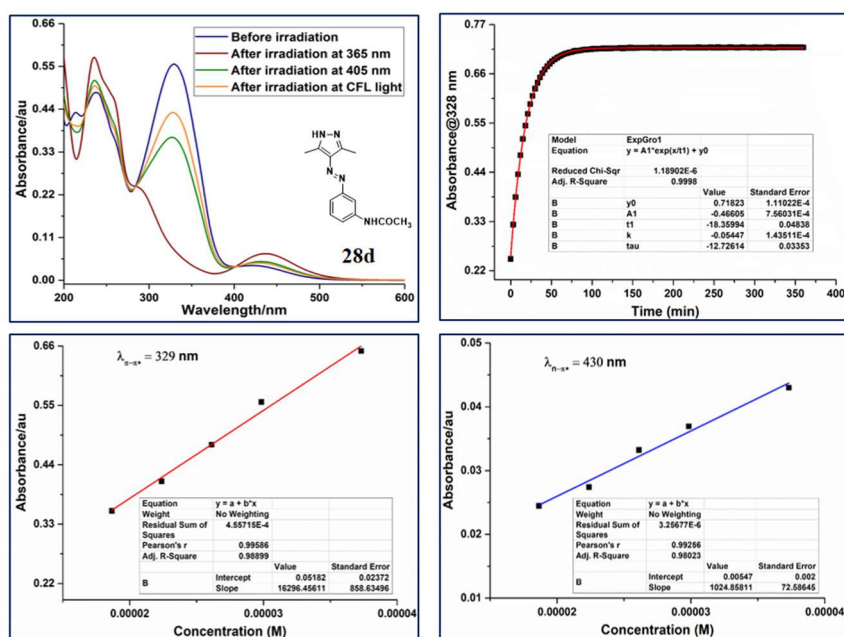


Figure 2B.28: UV-Vis photoswitching studies of **28d** (a) in CH₃CN solvent; (b) first-order kinetics plots; Estimation of molar extinction coefficient (in CH₃CN) for the (c) $\pi-\pi^*$ absorption and (d) $n-\pi^*$ absorption.

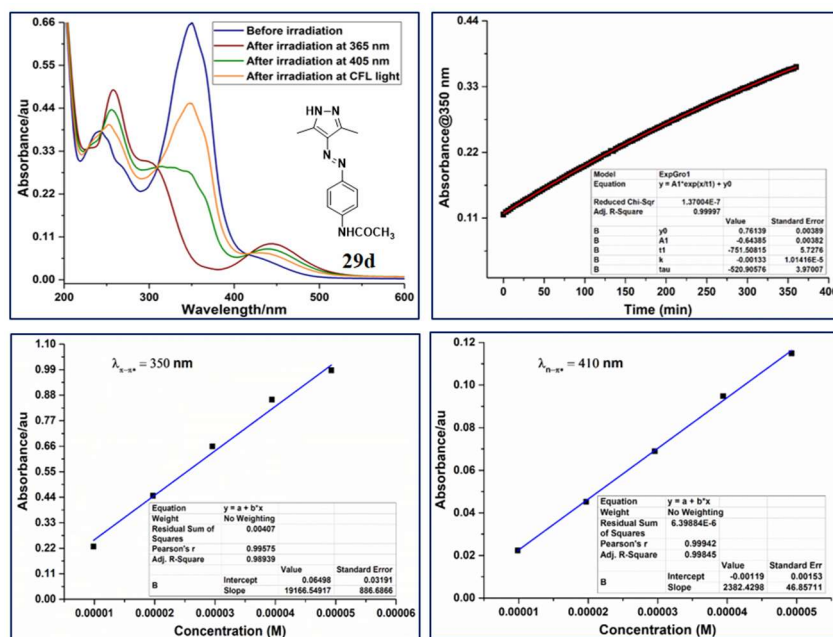


Figure 2B.29: UV-Vis photoswitching studies of **29d** (a) in CH₃CN solvent; (b) first-order kinetics plots; Estimation of molar extinction coefficient (in CH₃CN) for the (c) $\pi-\pi^*$ absorption and (d) $n-\pi^*$ absorption.

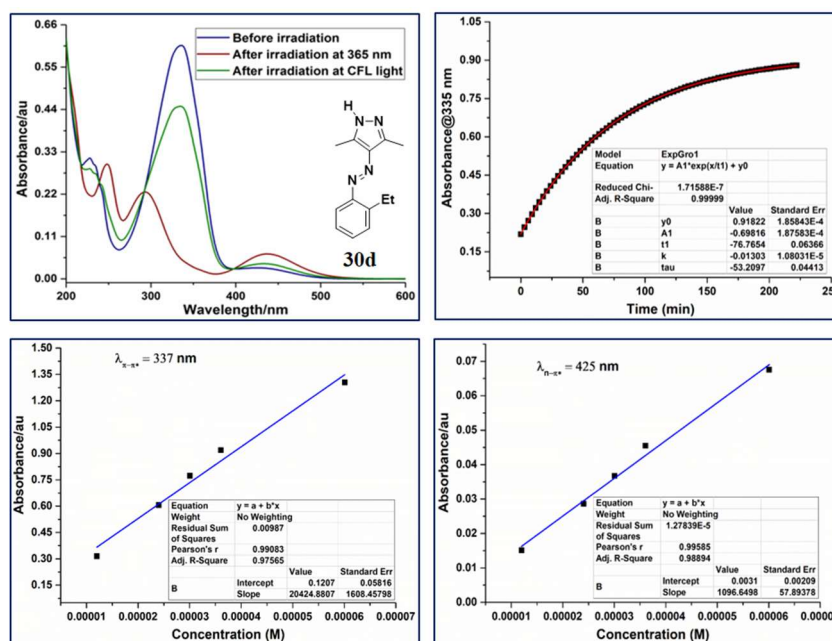


Figure 2B.30: UV-Vis photoswitching studies of **30d** (a) in CH₃CN solvent; (b) first-order kinetics plots; Estimation of molar extinction coefficient (in CH₃CN) for the (c) $\pi-\pi^*$ absorption and (d) $n-\pi^*$ absorption.

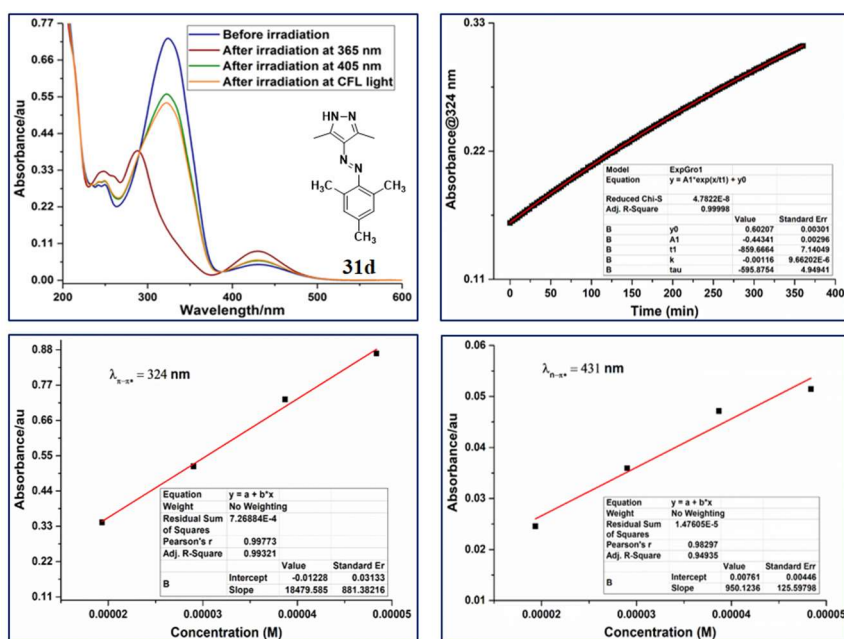


Figure 2B.31: UV-Vis photoswitching studies of **31d** (a) in CH_3CN solvent; (b) first-order kinetics plots; Estimation of molar extinction coefficient (in CH_3CN) for the (c) $\pi-\pi^*$ absorption and (d) $n-\pi^*$ absorption.

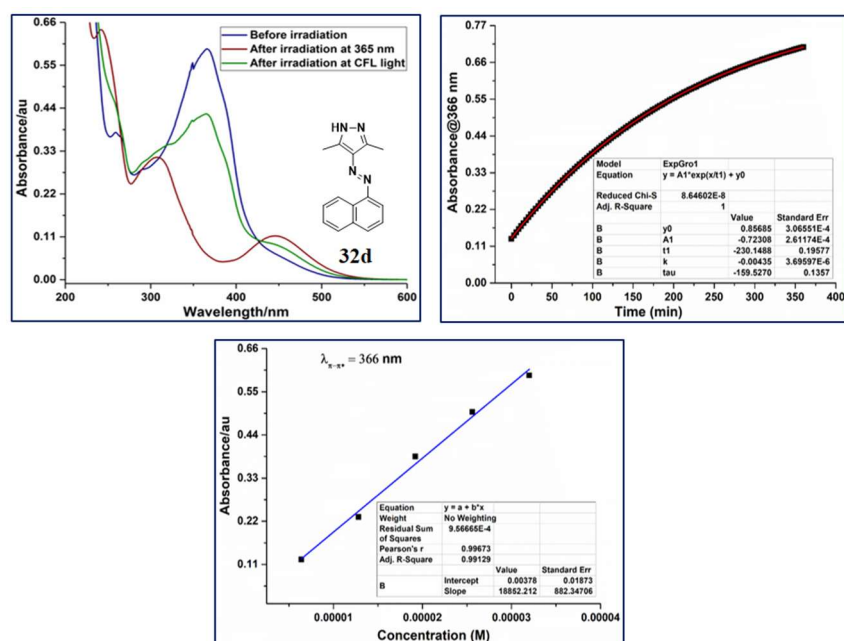


Figure 2B.32: UV-Vis photoswitching studies of **32d** (a) in CH_3CN solvent; (b) first-order kinetics plots; Estimation of molar extinction coefficient (in CH_3CN) for the (c) $\pi-\pi^*$ absorption and (d) $n-\pi^*$ absorption.

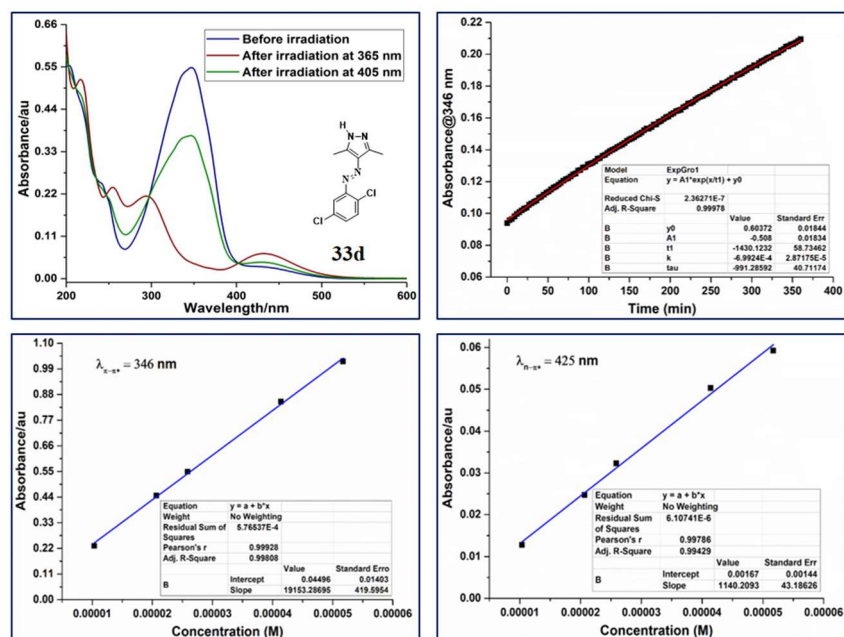


Figure 2B.33: UV-Vis photoswitching studies of **33d** (a) in CH_3CN solvent; (b) first-order kinetics plots; Estimation of molar extinction coefficient (in CH_3CN) for the (c) $\pi-\pi^*$ absorption and (d) $n-\pi^*$ absorption.

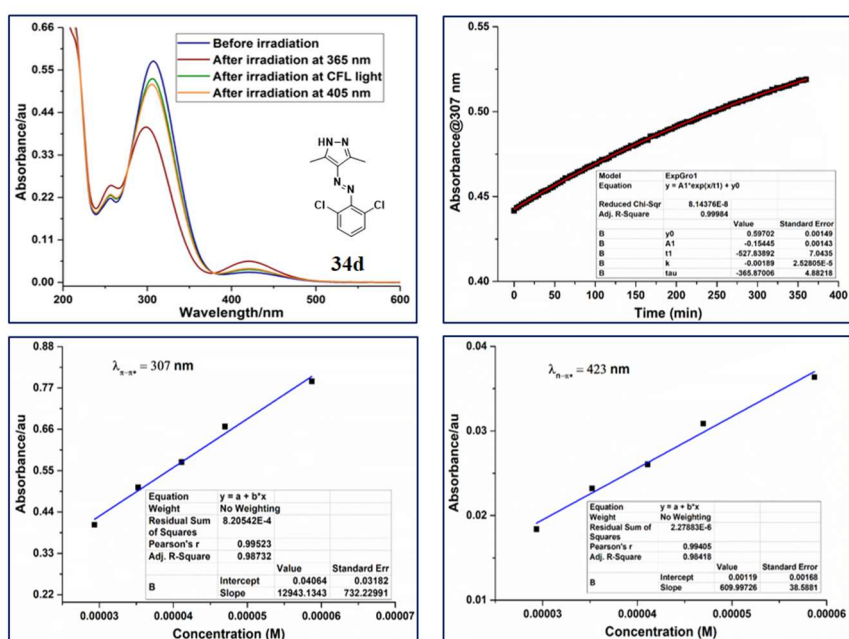


Figure 2B.34: UV-Vis photoswitching studies of **34d** (a) in CH_3CN solvent; (b) first-order kinetics plots; Estimation of molar extinction coefficient (in CH_3CN) for the (c) $\pi-\pi^*$ absorption and (d) $n-\pi^*$ absorption.

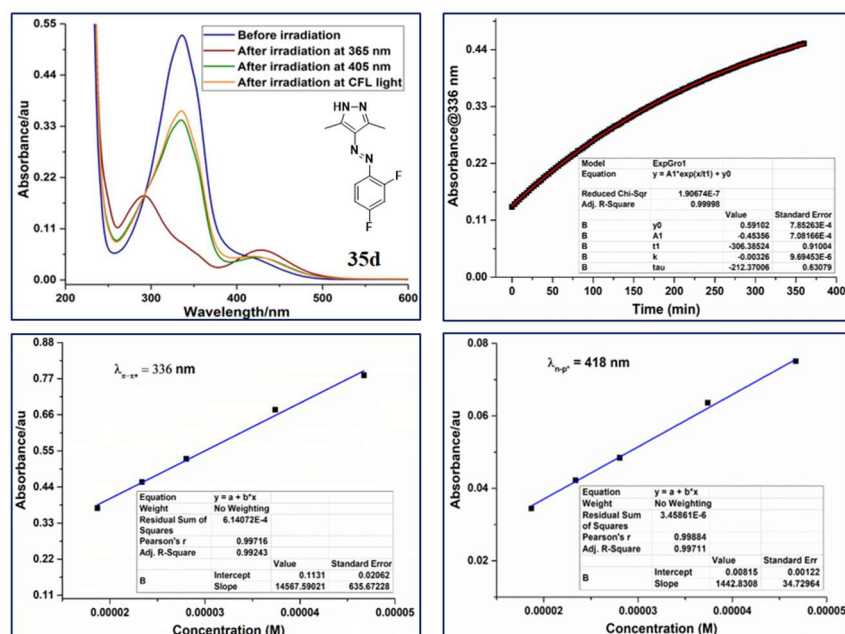


Figure 2B.30: UV-Vis photoswitching studies of **35d** (a) in CH_3CN solvent; (b) first-order kinetics plots; Estimation of molar extinction coefficient (in CH_3CN) for the (c) $\pi-\pi^*$ absorption and (d) $n-\pi^*$ absorption.

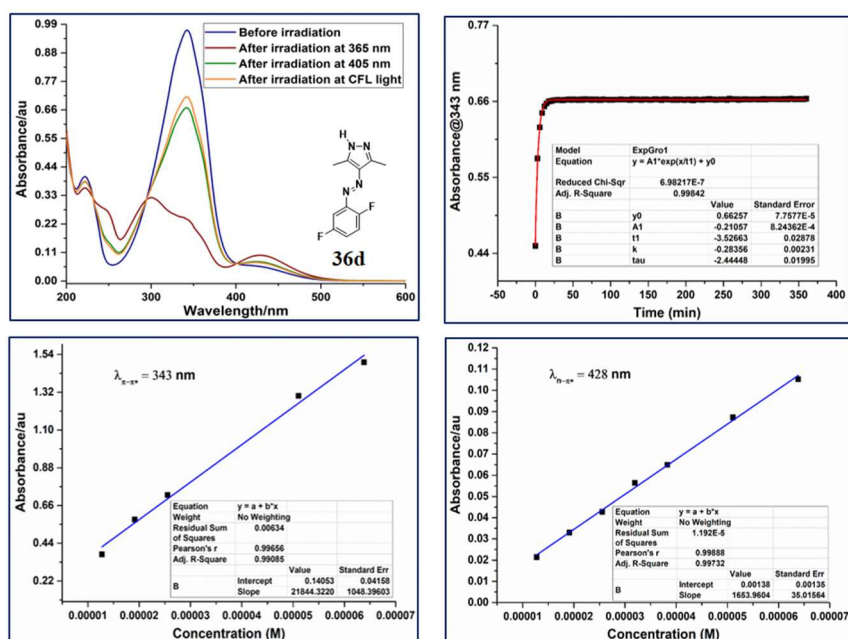


Figure 2B.36: UV-Vis photoswitching studies of **36d** (a) in CH_3CN solvent; (b) first-order kinetics plots; Estimation of molar extinction coefficient (in CH_3CN) for the (c) $\pi-\pi^*$ absorption and (d) $n-\pi^*$ absorption.

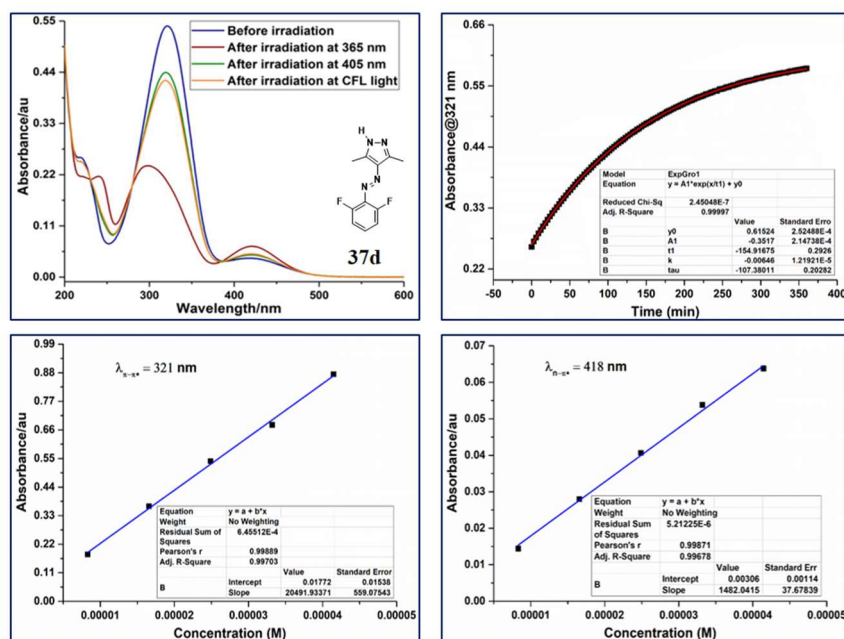


Figure 2B.37: UV-Vis photoswitching studies of **37d** (a) in CH_3CN solvent; (b) first-order kinetics plots; Estimation of molar extinction coefficient (in CH_3CN) for the (c) $\pi-\pi^*$ absorption and (d) $n-\pi^*$ absorption.

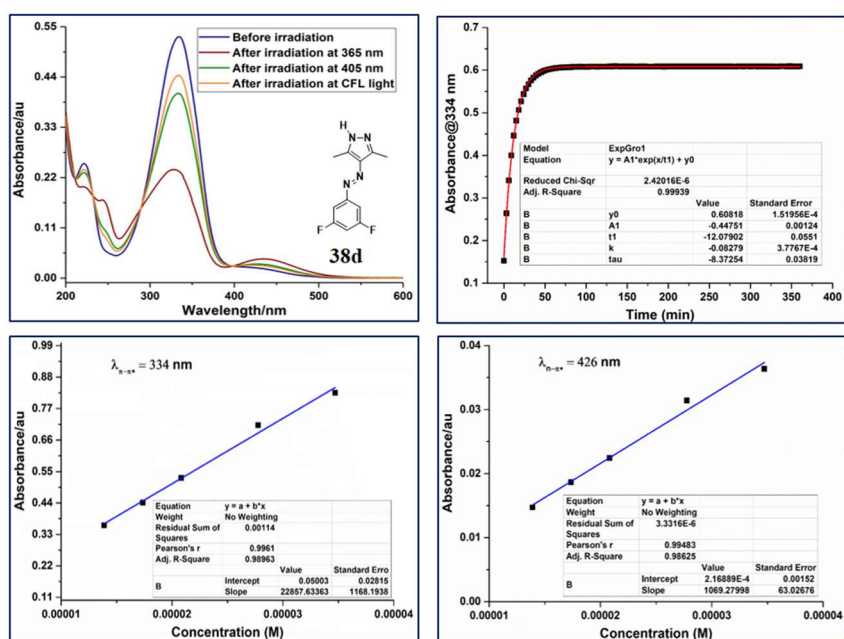
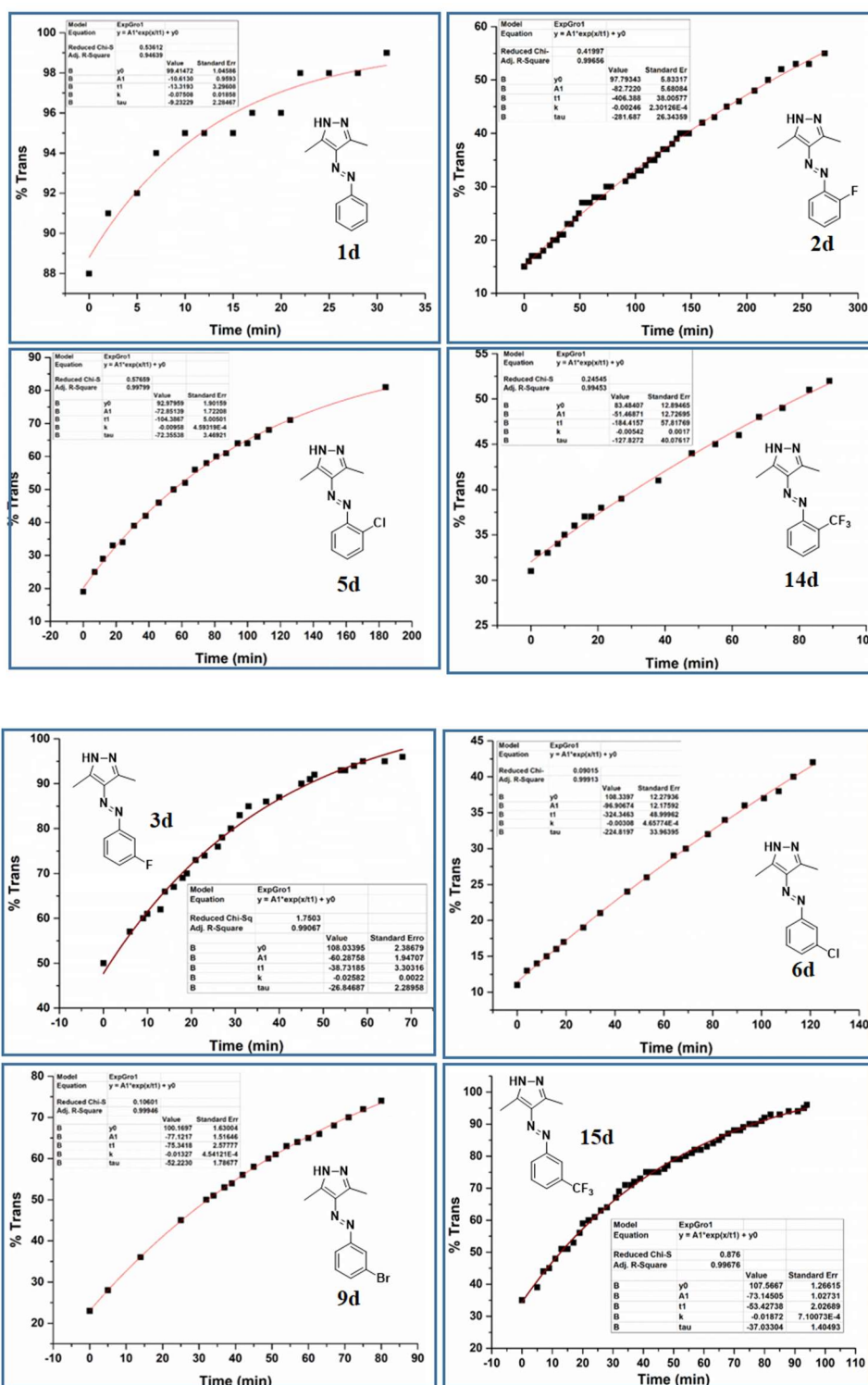
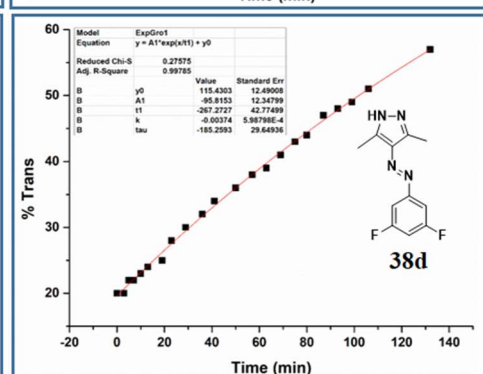
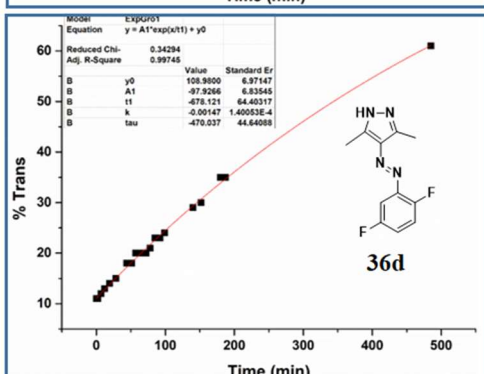
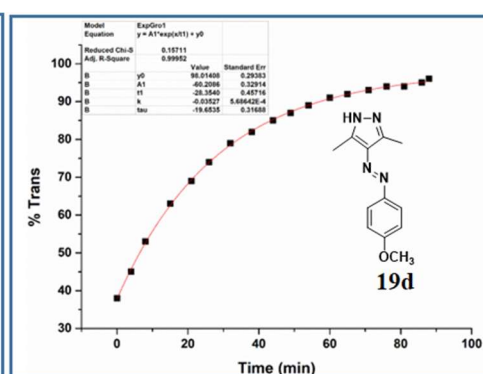
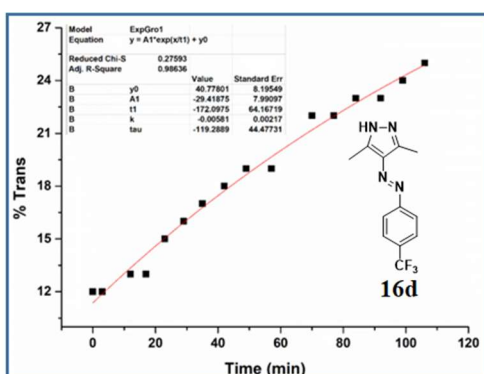
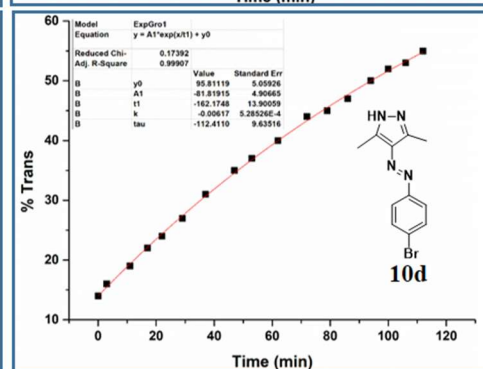
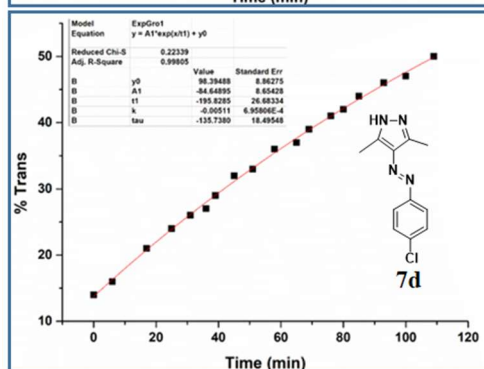
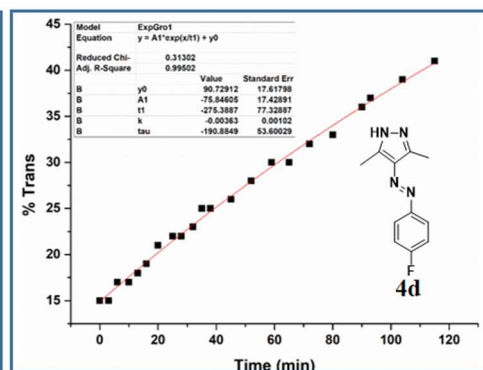
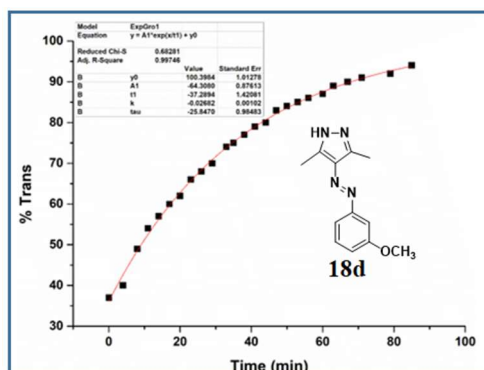


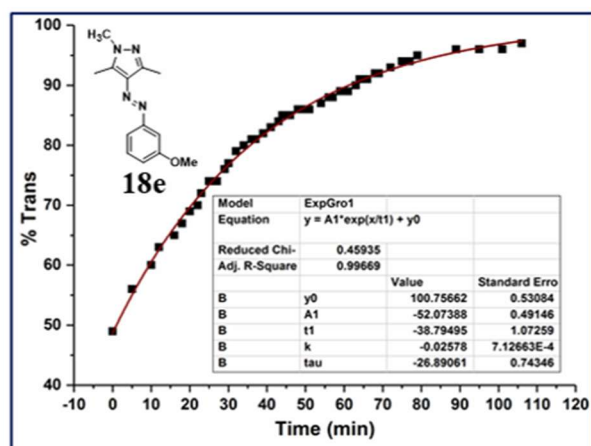
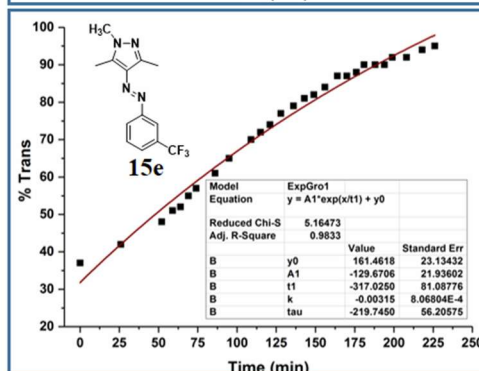
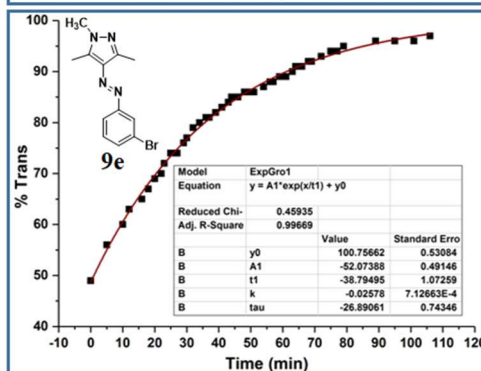
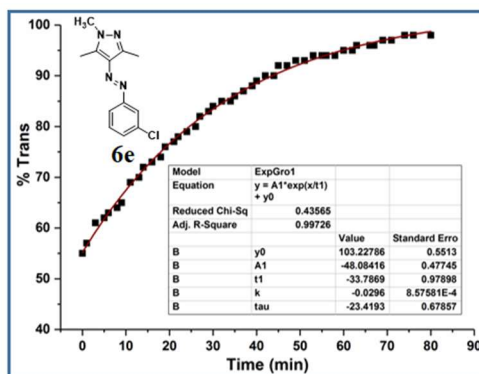
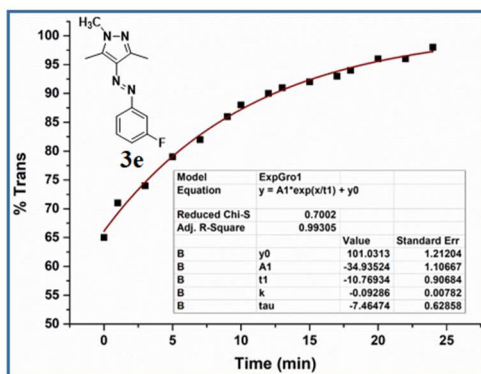
Figure 2B.38: UV-Vis photoswitching studies of **38d** (a) in CH_3CN solvent; (b) first-order kinetics plots; Estimation of molar extinction coefficient (in CH_3CN) for the (c) $\pi-\pi^*$ absorption and (d) $n-\pi^*$ absorption.

Appendix 2C:

NMR spectroscopic *Z-E* thermal reverse isomerization kinetics plots of phenylazopyrazole derivatives and *N*-methyl phenylazopyrazole derivatives in CD₃CN as a solvent at 298 K. Prior to the experiment, each sample has been irradiated at 365 nm light to attain a photostationary state.







Appendix 2D:

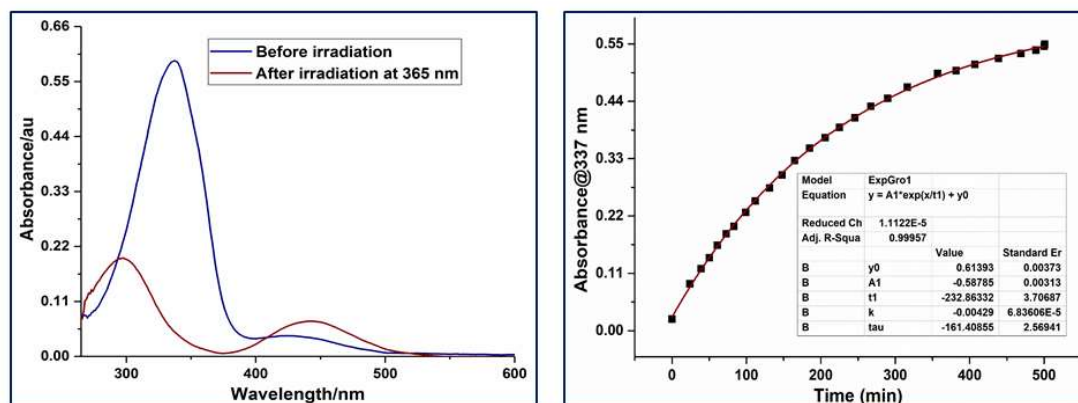


Figure 2D.1. UV-Vis photoswitching spectra (a) and kinetics plot (b) of **1e** in DMF at 60±1 °C.

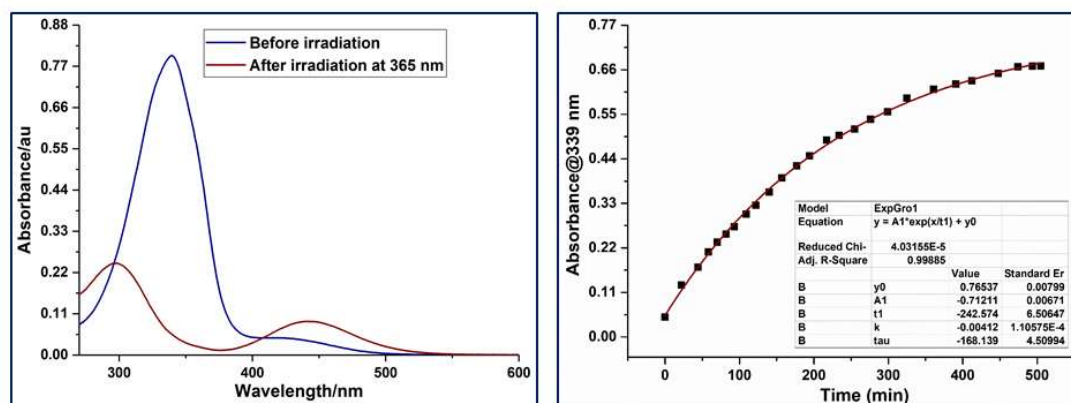


Figure 2D.2. UV-Vis photoswitching spectra (a) and kinetics plot (b) of **1e** in DMSO at 60±1 °C.

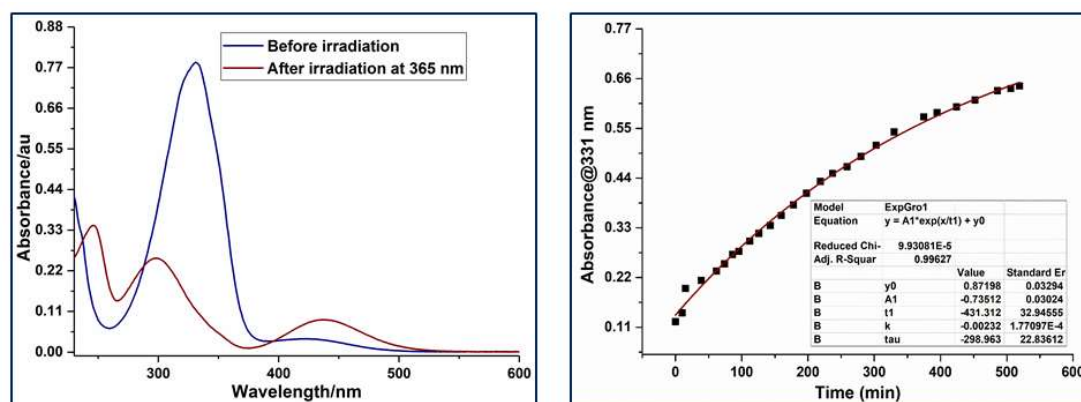


Figure 2D.3. UV-Vis photoswitching spectra (a) and kinetics plot (b) of **1d** in EtOH at 60±1 °C.

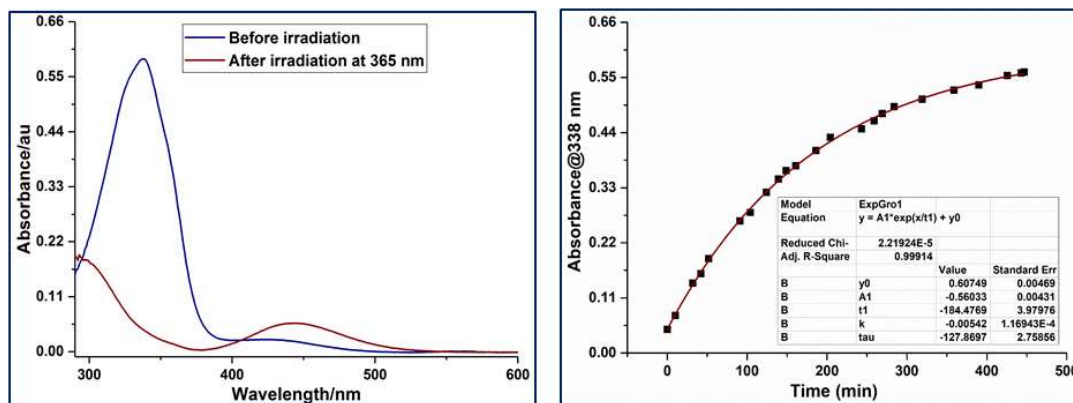


Figure 2D.4. UV-Vis photoswitching spectra (a) and kinetics plot (b) of **1d** in Toluene at 60±1 °C.

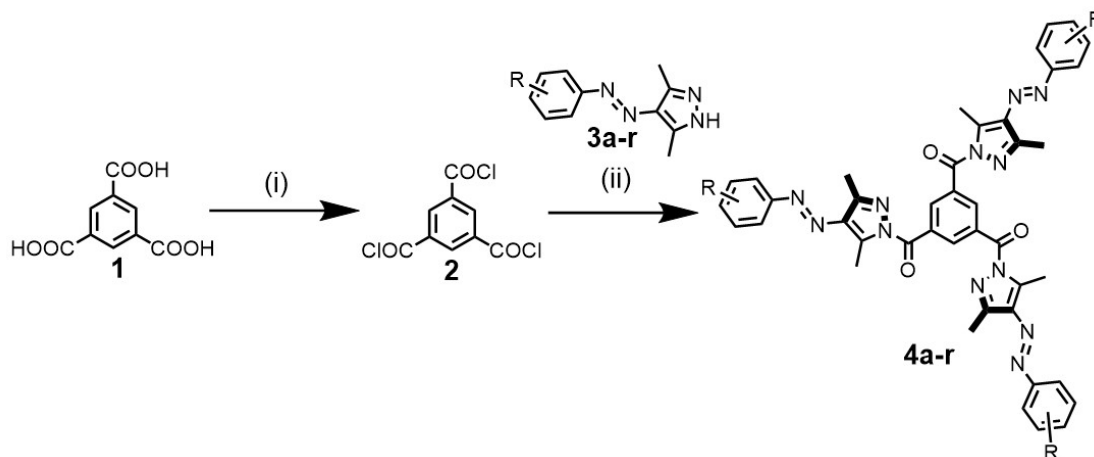
Chapter 3. Tripodal *N*-Functionalized Arylazo-3,5-dimethylpyrazole Derivatives of Trimesic Acid

3.1 Introduction

Photochromic materials are one of the versatile functional materials that can be useful in applications such as data storage, optical sensors, and rewritable imaging applications.¹⁻³ Various photoswitchable molecules such as stilbenes, spiropyrans, diarylethenes, fulgides etc are popularly used in this regard. Despite all these molecules, one of the most widely used systems is azobenzenes. Starting as dye molecules, it has evolved over the last century with a plethora of applications that include antibiotic drug (prontosil), indicator (methyl orange) and attained a status photoswitches. Since the discovery of its photoswitching properties due to *E-Z* isomerization, numerable applications of azobenzenes have been reported. The ease of synthesis and functionalization are the main reasons in this regard. In azobenzenes, the forward isomerization (*E* to *Z*) is a light induced process, whereas the reverse isomerization (*Z* to *E*) can be expected either through light or under dark. Due to thermal reverse isomerization, the molecules are expected to have a half-life, tuning of which is very crucial for various applications.

Recently bistable compounds showed promising applications in imaging, in particular reversible writing and erasing part.⁴ Mostly the light-driven switching has been used for printing, whereas thermal conditions are required for erasing. Apart from that, the systems need extensive synthesis or polymeric linkages for enabling the reversible writing and erasing processes.⁵⁻⁸ Due to the tunability in *Z*-isomer stability, we devised a simple strategy to connect multiple phenylazopyrazoles to a core moiety such that highly absorbing multistate photoswitchable compounds can be obtained. In this regard, we have designed and synthesized 18 phenylazopyrazole tricarboxamide based derivatives in good to excellent yields. Such molecules have several advantages such as ease of synthesis, the scope for derivatives, excellent multi-state photoswitching and higher conversion in photoisomerization, better solubility, long-term photoswitching stability and etc. This makes those molecules as potential candidates in reversible imaging and erasing processes. In this regard, our systems have advantages. Through these investigations, we discuss the synthesis, solution phase and solid-state photoswitching studies as a new class of multi-state and solid-state photoswitchable molecules.

3.2 Synthesis



Scheme 3.1. Synthesis of tripodal arylazo-3,5-dimethylpyrazole derivatives of trimesic acid **4a-r**. Conditions: (i) PCl₅, toluene, reflux, 3 h; (ii) Pyridine, toluene, reflux, 5 – 7 h.

Table 3.1. Synthesis of tripodal arylazo-3,5-dimethylpyrazole derivatives of trimesic acid **4a-r**.

S. No.	Compound	R=	%Yield ^a	S. No.	Compound	R=	%Yield ^a
1.	4a	H	69	10.	4j	4-CF ₃	85
2.	4b	3-F	67	11.	4k	2-NO ₂	72
3.	4c	4-F	81	12.	4l	3-NO ₂	92
4.	4d	3-Cl	80	13.	4m	4-NO ₂	92
5.	4e	4-Cl	82	14.	4n	4-I	80
6.	4f	3-Br	62	15.	4o	4-Me	68
7.	4g	4-Br	63	16.	4p	4-CN	73
8.	4h	2-CF ₃	89	17.	4q	4-OMe	69
9.	4i	3-CF ₃	88	18.	4r	3,5-di-F	70

^aIsolated yields

For synthesizing the target molecules, we have adopted a two-stage acid-amine coupling using trimesic acid and various substituted phenylazopyrazoles **3a-r**.⁹ (Scheme 3.1) In the first stage, the trimesic acid has been refluxed with PCl₅ in toluene to obtain the corresponding trimesoyl chloride, which was carefully taken to next stage without isolation and reacted with the respective arylazopyrazole derivatives in the presence of pyridine to obtain the tripodal target

molecules **4a-r** in good to excellent yields. (**Table 3.1**) All the target molecules **4a-r** have been characterized by using ^1H , ^{13}C -NMR, HRMS, IR and UV-Vis spectroscopic data.

3.3 Analysis of photoswitching studies using UV-Vis spectroscopy

All the synthesized molecules have been subjected to photoswitching in chloroform using UV-Vis spectroscopy at μM concentration. All the derivatives showed the appearance of a very strong $\pi-\pi^*$, and a weak $n-\pi^*$ absorption bands almost close to each other. (**Figure 3.1a**) Among them, 4- NO_2 , 4-I and 4- OCH_3 derivatives exhibited red shifts in both the bands relative to the parent. Due to the presence of three arylazopyrazole units and C_3 symmetric structure, their molar extinction coefficients were estimated to be two to three times higher than the corresponding unfunctionalized arylazopyrazoles with free NH. All of the derivatives exhibited nearly a quantitative photoswitching at 365 nm that can be rationalized based on the disappearance of the $\pi-\pi^*$ absorption of the *EEE*-isomer. Apparently, the expected *ZZZ*-isomer appeared with a blue shifted $\pi-\pi^*$ and $n-\pi^*$ absorption bands. Due to the appearance of only one set of $\pi-\pi^*$ and $n-\pi^*$ absorption bands, UV-Vis spectroscopy cannot be able to differentiate among the individual *EEZ*, *EZZ* and *ZZZ*-isomeric species. (**Figure 3.1e**) Interestingly, irradiation of the photoproducts of **4a** at 490 nm readily converted back to *EEE*-isomer. Similarly, all of the derivatives have also been subjected to reverse switching using different wavelengths of light. The individual wavelengths of light required for the reverse isomerization of various derivatives have been indicated along with their respective PSS composition in terms of *EEE*-isomer. (**Table 3. 2**)

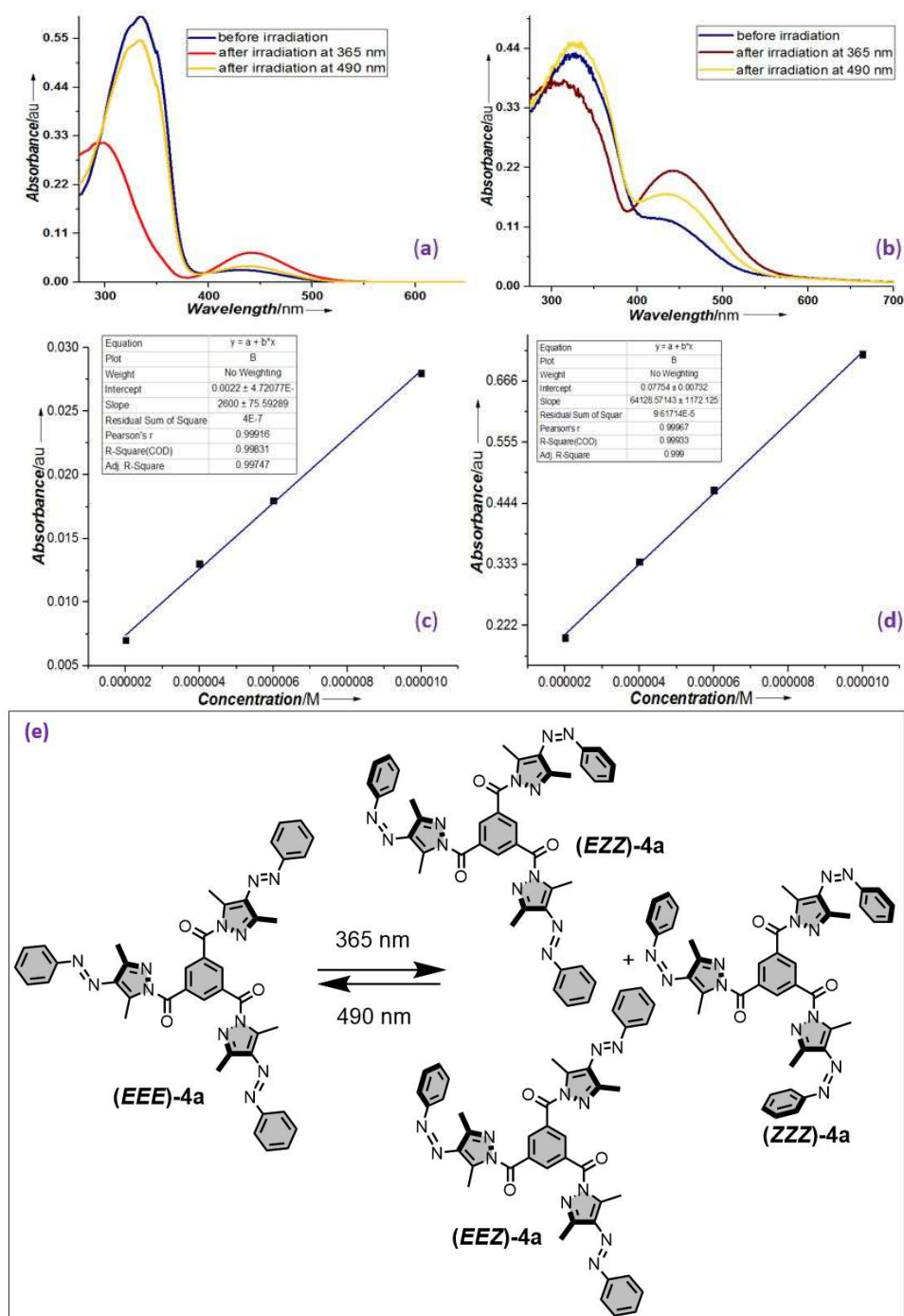


Figure 3.1. Photoswitching in **4a**: (a) UV-Vis spectroscopic data depicting photoswitching of **4a** in CHCl₃ (10 μM) with an insert showing the colour of solution, before and after irradiation at 365 nm; (b) UV-Vis spectroscopic data depicting photoswitching of **4a** in solid-state (KBr medium); Estimation of molar extinction coefficient (ϵ) of (c) n-π*, and (d) π-π* absorption bands in **4a**; (e) Possible photoisomerization products of **4a**.

Apart from that, we have also tested the photoswitching stability for reversibility for the parent compound **4a**. We have followed the reversible switching up to a maximum of 11 cycles, and we observed that the molecule did not show any fatigue. (**Figure 3.2**) The thermal stability of the *ZZZ*-isomer of the parent compound **4a** was also attempted. Due to the indistinguishable nature of the intermediates from the initial and final isomeric forms (*ZZZ*, *ZZE*, *ZEE* and *EEE*), and slowness of the reverse isomerization kinetics, we focused on the same experiment using NMR spectroscopy (*vide infra*).

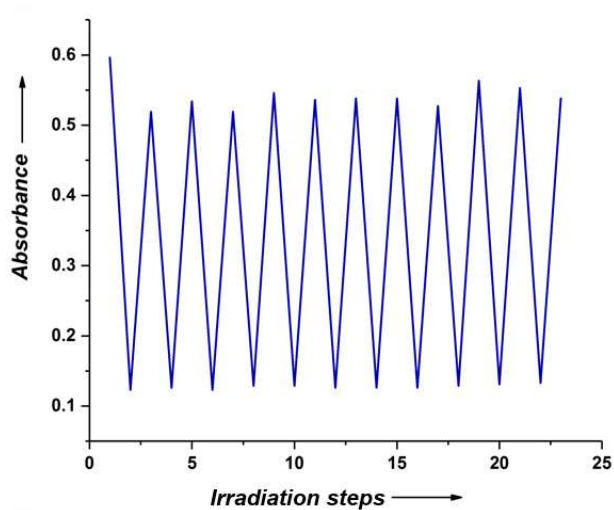


Figure 3.2. Long-term photoswitching stability of **4a** up to 11 cycles in CHCl_3 (For forward switching 365 nm was used, whereas reverse isomerization was induced using 490 nm light; absorbance changes at 352 nm).

Table 3.2. UV-Vis spectroscopic data of the **4a-r** in solution phase (CHCl₃) and solid phase (in KBr medium).

S. No.	Compound	R=	Concentration (μM)	Before irradiation (<i>EEE</i> -isomer)		After irradiation at 365 nm		PSS composition in solution phase photoswitching		The fraction of molecules undergoing photoswitching in solid phase	
				$\pi\text{-}\pi^* \lambda_{\text{max}} / (\epsilon)$	$n\text{-}\pi^* \lambda_{\text{max}} / (\epsilon)$	$\pi\text{-}\pi^* \lambda_{\text{max}}$	$n\text{-}\pi^* \lambda_{\text{max}}$	Forward <i>EEE-ZZZ</i> isomerization (in terms of % <i>EEE</i>)	Reverse <i>ZZZ-EEE</i> isomerization (in terms of % <i>EEE</i>) (Wavelength used for irradiation/nm)	Forward <i>EEE-ZZZ</i> isomerization	Reverse <i>ZZZ-EEE</i> isomerization (Wavelength used for irradiation/nm)
1	4a	H	10	334 (64126 ± 1172)	440 (2600 ± 75)	293	442	76	91	56	79
2	4b	3-F	9	336 (84181 ± 5251)	445 (3136 ± 114)	286	439	79	95	47	76
3	4c	4-F	5.4	335 (91126 ± 3684)	441 (3704 ± 35)	296	443	82	87	63	80
4	4d	3-Cl	7.3	337 (86337 ± 2187)	443 (2988 ± 164)	289	443	86	87	65	81
5	4e	4-Cl	5.5	341 (99190 ± 4483)	439 (4281 ± 142)	299	447	90	86	70	83
6	4f	3-Br	7.2	337 (73230 ± 4851)	444 (2744 ± 181)	287	444	85	91	59	80
7	4g	4-Br	8	342 (90500 ± 3117)	443 (3600 ± 152)	296	445	92	79	67	82
8	4h	2-CF ₃	10	337 (62700 ± 3865)	440 (1250 ± 76)	299	447	86	80	82	85
9	4i	3-CF ₃	8.5	334 (78014 ± 1019)	444 (2452 ± 144)	290	442	79	88	59	75
10	4j	4-CF ₃	15	334 (47645 ± 1606)	447 (1483 ± 74)	286	444	82	86	64	83
11	4k	2-NO ₂	13	336	432	-	-	-	-	96	96
12	4l	3-NO ₂	10	332 (69224 ± 3653)	447 (2086 ± 71)	256	442	69	81	76	86
13	4m	4-NO ₂	9.9	349 (77894 ± 2740)	447 (3636 ± 110)	287	454	80	83	95	95
14	4n	4-I	7.9	347 (84325 ± 3756)	447 (3885 ± 120)	304	446	92	84	66	83
15	4o	4-Me	9.8	341 (70532 ± 265)	444 (2666 ± 119)	300	443	87	79	67	86
16	4p	4-CN	10	343 (67360 ± 3226)	445 (2600 ± 40)	270	449	90	81	77	85
17	4q	4-OMe	9.4	352 (77889 ± 2225)	443 (3999 ± 108)	313	446	87	86	73	89
18	4r	3,5-diF	15	334 (72804 ± 2100)	436 (3580 ± 89)	289	444	83	73	85	82

3.4 Analysis of photoswitching studies using NMR spectroscopy

The photoswitching studies have also been carried out using $^1\text{H-NMR}$ spectroscopy at a relatively higher concentration in the range of mM. Unlike the UV-Vis spectroscopy, the NMR data was very useful in identification of the individual isomeric species such as *EEZ*, *EZZ* and *ZZZ*. Upon isomerization all of the protons experienced an upfield shift that progressively shifted towards the shielded region. Due to the overlapping nature, the individual isomeric species are indistinguishable on the basis of the protons attached to phenylazopyrazole units or the two methyl groups. In contrast, the chemical shifts of the benzene core protons are very useful in this regard. Due to the C_3 -symmetric structure, the three-benzene core protons of the parent **4a-*EEE*** appear as a singlet at 8.93 ppm. Upon isomerization with 365 nm wavelength light, we observed not only upfield shifts, but also the appearance of multiple signals. (**Figure 3.3**) The most downfield shifted singlet at 8.75 ppm is corresponding to the *ZZZ*-isomer. In between, the two singlets due to *EEE* and *ZZZ*-isomers, two sets of signals at an intensity ratio of 2:1 that can be rationalized as *EEZ* and *EZZ* isomers. For rationalizing the chemical shifts, we have utilized the NMR data from the kinetics experiments, the details of which will be explained in the following section. At different intervals of time, changes in the composition of individual isomers have been utilized in identifying the signals. Using the integral ratios of the benzene core protons, we were able to identify the PSS composition at both forward as well as reverse switching. (**Table 3.3** and **Appendix 3A**) Among the various derivatives, we observed, 4- OCH_3 and 4- CH_3 showed a maximum photoisomerization leading to *ZZZ*-isomer. On the other hand, 2- NO_2 derivative showed no switching at all. Presumably, this molecule might be switching back rapidly. In the case of 2-nitro derivative **4k**, the solution phase irradiation did not exhibit photoisomerization, however, in the solid phase (in KBr medium), it indeed produces appreciable changes in the absorption spectrum. Since the stability of the photoisomers is expected to be more in the solid phase, we observe the isomerization to a lesser extent. Hence, faster reverse isomerization might be responsible for no photoisomerization in the solution phase.

In order to understand whether the light induced isomerization is concentration dependent, we have performed the forward switching at different concentrations. The results revealed a low dependency of the concentration in photoswitching. Even at a concentration of 11 mM, we observed a conversion of 66% *ZZZ*-isomer, whereas no *EEE*-isomer was detected. (**Figure 3.4** and **Table 3.4**) The low dependency of the concentration in photoswitching is

contrary to a recent observation on *tris*-azobenzenes connected benzenetricarboxamides, where the forward photoswitching efficiency depends on the concentration due to the supramolecular interactions.^[19a] As we initially assumed, the presence of the two methyl groups at pyrazole prevented such interactions in **4a**, which might be responsible for moderate to good isomerization even at higher concentration.

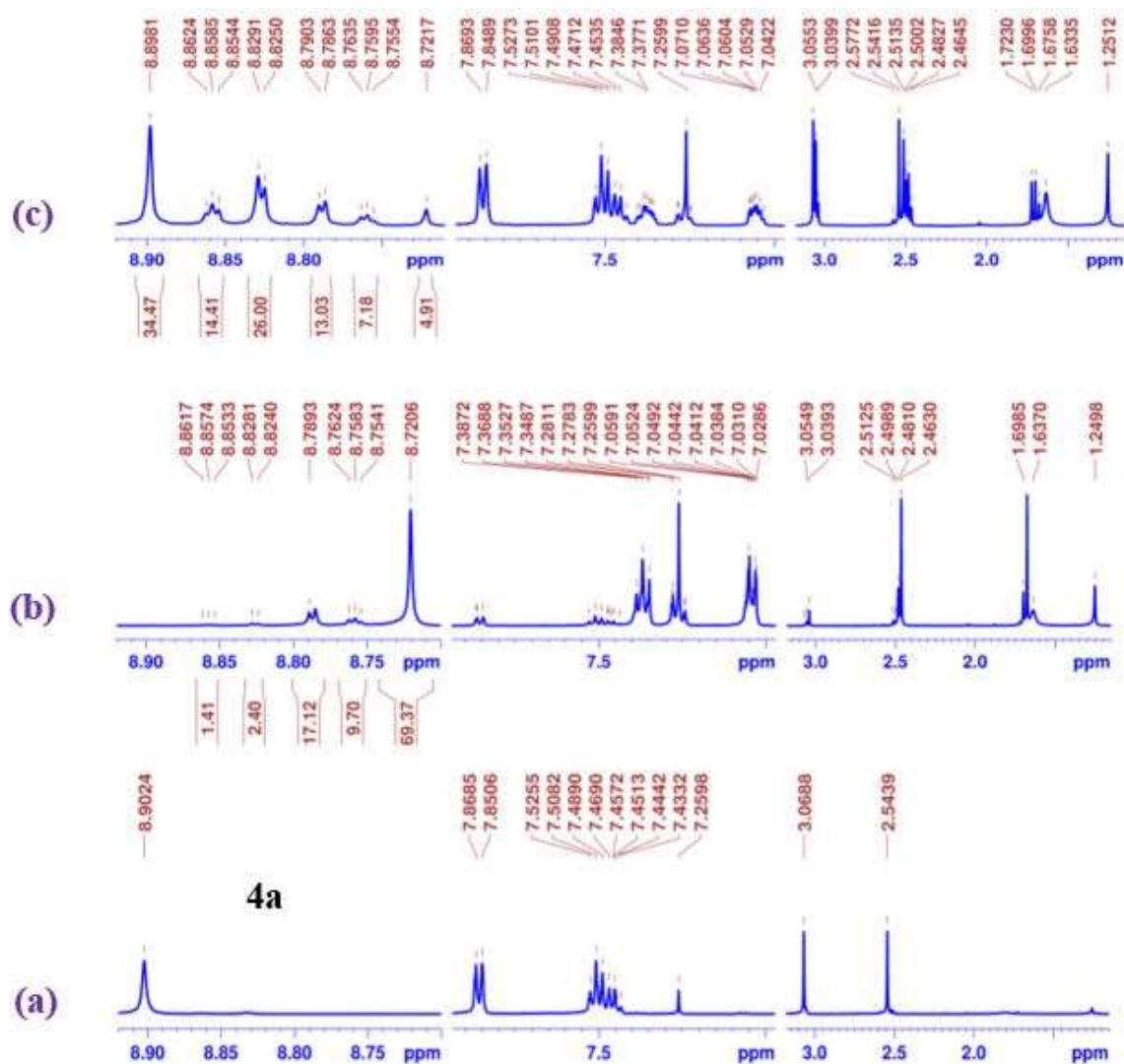


Figure 3.3: NMR photoswitching studies of **4a** in CDCl_3 (8.5 mM) (a) before irradiation; (b) after irradiation with 365 nm; (c) after irradiation with 490 nm.

Table 3.3. NMR studies of photoisomerization in tripodal arylazo-1*H*-3,5-dimethylpyrazole derivatives of trimesic acid **4a-r**.

S. No.	Compound	R=	λ (nm)	%Composition of individual isomers at PSS ^a			
				<i>EEE</i>	<i>EEZ</i>	<i>EZZ</i>	<i>ZZZ</i>
1.	4a	H	365	0	0	17	83
			490	35	40	20	5
2.	4b	3-F	365	0	7	31	62
			435	93	7	0	0
3.	4c	4-F	365	-	5	28	67
			490	76	21	3	0
4.	4d	3-Cl	365	3	16	40	41
			505	46	38	14	2
5.	4e	4-Cl	365	1	2	19	78
			450	41	34	18	7
6.	4f	3-Br	365	1	4	25	70
			505	48	37	13	2
7.	4g	4-Br	365	7	6	18	69
			435	32	23	22	13
8.	4h	2-CF ₃	365	2	4	27	67
			505	55	37	8	0
9.	4i	3-CF ₃	365	20	37	31	12
			490	60	32	8	-
10.	4j	4-CF ₃	365	1	7	33	59
			435	37	35	23	5
11.	4k	2-NO ₂	b	100	-	-	-
			b	100	-	-	-
12.	4l	3-NO ₂	365	6	24	41	29
			505	50	40	10	-
13.	4m	4-NO ₂	365	11	26	38	25
			505	84	16	-	-
14.	4n	4-I	365	20	35	32	13
			505	40	37	18	5
15.	4o	4-Me	365	10	19	34	37
			450	65	30	5	-
16.	4p	4-CN	365	1	5	25	68
			505	68	28	4	-
17.	4q	4-Ome	365	-	1	11	88
			505	72	25	3	-
18.	4r	3,5-di-F	365	17	22	34	27
			505	c	c	c	c

^aPSS has been established for individual derivatives through prolonged irradiation at 365 nm (forward isomerization from *EEE*-isomer, represented in normal font) such that no further isomerization happens; The compositions have been deduced using ¹H-NMR in CDCl₃ at 25 ± 1 °C; The integral ratios of benzene core protons have been used for the estimation of individual isomers; ^bNo photoisomerization was observed with different irradiation wavelengths; ^cDue to overlapping signals, the species were indistinguishable. (For all the

derivatives 8.5 mM concentration samples have been used, however, due to poor solubility, **4l** and **4r**, the exact concentrations were unknown.)

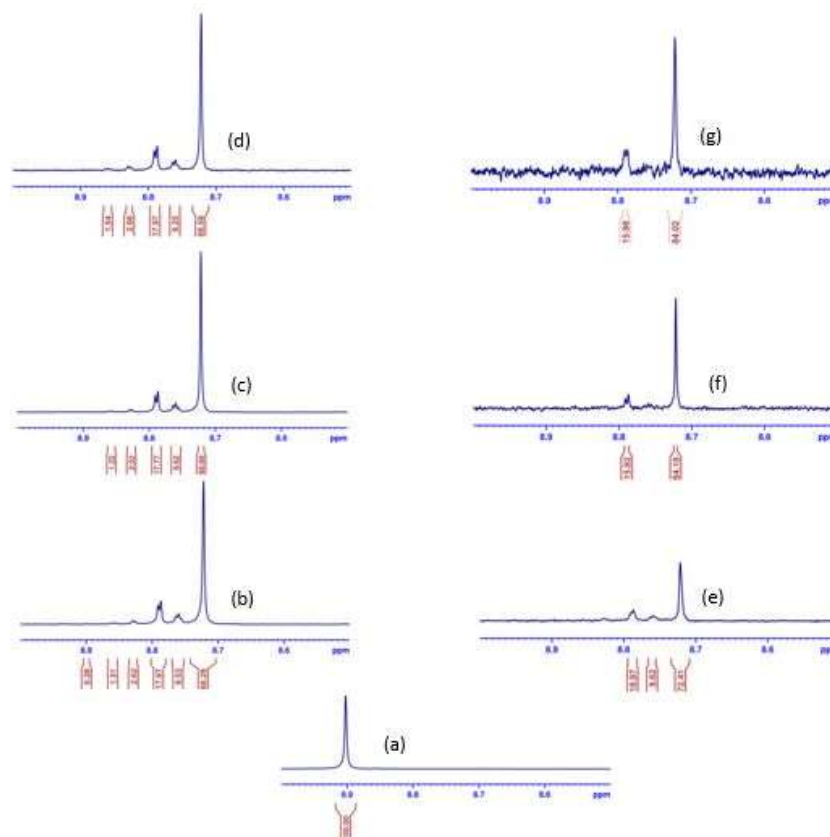


Figure 3.4. The composition of photoisomers of compound **4a** at different concentration: (a) *EEE-4a* spectrum at 11.43 mM (before irradiation); After irradiation of the sample at 365 nm, (b) at 11.43 mM; (c) at 5.72 mM; (d) at 2.86 mM; (e) at 1.43 mM; (f) at 0.71 mM and (g) at 0.36 mM. (All the $^1\text{H-NMR}$ spectra depict the signal(s) corresponding to benzene core protons in the aryl region of **4a**).

Table 3.4. Concentration dependency in photoswitching of **4a**.

S. No.	Composition at photostationary state ^a				Concentration (mM)
	% <i>EEE</i>	% <i>EEZ</i>	% <i>EZZ</i>	% <i>ZZZ</i>	
1 ^b	100	0	0	0	11.43
2	0	4	28	68	11.43
3	0	4	27	69	5.72
4	0	4	27	69	2.86
5	0	0	28	72	1.43
6	0	0	16	84	0.71
7	0	0	16	84	0.36

^aThe CDCl_3 solutions of **4a** in different concentrations have been subjected to 365 nm irradiation up to a maximum of 120 min, depending on the attainment of PSS. (The samples with low concentrations, 0.71 and 0.36 mM reached the PSS within 5 min of irradiation)

^bBefore irradiation.

3.5 Thermal reverse isomerization kinetics studies using NMR spectroscopy

In order to understand the stability of the *ZZZ*- and other isomers, the thermal reverse isomerization kinetics has been followed. In this regard, the parent compound **4a** was subjected to 365 nm irradiation to reach the PSS, followed by NMR spectroscopic studies that have been carried out at 25 ± 2 °C for more than 40 days. (Table 3. 5)

Table 3.5. Thermal reverse isomerization kinetics data of **4a** in CDCl_3 at 25 ± 2 °C using NMR spectroscopy.

S. No	Time (min)	% <i>ZZZ</i>	% <i>ZZE</i>	% <i>ZEE</i>	% <i>EEE</i>
1	0	71	26	3	0
2	45	71	26	3	0
3	61	70	27	3	0
4	1187	63	31	7	0
5	2645	57	35	7	1
6	4584	48	39	11	2
7	5931	41	42	15	2
8	7432	36	43	19	3
9	8701	33	43	20	4
10	10340	28	44	24	5
11	11589	26	44	25	6
12	13012	23	43	27	7
13	14543	19	42	31	8
14	15971	17	39	34	10
15	20294	11	36	39	15
16	21569	9	35	39	16
17	22830	8	36	39	17
18	24255	8	33	41	19
19	28873	6	27	43	25
20	31853	4	24	44	27
21	34322	3	20	45	34
22	38877	2	17	42	39
23	44423	1	14	40	44
24	55269	0	9	38	53
25	61295	0	5	35	60

In **4a**, upon isomerization using 365 nm light a mixture different photoisomers, namely *ZZZ*-, *ZZE*- and *ZEE*- along with the native isomer *EEE*-**4a** have been observed at PSS. The thermal reverse isomerization kinetics have been followed using a 400 MHz NMR at 298 K. For following the kinetics, the sample temperature has been maintained at 25 ± 2 °C. The collected data through NMR spectroscopy and changes in the composition of individual isomers over a period of 40 days have been shown. (Figure 3.5) We observed a consecutive reaction in three steps.

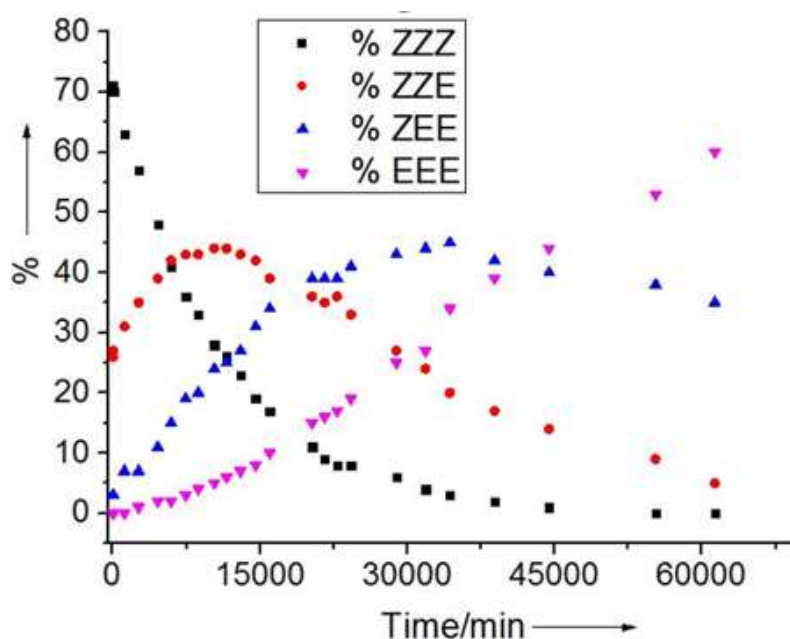


Figure 3.5. Thermal reverse isomerization kinetics profile of **4a** at 25 ± 2 °C using $^1\text{H-NMR}$.

The rate constants for the individual steps have been deduced by Mayank Saraswat using numerical solutions and fitting the data using a program ROOT (version 6.08) available online (in <https://root.cern.ch>.) The details of calculating the rate constants by numerically solving the rate expressions are indicated in Appendix. (**Appendix 3C**) For confirming the experimentally observed trend in the isomerization rates, DFT level computations at B3LYP/6-311G(d,p) level of theory have been performed. The trends in the computed rates and barriers have been indicated. (**Table 3.6**) Based on these data, it is evident that the ZZZ-isomer is more stable in solution phase. In figure S7 and table S3. Three consecutive reactions have been considered for obtaining the rate laws and corresponding rate constant for the thermal isomerization processes.

Table 3.6 Thermal reverse isomerization kinetics data of **4a**.

S. No.	Step	NMR Data ^a		Computed Barriers ^{b,d}
		k (min^{-1})	Half life ^c	
1	ZZZ - ZZE	$8.9876 \times 10^{-5} \pm 6.5434 \times 10^{-7}$	5.36	24.1(6)
2	ZZE - ZEE	$5.9765 \times 10^{-5} \pm 6.0645 \times 10^{-7}$	8.05	24.1(0)
3	ZEE - EEE	$2.9570 \times 10^{-5} \pm 5.4019 \times 10^{-7}$	16.27	24.1(6)

^aKinetics studies have been performed in CDCl_3 (8.5 mM) at 25 ± 2 °C; ^bB3LYP/6-311G(d,p) level of theory; ^cHalf-life in days; ^dEnergies in kcal/mol.

3.6 Solid-state photoisomerization

Similar to the solution phase photochemistry, solid-state photochemistry has also been followed using UV-Vis spectroscopy. The UV-Vis spectroscopic studies through reflectance mode in KBr medium showed prominent changes in the $n-\pi^*$ band. (**Figure 3.1b**) Therefore, the solid-state photoswitching studies have been extended to all of the derivatives using UV-Vis spectroscopy. In all of the cases, signals have been observed at $\pi-\pi^*$ and $n-\pi^*$ regions for the native sample in KBr medium. Upon irradiation with 365 nm, all derivatives exhibited prominent changes in the $n-\pi^*$ region. The increase in the intensity in that region clearly showed the isomerization.

The fraction of the sample that undergoes photoswitching has been estimated and tabulated. (**Table 3.2**) The percent conversion of the *EEE* isomer into the *ZZZ*, *ZZE* and *ZEE* photoisomers at the photostationary state by UV irradiation has been estimated on the basis of the following equation^[10] using the absorbance value changes in the $n-\pi^*$ region for the solid sample (in KBr medium) and in the $\pi-\pi^*$ region for the solution phase samples (in CHCl_3). Using the same expression, the reverse isomerization conversions at the PSS have also been obtained.

$$\% \text{ conversion of } EEE \text{ isomers} = 1 - \frac{\text{absorption after irradiation at 365 nm}}{\text{absorption before irradiation}}$$

In order to quantify the extent of isomerization, we have dissolved the irradiated sample (as a pellet in KBr medium) of **4b** in CDCl_3 under dark and immediately a $^1\text{H-NMR}$ has been recorded. The spectra showed that nearly 77% of sample underwent isomerization with the appearance of varying % of *EEZ*, *EZZ* and *ZZZ*-isomers. (**Figure 3.6**) Based on this observation, we have a clear evidence for the solid-state photoswitching. For selected derivatives, we have also performed the solid state switching for reversibility. The reversibility has been performed for 10 cycles by alternately irradiating the sample with 365 nm and 490 nm lights. In solid state also, these molecules showed consistency and switching stability.

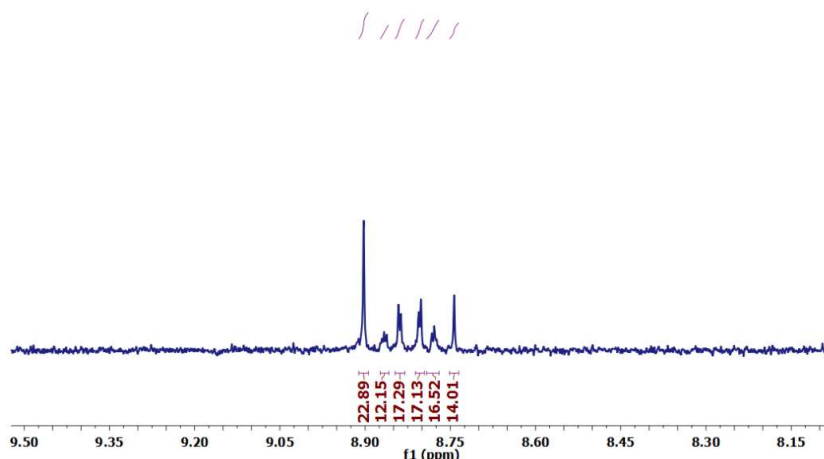


Figure 3.6: $^1\text{H-NMR}$ spectrum of **4b** in CDCl_3 (aromatic region corresponding to the benzene core protons) depicting the composition of individual isomers after irradiating the sample as a homogeneous mixture in KBr. (The irradiated sample was dissolved in CDCl_3 under dark and the $^1\text{H-NMR}$ has been recorded immediately)

3.7 Summary

In summary, 18 derivatives of tripodal arylazo-3,5-dimethylpyrazole-1-carboxamides have been synthesized in good to excellent yields. Due to the presence of methyl groups in the pyrazoles, their supramolecular interactions are hindered and so these molecules showed better solubility. Due to the presence of three switchable arylazopyrazole groups, not only they showed better light absorption properties, but also photoswitching ability predominantly towards high %ZZZ-isomer. The only exception is the 2-nitro derivative, which did not undergo isomerization at all, presumably experiencing faster reverse switching. Kinetics studies and reversibility studies using **4a** predicted the higher thermal stability of ZZZ-isomer and long-term switching prospects, respectively. Besides the solution phase switching properties, these class of molecules showed excellent solid state switching as well. The stability of the ZZZ-isomer and solid state photoswitching makes these molecules a new class of compounds that can be useful in various applications including the light-driven imaging and erasing.

3.6 Experimental Section

Arylazopyrazoles (**3a-r**) were prepared as mentioned in the procedure indicated in chapter 1. **General method for the synthesis of tripodal arylazo-3,5-dimethylpyrazole derivatives of trimesic acid 4a-r.** An oven dried 100 ml round bottom flask was charged with trimesic acid

(105.1 mg, 0.5 mmol) and phosphorus pentachloride (0.25 gm, 2.5 mmol) and refluxed in dry toluene (15 mL) under a nitrogen atmosphere for three hours to prepare trimesoyl chloride. This trimesoyl chloride was transferred (without isolation) to another oven dried 250 mL round bottom flask containing the corresponding arylazopyrazole **3a-r** (0.320 mg, 1.6 mmol), toluene (30 mL) and pyridine (0.791 mg, 10 mmol) under a nitrogen atmosphere at 0 °C. The Reaction mixture was stirred at 110 °C for 5-7 hours. The precipitate was filtered and washed well with dry ethanol to remove pyridine hydrochloride and the starting material to get the desired product.

Benzene-1,3,5-triyltris((3,5-dimethyl-4-((*E*)-phenyldiazenyl)-1*H*-pyrazol-1-yl)methanone) (**4a**):

Yellow solid, mp = 185-186 °C, 261.11 mg, 69% yield. ¹H NMR (400 MHz, CDCl₃) δ 2.54 (s, 9H), 3.07 (s, 9H), 7.44-7.53 (m, 9H), 7.85-7.87 (d, *J* = 7.3 Hz, 6H), 8.91 (s, 3H); ¹³C NMR (100 MHz, CDCl₃) δ 12.35, 15.38, 122.33, 129.08, 130.68, 132.77, 137.88, 137.93, 145.98, 146.31, 153.22, 166.79; HRMS (ESI-TOF): calcd. for C₄₂H₃₇N₁₂O₃[M+H]⁺: 757.3112, found: 757.3100; IR (ATR, cm⁻¹): 3054, 2918, 1706, 1581, 1440, 1406, 1346, 1287, 1215, 1176, 1078, 1042, 1012, 903, 850, 785, 770, 680, 650.

Benzene-1,3,5-triyltris((4-((*E*)-(3-fluorophenyl)diazenyl)-3,5-dimethyl-1*H*-pyrazol-1-yl)methanone) (**4b**):

Yellow solid, mp = 238-239°C, 271.62 mg, 67% yield. ¹H NMR (400 MHz, CDCl₃) δ 2.55 (s, 9H), 3.09 (s, 9H), 7.14-7.18 (t, *J* = 7.7 Hz, 3H), 7.45-7.55 (m, 6H), 7.68-7.70 (d, *J* = 7.7 Hz, 3H), 8.91 (s, 3H); ¹³C NMR (100 MHz, CDCl₃) δ 12.50, 15.53, 107.41, 107.63, 117.41, 117.63, 120.20, 130.33, 130.43, 132.81, 137.92, 138.10, 146.30, 146.89, 154.81, 154.88, 162.25, 164.71, 166.83; ¹⁹F NMR (376.5 MHz, CDCl₃) δ -111.30; HRMS (ESI-TOF): calcd. for C₄₂H₃₄F₃N₁₂O₃[M+H]⁺: 811.2829, found: 811.2868; IR (ATR, cm⁻¹): 3020, 1708, 1594, 1579, 1489, 1429, 1407, 1372, 1349, 1292, 1214, 1011, 669.

Benzene-1,3,5-triyltris((4-((*E*)-(4-fluorophenyl)diazenyl)-3,5-dimethyl-1*H*-pyrazol-1-yl)methanone) (**4c**):

Yellow solid, mp = 285-286°C, 328.37 mg, 81% yield. ¹H NMR (400 MHz, CDCl₃) δ 2.52 (s, 9H), 3.05 (s, 9H), 7.16-7.21 (t, *J* = 8.6 Hz, 6H), 7.85-7.89 (dd, *J* = 8.9, 5.2 Hz, 6H), 8.89 (s, 3H); ¹³C NMR (100 MHz, CDCl₃) δ 12.48, 15.53, 116.05, 116.28, 124.32, 124.41, 132.86, 137.89, 138.03, 146.13, 146.36, 149.85, 166.89; ¹⁹F NMR (376.5 MHz, CDCl₃) δ -113.02;

HRMS (ESI-TOF): calcd. for $C_{42}H_{34}F_3N_{12}O_3[M+H]^+$: 811.2829, found: 811.2720; IR (ATR, cm^{-1}): 3115, 1705, 1594, 1499, 1470, 1434, 1405, 1378, 1347, 1289, 1229, 1174, 1136, 1089, 1040, 1020, 1009, 989, 934, 897, 837, 817, 758, 746, 736, 728, 712, 671, 640, 627.

Benzene-1,3,5-triyltris((4-((*E*)-(3-chlorophenyl)diazenyl)-3,5-dimethyl-1*H*-pyrazol-1-yl)methanone) (**4d**):

Yellow solid, mp = 219-220°C, 344.0628 mg, 80% yield. 1H NMR (400 MHz, $CDCl_3$) δ 2.52 (s, 3H), 3.07 (s, 3H), 7.40-7.46 (m, 6H), 7.75-7.78 (d, $J = 6.4$ Hz, 3H), 7.83 (s, 3H), 8.91 (s, 3H); HRMS (ESI-TOF): calcd. for $C_{42}H_{34}Cl_3N_{12}O_3[M+H]^+$: 859.1942, found: 859.1988, 861.1957; IR (ATR, cm^{-1}): 3115, 2918, 1726, 1710, 1576, 1426, 1403, 1372, 1345, 1291, 1269, 1218, 1189, 1174, 1019, 924, 902, 879, 782, 757, 734, 713, 673.

Benzene-1,3,5-triyltris((4-((*E*)-(4-chlorophenyl)diazenyl)-3,5-dimethyl-1*H*-pyrazol-1-yl)methanone) (**4e**):

Yellow solid, mp = 275-276°C, 352.66 mg, 82% yield. 1H NMR (400 MHz, $CDCl_3$) δ 2.52 (s, 9H), 3.06 (s, 9H), 7.46-7.48 (d, $J = 8.7$ Hz, 3H), 7.79-7.81 (d, $J = 8.7$ Hz, 6H), 8.90 (s, 3H); ^{13}C NMR (100 MHz, $CDCl_3$) δ 12.51, 15.54, 123.70, 129.47, 132.84, 136.68, 138.00, 138.06, 146.34, 146.50, 151.71, 166.86; HRMS (ESI-TOF): calcd. for $C_{42}H_{34}Cl_3N_{12}O_3[M+H]^+$: 859.1942, found: 859.2005; IR (ATR, cm^{-1}): 3116, 2920, 2851, 1719, 1707, 1579, 1498, 1482, 1426, 1406, 1374, 1345, 1301, 1287, 1220, 1175, 1091, 1047, 927, 894, 830, 783, 757.

Benzene-1,3,5-triyltris((4-((*E*)-(3-bromophenyl)diazenyl)-3,5-dimethyl-1*H*-pyrazol-1-yl)methanone) (**4f**):

Yellow solid, mp = 245-246°C, 307.99 mg, 62% yield. 1H NMR (400 MHz, $CDCl_3$) δ 2.52 (s, 9H), 3.08 (s, 9H), 7.37-7.41 (t, $J = 7.6$ Hz, 3H), 7.56-7.58 (d, $J = 7.3$ Hz, 3H), 7.80-7.82 (d, $J = 7.4$ Hz, 3H), 7.98 (s, 3H), 8.90 (s, 3H); ^{13}C NMR (100 MHz, $CDCl_3$) δ 12.55, 15.58, 122.41, 123.28, 124.39, 130.60, 132.81, 133.42, 137.99, 138.10, 146.28, 147.02, 154.23, 166.83; HRMS (ESI-TOF): calcd. for $C_{42}H_{34}Br_3N_{12}O_3[M+H]^+$: 991.0427, found: 993.0449; IR (ATR, cm^{-1}): 3116, 2924, 1720, 1700, 1579, 1499, 1478, 1462, 1431, 1402, 1380, 1345, 1273, 1216, 1186, 1175, 1119, 1055, 1046, 1019, 939, 907, 879, 837, 800, 719, 648.

Benzene-1,3,5-triyltris((4-((*E*)-(4-bromophenyl)diazenyl)-3,5-dimethyl-1*H*-pyrazol-1-yl)methanone) (**4g**):

Yellow solid, mp = 236-236°C, 312.96 mg, 63% yield. ¹H NMR (400 MHz, CDCl₃) δ 2.52 (s, 9H), 3.05 (s, 9H), 7.62-7.64 (d, *J* = 8.3 Hz, 3H), 7.72-7.74 (d, *J* = 8.4 Hz, 6H), 8.89 (s, 3H); ¹³C NMR (100 MHz, CDCl₃) δ 12.52, 15.57, 123.94, 125.10, 132.44, 132.81, 138.00, 138.06, 146.32, 146.60, 152.04, 166.84; HRMS (ESI-TOF): calcd. for C₄₂H₃₄Br₃N₁₂O₃[M+H]⁺: 991.0427, found: 991.0389; IR (ATR, cm⁻¹): 3115, 2925, 2349, 1722, 1708, 1578, 1498, 1477, 1427, 1406, 1375, 1345, 1301, 1286, 1220, 1174, 1122, 1094, 1068, 1047, 1019, 1006, 961, 927, 893, 838, 826, 780, 758, 732, 713.

Benzene-1,3,5-triyltris((3,5-dimethyl-4-((*E*)-(2-(trifluoromethyl)phenyl)diazenyl)-1*H*-pyrazol-1-yl)methanone) (**4h**):

Yellow solid, mp = 262-263°C, 427.57 mg, 89% yield. ¹H NMR (400 MHz, CDCl₃) δ 2.53 (s, 9H), 3.10 (s, 9H), 7.52-7.56 (t, *J* = 6.9 Hz, 3H), 7.63-7.67 (t, *J* = 7.9 Hz, 3H), 7.81-7.83 (d, *J* = 7.6 Hz, 6H), 8.91 (s, 3H); ¹³C NMR (100 MHz, CDCl₃) δ 12.49, 15.30, 115.90, 126.66, 128.08, 128.39, 130.19, 132.67, 132.80, 138.07, 138.65, 146.50, 147.91, 150.10, 166.83; ¹⁹F NMR (376.5 MHz, CDCl₃) δ -61.41; HRMS (ESI-TOF): calcd. for C₄₅H₃₄F₉N₁₂O₃[M+H]⁺: 961.2733, found: 961.2696; IR (ATR, cm⁻¹): 3137, 2934, 1712, 1696, 1600, 1579, 1517, 1495, 1435, 1407, 1373, 1350, 1310, 1285, 1268, 1219, 1196, 1168, 1107, 1052, 1035, 1020, 953, 911, 889, 756, 732, 717, 653.

Benzene-1,3,5-triyltris((3,5-dimethyl-4-((*E*)-(3-(trifluoromethyl)phenyl)diazenyl)-1*H*-pyrazol-1-yl)methanone) (**4i**):

Yellow solid, mp = 256-257°C, 422.76 mg, 88% yield. ¹H NMR (400 MHz, CDCl₃) δ 2.55 (s, 9H), 3.09 (s, 9H), 7.61-7.65 (t, *J* = 7.7 Hz, 3H), 7.70-7.72 (d, *J* = 7.5 Hz, 3H), 8.02-8.04 (d, *J* = 7.8 Hz, 3H), 8.10 (s, 3H), 8.93 (s, 3H); ¹³C NMR (100 MHz, CDCl₃) δ 12.57, 15.59, 119.51, 122.65, 125.47, 127.05, 129.83, 131.69, 132.02, 132.80, 138.03, 138.13, 146.24, 147.26, 153.26, 166.81; ¹⁹F NMR (376.5 MHz, CDCl₃) δ -65.87; HRMS (ESI-TOF): calcd. for C₄₅H₃₄F₉N₁₂O₃[M+H]⁺: 961.2733, found: 961.2770; IR (ATR, cm⁻¹): 3123, 1701, 1581, 1493, 1335, 1404, 1382, 1372, 1350, 1327, 1295, 1218, 1184, 1166, 1120, 1092, 1045, 1022, 1003, 933, 906, 803, 736, 718, 691, 657.

Benzene-1,3,5-triyltris((3,5-dimethyl-4-((*E*)-(4-(trifluoromethyl)phenyl)diazenyl)-1*H*-pyrazol-1-yl)methanone) (**4j**):

Yellow solid, mp = 237-238°C, 408.35 mg, 85% yield. ¹H NMR (400 MHz, CDCl₃) δ 2.54 (s, 9H), 3.09 (s, 9H), 7.75-7.77 (d, *J* = 8.3 Hz, 6H), 7.92-7.94 (d, *J* = 8.2 Hz, 6H), 8.92 (s, 3H); ¹³C NMR (100 MHz, CDCl₃) δ 12.55, 15.59, 122.63, 126.41, 126.45, 131.87, 132.30, 132.73, 138.15, 146.17, 147.49, 155.09, 166.78; ¹⁹F NMR (376.5 MHz, CDCl₃) δ 65.69; HRMS (ESI-TOF): calcd. for C₄₅H₃₄F₉N₁₂O₃[M+H]⁺: 961.2733, found: 961.2776; IR (ATR, cm⁻¹): 3128, 3088, 2931, 1703, 1613, 1574, 1427, 1406, 1361, 1320, 1290, 1221, 1169, 1114, 1065, 1013, 894, 847, 828, 742, 717, 648.

Benzene-1,3,5-triyltris((3,5-dimethyl-4-((*E*)-(2-nitrophenyl)diazenyl)-1*H*-pyrazol-1-yl)methanone) (**4k**):

Orange solid, mp = 242-243°C, 321.06 mg, 72% yield. ¹H NMR (400 MHz, CDCl₃) δ 2.45 (s, 9H), 3.08 (s, 9H), 7.53-7.57 (t, *J* = 7.5 Hz, 3H), 7.68-7.72 (m, 6H), 7.86-7.88 (d, *J* = 7.9 Hz, 3H), 8.89 (s, 3H); ¹³C NMR (100 MHz, CDCl₃) δ 12.51, 15.45, 118.17, 124.03, 130.42, 132.70, 132.92, 138.11, 138.64, 145.74, 146.42, 147.80, 148.43, 166.73; HRMS (ESI-TOF): calcd. for C₄₂H₃₄N₁₅O₉[M+H]⁺: 892.2664, found: 892.2626; IR (ATR, cm⁻¹): 2927, 1729, 1700, 1580, 1535, 1514, 1472, 1428, 1406, 1340, 1288, 1222, 1175, 1139, 1118, 1086, 1044, 1012, 954, 888, 857, 772, 745, 716, 668, 609.

Benzene-1,3,5-triyltris((3,5-dimethyl-4-((*E*)-(3-nitrophenyl)diazenyl)-1*H*-pyrazol-1-yl)methanone) (**4l**):

Orange solid, mp = 216-217°C, 410.24 mg, 92% yield. ¹H NMR (400 MHz, CDCl₃) δ 2.56 (s, 9H), 3.11 (s, 9H), 7.68-7.72 (t, *J* = 8 Hz, 3H), 8.18-8.20 (d, *J* = 7.8 Hz, 3H), 8.30-8.32 (d, *J* = 7.0 Hz, 3H), 8.66 (s, 3H), 8.93 (s, 3H); HRMS (ESI-TOF): calcd. for C₄₂H₃₄N₁₅O₉[M+H]⁺: 892.2664, found: 892.2638; IR (ATR, cm⁻¹): 3104, 2924, 2355, 2262, 1702, 1609, 1580, 1530, 1503, 1470, 1432, 1403, 1372, 1344, 1290, 1219, 1173, 1120, 1076, 1043, 1020, 1003, 944, 904, 867, 855, 804, 787, 666.

Benzene-1,3,5-triyltris((3,5-dimethyl-4-((*E*)-(4-nitrophenyl)diazenyl)-1*H*-pyrazol-1-yl)methanone) (**4m**):

Orange solid, mp = 234-235°C, 410.24 mg, 92% yield. ¹H NMR (400 MHz, CDCl₃) δ 2.55 (s, 9H), 3.11 (s, 9H), 7.96-7.98 (d, *J* = 8.6 Hz, 6H), 8.37-8.39 (d, *J* = 8.6 Hz, 6H), 8.93 (s, 3H);

^{13}C NMR (100 MHz, CDCl_3) δ 12.62, 15.62, 123.05, 124.94, 132.71, 138.20, 138.46, 146.09, 148.40, 148.61, 156.44, 166.69; HRMS (ESI-TOF): calcd. for $\text{C}_{42}\text{H}_{34}\text{N}_{15}\text{O}_9[\text{M}+\text{H}]^+$: 892.2664, found: 892.2637; IR (ATR, cm^{-1}): 3104, 2927, 1770, 1699, 1607, 1575, 1523, 1466, 1432, 1403, 1373, 1336, 1285, 1219, 1170, 1149, 1103, 1043, 1018, 1005, 893, 859, 830, 775, 755, 726, 717, 679,

Benzene-1,3,5-triyltris((4-((*E*)-(4-iodophenyl)diazenyl)-3,5-dimethyl-1*H*-pyrazol-1-yl)methanone) (**4n**):

Yellow solid, mp = 233-234°C, 453.81 mg, 80% yield. ^1H NMR (400 MHz, CDCl_3) δ 2.51 (s, 9H), 3.05 (s, 9H), 7.57-7.59 (d, $J = 8.6$ Hz, 6H), 7.83-7.85 (d, $J = 8.6$ Hz, 6H), 8.89 (s, 3H); ^{13}C NMR (100 MHz, CDCl_3): δ 12.52, 15.56, 97.28, 124.07, 132.80, 138.00, 138.08, 138.46, 146.33, 146.63, 152.65, 166.83; HRMS (ESI-TOF): calcd. for $\text{C}_{42}\text{H}_{34}\text{I}_3\text{N}_{12}\text{O}_3[\text{M}+\text{H}]^+$: 1135.0011, found: 1135.0063; IR (ATR, cm^{-1}): 3115, 2921, 2349, 1726, 1711, 1580, 1496, 1475, 1426, 1404, 1387, 1344, 1286, 1221, 1176, 1046, 1003, 825, 777, 758, 735, 628, 609.

Benzene-1,3,5-triyltris((3,5-dimethyl-4-((*E*)-*p*-tolyl)diazenyl)-1*H*-pyrazol-1-yl)methanone) (**4o**):

Yellow solid, mp = 235-236°C, 271.63 mg, 68% yield. ^1H NMR (400 MHz, CDCl_3) δ 2.44 (s, 9H), 2.53 (s, 9H), 3.05 (s, 9H), 7.29-7.31 (d, $J = 8.1$ Hz, 6H), 7.75-7.77 (d, $J = 8.2$ Hz, 6H), 8.90 (s, 3H); ^{13}C NMR (100 MHz, CDCl_3) δ 12.47, 15.51, 21.63, 122.41, 129.84, 132.90, 137.98, 141.31, 145.59, 146.50, 151.46, 166.93; HRMS (ESI-TOF): calcd. for $\text{C}_{45}\text{H}_{43}\text{N}_{12}\text{O}_3[\text{M}+\text{H}]^+$: 799.3581, found: 799.3545; IR (ATR, cm^{-1}): 3112, 2925, 2349, 1721, 1708, 1602, 1583, 1502, 1434, 1408, 1377, 1345, 1309, 1289, 1219, 1177, 1150, 1120, 1104, 1043, 1019, 1007, 894, 821, 759, 737, 709, 674, 623.

4,4',4''-(((1*E*,1'*E*,1''*E*)-((benzene-1,3,5-tricarbonyl)tris(3,5-dimethyl-1*H*-pyrazole-1,4-diyl))tris(diazeno-2,1-diyl))tribenzonitrile (**4p**):

Orange solid, mp = 260-261°C, 303.63 mg, 73% yield. ^1H NMR (400 MHz, CDCl_3) δ 2.53 (s, 9H), 3.09 (s, 9H), 7.79-7.81 (d, $J = 8.3$ Hz, 3H), 7.91-7.93 (d, $J = 8.3$ Hz, 6H), 8.92 (s, 3H); ^{13}C NMR (100 MHz, CDCl_3) δ 12.57, 15.59, 113.74, 118.65, 122.99, 132.71, 133.38, 138.18, 138.30, 146.11, 148.04, 155.20, 166.70; HRMS (ESI-TOF): calcd. for $\text{C}_{45}\text{H}_{34}\text{N}_{15}\text{O}_3[\text{M}+\text{H}]^+$: 832.2969, found: 832.2938; IR (ATR, cm^{-1}): 3114, 2923, 2851, 2228, 1704, 1578, 1497, 1427, 1406, 1371, 1343, 1285, 1220, 1174, 1103, 1042, 1011, 893, 846, 794, 758, 721, 647.

Benzene-1,3,5-triyltris((4-((*E*)-(4-methoxyphenyl)diazenyl)-3,5-dimethyl-1*H*-pyrazol-1-yl)methanone) (**4q**):

Yellow solid, mp = 250-251°C, 292.18 mg, 69% yield. ¹H NMR (400 MHz, CDCl₃) δ 2.52 (s, 9H), 3.04 (s, 9H), 3.90 (s, 9H), 6.99-7.01 (d, *J* = 8.6 Hz, 6H), 7.84-7.86 (d, *J* = 8.7 Hz, 6H), 8.88 (s, 3H); ¹³C NMR (100 MHz, CDCl₃) δ 12.46, 15.50, 55.74, 114.32, 124.22, 132.96, 137.94, 140.88, 144.94, 146.59, 147.77, 161.92, 166.97; HRMS (ESI-TOF): calcd. for C₄₅H₄₃N₁₂O₆[M+H]⁺: 847.3429, found: 847.3455; IR (ATR, cm⁻¹): 2836, 1704, 1599, 1585, 1503, 1464, 1433, 1417, 1372, 1350, 1314, 1290, 1247, 1177, 1147, 1104, 1031, 1020, 1007, 898, 832, 804, 769, 758, 738, 724, 711, 637, 614.

Benzene-1,3,5-triyltris((4-((*E*)-(3,5-difluorophenyl)diazenyl)-3,5-dimethyl-1*H*-pyrazol-1-yl)methanone) (**4r**):

Yellow solid, mp = 263-264°C, 302.67mg, 70% yield. ¹H NMR (400 MHz, CDCl₃) δ 2.51 (s, 9H), 3.07 (s, 9H), 6.89-6.92 (t, *J* = 8.5 Hz, 3H), 7.39-7.40 (d, *J* = 5.6 Hz, 6H), 8.91 (s, 3H); HRMS (ESI-TOF): calcd. for C₄₂H₃₁F₆N₁₂O₃[M+H]⁺: 865.2546, found: 865.2543. IR (ATR, cm⁻¹): 3095, 2925, 2349, 1714, 1614, 1599, 1578, 1499, 1483, 1452, 1432, 1407, 1378, 1349, 1282, 1226, 1202, 1179, 1118, 1043, 1013, 993, 980, 915, 869, 852, 757, 729, 716, 665, 621.

3.7 References:

- (a) Laurent,; Dürr, H. *Pure Appl. Chem.* **2001**, *73*, 639-665. (b) Dürr, H.; Laurent, H. B.-*Photochromism: Molecules and Systems*, Elsevier, Amsterdam, 2003. (c) Irie, M.; Fukaminato, T.; Matsuda, K.; Kobatake, S. *Chem. Rev.* **2014**, *114*, 12174-12277. (d) Irie, M. *Pure Appl. Chem.* **2015**, *87*, 617-626; (e) Zhang, J.; Zou, Q.; Tian, H. *Adv. Mater.* **2013**, *25*, 378-399. (f) Mukhopadhyay, A.; Moorthy, J. N. *J. Photochem. Photobiol. C* **2016**, *29*, 73-106. (g) Pariani, G.; Quintavalla, M.; Colella, L.; Oggioni, L.; Castagna, R.; Ortica, F.; Bertarelli, C.; Bianco, A. *J. Phys. Chem. C* **2017**, *121*, 23592-23598.
- (a) Irie, M. *Photoreactive Materials for Ultrahigh-density Optical Memory*, Elsevier, Amsterdam, 1993; (b) Ikeda, T.; Tsutsumi, O. *Science* **1995**, *268*, 1873-1875. (c) Irie, M. *Chem. Rev.* **2000**, *100*, 1685-1716. (d) Kawata, S.; Kawata, Y. *Chem. Rev.* **2000**, *100*, 1777-1788.
- (a) Lee, J.; Choi, E. J.; Kim, I.; Lee, M.; Satheeshkumar, C.; Song, C. *Sensors* **2017**, *17*, 1816-1826; (b) Klajn, R. *Chem. Soc. Rev.* **2014**, *43*, 148-184. (c) Xie, X.; Mistlberger, G.; Bakker, E. *J. Am. Chem. Soc.*, **2012**, *134*, 16929-16932. (d) Natali, M. Giordani, S. *Chem. Soc. Rev.* **2012**, *41*, 4010-4029.

4. (a) Harada, J.; Kawazoe, Y.; Ogawa, K. *Chem. Commun.* **2010**, *46*, 2593-2595. (b) Hadjoudis, E.; Mavridis, I. M. *Chem. Soc. Rev.* **2004**, *33*, 579-588. (c) Guo, J.; Jia, D.; Liu, L.; Yuan, H.; Li, F. *J. Mater. Chem.* **2011**, *21*, 3210-3215. (d) Robert, F.; Naik, A. D.; Tinant, B.; Robiette, R.; Garcia, Y. *Chem. Eur. J.* **2009**, *15*, 4327-4342. (e) Moorthy, J. N.; Mal, P.; Natarajan, R.; Venugopalan, P. *Org. Lett.* **2001**, *3*, 1579-1582. (f) Luo, Q.; Cao, F.; Xiong, C.; Dou, Q.; Qu, D. -H. *J. Org. Chem.* **2017**, *82*, 10960-10967.
5. Qi, Q.; Li, C.; Liu, X.; Jiang, S.; Xu, Z.; Lee, R.; Zhu, M.; Xu, B.; Tian, W. *J. Am. Chem. Soc.* **2017**, *139*, 16036-16039.
6. Zhou, H.; Xue, C.; Weis, P.; Suzuki, Y.; Huang, S.; Koynov, K.; Auernhammer, G. K.; Berger, R.; Butt, H. J.; Wu, S. *Nat. Chem.* **2017**, *9*, 145-151.
7. Kobatake, S.; Yamashita, I. *Tetrahedron* **2008**, *64*, 7611-7618.
8. Frolova, L. A.; Rezvanova, A. A.; Lukyanov, B. S.; Sanina, N. A.; Troshin, P. A.; Aldoshin, S. M. *J. Mater. Chem. C*, **2015**, *3*, 11675-11680.
9. Devi, S.; Saraswat, M.; Grewal, S.; Venkataramani, S. *J. Org. Chem.*, **2018**, *83*, 4307-4322.
10. Ghebreyessus, K.; Cooper, S. M. *Organometallics* **2017**, *36*, 3360-3370.

Appendix 3A

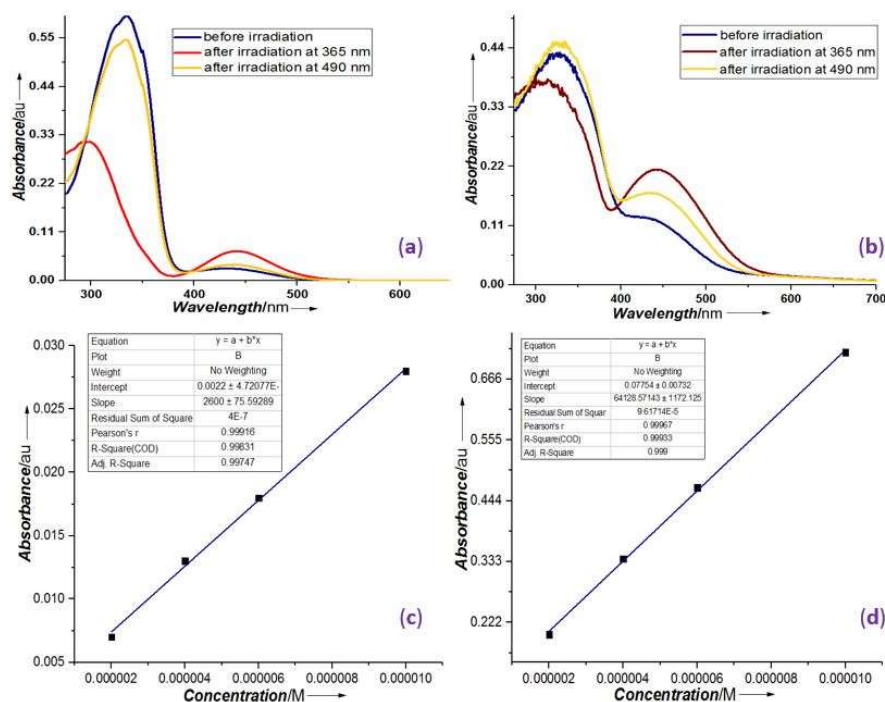


Figure 3A1: UV-Vis photoswitching studies of **4a** (a) in CHCl₃ solvent (10.0 μM); (b) in KBr solid medium; Estimation of molar extinction coefficient for the (c) n-π* absorption and (d) π-π* absorption.

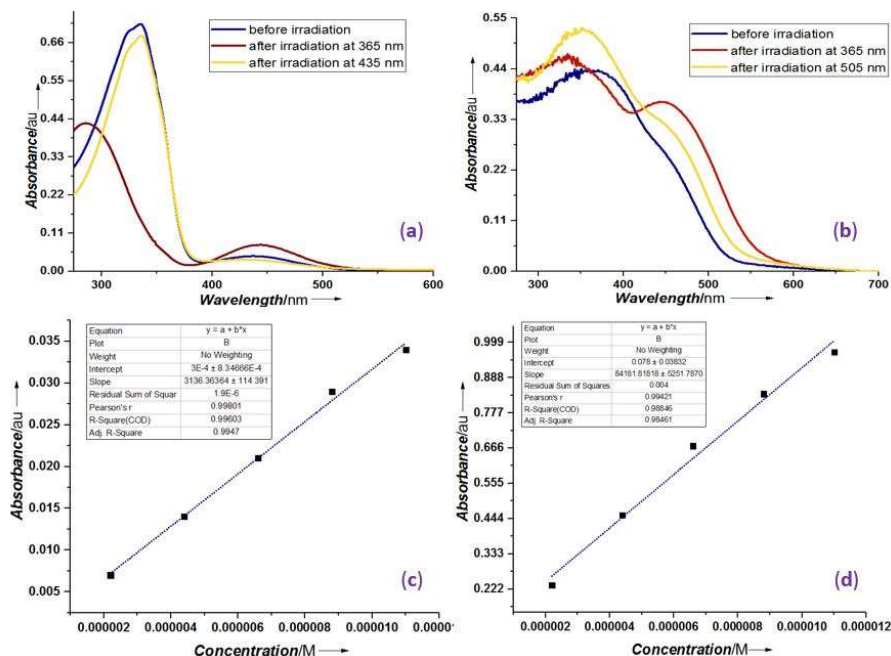


Figure 3A2: UV-Vis photoswitching studies of **4b** (a) in CHCl₃ solvent (9.0 μM); (b) in KBr solid medium; Estimation of molar extinction coefficient for the (c) n-π* absorption and (d) π-π* absorption.

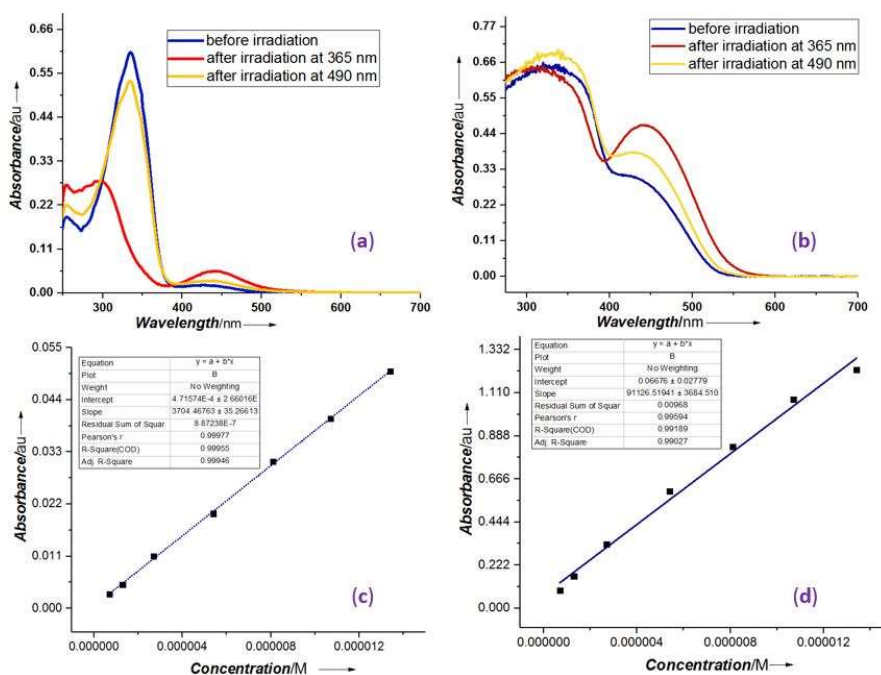


Figure 3A3: UV-Vis photoswitching studies of **4c** (a) in CHCl_3 solvent ($5.4 \mu\text{M}$); (b) in KBr solid medium; Estimation of molar extinction coefficient for the (c) $n-\pi^*$ absorption and (d) $\pi-\pi^*$ absorption.

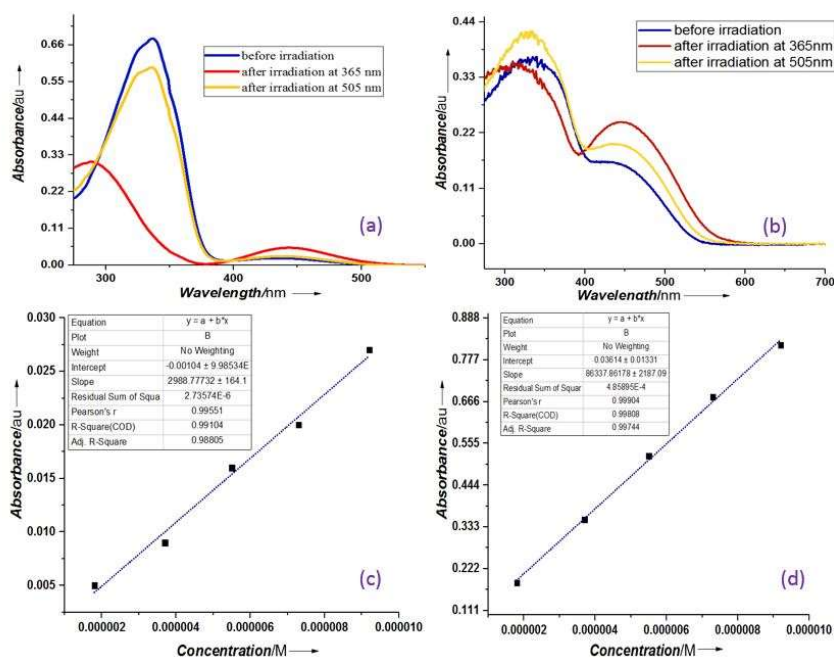


Figure 3A4: UV-Vis photoswitching studies of **4d** (a) in CHCl_3 solvent ($7.3 \mu\text{M}$); (b) in KBr solid medium; Estimation of molar extinction coefficient (in CHCl_3) for the (c) $n-\pi^*$ absorption and (d) $\pi-\pi^*$ absorption.

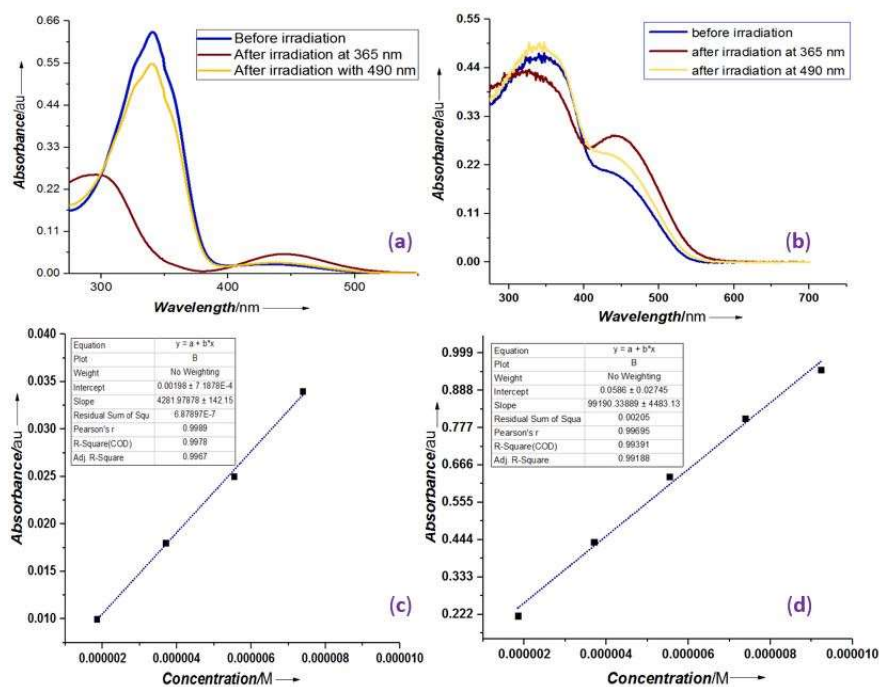


Figure 3A5: UV-Vis photoswitching studies of **4e** (a) in CHCl₃ solvent (5.5 μM); (b) in KBr solid medium; Estimation of molar extinction coefficient (in CHCl₃) for the (c) n-π* absorption and (d) π-π* absorption.

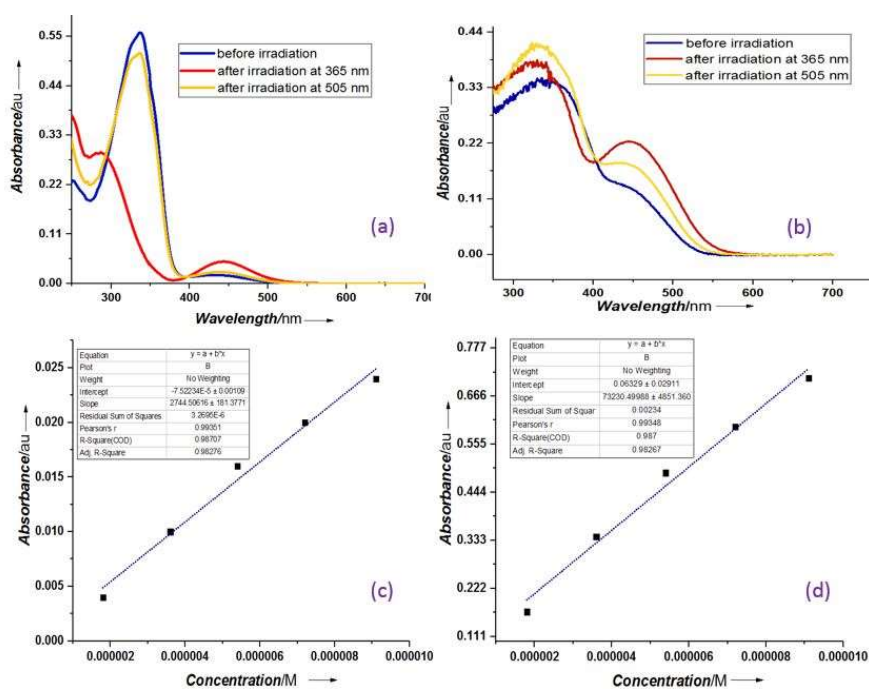


Figure 3A6: UV-Vis photoswitching studies of **4f** (a) in CHCl₃ solvent (7.2 μM); (b) in KBr solid medium; Estimation of molar extinction coefficient (in CHCl₃) for the (c) n-π* absorption and (d) π-π* absorption.

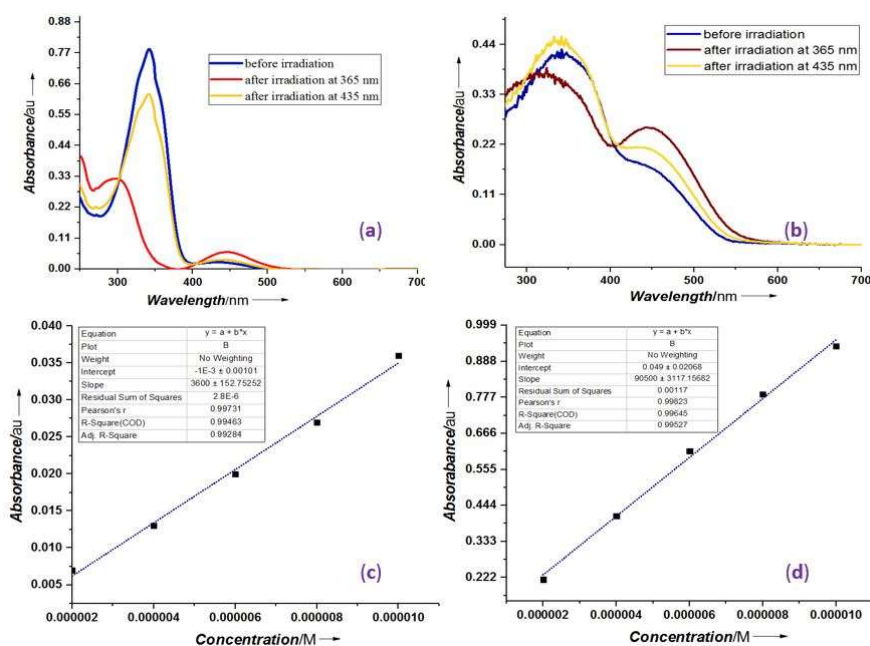


Figure 3A7: UV-Vis photoswitching studies of **4g** (a) in CHCl_3 solvent ($8.0 \mu\text{M}$); (b) in KBr solid medium; Estimation of molar extinction coefficient (in CHCl_3) for the (c) $n-\pi^*$ absorption and (d) $\pi-\pi^*$ absorption.

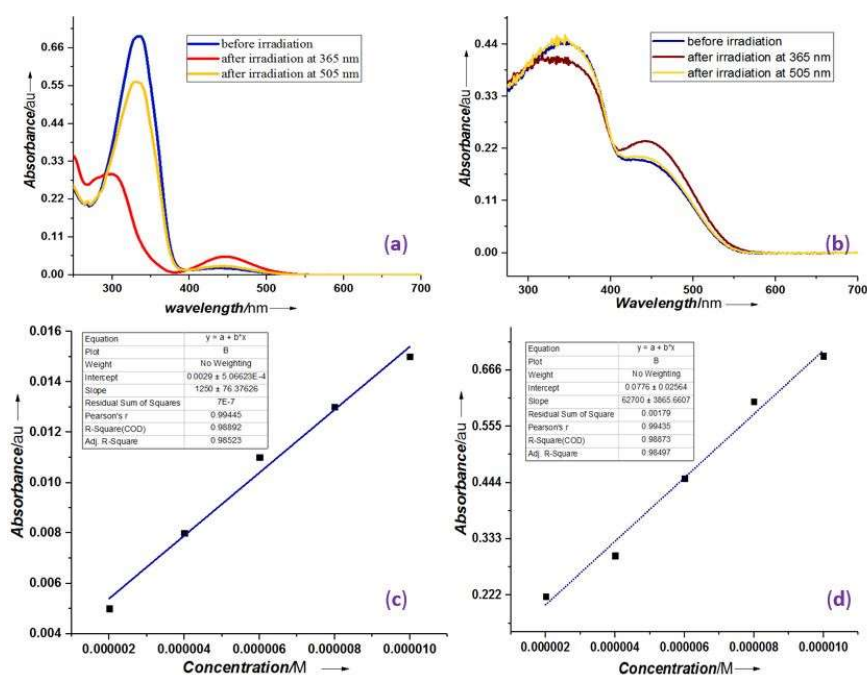


Figure 3A8: UV-Vis photoswitching studies of **4h** (a) in CHCl_3 solvent ($10 \mu\text{M}$); (b) in KBr solid medium; Estimation of molar extinction coefficient (in CHCl_3) for the (c) $n-\pi^*$ absorption and (d) $\pi-\pi^*$ absorption.

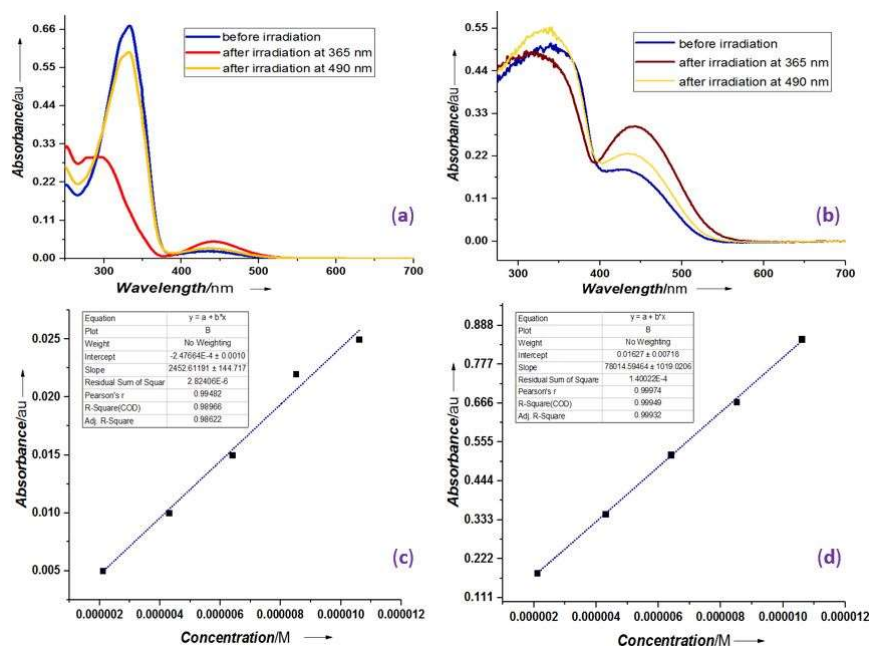


Figure 3A9: UV-Vis photoswitching studies of **4i** (a) in CHCl₃ solvent (8.5 μM); (b) in KBr solid medium; Estimation of molar extinction coefficient (in CHCl₃) for the (c) n-π* absorption and (d) π-π* absorption.

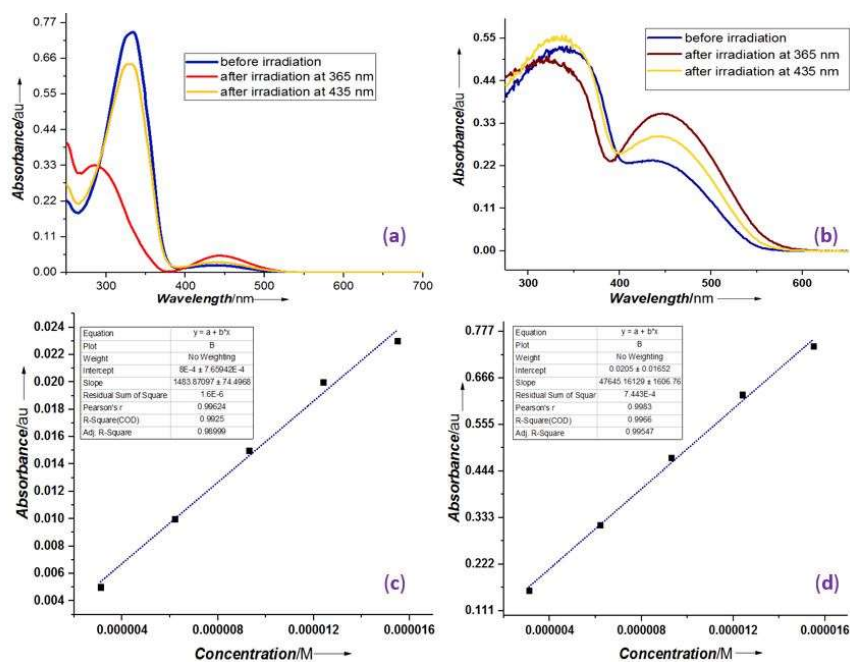


Figure 3A10: UV-Vis photoswitching studies of **4j** (a) in CHCl₃ solvent (15 μM); (b) in KBr solid medium; Estimation of molar extinction coefficient (in CHCl₃) for the (c) n-π* absorption and (d) π-π* absorption.

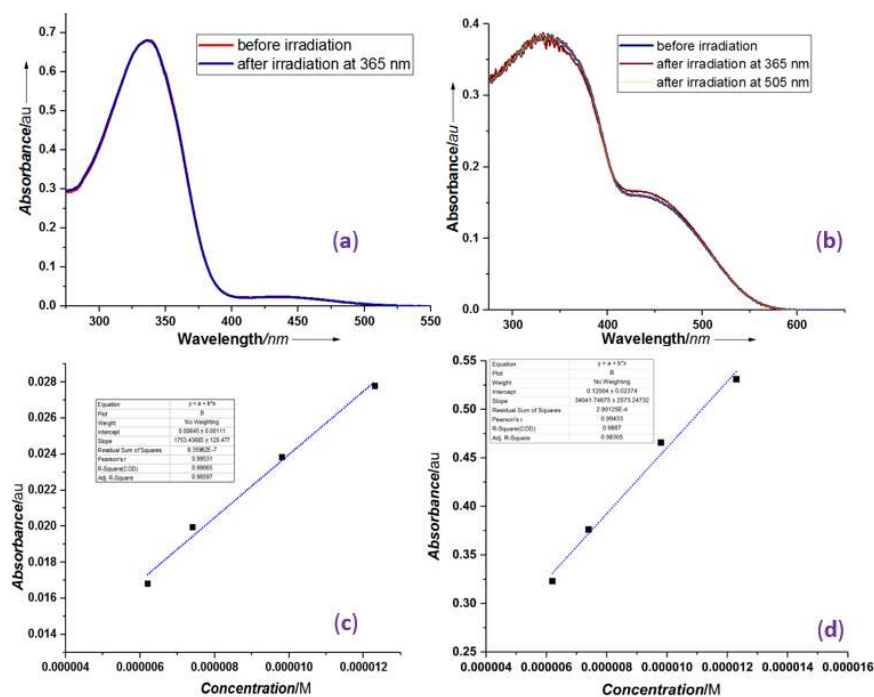


Figure 3A11: UV-Vis photoswitching studies of **4k** (a) in CHCl_3 solvent (μM); (b) in KBr solid medium; Estimation of molar extinction coefficient (in CHCl_3) for the (c) $n-\pi^*$ absorption and (d) $\pi-\pi^*$ absorption.

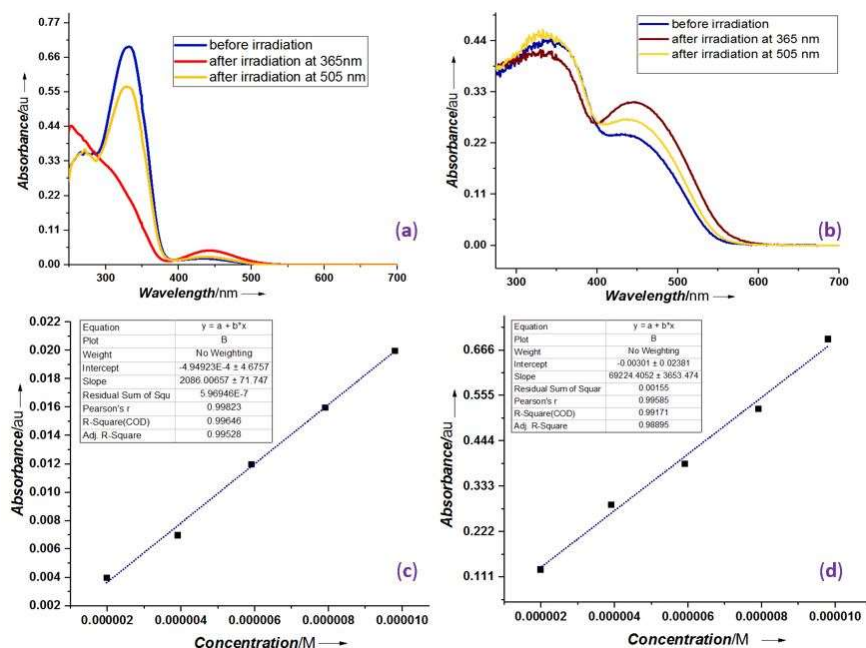


Figure 3A12: UV-Vis photoswitching studies of **4l** (a) in CHCl_3 solvent ($10 \mu\text{M}$); (b) in KBr solid medium; Estimation of molar extinction coefficient (in CHCl_3) for the (c) $n-\pi^*$ absorption and (d) $\pi-\pi^*$ absorption.

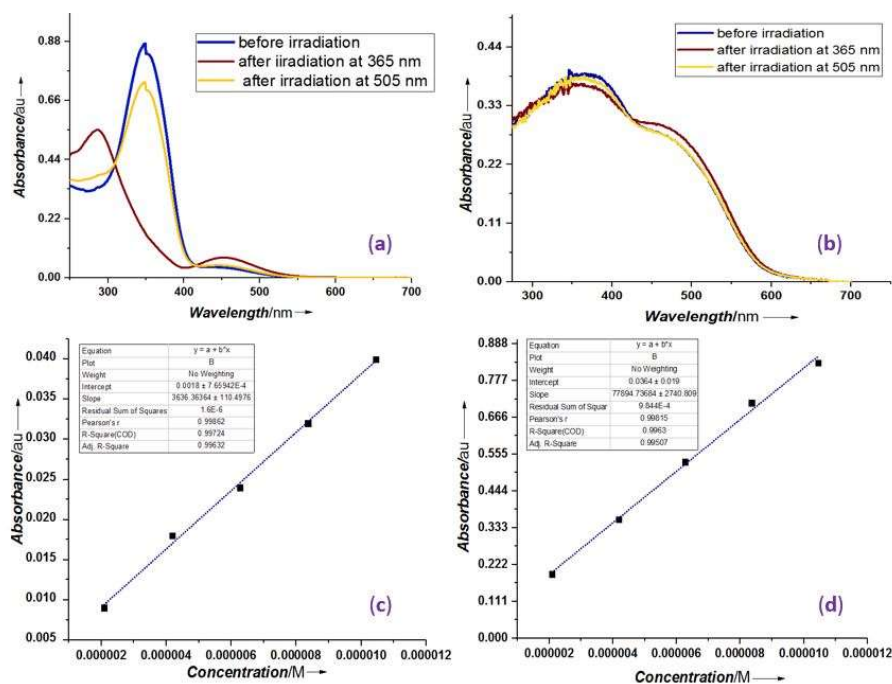


Figure 3A13: UV-Vis photoswitching studies of **4m** (a) in $CHCl_3$ solvent (9.9 μM); (b) in KBr solid medium; Estimation of molar extinction coefficient (in $CHCl_3$) for the (c) $n-\pi^*$ absorption and (d) $\pi-\pi^*$ absorption.

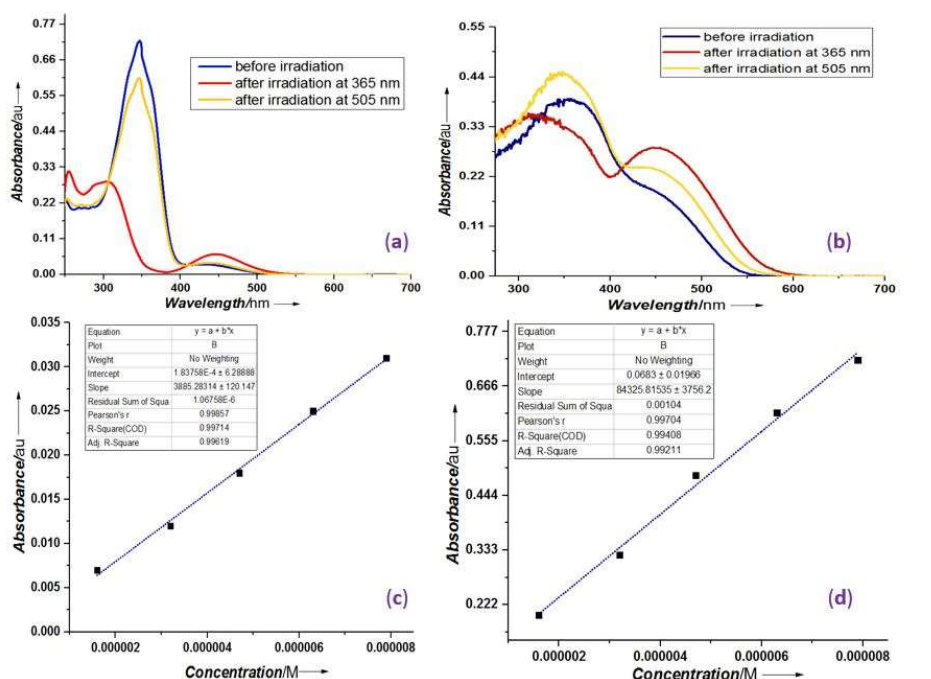


Figure 3A14: UV-Vis photoswitching studies of **4n** (a) in $CHCl_3$ solvent (7.9 μM); (b) in KBr solid medium; Estimation of molar extinction coefficient (in $CHCl_3$) for the (c) $n-\pi^*$ absorption and (d) $\pi-\pi^*$ absorption.

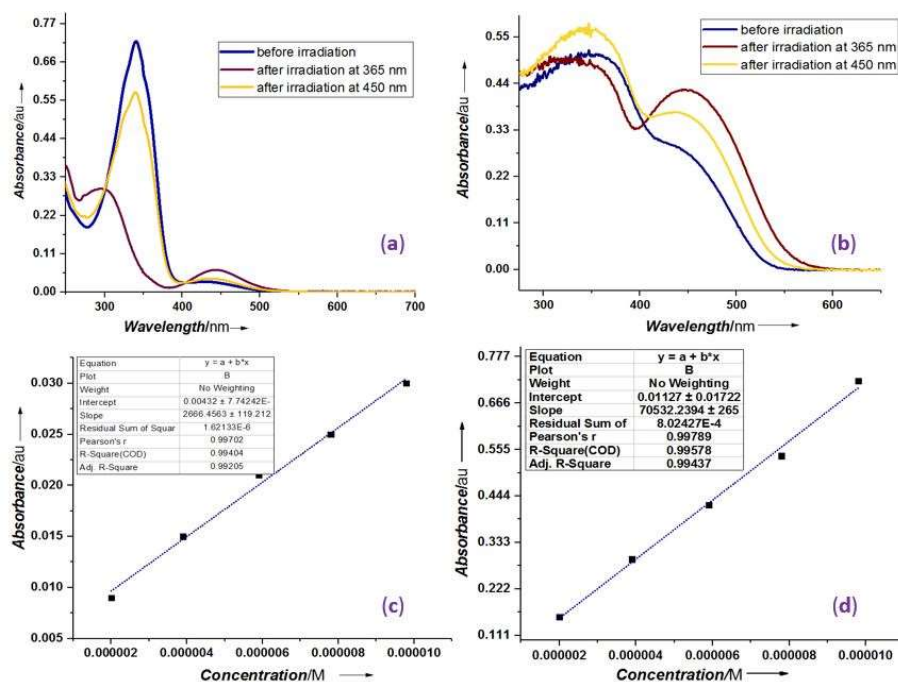


Figure 3A15: UV-Vis photoswitching studies of **4o** (a) in CHCl_3 solvent (9.8 μM); (b) in KBr solid medium; Estimation of molar extinction coefficient (in CHCl_3) for the (c) $n-\pi^*$ absorption and (d) $\pi-\pi^*$ absorption.

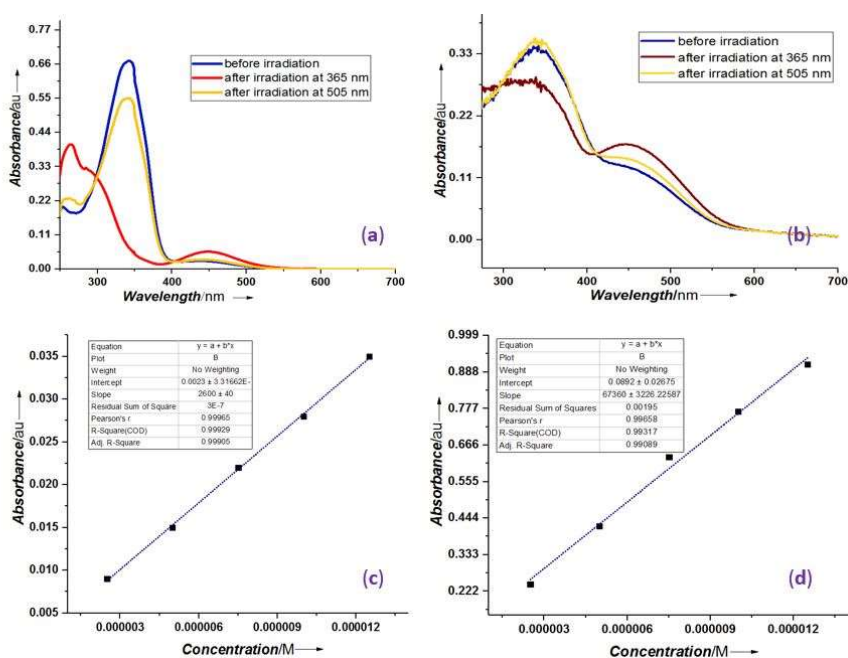


Figure 3A16: UV-Vis photoswitching studies of **4p** (a) in CHCl_3 solvent (10 μM); (b) in KBr solid medium; Estimation of molar extinction coefficient (in CHCl_3) for the (c) $n-\pi^*$ absorption and (d) $\pi-\pi^*$ absorption.

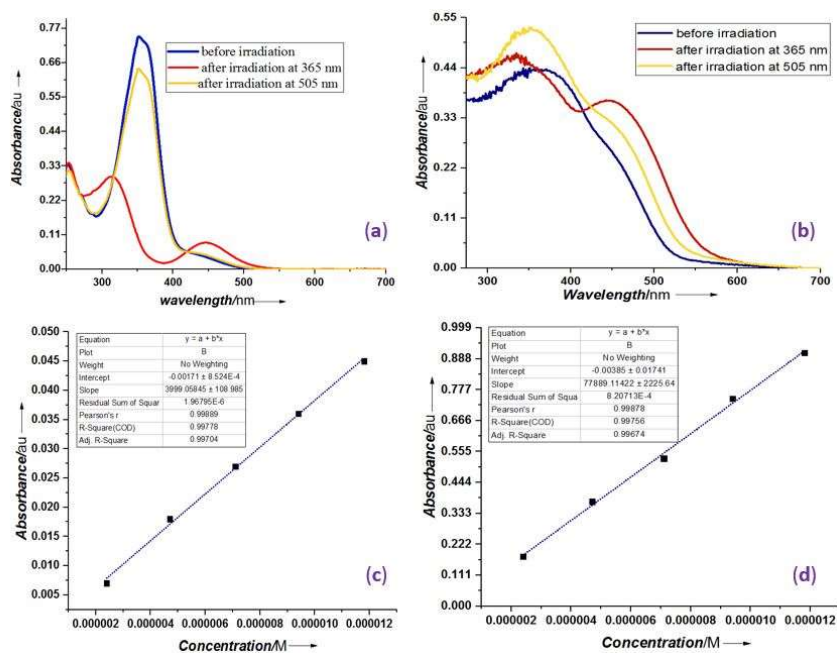


Figure 3A17: UV-Vis photoswitching studies of **4q** (a) in CHCl₃ solvent (9.4 μM); (b) in KBr solid medium; Estimation of molar extinction coefficient (in CHCl₃) for the (c) n-π* absorption and (d) π-π* absorption.

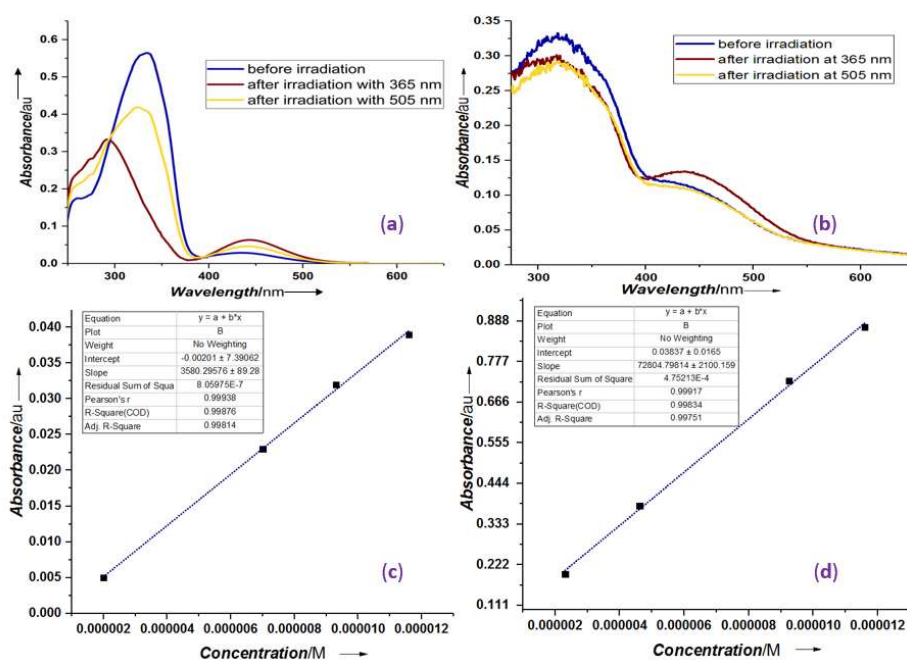


Figure 3A18: UV-Vis photoswitching studies of **4r** (a) in CHCl₃ solvent (15 μM); (b) in KBr solid medium; Estimation of molar extinction coefficient (in CHCl₃) for the (c) n-π* absorption and (d) π-π* absorption.

Appendix 3B

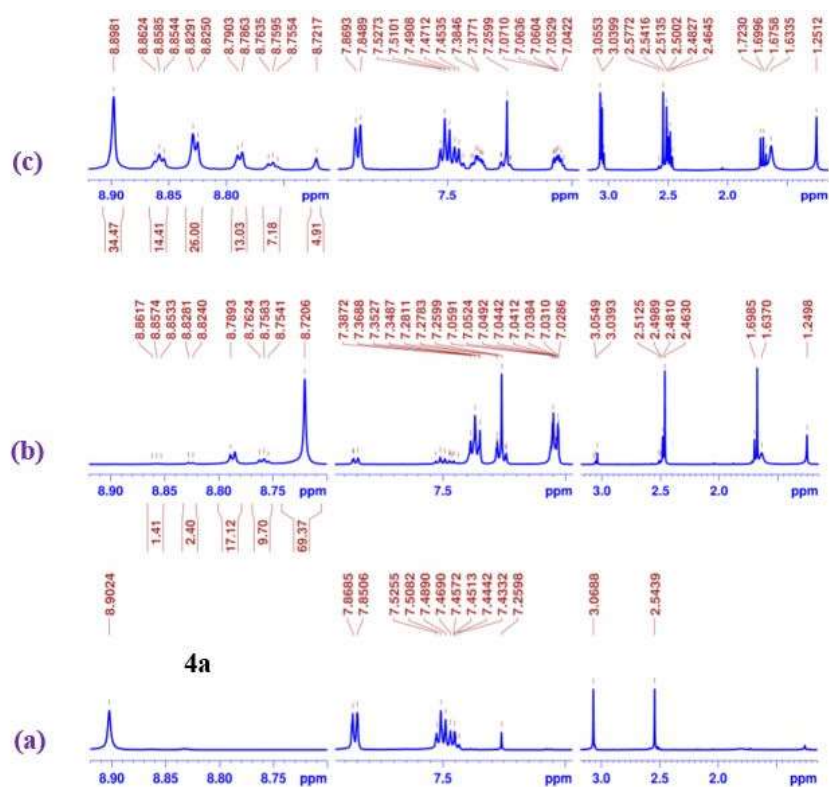


Figure 3B.1: NMR photoswitching studies of **4a** in CDCl_3 (8.5 mM) (a) before irradiation; (b) after irradiation with 365 nm; (c) after irradiation with 490 nm.

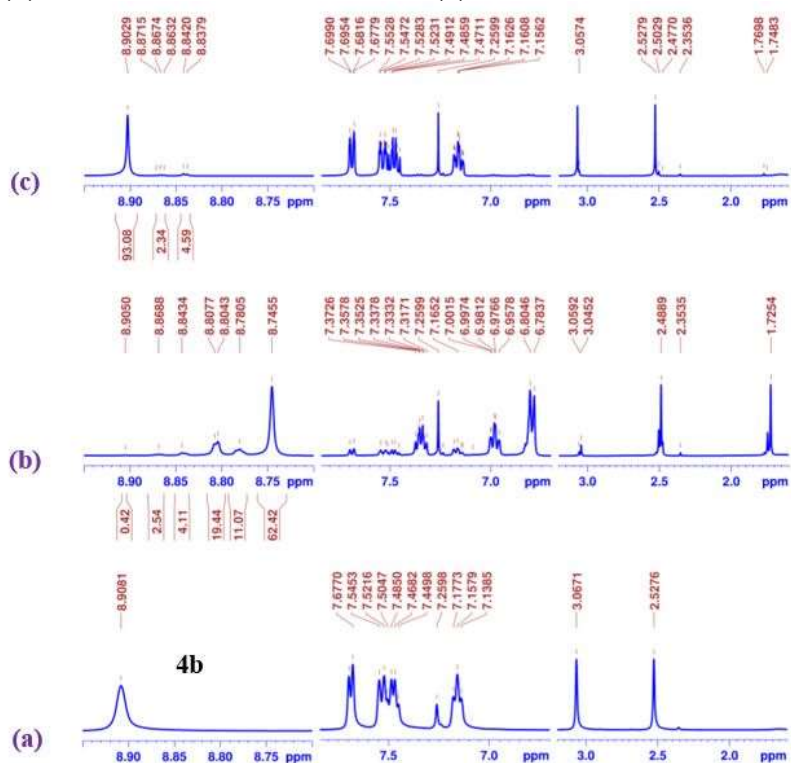


Figure 3B.2: NMR photoswitching studies of **4b** in CDCl_3 (8.5 mM) (a) before irradiation; (b) after irradiation with 365 nm; (c) after irradiation with 435 nm.

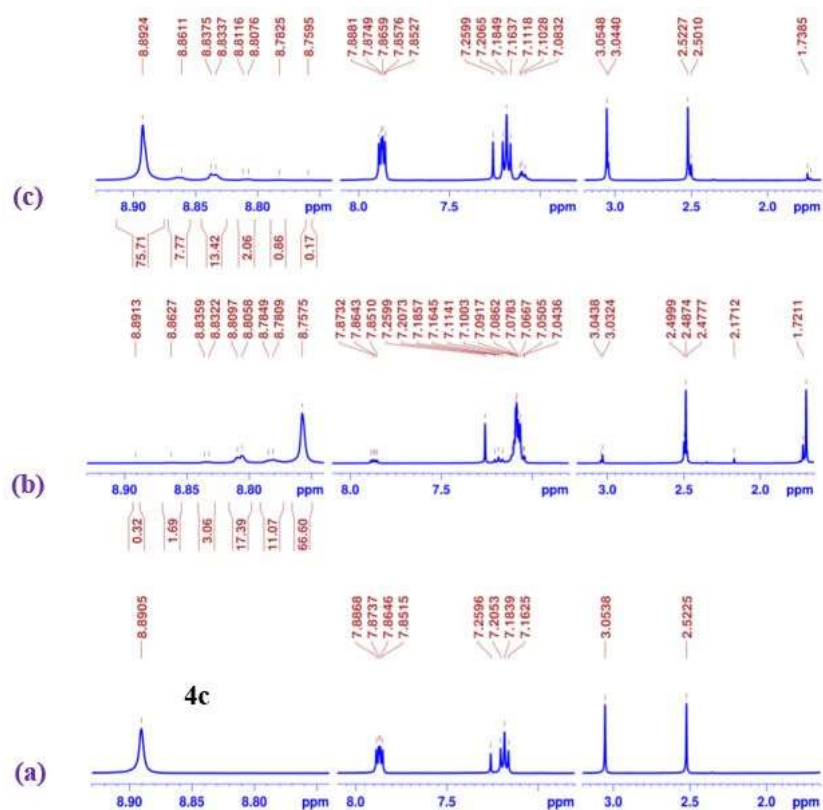


Figure 3B.3: NMR photoswitching studies of **4c** in CDCl_3 (8.5 mM) (a) before irradiation; (b) after irradiation with 365 nm; (c) after irradiation with 490 nm.

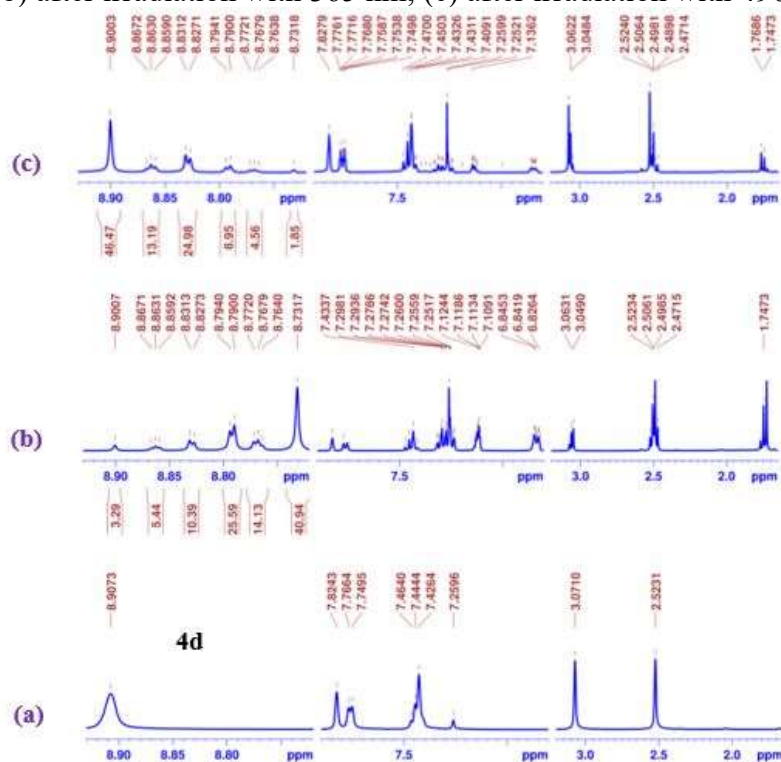


Figure 3B.4: NMR photoswitching studies of **4d** in CDCl_3 (8.5 mM) (a) before irradiation; (b) after irradiation with 365 nm; (c) after irradiation with 505 nm.

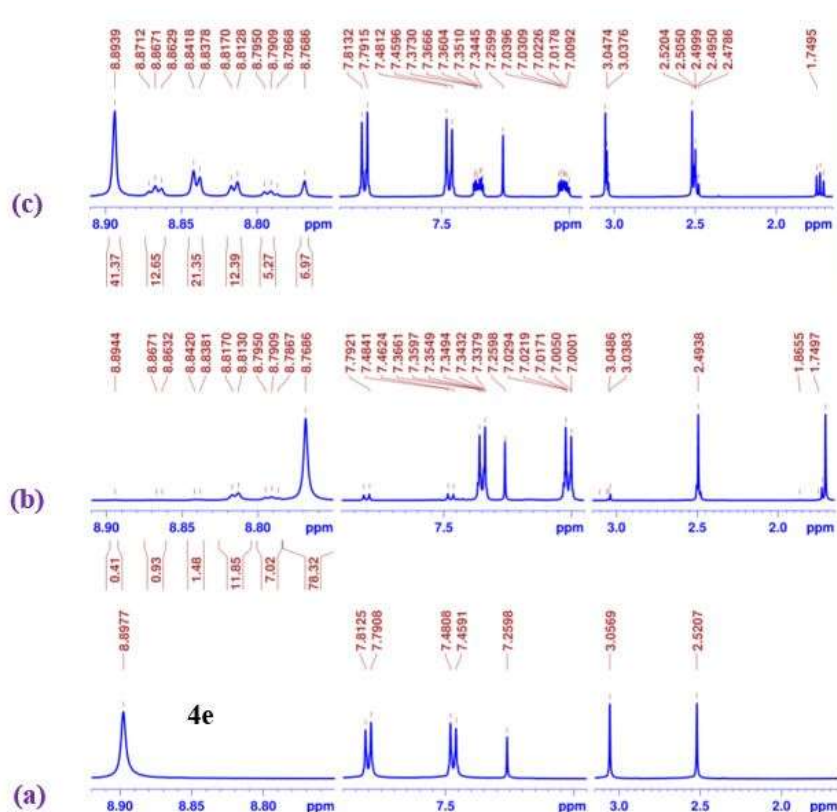


Figure 3B.5: NMR photoswitching studies of **4e** in CDCl_3 (8.5 mM) (a) before irradiation; (b) after irradiation with 365 nm; (c) after irradiation with 450 nm.

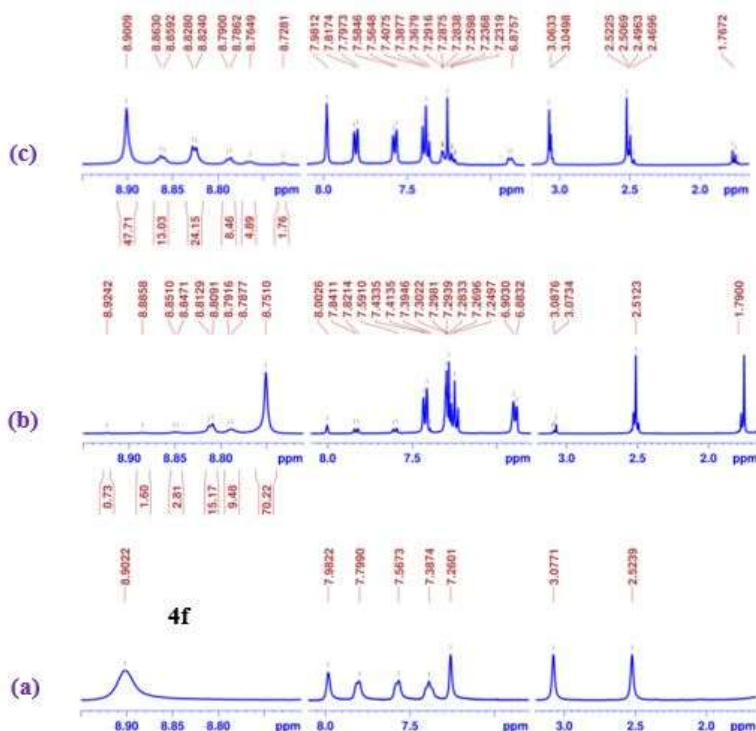


Figure 3B.6: NMR photoswitching studies of **4f** in CDCl_3 (8.5 mM) (a) before irradiation; (b) after irradiation with 365 nm; (c) after irradiation with 505 nm.

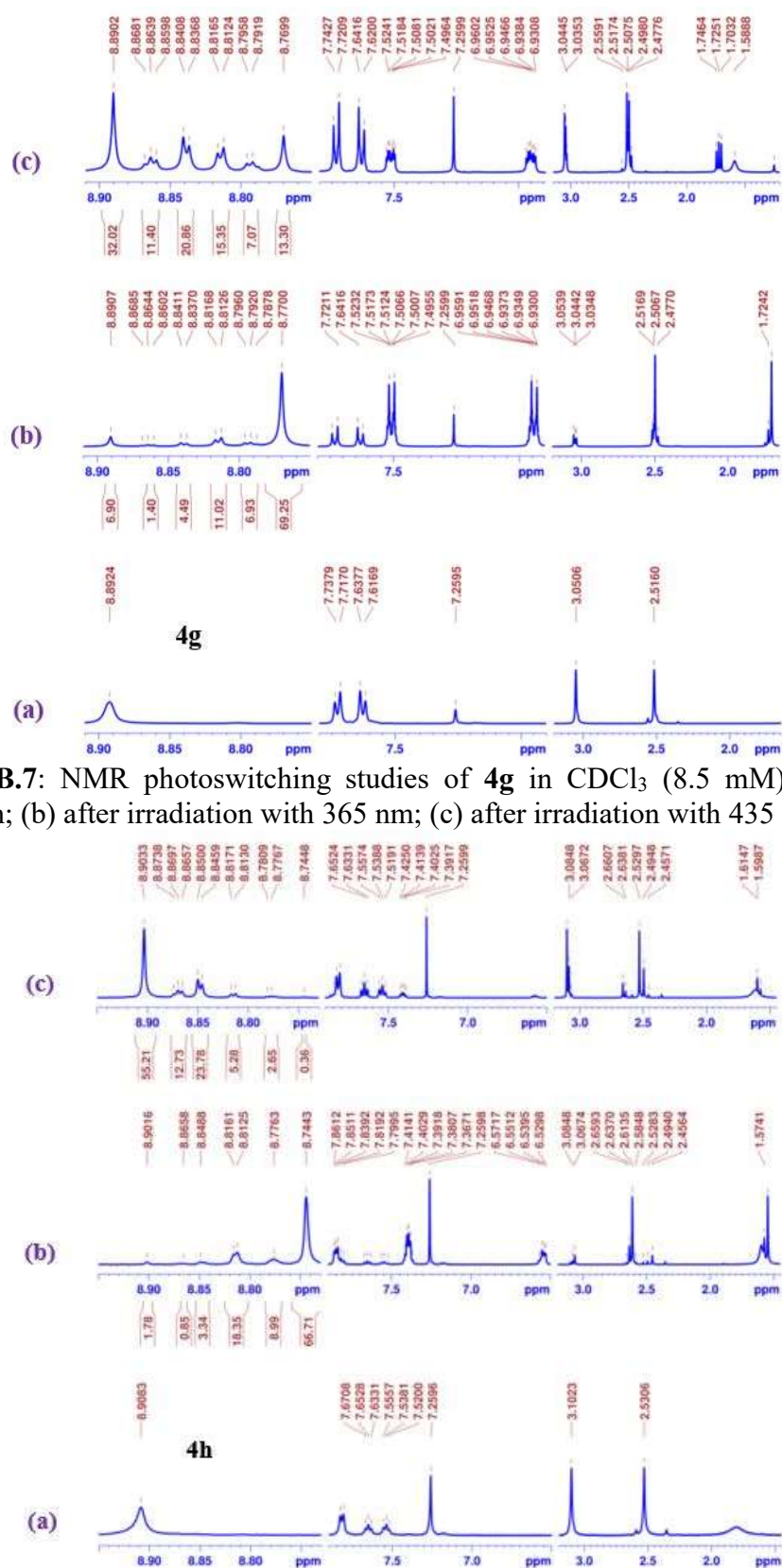


Figure 3B.8: NMR photoswitching studies of **4h** in CDCl_3 (8.5 mM) (a) before irradiation; (b) after irradiation with 365 nm; (c) after irradiation with 505 nm.

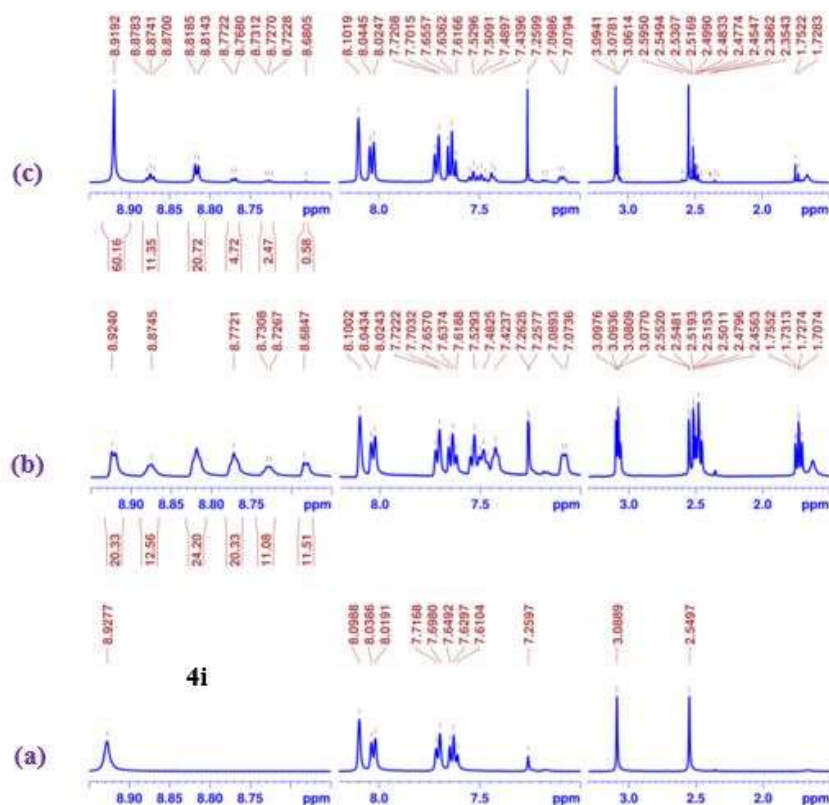


Figure 3B.9: NMR photoswitching studies of **4i** in CDCl_3 (8.5 mM) (a) before irradiation; (b) after irradiation with 365 nm; (c) after irradiation with 490 nm.

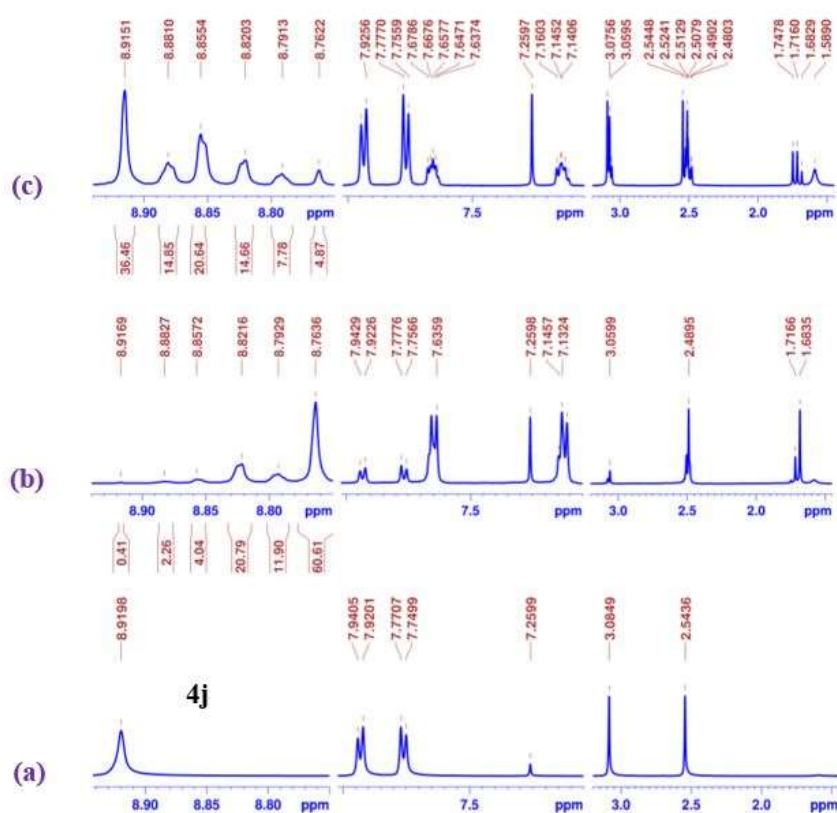


Figure 3B.10: NMR photoswitching studies of **4j** in CDCl_3 (8.5 mM) (a) before irradiation; (b) after irradiation with 365 nm; (c) after irradiation with 435 nm.

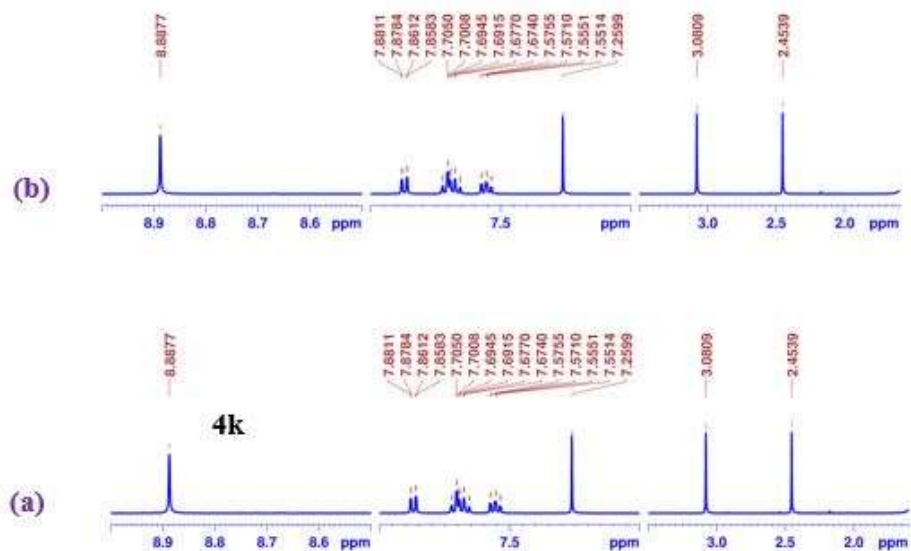


Figure 3B.11: The molecule **4k** did not show photoswitching in CDCl_3 (8.5 mM) (a) before irradiation; (b) after irradiation with 365 nm.

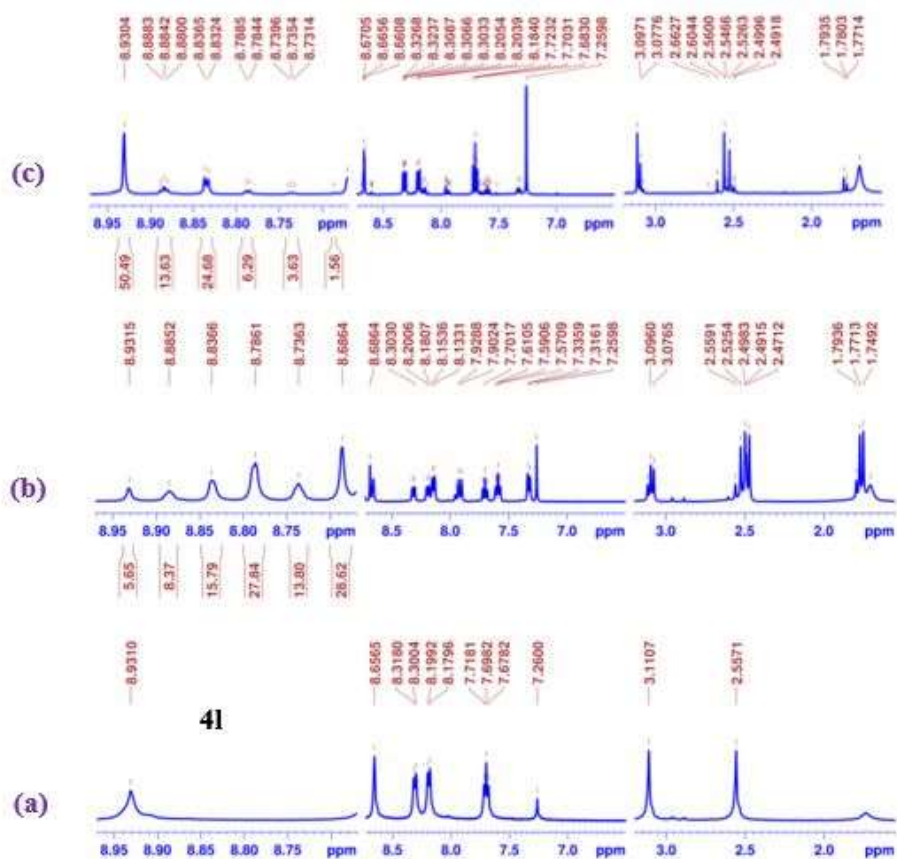


Figure 3B.12: NMR photoswitching studies of **4l** in CDCl_3 (8.5 mM) (a) before irradiation; (b) after irradiation with 365 nm; (c) after irradiation with 505 nm.

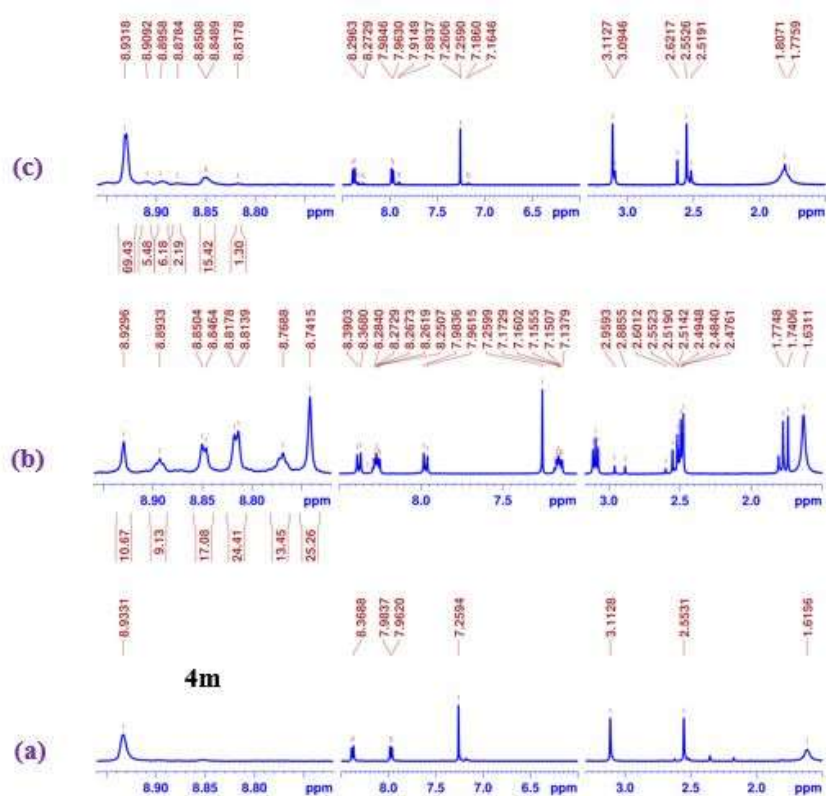


Figure 3B.13: NMR photoswitching studies of **4m** in CDCl_3 (8.5 mM) (a) before irradiation; (b) after irradiation with 365 nm; (c) after irradiation with 505 nm.

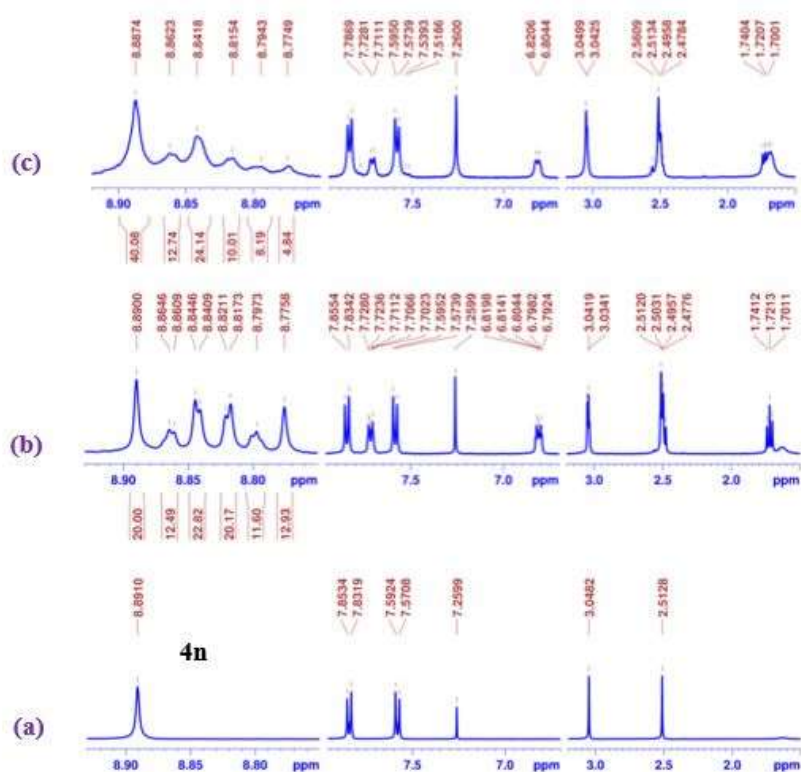


Figure 3B.14: NMR photoswitching studies of **4n** in CDCl_3 (8.5 mM) (a) before irradiation; (b) after irradiation with 365 nm; (c) after irradiation with 505 nm.

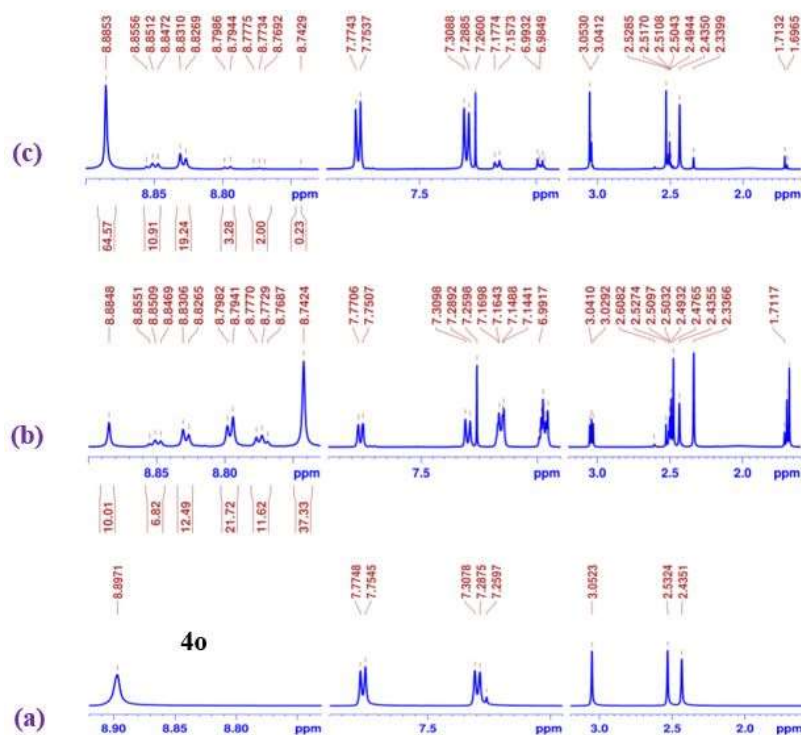


Figure 3B.15: NMR photoswitching studies of **4o** in CDCl_3 (8.5 mM) (a) before irradiation; (b) after irradiation with 365 nm; (c) after irradiation with 450 nm.

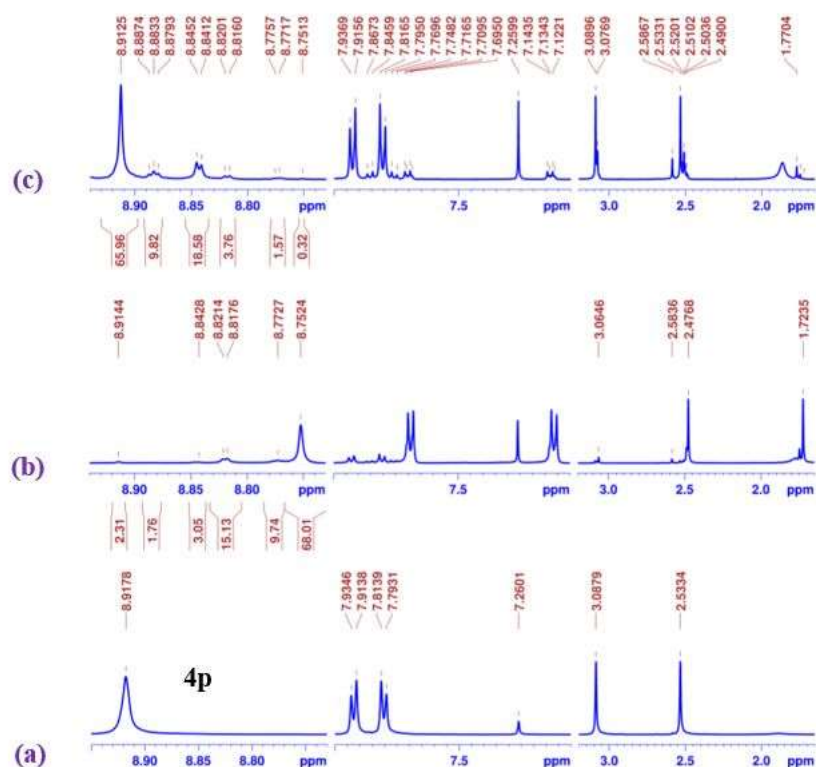


Figure 3B.16: NMR photoswitching studies of **4p** in CDCl_3 (8.5 mM) (a) before irradiation; (b) after irradiation with 365 nm; (c) after irradiation with 505 nm.

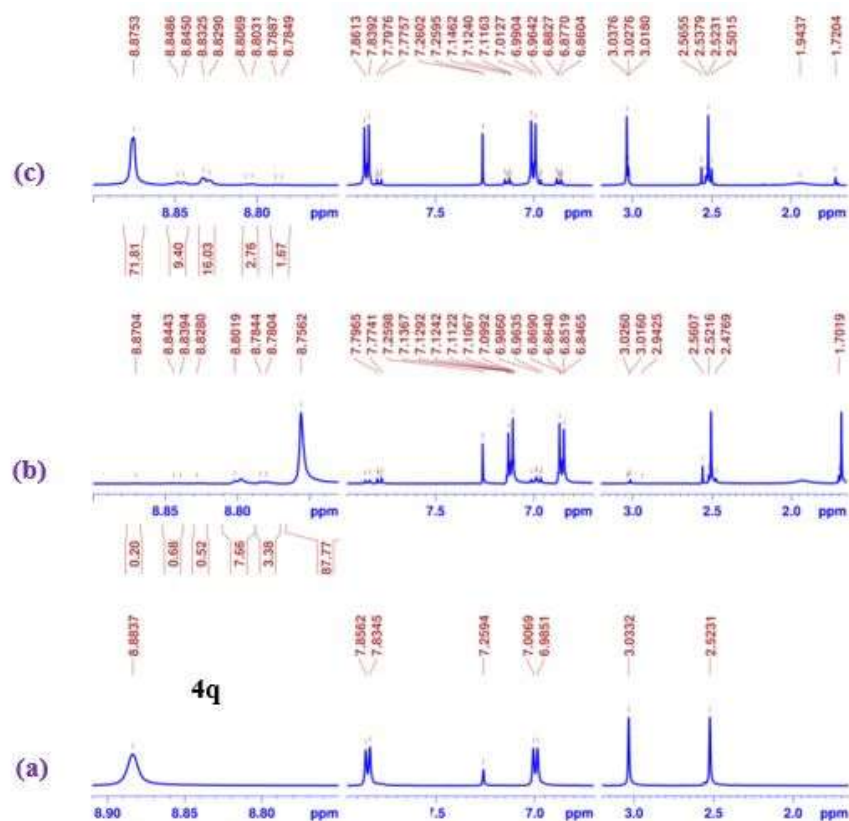


Figure 3B.17: NMR photoswitching studies of **4q** in CDCl₃ (8.5 mM) (a) before irradiation; (b) after irradiation with 365 nm; (c) after irradiation with 505 nm.

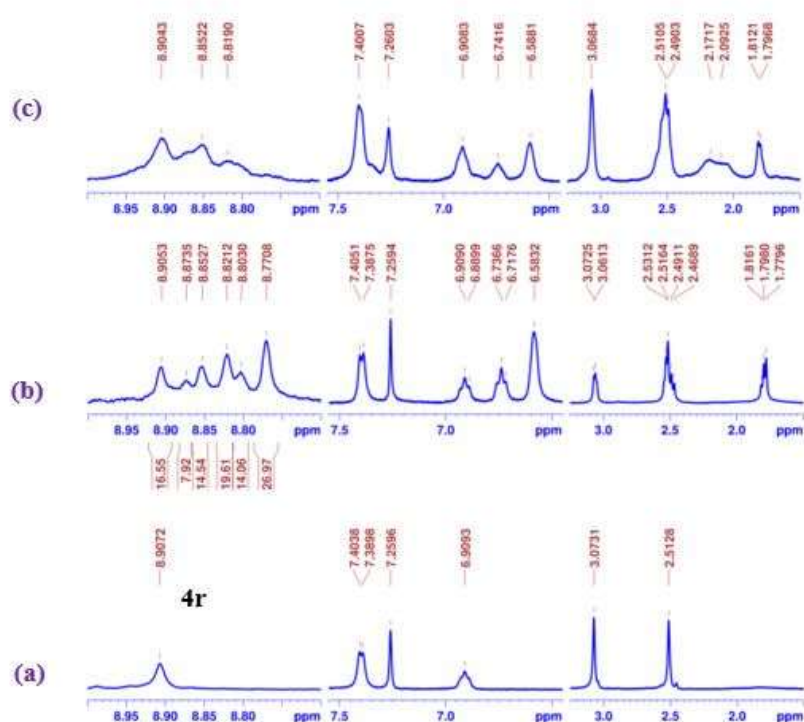
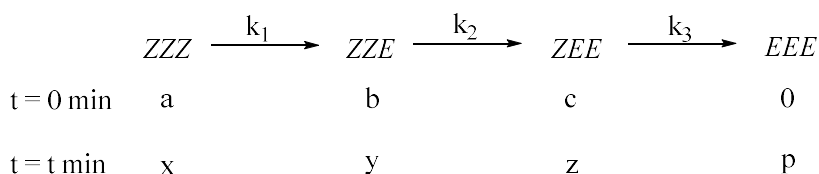


Figure 3B.18: NMR photoswitching studies of **4r** in CDCl₃ (concentration unknown due to poor solubility and precipitation) (a) before irradiation; (b) after irradiation with 365 nm; (c) after irradiation with 505 nm.

Appendix 3C



total concentration (at time $t = 0$ min) $u = a + b + c$

total concentration (at time $t = t$ min) $u = x + y + z + p$

a , b and c are the initial concentrations of ZZZ , ZZE and ZEE , respectively.

x , y , z and p are the concentrations of ZZZ , ZZE , ZEE and EEE , respectively during the kinetics at any given time " t ".

Change in the concentration of ZZZ isomer

$$-\frac{d[ZZZ]}{dt} = k_1[ZZZ]$$

Or

$$-\frac{d[x]}{dt} = k_1[x]$$

$$x = ae^{-k_1 t} \dots\dots\dots(\text{Eqn1})$$

Change in the concentration of ZZE isomer

$$-\frac{d[ZZE]}{dt} = k_2[ZZE] - k_1[ZZZ]$$

$$-\frac{d[y]}{dt} = k_2[y] - k_1[x]$$

$$y(t) = Ae^{-k_2 t} + a \frac{k_1}{(k_2 - k_1)} e^{-k_1 t}$$

Initial condition $t = 0$, $y = b$, then $A = b - a \frac{k_1}{(k_2 - k_1)}$

$$y = \left(b - a \frac{k_1}{k_2 - k_1}\right) e^{-k_2 t} + a \frac{k_1}{(k_2 - k_1)} e^{-k_1 t} \dots\dots\dots(\text{Eqn 2})$$

Change in the concentration of ZEE isomer

$$-\frac{d[ZEE]}{dt} = k_3[ZEE] - k_2[ZZE]$$

$$-\frac{d[c]}{dt} = k_3[c] - k_2[y]$$

$$Z(t) = \left(b - a \frac{k_1}{k_2 - k_1}\right) \left(\frac{k_2}{k_3 - k_2}\right) e^{-k_2 t} + a \frac{k_1}{(k_2 - k_1)} \left(\frac{k_2}{k_3 - k_1}\right) e^{-k_1 t} + C e^{-k_3 t}$$

Initial condition $t = 0, z = c,$
 Then $C = [c - (b - a \frac{k_1}{(k_2 - k_1)}) (\frac{k_2}{(k_3 - k_2)}) - a \frac{k_1}{(k_2 - k_1)} \frac{k_2}{(k_3 - k_1)}] e^{-k_3 t}$

$$z(t) = (b - a \frac{k_1}{k_2 - k_1}) \frac{k_2}{(k_3 - k_2)} e^{-k_2 t} + a \frac{k_1}{(k_2 - k_1)} \frac{k_2}{(k_3 - k_1)} e^{-k_1 t} + [c - (b - a \frac{k_1}{k_2 - k_1}) \frac{k_2}{(k_3 - k_2)} - a \frac{k_1}{(k_2 - k_1)} \frac{k_2}{(k_3 - k_1)}] e^{-k_3 t} \dots\dots\dots(\text{Eqn 3})$$

All the rate constants have been estimated from the data points by fitting them using ROOT (version 6.08) programme. (available at <https://root.cern.ch/>) Rate constants k_1, k_2 and k_3 have been estimated from the Eqn 1, Eqn 2 and Eqn 3, respectively.

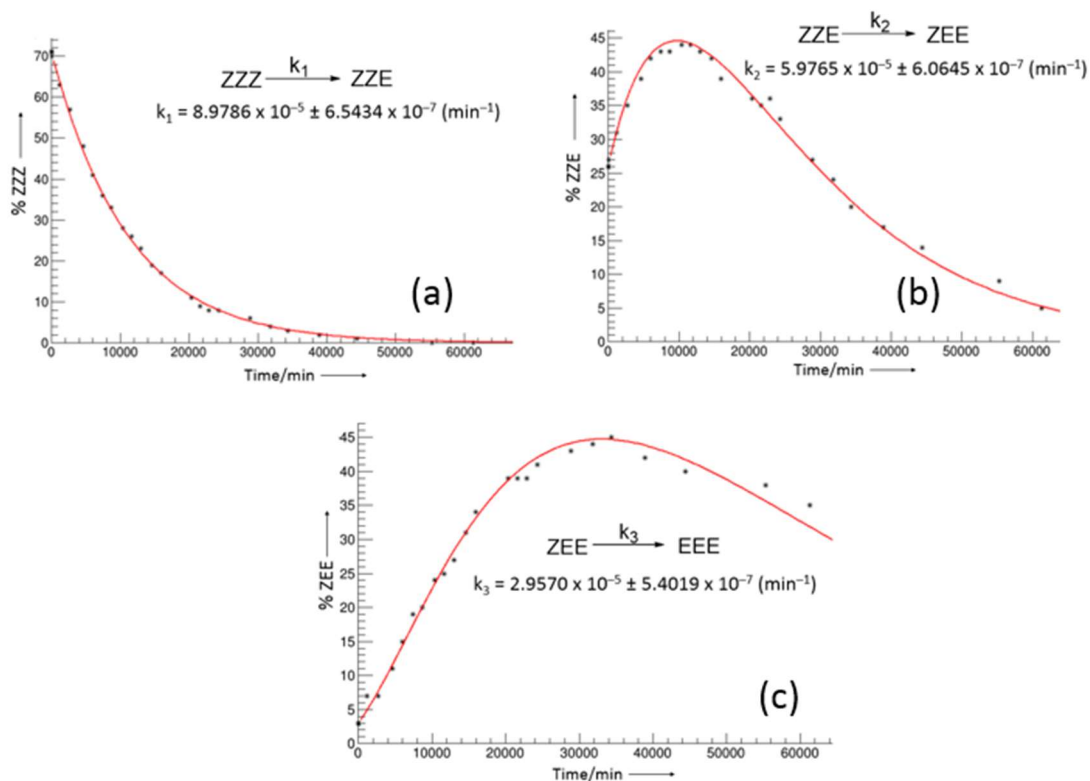


Figure 3C1: Plots corresponding to the fitting of the thermal reverse isomerization kinetics and deducing the rate constants using the ROOT programme for the processes: (a) ZZZ-ZZE, (b) ZZE-ZEE and (c) ZEE- EEE, respectively.

Chapter 4. Photoswitchable discotic liquid crystals

4.1 Introduction

Recently, there have been increasing interest in discotic liquid crystalline (DLC) materials^[1-3] endowed with photoresponsive groups.^[4a] These materials have emerged as fascinating functional materials as it combines the optical properties of the photochromic group and self-assembling and dynamic features of DLCs.^[4b,c] Photochromic liquid crystals (LC) are very useful as they can change their mesomorphic state upon irradiation.^[5-7] Among the various photochromic groups like spirooxazines, diarylethenes, azobenzene etc., azobenzene systems^[4b,5-7] are widely studied owing to the rich photochemistry of azobenzene chromophores and the ease of functionalization. Usually, the LC phases of azobenzene incorporated compounds changed to the isotropic phase on irradiation because of the destabilization in the LC phases due to *Z*-azobenzene.^[8] Azobenzenes compounds can be very useful in making light modulated switches.^[9-11]

The planar structural feature in *E*-isomer of azobenzenes, and the versatile tunability of it provides many opportunities in design and incorporation of azobenzenes in the molecular systems. Particularly when multiple azobenzenes are introduced through amide linkages, the resulting system can form an interesting supramolecular assembly. The π - π stacking provides the necessary driving force in this regard. Such systems have found applications in remote-controllable actuators^{6c}, photoresponsive surfactants¹², and light induced mass transport¹³ etc. Lee et al. explored the stimulus responsive supramolecular assemblies such as fibres, gels, and spheres using these photoswitchable triamides.¹⁴ Recently, Thiele and coworkers reported the *cis-trans* isomerization processes of multi-state photochromic benzenetricarboxamide system using in-situ NMR spectroscopy.¹⁵ The photoisomerization and the reverse thermal isomerization processes are not cooperative. and equally depending on the concentration.

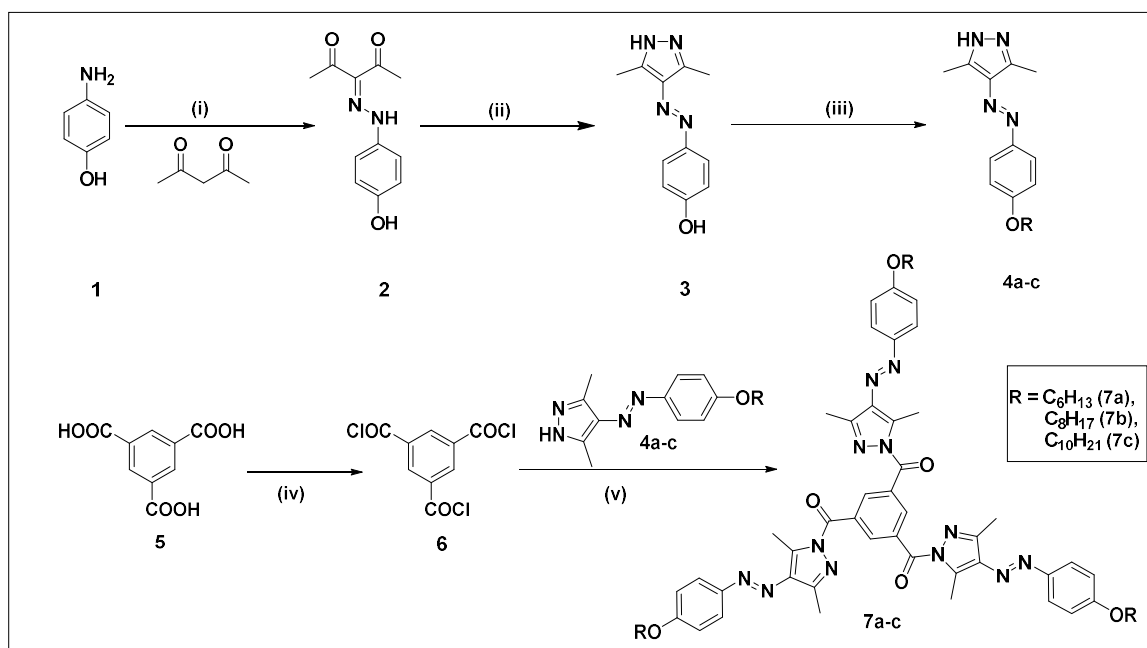
Interestingly, the use of such azobenzene attached benzenetricarboxamide cores in the making of liquid crystals has not been investigated so far. Furthermore, the utilization of these azobenzenetricarboxamide based core can create discotic liquid crystals, due to the well-known behaviour for the formation of columnar mesophase. Considering the fact that these cores are found to be C_3 symmetric with a propeller-like structure, the aggregation of the alkyl chain extensions from the core can presumably provide a large porous architecture. In this context, we designed two different C_3 -symmetric azoarene incorporated benzenetricarboxamide core

with alkyl connected through an ethereal linkage. In the first design, we utilized the 4-alkoxyphenylazopyrazole derivatives, whereas in the later, we utilized the 4-alkoxyphenylazobenzene tricarboxamide derivatives. Herein, we discuss the investigations on the liquid crystalline properties and photoswitching behaviour of both of those systems.

4.2 Tripodal alkoxyphenylazopyrazole based derivatives of trimesic acid

4.2.1 Synthesis

After the successful design and synthesis of the arylazopyrazole based benzene tricarboxamides, we paid our attention to derivatize them towards making discotic liquid crystals. In this regard, we designed the target molecules in such a way by considering arylazopyrazole based benzene tricarboxamides as our core and introduced the flexibility by attaching peripheral alkoxy groups. In this regard, three analogous target molecules **7a-c** by varying the alkoxy chains viz, C₆, C₈ and C₁₀ have been synthesized as follows. (**Scheme 4.1**)



Scheme 4.1: Synthesis of tripodal alkoxy chain connected arylazo-3,5-dimethylpyrazole derivatives of trimesic acid **7a-c**. (i) conc. HCl, NaNO₂, Aq. NaOAc, 0 °C, 4 h, 87%; (ii) NH₂NH₂.2HCl Na₂CO₃, EtOH, Reflux, 13 h, 79%; (iii) K₂CO₃, R-Br, cat. KI, dry DMF, 100 °C, 24 h; **4a**-71%, **4b**-72%, **4c**-71%; (iv) PCl₅, Toluene, reflux; (v) pyridine, Toluene, RT, 12 h, **7a**-96%, **7b**-95%, **7c**-98%.

4.2.2. Photoswitching Studies:

All of the three target molecules have been subjected to photochemistry by using UV-Vis spectroscopic technique. All of them exhibited similar UV-Vis spectral data with almost identical absorption maxima. Even after switching with 365 nm light, the spectral appearance did not differ much. The spectral data are included below. (**Figure 4.1** and **Table 4.1**)

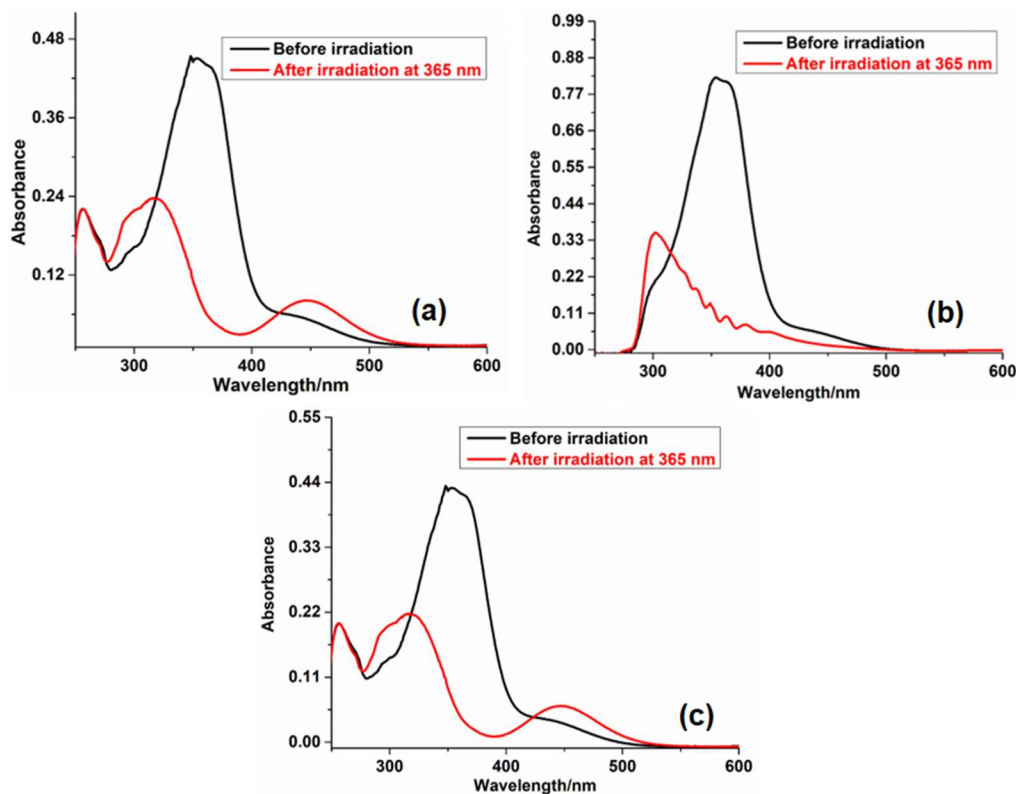


Figure 4.1. Photoswitching studies using UV-Vis spectroscopy for the target molecules (a) **7a**; (b) **7b**; (c) **7c**. All the spectra are recorded in CHCl_3 ; (Black – Before irradiation; Red - After irradiation at 365 nm).

Table 4.1. Spectral properties of all-*trans* and -*cis* isomers using UV-Vis spectroscopy in CHCl_3 at 25 °C.

S. No.	Compound	λ_{max} (EEE)	λ_{max} (After irradiation)
1	7a	353	316, 447
2	7b	353	316, 445
3	7c	353	316, 446

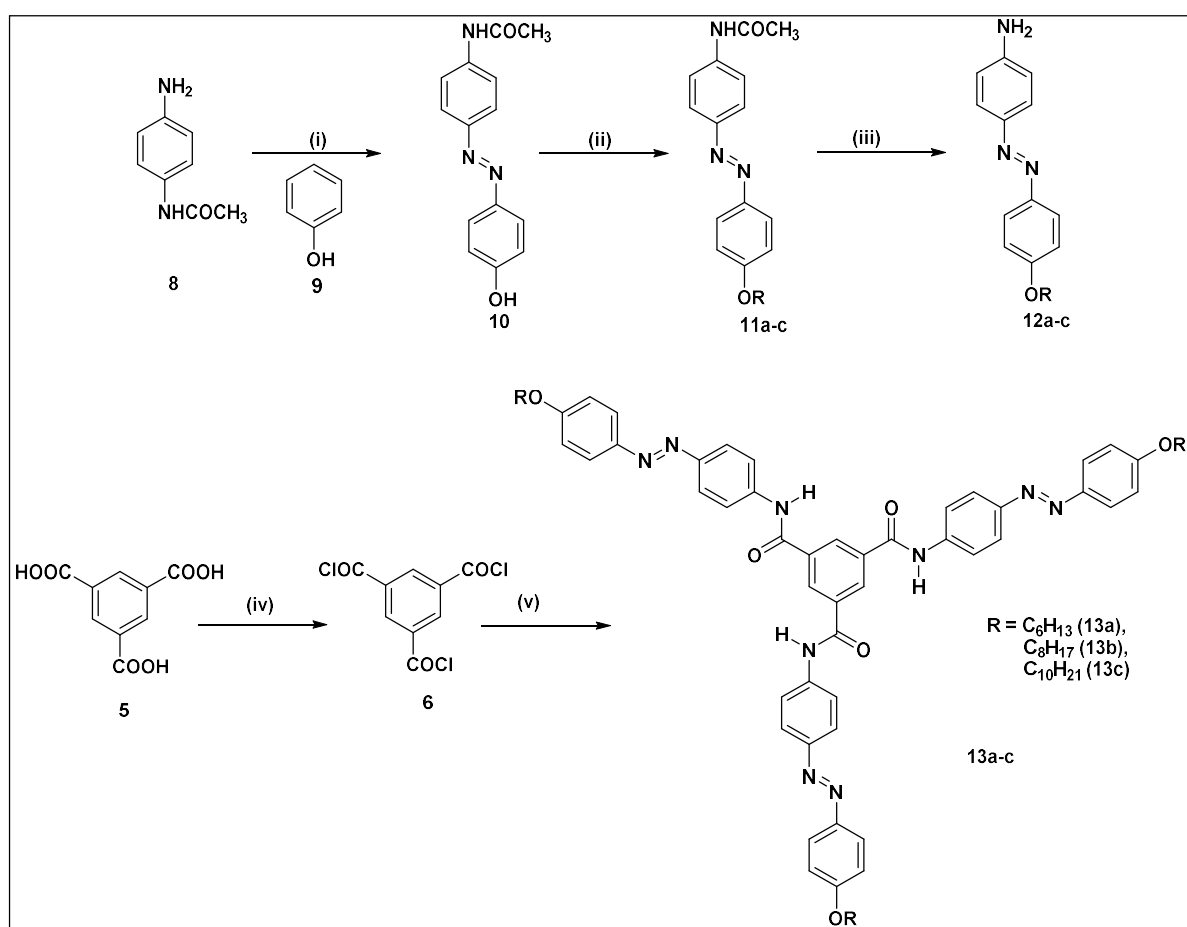
4.2.3. Liquid crystalline studies

After the successful synthesis and photoswitching studies, we have tested these molecules for liquid crystalline properties in collaboration with Dr. Santanu Kumar Pal's group. The preliminary Polarized Optical Images (POM) showed that these molecules were

lacking liquid crystalline properties. Presumably the methyl groups of pyrazole units in the core moiety did not allow the molecules to stack. So, we could not utilize these molecules as photoswitchable liquid crystals. This led to redesign our molecules in such a way that they are stable as well as decorated with photoswitchable moieties in the core to enable it as a photoswitchable discotic liquid crystals.

4.3 Alkoxyphenylazobenzene based tricarboxamide derivatives

4.3.1 Synthesis:



Scheme 4.2: Synthesis of aminoazobenzene incorporated tripodal molecules **13a-c**. (i) conc. HCl, NaNO₂, Phenol, Aq. NaOAc, 0 °C, 4 h, 91%; (ii) K₂CO₃, R-Br, cat. KI, dry DMF, 100 °C, 6-8 h; (iii) Conc. HCl, EtOH, reflux, 5-6 h, **12a**-82%, **12b**-84%, **12c**-84%; (iv) PCl₅, Toluene, reflux; (v) pyridine, Toluene, RT, 12 h, **13a**-76%, **13b**-72%, **13c**-75%.

The target molecules **13a-c** have been synthesized using 4-aminoacetanilide **8** as the starting material. (**Scheme 4.2**) The compound **8** has been diazotized and treated with phenol to obtain the hydroxyazobenzene derivative **9** as per the literature procedure.¹⁶ In order to obtain the ethers **3a-c**, the *O*-alkylation has been performed with different alkyl bromides (*n*-hexyl, *n*-octyl and *n*-pentyl bromides) using potassium carbonate as a base in the presence of a catalytic quantity of potassium iodide. Without purification of the acetanilide derivatives **11a-c**, they were subjected to acid hydrolysis led to their corresponding amine products **12a-c** in good yields. Finally the *in situ* generated trimesoyl chloride **6** has been used to react with the amine compounds **12a-c** to obtain the corresponding triamide target molecules **13a-c**. All the intermediates and the target molecules have been characterized by ¹H, ¹³C-NMR, IR, UV-Vis and HRMS spectral techniques.

4.3.2. Photoswitching Studies

UV-Vis Spectroscopy: The photoswitching behaviour of all the target molecules **13a-c** have been performed in CHCl₃ and DMSO as solvents at room temperature using UV-Vis spectroscopy. All the three targets showed almost identical absorption spectra for both *trans* as well as *cis* isomers. A band with a λ_{max} at 369 nm has been attributed to the π - π^* absorption of *trans* isomer, whereas the n - π^* absorption band appeared as a shoulder in all the three targets. (**Figure 4.2**) This clearly indicated that the chain length did not perturb the absorption spectrum of all the three molecules at all. Also, switching behaviour was found to be quite similar in all the three molecules. Upon irradiation at 365 nm light, the molecules were found to isomerize to all-*cis* isomers, inferred from the spectral changes in the π - π^* and n - π^* absorptions. To envisage the thermal stability of the *cis* isomer, kinetics have been followed for all the three isomers. The net rate of formation of all-*trans* isomer is found to decrease upon increasing the alkyl chain length. (**Table 4.2** and **Appendix 4A**).

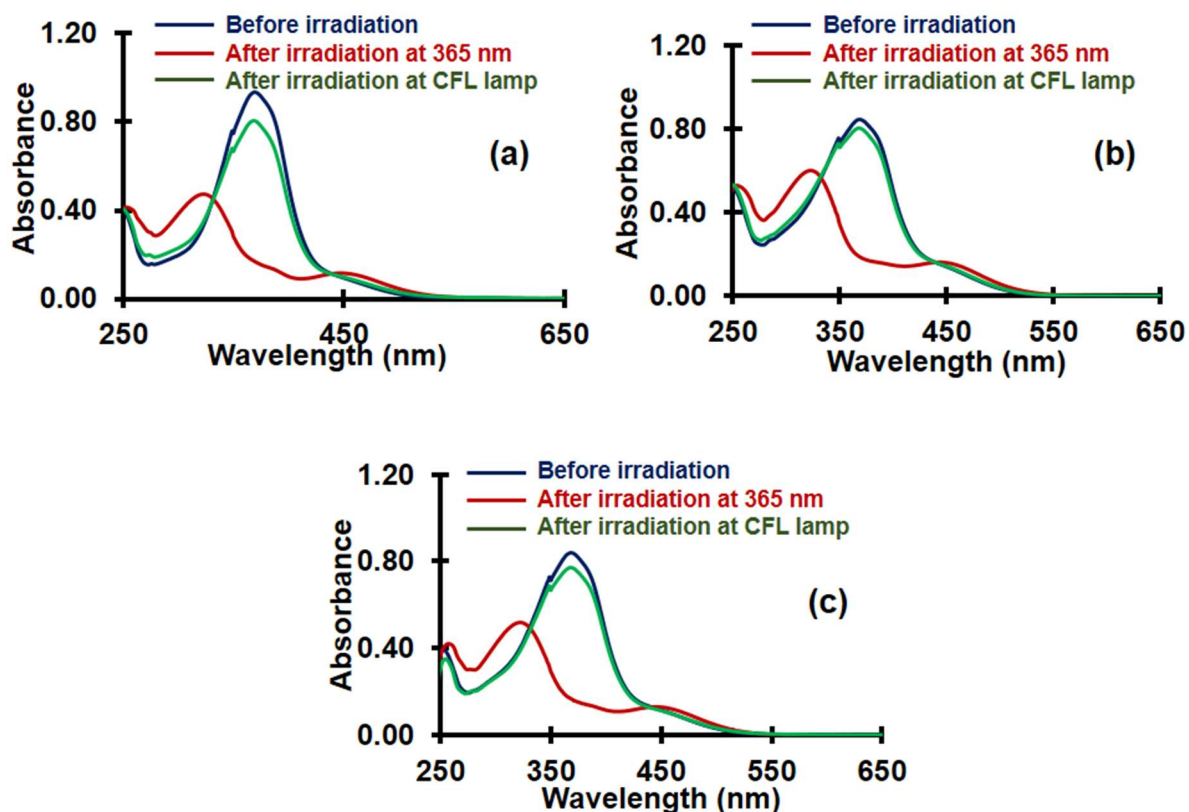


Figure 4.2. Photoswitching behaviour using UV-Vis spectroscopy for the target molecules (a) **13a**; (b) **13b**; (c) **13c**. All the spectra are recorded in CHCl_3 ; (Colour codes: Blue colour - spectra due to the all-*trans*; red colour - spectra recorded after irradiation at 365 nm; green colour - spectra recorded after reverse switching using white light (CFL lamp)).

Table 4.2. Spectral properties and solution phase formation rate constants of all-*trans* isomers using UV-Vis spectroscopy.

S. No.	Compound	λ_{max} (<i>Trans</i>)	λ_{max} (<i>Cis</i>)	k (sec^{-1}) ^a	Half life (min) ^a
1	13a	369 (CHCl_3)	323, 446 (CHCl_3)	2.82×10^{-5}	410
		375 (DMSO)	320, 448 (DMSO)		
2	13b	369 (CHCl_3)	323, 446 (CHCl_3)	4.00×10^{-5}	286
		375 (DMSO)	320, 448 (DMSO)		
3	13c	369 (CHCl_3)	323, 446 (CHCl_3)	4.32×10^{-5}	267
		375 (DMSO)	320, 448 (DMSO)		

^aRate constants and the half-lives have been measured in DMSO at 25 °C.

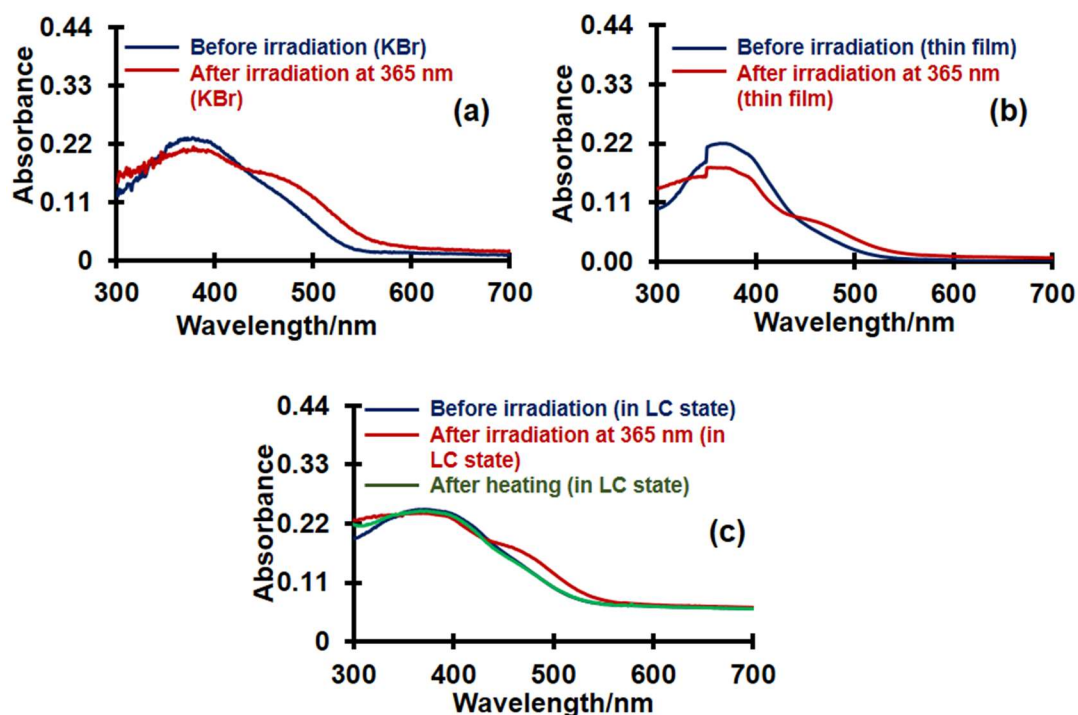


Figure 4.3. Photoswitching behaviour in the solid-state for **13a**: (a) in KBr; (b) in a thin film; (c) in LC state. The black coloured spectra are due to the all-*trans* (*EEE*) isomer (before irradiation), whereas the red one indicates the changes after irradiation at 365 nm. The spectra appearing in blue in (c) was observed after reverse switching on heating.

Interestingly, the compounds were showing photoswitching behaviour in the solid-state also. The solid-state reflectance mode absorption spectra of the irradiated sample showed a significant increase in the $n-\pi^*$ region along with a decrease in the $\pi-\pi^*$ absorption band, which clearly indicates the *E-Z* isomerization (**Figure 4.3**). Firstly, the solid-state UV-Vis spectrum of **13a** has been recorded in KBr (**Figure 4.3a**). The one band at 377 nm was observed corresponding to $\pi-\pi^*$ transition in its trans state. After irradiating the sample for 10 min with 365 nm UV light, it shows two bands at 377 nm and 445 nm which have been attributed to $\pi-\pi^*$ and $n-\pi^*$ transitions, respectively. Secondly, the solid-state UV-Vis spectra were recorded in the form of a thin film of **13a** (**Figure 4.3b**). In a similar manner (as in KBr), the one peak was perceived at 365 nm in its trans state, however, little blue-shifted as compared to KBr one and after irradiation for 10 min it shows two peaks at 345 nm for $\pi-\pi^*$ and 445 nm $n-\pi^*$ transitions. Thirdly the solid-state UV-Vis studies were carried out in its LC state (**Figure 4.3c**). For that the compound **13a** was first heated to its isotropic temperature and then cooled back to room temperature LC state as observed through POM. Then the same sample was

subjected to UV-Vis which shows one peak at 370 nm corresponding to π - π^* transitions in its trans configuration. On irradiating the sample with 365 nm UV light for 15 min, the compound switches to its *cis* configuration, which gives rise to two peaks at 370 nm and 445 nm identified as π - π^* and n - π^* transitions. And on heating the sample (criteria for reverts back the trans configuration), the n - π^* peak disappears (**Figure 4.3c**) which indicates that *cis* configuration has changed back to its stable trans configuration. However, after observing the irradiated film under POM, the optical textures for irradiated LC sample still retained the same without exhibiting any appreciable change in the mesophase. Although the sample was also irradiating for a long time to observe some change in the POM textures but no change was detected. This indicates that the columnar self-assembly has not perturbed when the molecule is going from its trans-state to *cis*-state which probably because the azobenzene is acting as a flexible part as that of alkyl chains. All of these experimental evidences clearly envisage the possibility of photoswitching in these target molecules.

NMR Spectroscopy: All the three target molecules (**13a-c**) possess three photochromic groups, hence, there can be a maximum of four possible isomeric species, namely *EEE*, *EEZ*, *EZZ* and *ZZZ* that can exist under photoswitching conditions. Since UV-Vis spectroscopy is unable to differentiate between these individual species, we shifted our attention to NMR spectroscopy for understanding their presence. The NMR spectra of all the three targets recorded in CDCl_3 showed broadness in almost all the signals even at a lower concentration. Presumably the aggregation or supramolecular π -stacking interactions lead to the broadness. As a result, the photoswitching studies were not clear. On the other hand, when the spectra were recorded using $\text{DMSO-}d_6$, the signals were found to be well-resolved and appeared sharp. Besides that, we also observed the formation of a photostationary state upon irradiation at 365 nm, where all of the four species coexist. (**Figure 4.4** and **4.5**) Based on the spectral changes, we observed that upon *E* to *Z* isomerization, the signals were found to be shifted to the upfield region. Due to non-overlapping nature, the aromatic benzene core protons (appeared as a singlet in *EEE*-isomer) have been used for identifying the individual isomers. Indeed, with each successive *E* to *Z* isomerization step, this signal was separated into two singlets before appearing once again as a simple singlet in the case of *ZZZ*-isomer. Also, the signals were clearly showed a progressive upfield shift as a result of gaining more *Z*-configuration. At the PSS, the major species was found to be *ZZZ*-isomer, which showed a maximum upfield shifting of the benzene core protons. The appearance of signals with 1:2 and 2:1 integral ratios have

been used to differentiate between the *EEZ* and *ZZE*-isomers. Based on the photoswitching studies, it is clear that maximum *ZZZ*-isomer conversion (64%) can be achieved at 14.1 mM concentration. The corresponding amide -NH signal also showed a similar kind of trend, which also can be useful in identifying the individual species.

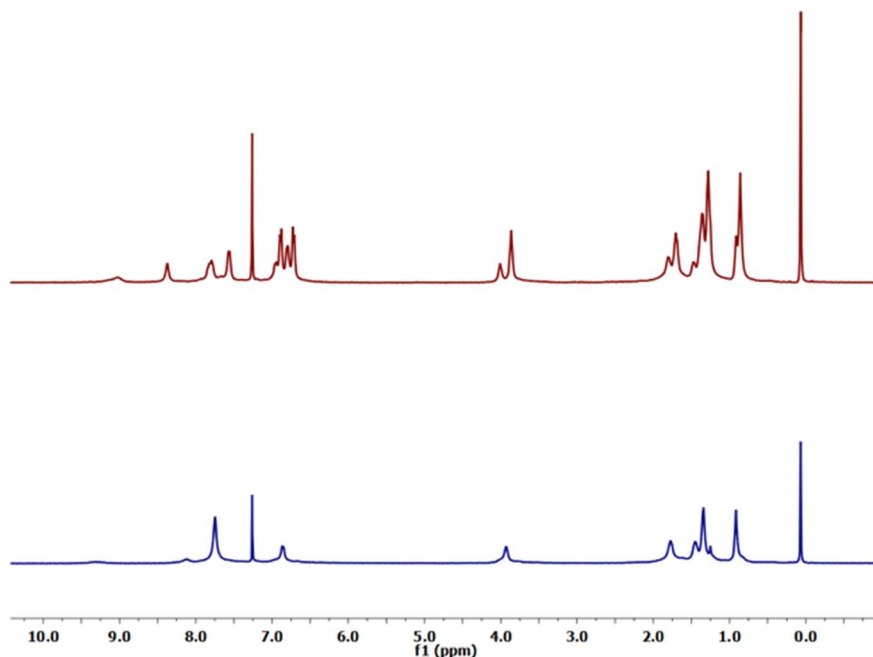


Figure 4.4. NMR spectra of (a) The spectra shown in blue colour is corresponding to (*EEE*)-**13a** as a 4.8 mM concentration in CDCl₃. (b) The red colour spectrum is corresponding to the same solution subjected to irradiation at 365 nm for 1 h.

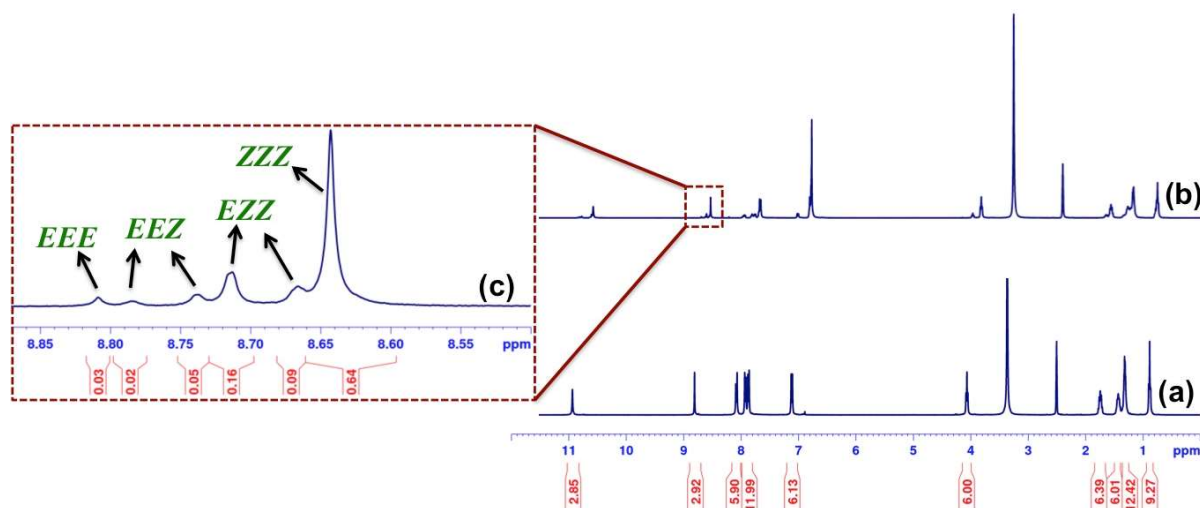


Figure 4.5. NMR spectra of **13a**. (a) The spectrum corresponding to (*EEE*)-**13a** as a 14.1 mM concentration in DMSO-*d*₆. (b) The spectrum corresponds to the same solution after subjected to irradiation at 365 nm for 130 min. (c) The expanded region corresponding to benzene core protons of spectrum “b” with normalized integral values corresponding to *EEE*, *EEZ*, *EZZ* and *ZZZ* isomers of **13a**.

4.3.3 Thermal behaviour

The thermal behaviour of the newly synthesized target molecules **13a-c** were first studied by polarised optical microscopy (POM) and differential scanning calorimetry (DSC). All the compounds were found to exhibit liquid crystalline behaviour at ambient temperature. Under POM, compound **13a** consisting peripheral chain length of six exhibiting liquid crystalline behaviours at room temperature (but the textures mobility was less) and melts into an isotropic liquid at 238 °C. On cooling from its isotropic melt, it exhibits needle-like textures consisting rectilinear defects and homeotropic domains (**Figure 4.6a**) specifies Col_h mesophase, which then transforms to four brushes textures (**Figure 4.6b & c**) at 160.4 °C representative of Col_r mesophase which then stays up to room temperature (**Figure 4.6d**). Unexpectedly in DSC, no thermal transition was observed, which may be because of low enthalpy change involved in the transitions although the mesomorphic behavioural change was very clearly and simply observed from POM and X-ray diffraction (XRD) studies. Compound **13b** also exhibiting liquid crystalline behaviour at room temperature which on pressing gives some birefringence texture (**Figure 4.7a**) which was not so clear and further phase confirmation leads to the existence of Col_h phase as done by XRD technique (**Appendix 4A**). And also on shearing in one direction the compound was giving homogeneous domains (**Figure 4.7b**) which is a characteristic of liquid crystal.

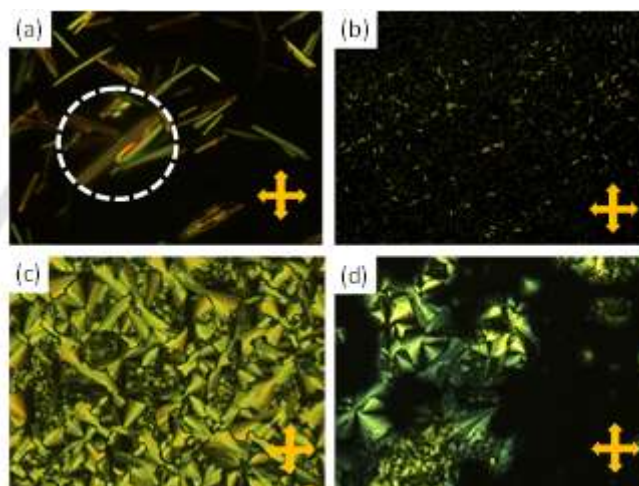


Figure 4.6. Photomicrographs of compound **13a**: (a) at 220 °C (Col_h , X500) (b) at 160.4 °C (transition from Col_h to Col_r , X100) (c) at 120 °C (Col_r , X500) (d) at room temperature (X500), on cooling from isotropic liquid with a scan rate of 5 °C/min.

In DSC, it shows mesophase to isotropic transition at 190 °C while on cooling it shows no observable transition may be due to the same reason as explained before. Similar to

compound **13b**, compound **13c** also giving birefringent textures but in some areas, rectilinear defects characteristic of Col_h phase (**Figure 4.7c**) were found. And on heating, it exhibits mesophase to isotropic transition at 175 °C. So, all the compounds exhibit enantiotropic mesomorphic behaviour as very well observed by POM and X-ray studies but unpredictably, some of the transitions were not observed from DSC because of some low enthalpy change involved in the transitions as reported in the earlier reports also.^[17-19]

In all of the three compounds, we have noted that textures mobility on pressing the top of glass slide was less which may be due to the strong amide interactions (three amide bonds present in the compound) with the hydrophilic glass surface, as the compounds were sandwiched between the two glass surfaces.

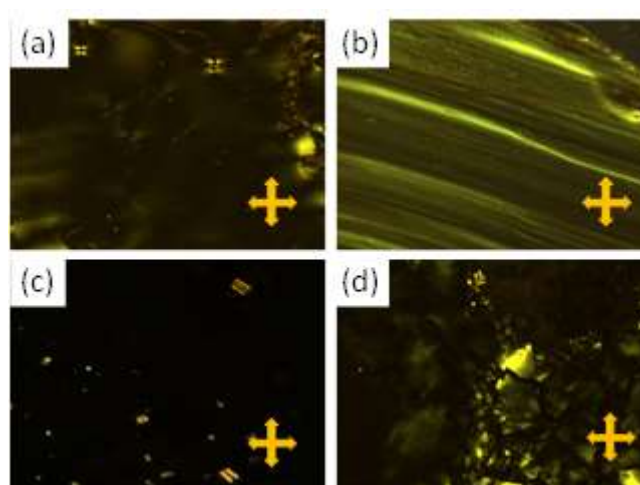


Figure 4.7. Photomicrographs of compound **13b** (a) at 68.6 °C (Col_h, X100) (b) at room temperature (Col_h, X100), for compound **13c** (c) at 69.2 °C (Col_h, X500) (d) at 35.2 °C (X200), observed on cooling with a scan rate of 5 °C/min.

Table 4.3. Thermal properties of the target compounds.

Compound	Phase transitions, T [°C]
13a	Col _r 165 Col _h 238 Iso ^[a]
	Iso 230 Col _h 160.4 Col _r ^[a]
13b	Col _h 190 Iso ^[b]
	Iso 185 Col _h ^[a]
13c	Col _h 175 Iso ^[b]
	Iso 165 Iso ^[a]

[a] Transition temperature from POM & X-ray. [b] Transition temperature from POM, DSC & X-ray. Abbreviations: Col_r= Columnar rectangular, Col_h= Columnar hexagonal, Iso= isotropic liquid.

4.4 Summary

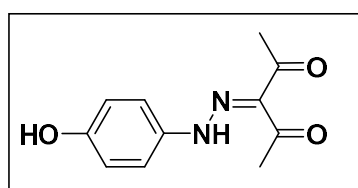
Through these investigations, we have synthesized six long chain alkoxy azoarene connected derivatives of trimesic acid (**7a-c** and **13a-c**). All of the six target molecules showed solution state photoswitching. Under μM concentration range, all of the six molecules showed nearly complete photoswitching that was realized from the UV-Vis spectroscopy. However, at a higher concentration in the mM range they were found to show partial photoswitching, which was confirmed by the NMR spectroscopy. Interestingly, all of them exhibited solid state photoswitching. Due to the lack of supramolecular π -stacking interactions, the pyrazole-based derivatives **7a-c** exhibited no discotic liquid crystalline behaviour. In contrast, the targets **13a-c** showed DLC properties. Interestingly, **13a** exhibited temperature-dependent changes in the mesophases. A columnar rectangular phase was observed at low temperature, whereas, a columnar hexagonal at higher temperature was seen. The other two higher homologues **13b,c** revealed only columnar hexagonal phases at all temperature ranges. Thus, the tris-azobenzenetricarboxamides based systems are found to be versatile DLCs.

4.5 Experimental Section

General procedure for the synthesis of target compounds, **7a-c**:

3-(2-(4-Hydroxyphenyl)hydrazono)pentane-2,4-dione (**2**):

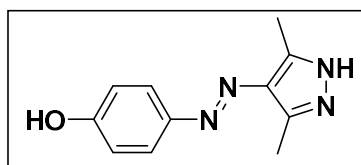
A mixture of aniline or substituted anilines (20.0 mmol) and deionized water in a two neck round bottom flask was cooled to 0 °C. To this 37% conc. HCl (6.5 mL) was added and stirred to get a clear solution. Then a cold aqueous solution of sodium nitrite (1.52 g, 22.0 mmol in 20 mL of water) was added dropwise into the reaction mixture slowly. After the addition, the diazonium salt started forming. The reaction mixture was allowed to stir for half an hour for completion. Afterwards, at 0 °C a cold aqueous solution of sodium acetate (5.90 g, 70.0 mmol) and acetylacetone (2.00 g, 20.0 mmol in 100 mL of water and 10 ml of ethanol) was added. The reaction was continued at room temperature and was monitored by TLC. After completion of the reaction, the reaction mixture was filtered off to obtain a yellow-orange solid product, which was dried under vacuum to yield the desired product.



Yellow solid, mp = 168-171 °C, 191.6 mg, 87% yield. ^1H NMR (400 MHz, DMSO- d_6) δ 2.37 (s, 3H), 2.46 (s, 3H), 6.83–6.85 (d, J = 8.8 Hz, 2H), 7.42–7.44 (d, J = 8.8 Hz, 2H), 9.67 (s, 1H, OH), 14.51 (s, 1H); ^{13}C NMR (100 MHz, DMSO- d_6) δ 29.89, 31.56, 116.53, 116.60, 118.50, 132.51, 134.14, 156.35, 196.38; HRMS (ESI-TOF): calcd. for $\text{C}_{11}\text{H}_{12}\text{N}_2\text{O}_3[\text{M}-\text{H}]^+$: 219.0770, found: 219.0758.

(*E*)-4-((3,5-Dimethyl-1*H*-pyrazol-4-yl)diazenyl)phenol (**3**):

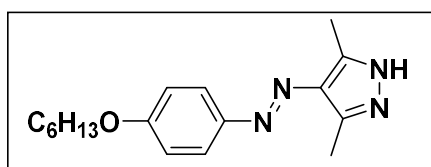
A mixture of arylazoacetylacetone derivative (1.0 mmol), hydrazine dihydrochloride (2.0 mmol) and Na_2CO_3 (4.0 mmol) in 10 mL absolute ethanol was refluxed. The reaction was followed using TLC upto the completion of the reaction. After completion of the reaction, the product was purified by column chromatography. (Eluent: 1:1 ethylacetate/n-hexane)



Yellow solid, mp = 198-205 °C, 170.8 mg, 79% yield. ^1H NMR (400 MHz, DMSO- d_6) δ 2.40 (s, 3H), 2.46 (s, 3H), 6.86-6.89 (d, J = 8.9 Hz, 2H), 7.61-7.63 (d, J = 8.9 Hz, 2H), 9.97 (s, 1H, OH), 12.72 (s, 1H, NH); ^{13}C NMR (100 MHz, DMSO- d_6) δ 10.4, 14.1, 116.1, 123.6, 134.2, 137.7, 142.9, 146.6, 159.5; HRMS (ESI-TOF) calcd. for $\text{C}_{11}\text{H}_{12}\text{N}_4\text{O}[\text{M}+\text{H}]^+$: 217.1089, found: 217.1081; IR (ATR, cm^{-1}): 3291, 3190, 3119, 2917, 1482, 1420, 1134, 1061, 825.

General method for the synthesis of alkoxy arylazopyrazole derivatives 4a-c: To a dry DMF (35 mL) solution of compound 3 (14.5 mM), potassium carbonate (14.5 mM) and a pinch of potassium iodide have been charged and stirred at RT. After ten minutes alkyl bromide (14.5 mM) was added slowly and then the reaction mixture was heated to 100 °C. The reaction was monitored by TLC and after the completion, the DMF was evaporated under vacuum.

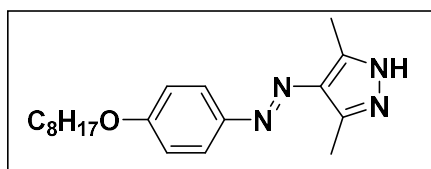
(*E*)-4-((4-(Hexyloxy)phenyl)diazenyl)-3,5-dimethyl-1*H*-pyrazole (**4a**):



Yellow Solid, mp = 168-170 °C, 213.3 mg, 71% yield. ^1H NMR (400 MHz, CDCl_3) δ 0.91-0.94 (t, J = 6.7 Hz, 3H), 1.35-1.36 (m, 4H), 1.45-1.50 (m, 2H), 1.78-1.85 (m, 2H), 2.59 (s,

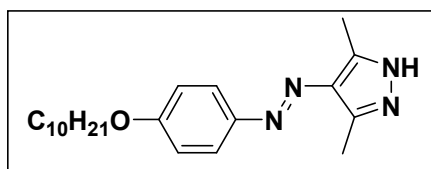
6H), 4.00-4.03 (t, $J = 6.6$ Hz, 2H), 6.95-6.97 (d, $J = 8.4$ Hz, 2H), 7.76-7.79 (d, $J = 8.3$ Hz, 2H); ^{13}C NMR (100 MHz, CDCl_3) δ 12.26, 14.28, 22.74, 25.84, 29.34, 31.73, 68.41, 114.67, 123.48, 134.60, 141.08, 147.80, 160.60; HRMS (ESI-TOF) calcd. for $\text{C}_{17}\text{H}_{24}\text{N}_4\text{O}[\text{M}+\text{H}]^+$: 301.2028, found 301.2020; IR (ATR, cm^{-1}): 3110, 2927, 1488, 1410, 1144, 1051, 826 640, 675.

(*E*)-3,5-Dimethyl-4-((4-(octyloxy)phenyl)diazenyl)-1*H*-pyrazole (**4b**):



Yellow Solid, mp = 165-167 °C, 229.9 mg, 70% yield ^1H NMR (400 MHz, CDCl_3) δ 0.88-0.91 (t, $J = 6.8$ Hz, 3H), 1.30-1.33 (m, 8H), 1.44-1.49 (m, 2H), 1.78-1.85 (m, 2H), 2.60 (s, 6H), 4.00-4.03 (t, $J = 6.5$ Hz, 2H), 6.95-6.97 (d, $J = 8.1$ Hz, 2H), 7.76-7.78 (d, $J = 8.0$ Hz, 2H); ^{13}C NMR (100 MHz, CDCl_3) δ 12.24, 14.24, 22.79, 26.17, 29.38, 29.50, 31.95, 68.41, 114.67, 123.48, 134.59, 141.03, 147.80, 160.59; HRMS (ESI-TOF) calcd. for $\text{C}_{21}\text{H}_{32}\text{N}_4\text{O}[\text{M}+\text{H}]^+$: 329.2341, found 329.2326; IR (ATR, cm^{-1}): 3150, 3111, 2901, 1472, 1408, 1144, 1091, 825, 686, 644.

(*E*)-4-((4-(Decyloxy)phenyl)diazenyl)-3,5-dimethyl-1*H*-pyrazole (**4c**):



Yellow Solid, mp = 166-168 °C, 256.6 mg, 72% yield ^1H NMR (400 MHz, CDCl_3) δ 0.87-0.92 (t, $J = 7.0$ Hz, 3H), 1.28-1.35 (m, 12H), 1.46-1.49 (m, 2H), 1.79-1.83 (m, 2H), 2.60 (s, 6H), 4.00-4.03 (t, $J = 6.6$ Hz, 2H), 6.95-6.97 (d, $J = 9.0$ Hz, 2H), 7.76-7.79 (d, $J = 9.0$ Hz, 2H); ^{13}C NMR (100 MHz, CDCl_3) δ 12.26, 14.27, 22.83, 26.17, 29.37, 29.47, 29.55, 29.70, 29.72, 32.04, 68.41, 114.67, 123.48, 134.60, 141.07, 147.80, 160.60; HRMS (ESI-TOF) calcd. for $\text{C}_{21}\text{H}_{32}\text{N}_4\text{O}[\text{M}+\text{H}]^+$: 357.2654, found 357.2610; IR (ATR, cm^{-1}): 3130, 3110, 2912, 1480, 1405, 1139, 1081, 828, 660, 651.

General method for the synthesis of tripodal alkoxy arylazo-3,5-dimethylpyrazole derivatives of trimesic acid 7a-c: An oven dried 100 ml round bottom flask was charged with trimesic acid (0.5 mmol) and phosphorus pentachloride (2.5 mmol) and refluxed in dry toluene

(15 mL) under a nitrogen atmosphere for three hours to prepare trimesoyl chloride. This trimesoyl chloride was transferred (without isolation) to another oven dried 250 mL round bottom flask containing the corresponding arylazopyrazole **4a-c** (1.6 mmol), toluene (30 mL) and pyridine (10 mmol) under a nitrogen atmosphere at 0 °C. The Reaction mixture was stirred at 110 °C for 5-7 hours. The precipitate was filtered and washed well with dry ethanol to remove pyridine hydrochloride and the starting material to get the desired product.

Benzene-1,3,5-triyltris((4-((*E*)-(4-(hexyloxy)phenyl)diazenyl)-3,5-dimethyl-1*H*-pyrazol-1-yl)methanone) (**7a**):

Yellow Solid, mp = 107-109 °C, 1015.1 mg, 96% yield. ¹H NMR (400 MHz, CDCl₃) δ 0.92 (t, 9H), 1.36 (m, 12H), 1.49 (m, 6H), 1.80-1.84 (m, 6H), 2.52 (s, 9H), 3.03 (s, 9H), 4.01-4.04 (t, *J* = 6.4 Hz, 6H), 6.97-6.99 (d, *J* = 8.3 Hz, 6H), 7.82-7.84 (d, *J* = 8.3 Hz, 6H), 8.90 (s, 3H); ¹³C NMR (100 MHz, CDCl₃) δ 12.44, 14.19, 15.48, 22.74, 25.83, 29.30, 31.72, 68.49, 114.79, 124.19, 132.94, 137.89, 137.93, 144.81, 146.59, 147.58, 161.56, 166.95; HRMS (ESI-TOF) calcd for C₆₀H₇₂N₁₂O₆[M+H]⁺: 1057.5776, found 1057.5731; IR (ATR, cm⁻¹): 3335, 3013, 2991, 2910, 2781, 2655, 2576, 1651, 1530, 1400, 1321, 960, 830, 665, 641.

Benzene-1,3,5-triyltris((3,5-dimethyl-4-((*E*)-(4-(octyloxy)phenyl)diazenyl)-1*H*-pyrazol-1-yl)methanone) (**7b**):

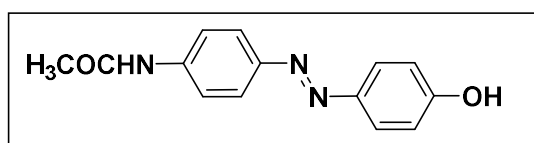
Yellow Solid, mp = 122-124 °C, 1084.6 mg, 95% yield. ¹H NMR (400 MHz, CDCl₃) δ 0.88-0.91 (t, *J* = 6.7 Hz, 9H), 1.30-1.34 (m, 24H), 1.45-1.48 (m, 6H), 1.79-1.85 (m, 6H), 2.52 (s, 9H), 3.03 (s, 9H), 4.02-4.05 (t, *J* = 6.5 Hz, 6H), 6.97-7.00 (d, *J* = 8.8 Hz, 6H), 7.82-7.85 (d, *J* = 8.8 Hz, 6H), 8.88 (s, 3H); ¹³C NMR (100 MHz, CDCl₃) δ 12.45, 14.27, 15.50, 22.81, 26.16, 29.34, 29.38, 29.50, 31.96, 68.50, 114.78, 124.19, 132.94, 137.87, 137.92, 144.81, 146.59, 147.56, 161.55, 166.95; HRMS (ESI-TOF) calcd. for C₆₆H₈₄N₁₂O₆[M+H]⁺: 1141.6715, found 1141.6741; IR (ATR, cm⁻¹): 3330, 3010, 2981, 2908, 2771, 2650, 2581, 1660, 1520, 1402, 1311, 961, 832, 672, 651.

Benzene-1,3,5-triyltris((4-((*E*)-(4-(decyloxy)phenyl)diazenyl)-3,5-dimethyl-1*H*-pyrazol-1-yl)methanone) (**7c**):

Yellow Solid, mp = 116-118 °C, 1201.2 mg, 98% yield. ¹H NMR (400 MHz, CDCl₃) δ 0.87-0.90 (t, *J* = 6.8 Hz, 9H), 1.28 (m, 36H), 1.44-1.48 (m, 6H), 1.78-1.84 (m, 6H), 2.52 (s, 9H), 3.03 (s, 9H), 4.02-4.05 (t, *J* = 6.5 Hz, 6H), 6.97-7.00 (d, *J* = 8.7 Hz, 6H), 7.82-7.85 (d, *J* = 8.6

Hz, 6H), 8.88 (s, 3H); ^{13}C NMR (100 MHz, CDCl_3) δ 12.32, 14.14, 15.35, 22.70, 26.03, 29.21, 29.34, 29.40, 29.57, 29.59, 31.91, 68.38, 114.67, 124.06, 132.82, 137.74, 137.81, 44.67, 146.47, 147.45, 161.43, 166.83; HRMS (ESI-TOF) calcd. for $\text{C}_{72}\text{H}_9\text{N}_{12}\text{O}_6[\text{M}+\text{H}]^+$: 1225.7654, found: 1225.7703; IR (ATR, cm^{-1}): 3338, 3018, 2981, 2918, 2772, 2671, 2567, 1661, 1527, 1415, 1319, 970, 837, 668, 643.

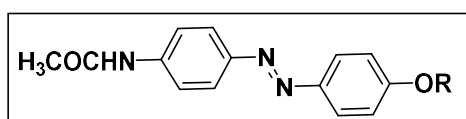
Synthesis of (*E*)-*N*-(4-((4-hydroxyphenyl)diazenyl)phenyl)acetamide (**10**):



A mixture of *p*-aminoacetanilide (3.3 g, 22 mM) and deionized water in a two neck round bottom flask was cooled to 0 °C. To this 37% conc. HCl (6.5 mL) was added and stirred to get a clear solution. Then a cold aqueous solution of sodium nitrite (1.52 g, 22 mM in 20 mL of water) was added dropwise into the reaction mixture. After the addition, the diazonium salt started forming. The reaction mixture was allowed to stir for half an hour for completion. After half an hour, at 0 °C a cold aqueous solution of sodium acetate (5.9 g, 70 mM) and phenol (2.16 g, 23 mM in 100 mL of water) was added. The reaction was monitored by TLC. After completion of the reaction, the reaction mixture was filtered off and to obtain an orange solid product, which was dried under vacuum to yield the desired product. 3 h (Yield = 91%)

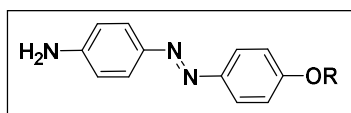
Dark orange solid, m.p. = 157-161 °C, ^1H NMR (400 MHz, $\text{DMSO}-d_6$) δ 2.10 (s, 3H, -COCH₃), 6.92-6.94 (d, J = 8.4 Hz, 2H), 7.74-7.78 (m, 2H), 10.30 (s, 1H, -OH); ^{13}C NMR (100 MHz, $\text{DMSO}-d_6$) δ 24.59, 116.43, 119.58, 123.45, 124.97, 141.87, 145.52, 148.02, 161.42, 169.19; HRMS (ESI-TOF) calcd. for $\text{C}_{14}\text{H}_{14}\text{N}_3\text{O}_2[\text{M}+\text{H}]^+$: 255.1008, found: 256.1086; IR (ATR, cm^{-1}): 640, 675, 834, 965, 1142, 1226, 1264, 1322, 1369, 1401, 1500, 1529, 1587, 1651, 2586, 2660, 2789, 2920, 2998, 3043, 3341.

General procedure for the synthesis of (*E*)-*N*-(4-((4-alkoxyphenyl)diazenyl)phenyl)acetamide (11a-c**):**



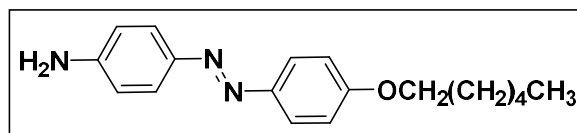
To a dry DMF (35 mL) solution of compound 1 (3.7 g, 14.5 mM), potassium carbonate (20.04 g, 14.5 mM) and a pinch of potassium iodide have been charged and stirred at RT. After ten minutes alkyl bromide (2.4 g, 14.5 mM) was added slowly and then the reaction mixture was heated to 100 °C. The reaction was monitored by TLC and after the completion, the DMF was evaporated under vacuum. The crude compound was used for the hydrolysis step without further purification. (5 h)

General procedure for the synthesis of (*E*)-4-((4-alkoxyphenyl)diazenyl)aniline (12a-c**):**



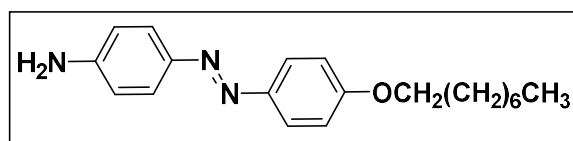
To the crude p-alkoxyazoacetanilide derivatives (**3a-c**) (1.75 g, 5.16 mM) in ethanol (150 mL), 37% con. HCl (4 mL) was added and let it refluxed. The reaction was monitored by TLC. After completion of the reaction, the reaction mixture was neutralised by adding an aqueous sodium bicarbonate solution. The extraction of the reaction mixture was done in ethyl acetate. The extracted organic layer was washed with brine solution and evaporated to dryness and was subjected to purification by column chromatography. (Eluent: ethylacetate:n-hexane 20:80)

(*E*)-4-((4-(hexyloxy)phenyl)diazenyl)aniline (12a**):**



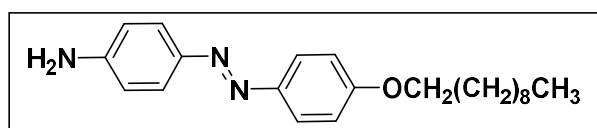
Orange Solid, m.p. = 96-99 °C, 243.86 mg, 82% yield. ¹H NMR (400 MHz, CDCl₃) δ 0.92-0.96 (t, *J* = 7.0 Hz, 3H), 1.36-1.40 (m, 4H), 1.48-1.50 (m, 2H), 1.82-1.85 (quin., 2H), 4.02 (br, 2H, -NH₂), 4.03-4.06 (t, *J* = 6.6 Hz, 2H), 6.75-6.77 (d, *J* = 8.7 Hz, 2H), 6.99-7.01 (d, *J* = 8.9 Hz, 2H), 7.78-7.80 (d, *J* = 8.7 Hz, 2H), 7.84-7.87 (d, *J* = 8.9 Hz, 2H); ¹³C NMR (100 MHz, CDCl₃) δ 14.07, 22.63, 25.73, 29.21, 31.61, 68.30, 114.63, 114.74, 124.04, 124.64, 145.66, 147.05, 148.93, 160.81; HRMS (ESI-TOF) calcd. for C₁₈H₂₄N₃O[M+H]⁺: 298.1919, found 298.1906; IR (ATR, cm⁻¹): 633, 717, 825, 1008, 1112, 1130, 1240, 1299, 1384, 1498, 1580, 2000, 2854, 2923, 3037, 3379, 3481.

(*E*)-4-((4-(octyloxy)phenyl)diazenyl)aniline (**12b**):



Orange Solid, m.p. = 105-108 °C, 273.4 mg, 84% yield. ¹H NMR (400 MHz, CDCl₃) δ 0.91-0.94 (t, *J* = 6.8 Hz, 3H), 1.32-1.37 (m, 8H), 1.46-1.54 (m, 2H), 1.81-1.85 (quin., 2H), 4.01 (br, 2H, -NH₂), 4.02-4.05 (t, *J* = 6.5 Hz, 2H), 6.74-6.76 (d, *J* = 8.6 Hz, 2H), 6.99-7.02 (d, *J* = 8.9 Hz, 2H), 7.79-7.81 (d, *J* = 8.6 Hz, 2H), 7.86-7.88 (d, *J* = 8.8 Hz, 2H); ¹³C NMR (100 MHz, CDCl₃) δ 14.17, 22.71, 26.07, 29.27, 29.29, 29.41, 31.86, 68.32, 114.66, 114.74, 124.06, 124.66, 145.63, 147.06, 149.00, 160.82; HRMS (ESI-TOF) calcd. for C₂₀H₂₈N₃O[M+H]⁺: 326.2232, found: 326.2247; IR(ATR, cm⁻¹): 632, 716, 826, 1010, 1132, 1239, 1297, 1387, 1460, 1494, 1582, 2548, 2853, 2922, 3037, 3192, 3380, 3480.

(*E*)-4-((4-(decyloxy)phenyl)diazenyl)aniline (**12c**):



Orange Solid, m.p. = 111-113 °C, 296.9 mg, 84% yield. ¹H NMR (400 MHz, CDCl₃) δ 0.92-0.93 (t, *J* = 6.7 Hz, 3H), 1.31-1.36 (m, 12H), 1.48-1.52 (m, 2H), 1.82-1.85 (quin., 2H), 4.01 (br, 2H, -NH₂), 4.03-4.06 (t, *J* = 6.5 Hz, 2H), 6.75-6.77 (d, *J* = 8.1 Hz, 2H), 6.99-7.01 (d, *J* = 8.2 Hz, 2H), 7.78-7.80 (d, *J* = 7.8 Hz, 2H), 7.85-7.87 (d, *J* = 8.0 Hz, 2H); ¹³C NMR (100 MHz, CDCl₃) δ 14.15, 22.70, 26.04, 29.25, 29.34, 29.42, 29.58, 29.59, 31.91, 68.31, 114.63, 114.72, 124.03, 124.63, 145.66, 147.05, 148.92, 160.80; HRMS (ESI-TOF) calcd. for C₂₂H₃₂N₃O[M+H]⁺: 354.2545, found: 354.2545; IR (ATR, cm⁻¹): 634, 714, 829, 1014, 1057, 1139, 1238, 1303, 1392, 1462, 1499, 1584, 2642, 2851, 2914, 3040, 3205, 3346, 3476.

General synthetic procedure for the synthesis of **13a-c**:

To the trimesic acid (0.05 g, 0.24 mM) in a two neck round bottom flask, dry toluene (25 mL) was added under the argon atmosphere. To the insoluble reaction mixture, PCl₅ (0.25 g, 1.2 mM) was added in portions. After the complete addition of PCl₅, the reaction mixture was refluxed upto the formation of a transparent reaction mixture. (Note: The trimesylchloride is highly sensitive to moisture) A mixture of **12a-c** (0.35 g, 1.2 mM), pyridine (0.19 g, 2.4 mM) and dry toluene (50 mL) have been taken in a two neck round bottom flask and stirred for ten

minutes under an argon atmosphere and cooled to 0 °C. Now trimesoyl chloride solution in toluene from the previous stage of the reaction was carefully transferred into this reaction mixture. The reaction mixture was then allowed to stir at room temperature and the reaction was monitored by TLC. After the completion of the reaction, the toluene was evaporated in a rotary evaporator. Then the crude product was purified by column chromatography on silica gel (EtOAc:n-hexanes = 40:60) to obtain a pure product as dark orange colour solids.

*N*¹,*N*³,*N*⁵-tris(4-((*E*)-(4-(hexyloxy)phenyl)diazenyl)phenyl)benzene-1,3,5-tricarboxamide

(13a):

Yellow solid, m.p: see Table 4.3, 796.7 mg, 76% yield. ¹H NMR (400 MHz, CDCl₃) δ 0.94 (t, *J* = 5.3 Hz, 9H), 1.36 (br, 12H), 1.47 (t, *J* = 5.7 Hz, 6H), 1.79 (t, *J* = 5.7 Hz, 6H), 3.92 (t, *J* = 6.6 Hz, 6H), 6.81-6.84 (d, *J* = 8.0 Hz, 6H), 7.74 (br, 21H), 9.87 (br, 3H, N-H); ¹³C NMR (100 MHz, CDCl₃) δ 14.09, 22.64, 25.74, 29.26, 31.68, 68.20, 114.42, 120.43, 123.57, 124.78, 128.71, 135.70, 139.47, 146.74, 149.47, 161.32, 165.61; IR (ATR, cm⁻¹): 624, 719, 839, 935, 1011, 1104, 1138, 1150, 1241, 1301, 1315, 1402, 1417, 1454, 1469, 1496, 1522, 1582, 1593, 1651, 1660, 2859, 2927, 3296, 3418; HRMS (MALDI) calcd. for C₆₃H₆₉N₉O₆[M+H]⁺: 1048.5449, found: 1048.5369.

*N*¹,*N*³,*N*⁵-tris(4-((*E*)-(4-(octyloxy)phenyl)diazenyl)phenyl)benzene-1,3,5-tricarboxamide

(13b):

Yellow solid, m.p: see Table 4.3, 815.4 mg, 72% yield. ¹H NMR (400 MHz, CDCl₃) δ 0.92 (t, *J* = 6.7 Hz, 9H), 1.32 (br, 24H), 1.47 (t, *J* = 6.8 Hz, 6H), 1.80 (t, *J* = 5.5 Hz, 6H), 3.94 (t, *J* = 4.3 Hz, 6H), 6.83-6.85 (d, *J* = 8.3 Hz, 6H), 7.76 (br, 21H), 9.91 (br, 3H, N-H); ¹³C NMR (100 MHz, CDCl₃) δ 14.16, 22.72, 26.10, 29.32, 29.50, 31.90, 68.23, 114.42, 120.45, 123.63, 124.80, 128.73, 135.81, 139.47, 146.76, 149.54, 161.33, 165.79; HRMS (MALDI) calcd. for C₆₉H₈₁N₉O₆[M+H]⁺: 1132.6388, found: 1132.6343; IR (ATR, cm⁻¹): 623, 719, 789, 833, 910, 962, 1020, 1104, 1138, 1238, 1301, 1402, 1417, 1454, 1468, 1496, 1520, 1581, 1594, 1658, 2853, 2922, 3018, 3306.

*N*¹,*N*³,*N*⁵-tris(4-((*E*)-(4-(decyloxy)phenyl)diazenyl)phenyl)benzene-1,3,5-tricarboxamide

(13c):

Yellow solid, m.p: see Table 4.3, 912.5 mg, 75% yield. ¹H NMR (400 MHz, CDCl₃) δ 0.92 (t, *J* = 6.9 Hz, 9H), 1.31 (br, 28H), 1.47 (br, 6H), 1.80 (t, *J* = 6.5 Hz, 6H), 3.93 (t, *J* = 6.3 Hz, 6H),

6.83-6.85 (d, $J=7.7$ Hz, 6H), 7.76 (br, 21H), 9.89 (br, 3H, N-H); ^{13}C NMR (100 MHz, CDCl_3) δ 14.17, 22.74, 26.11, 29.36, 29.42, 29.59, 29.69, 31.97, 68.23, 114.43, 120.52, 123.52, 124.77, 128.86, 135.45, 139.39, 146.69, 149.40, 161.36, 165.27; HRMS (MALDI) calcd. for $\text{C}_{75}\text{H}_{93}\text{N}_9\text{O}_6[\text{M}+\text{H}]^+$: 1216.7327, found: 1216.7275. IR (ATR, cm^{-1}): 624, 719, 835, 943, 1013, 1104, 1139, 1240, 1302, 1402, 1417, 1454, 1468, 1497, 1524, 1582, 1595, 1659, 2852, 2921, 3047, 3307.

4.6 References

1. (a) Kumar, S. *Chem. Soc. Rev.* **2006**, *35*, 83-109. (b) Kumar, S. *Liq. Cryst.* **2004**, *31*, 1037-1059.
2. Cammidge, A. N.; Bushby R. J. in *Handbook of Liquid Crystals, Vol. 7* (Eds. Demus, D.; Goodby, J. W.; Gray, G. W.; Spiess, H. W.; Vill V.), Wiley- WCH, Weinheim, **1998**, pp 693.
3. (a) Bushby, R. J.; Kawata, K. *Liq. Cryst.* **2011**, *38*, 1415-1426. (b) Wohrle, T.; Wurzbach, I.; Kirres, J.; Kostidou, A.; Kapernaum, N.; Litterscheidt, J.; Haenle, J. C.; Staffeld, P.; Baro, A.; Giesselmann, F.; Laschat, S. *Chem. Rev.* **2016**, *116*, 1139-1241.
4. (a) Ichimura, K.; Furumi, S.; Morino, S.Y.; Kidowaki, M.; Nakagawa, M.; Ogawa, M.; Nishiura, Y. *Adv. Mater.* **2000**, *12*, 950-953. (b) Bisoyi, H. K.; Li, Q. *Chem. Rev.* **2016**, *116*, 15089-15166. (c) Alaasar, M.; Poppe, S.; Dong, Q.; Liu, F.; Tschierske, C. *Angew. Chem., Int. Ed.*, **2017**, *56*, 10801-10805.
5. (a) Irie, M. *Chem. Rev.* **2000**, *100*, 1685-1716. (b) Frigoli, M.; Mehl, G. H. *Chem. Commun.* **2004**, *0*, 2040-2041. (c) Frigoli, M.; Mehl, G. H. *Eur. J. Org. Chem.* **2004**, 636-642. (d) Frigoli, M.; Mehl, G. H. *Mol. Cryst. Liq. Cryst.* **2005**, *430*, 123-126. (e) Eelkema, R. *Liq. Cryst.* **2011**, *38*, 1641-1652. (f) Zep, A.; Wojcik, M. M.; Lewandowski, W.; Sitkowska, K.; Prominski, A.; Mieczkowski, J.; Pocięcha, D.; Gorecka, E. *Angew. Chem., Int. Ed.* **2014**, *53*, 13725-13728. (g) Yamakado, R.; Hara, M.; Nagano, S.; Seki, T.; Maeda, H. *Chem. - Eur. J.* **2017**, *23*, 9244-9248.
6. (a) Chen, Y.; Harrison, W.T.; Imrie, C.T.; Ryder, K.S. *J. Mater. Chem.* **2002**, *12*, 579-585. (b) Li, Q.; Kim, J.; Park, H. S.; Williams, J. *Chem. Mater.* **2005**, *17*, 6018-6021. (c) Choi, Y.-J.; Kim, D.-Y.; Park, M.; Yoon, W.-J.; Lee, Y.; Hwang, J.-K.; Chiang, Y.-W.; Kuo, S.-W.; Hsu, C.-H.; Jeong, K.-U. *ACS Appl. Mater. Interfaces* **2016**, *8*, 9490-9498. (d) Pan, S.; Ni, M.; Mu, B.; Li, Q.; Hu, X.-Y.; Lin, C.; Chen, D.; Wang, L. *Adv. Funct. Mater.* **2015**, *25*, 3571-3580.

7. (a) Sung, J. H.; Hirano, S.; Tsutsumi, O.; Kanazawa, A.; Shiono, T.; Ikeda, T. *Chem. Mater.* **2002**, *14*, 385-391. (b) Adachi, H.; Hirai, Y.; Ikeda, T.; Maeda, M.; Hori, R.; Kutsumizu, S.; Haino, T. *Org. Lett.* **2016**, *18*, 924-927. (c) Kreger, K.; Wolfer, P.; Audorff, H.; Kador, L.; Stingelin-Stutzmann, N.; Smith, P.; Schmidt, H.-W. *J. Am. Chem. Soc.* **2010**, *132*, 509-516.
8. Pfltscher, M.; Wölper, C.; Gutmann, J. S.; Mezger, M.; Giese, M. *Chem. Commun.* **2016**, *52*, 8549-8552.
9. (a) Dugave, C.; Demange, L. *Chem. Rev.* **2003**, *103*, 2475-2532. (b) Garcia-Amoros, J.; Velasco, D. *Beilstein J. Org. Chem.* **2012**, *8*, 1003-1017.
10. (a) Kobatake, S.; Takami, S.; Muto, H.; Ishikawa, T.; Irie, M. *Nature*, **2007**, *446*, 778-781. (b) Guo, S.; Matsukawa, K.; Miyata, T.; Okubo, T.; Kuroda, K.; Shimojima, A. *J. Am. Chem. Soc.* **2015**, *137*, 15434–15440. (c) Merino, E.; Ribagorda, M. *Beilstein J. Org. Chem.* **2012**, *8*, 1071-1090.
11. (a) Henzl, J.; Mehlhorn, M.; Gawronski, H.; Rieder, K.-H.; Morgenstern, K. *Angew. Chem., Int. Ed.* **2006**, *45*, 603-606. (b) Beharry, A. A.; Woolley, G. A. *Chem. Soc. Rev.* **2011**, *40*, 4422-4437.
12. Huang, Y.; Kim, D.-H. *Nanoscale* **2012**, *4*, 6312-6317.
13. Goldenberg, L. M.; Kulikovskiy, L.; Kulikovska, O.; Tomczyk, J.; Stumpe, J. *Langmuir* **2010**, *26*, 2214-2217.
14. Lee, S.; Oh, S.; Lee, J.; Malpani, Y.; Jung, Y.-S.; Kang, B.; Lee, J. Y.; Ozasa, K.; Isoshima, T.; Lee, S. Y.; Hara, M.; Hashizume, D.; Kim, J.-M. *Langmuir* **2013**, *29*, 5869-5877.
15. Kind, J.; Kaltschnee, L.; Leyendecker, M.; Thiele, C. M. *Chem. Commun.* **2016**, *52*, 12506-12509.
16. Cârlescu, I.; Scutaru, A. M.; Apreutesei, D.; Alupei, V.; Scutaru, D. *Liquid Crystals*, **2007**, *34*, 775-785.
17. Bala, I.; Gupta, S. P.; De, J.; Pal, S. K.; *Chem. - Eur. J.* **2017**, *23*, 12767-12778.
18. Luo, J.; Zhao, B.; Chan, H. S. O.; Chi, C. *J. Mater. Chem.* **2010**, *20*, 1932-1941.
19. Foster, E. J.; Lavigueur, C.; Ke, Y.-C.; Williams, V. E. *J. Mater. Chem.* **2005**, *15*, 4062-4068.

Appendix 4A

Kinetics plots for the formation constants of all-*trans* isomers using UV-Vis spectroscopy:

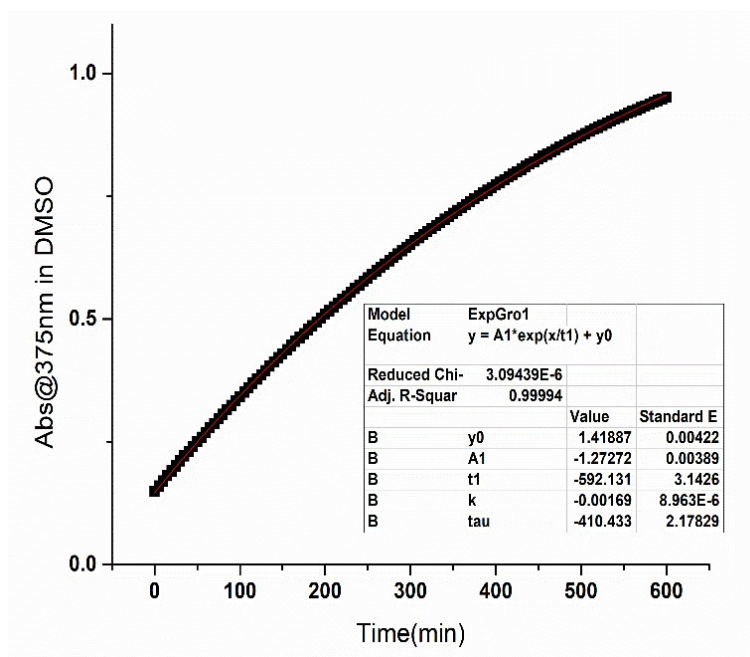


Figure 4A.1. First order formation kinetics for the reverse switching in **13a** (10.8 mM solution in DMSO)

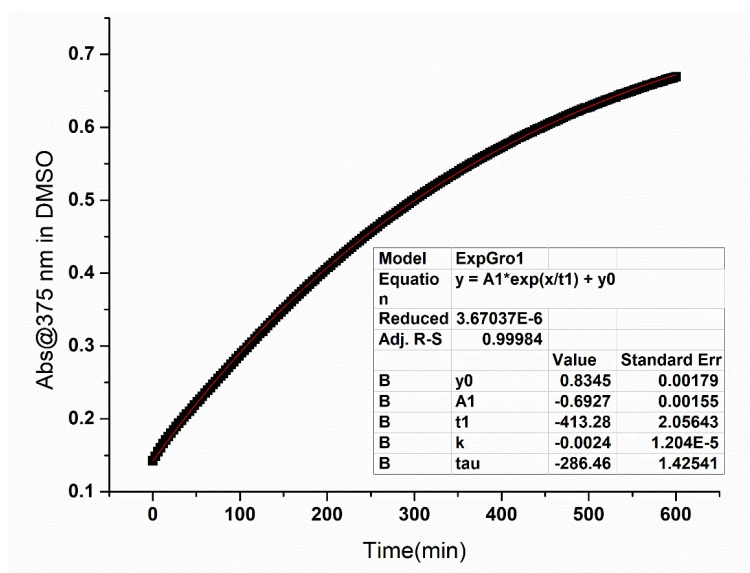


Figure 4A.2. First order formation kinetics for the reverse switching in **13b** (8.0 mM solution in DMSO)

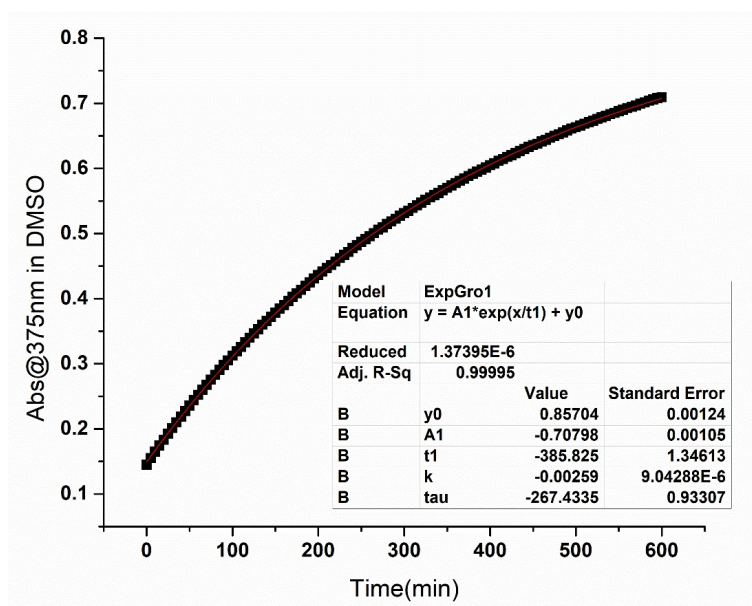


Figure 4A.3. First order formation kinetics for the reverse switching in **13c** (7.5 mM solution in DMSO)

Appendix 4B

X-ray diffraction (XRD) studies: X-ray scattering experiments were performed to deduce the exact structure of the assembly of the mesophases. The compound **13a** at a lower temperature, in the temperature range of 25 °C to 160 °C exhibits many peaks in the small angle region. In addition, there are h_a and h_c peaks in the wide angle region. The h_a peak is mainly originated due to the liquid-like the order of the fluid chain and h_c peak appears due to the core-core separation and it is indicative of π - π interaction, reflecting the columnar nature of the mesophase (**Figure 4B.1**). The peaks of the small angle could be indexed on the rectangular lattice. The calculated 2D lattice parameters are $a = 57.2 \text{ \AA}$, $b = 44.84 \text{ \AA}$ (at 140 °C). The h_c peak set the value of the of the other lattice parameter i.e. $c = 3.89 \text{ \AA}$. The details are summarized in the Table 3. In brief, the observed phase is Col_r . Further, this phase transformed into Col_h phase at temperature of 160.4 °C, and persists in the temperature range of 160.4 °C to 238 °C. The phase is confirmed by the observation of three peaks in the small angle region with d-spacing in ratios $1:1/\sqrt{3}:1/\sqrt{7}$ and these peaks were assigned to reflections from (10), (11) and (21) planes, respectively of the hexagonal lattice (**Figure 4B.1b**, and **Table 4B.1**).

Further, h_a and h_c peaks were also observed in the wide angle region where h_c peak confirmed its columnar nature. The calculated lattice parameter is found to be $a = 39.24 \text{ \AA}$ and the other lattice parameter which is set by the value of the spacing of h_c peak i.e. $c = 3.62 \text{ \AA}$. In summary, the compound **13a** exhibit Col_r phase at lower temperature (25-160 °C) and Col_h phase at higher temperature (160.4-238 °C). This phase behaviour is also well supported by POM.

In contrast, compounds **13b** and **13c** showed only Col_h phase (**Figure 4B.1c** and **4B.1d**). The lattice parameters are found to be $a = 43.35 \text{ \AA}$ and 49.74 \AA (**Table 4B.1**), respectively, which reflect the increasing trend. This trend is obvious because the periphery chain length (size of the molecule) is increasing from compound **13a** to **13c**.

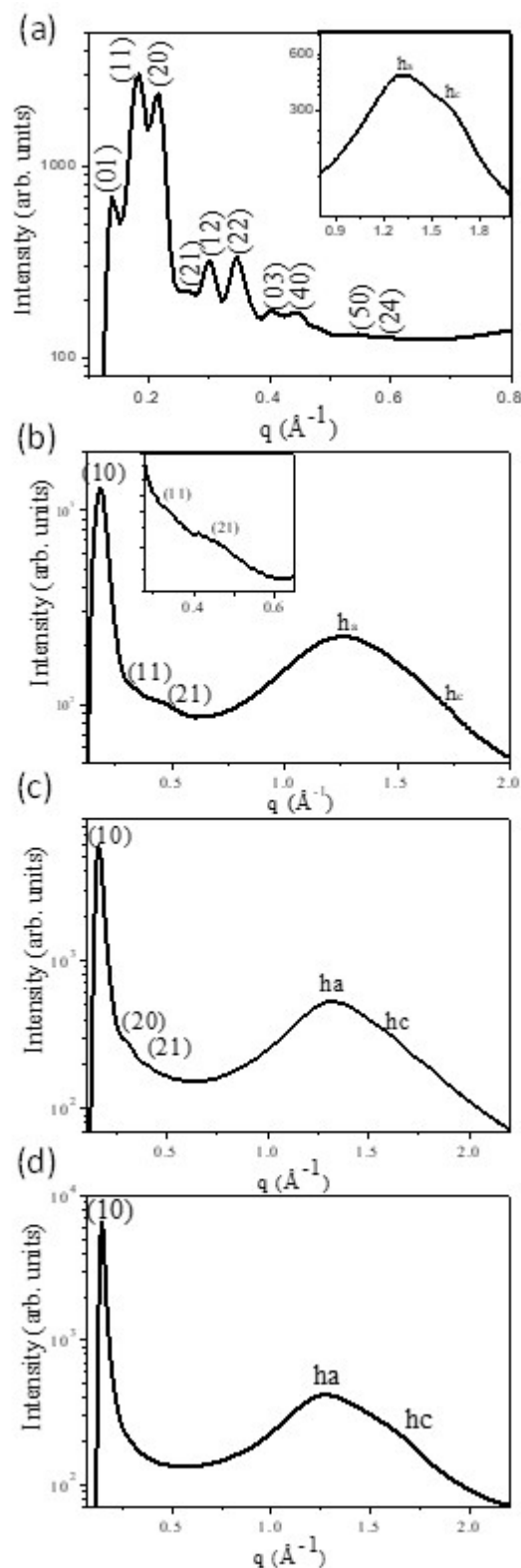


Figure 4B.1. X-ray diffraction pattern: (a) compound **13a** in the Col_r at 140°C ; (b) compound **13a** in the Col_h at 190°C ; (c) compound **13b** in the Col_h at 25°C ; (d) compound **13c** in the Col_h at 115°C , obtained on cooling from the isotropic liquid, h_a and h_c are the spacings appear due to alkyl chain-chain and core-core correlation, respectively.

Table 4B.1. The Indices, observed and calculated d -spacings and planes of the diffraction peaks of the lattices.

Compounds	T (°C)	Phase	Lattice constants (Å)	d_{obs} (Å) ^[a]	d_{cal} (Å) ^[b]	Miller Indices (hk)
13a	140	Col _r	a = 57.20	44.78	44.84	01
			b = 44.84	35.16	35.29	11
			c = 3.89	28.91	28.6	20
				23.90	24.11	21
				20.83	20.87	12
				17.93	17.65	22
				15.28	14.95	03
				14.14	14.30	40
				11.46	11.44	50
				10.59	10.44	24
				9.93	9.66	34
				9.54	9.53	60
					4.81	h_a
					3.8	h_c
13b	190	Col _h	a = 39.24	33.99		10
			c = 3.62	19.57		11
				13.15		21
				4.95		h_a
				3.62		h_c
13c	25	Col _h	a = 45.47	39.38	39.38	10
			c = 3.88	19.89	19.69	20
				15.14	14.88	21
				4.79		h_a
				3.88		h_c
13c	115	Col _h	a = 49.76	43.09	43.09	10
			c = 3.62	4.94		h_a
				3.73		h_c

[a] d_{obs} : experimental d -spacing. [b] d_{cal} : calculated d -spacing for Col_r by using the relation: $\frac{1}{d^2} = \left[\frac{h^2}{a^2} + \frac{k^2}{b^2} \right]$; for Col_h : $\frac{1}{d^2} = \left[\frac{h^2}{a^2} + \frac{k^2}{a^2} \right]$ h, k are the indices of the reflections corresponding to the columnar rectangular phase (Col_r) and columnar hexagonal phase (Col_h); a, b & c are the unit cell parameters, h_a & h_c spacings appear due to alkyl chain-chain and core-core correlation, respectively.

Reconstructed electron density maps: Electron density map for the columnar rectangular and hexagonal phase of compound **13a** was reconstructed (**Figure 4B.2a,b**). The procedure to reconstruct the electron density map is described in the earlier literature.^[18,21]

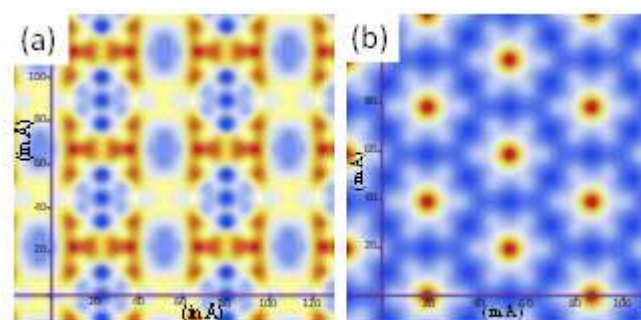


Figure 4B.2. (a) Reconstructed electron density map of columnar rectangular (Col_r) and (b) columnar hexagonal (Col_h) phase. The red represents the highest electron density and deep blue is the lowest.

Appendix 4C

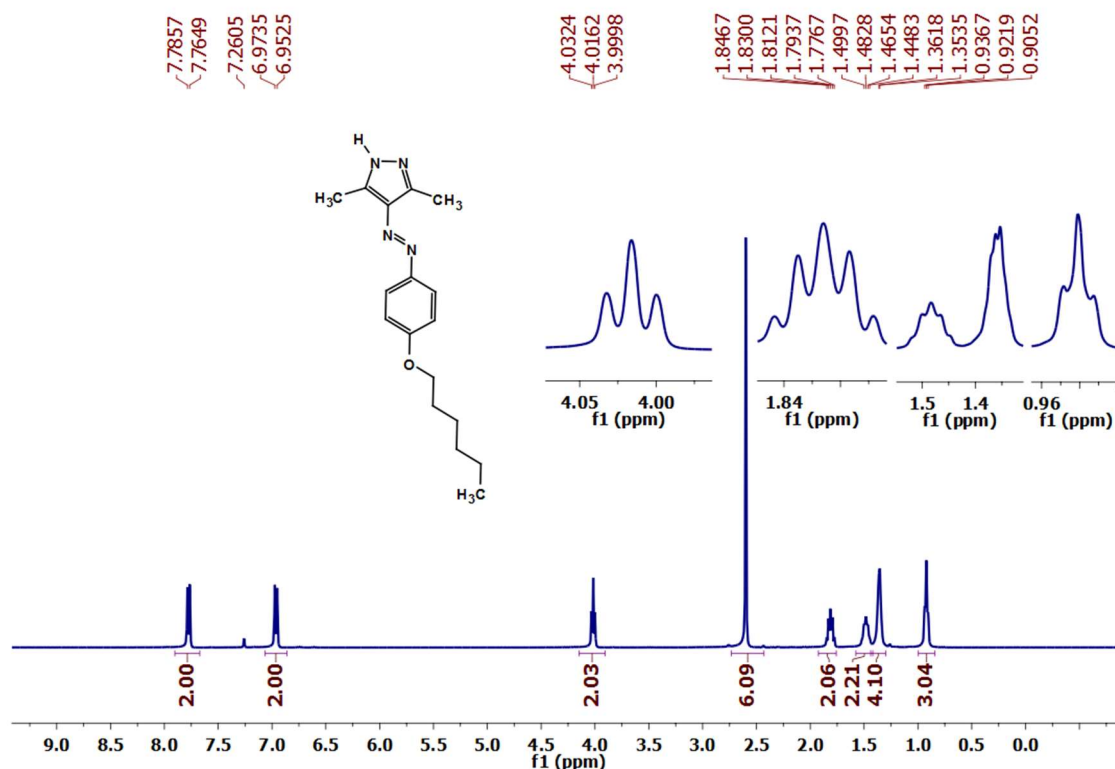


Figure 4C.1. ^1H NMR spectrum of *(E)*-4-((4-(hexyloxy)phenyl)diazenyl)-3,5-dimethyl-1*H*-pyrazole (**4a**)

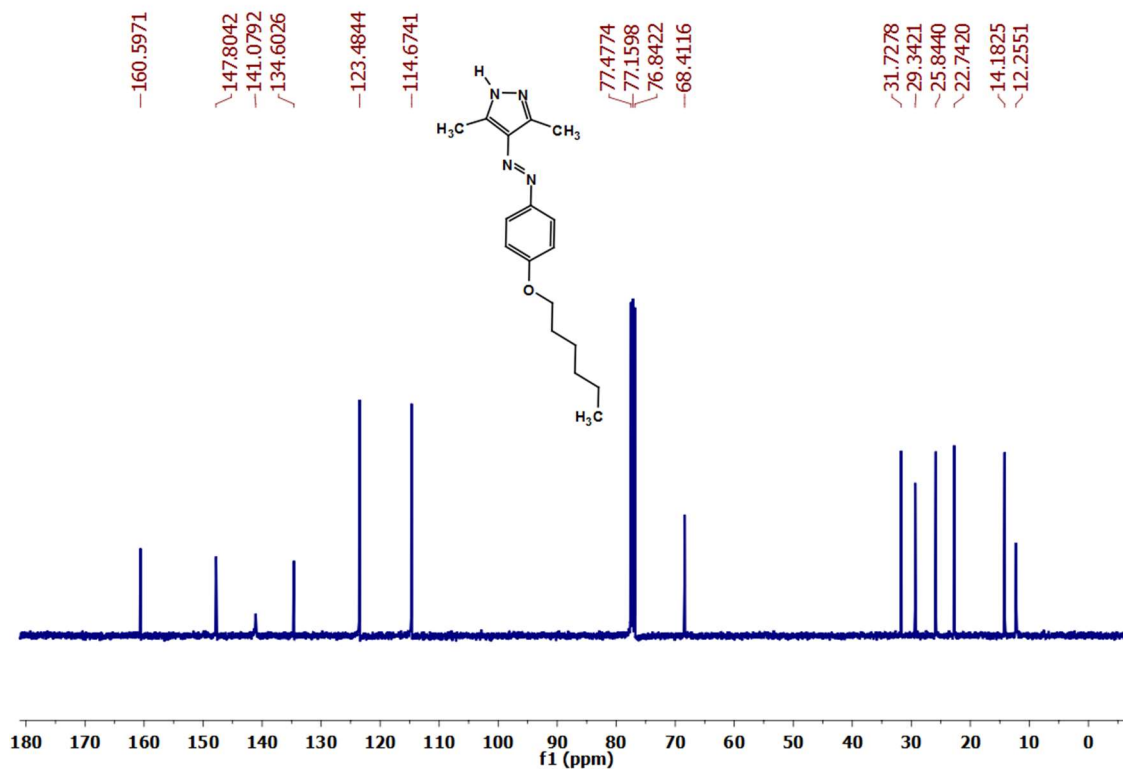


Figure 4C.2. ^{13}C NMR spectrum of *(E)*-4-((4-(hexyloxy)phenyl)diazenyl)-3,5-dimethyl-1*H*-pyrazole (**4a**)

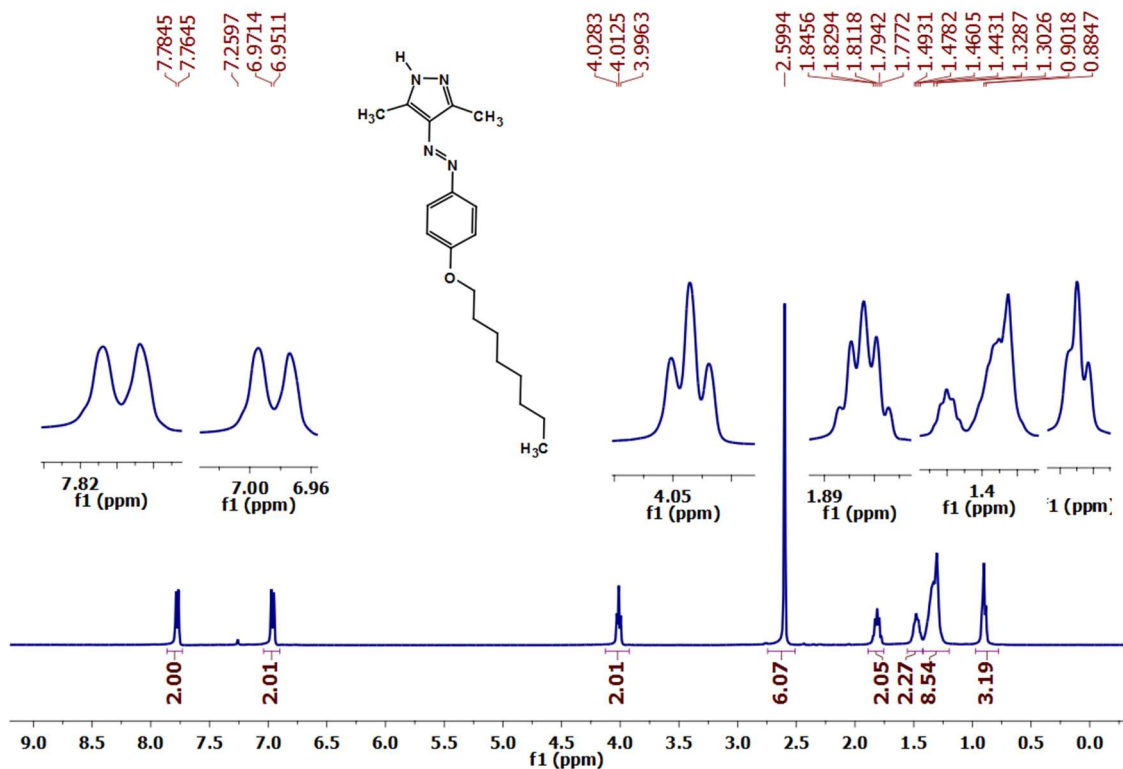


Figure 4C.3. ^1H NMR spectrum of (*E*)-3,5-dimethyl-4-((4-(octyloxy)phenyl)diazenyl)-1*H*-pyrazole (**4b**)

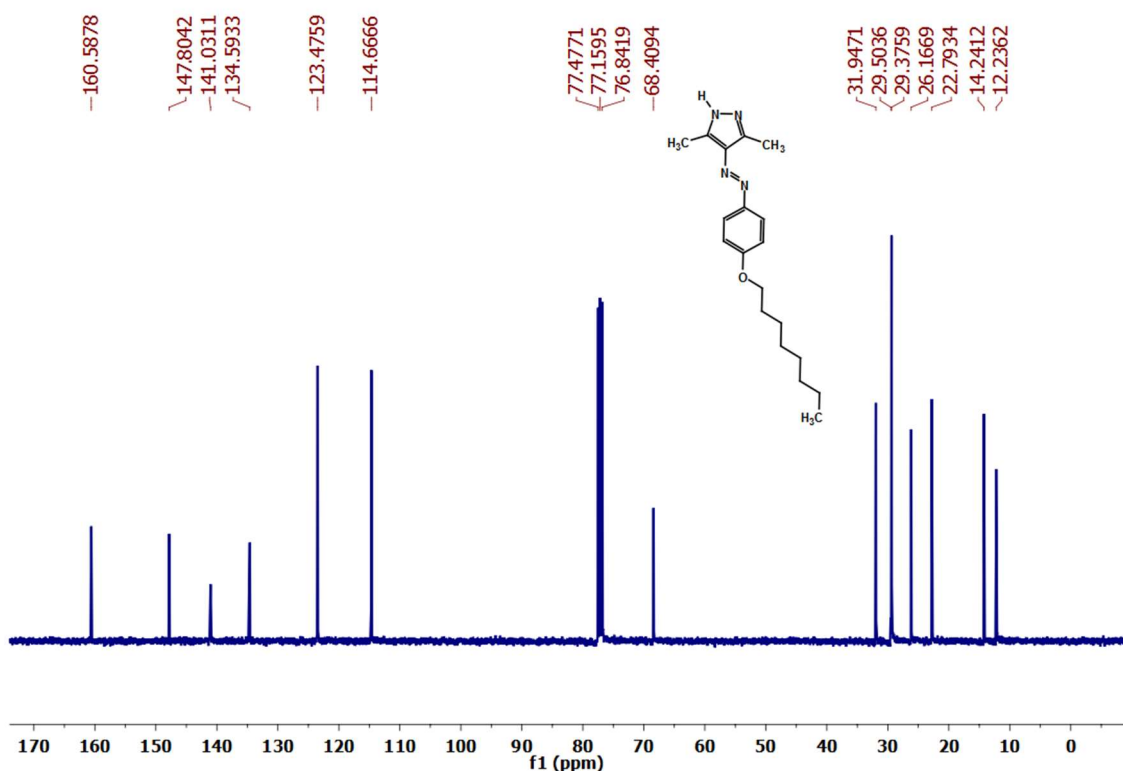


Figure 4C.4. ^{13}C NMR spectrum of (*E*)-3,5-dimethyl-4-((4-(octyloxy)phenyl)diazenyl)-1*H*-pyrazole (**4b**)

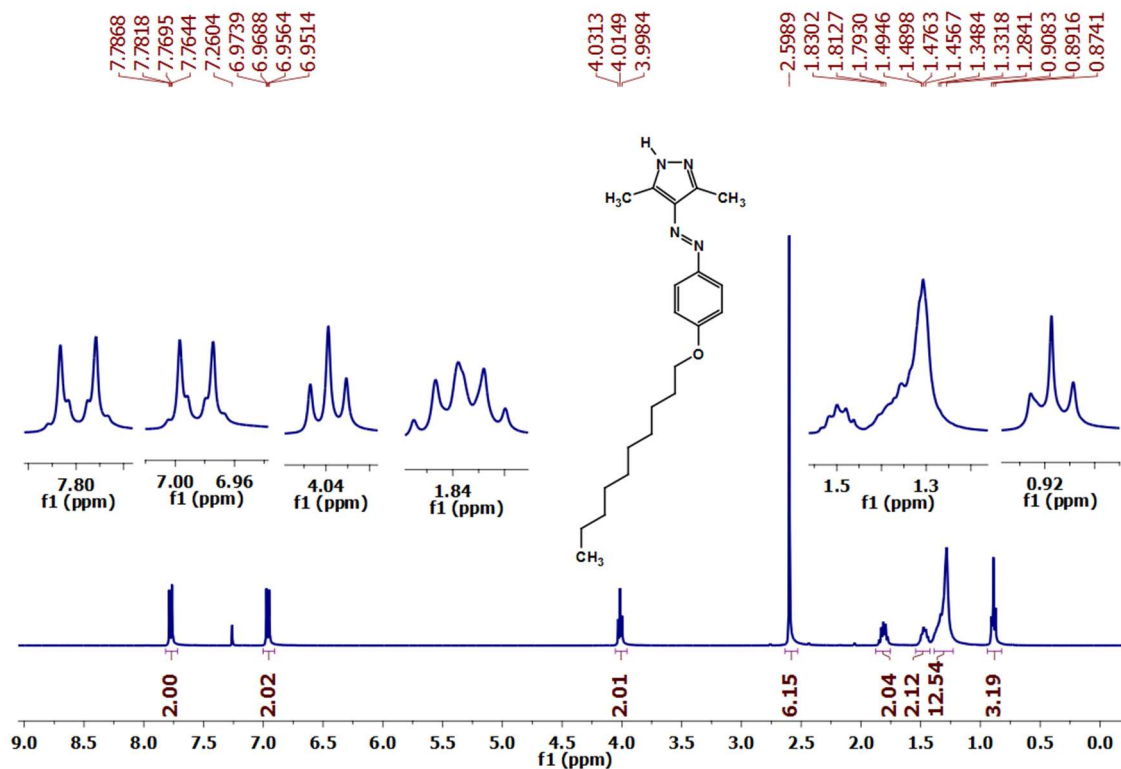


Figure 4C.5. ¹H NMR spectrum of *(E)*-4-((4-(decyloxy)phenyl)diazenyl)-3,5-dimethyl-1*H*-pyrazole (**4c**)

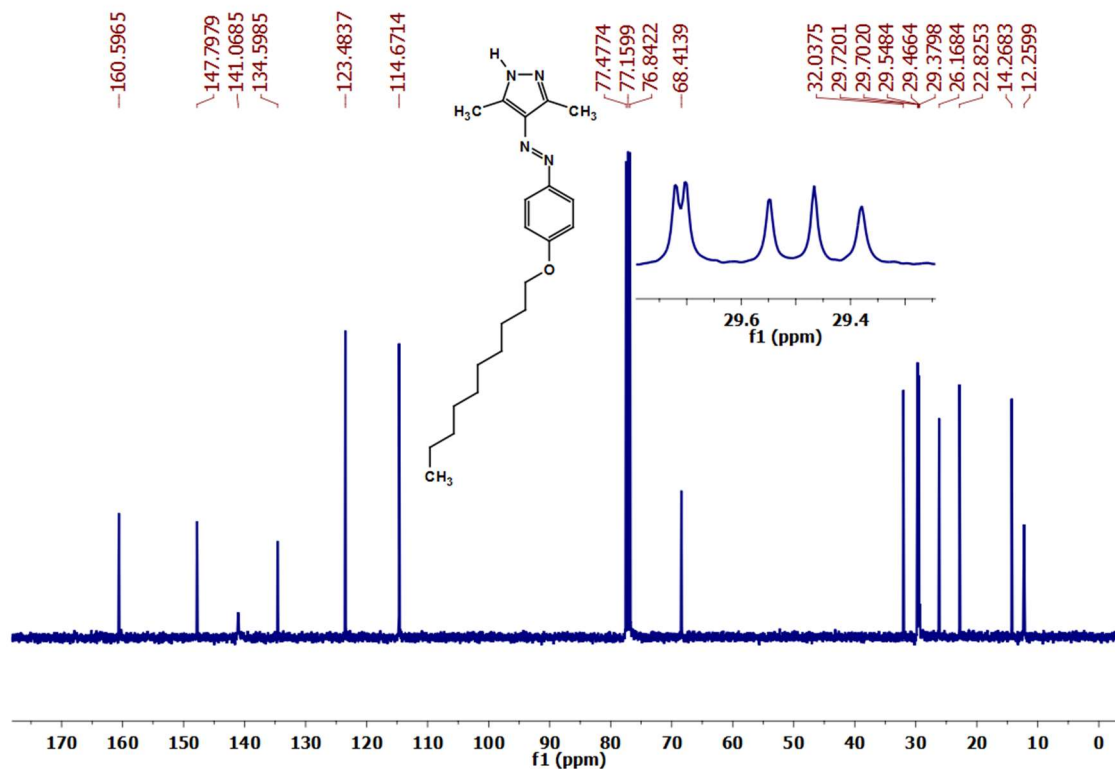


Figure 4C.6. ¹³C NMR spectrum of *(E)*-4-((4-(decyloxy)phenyl)diazenyl)-3,5-dimethyl-1*H*-pyrazole (**4c**)

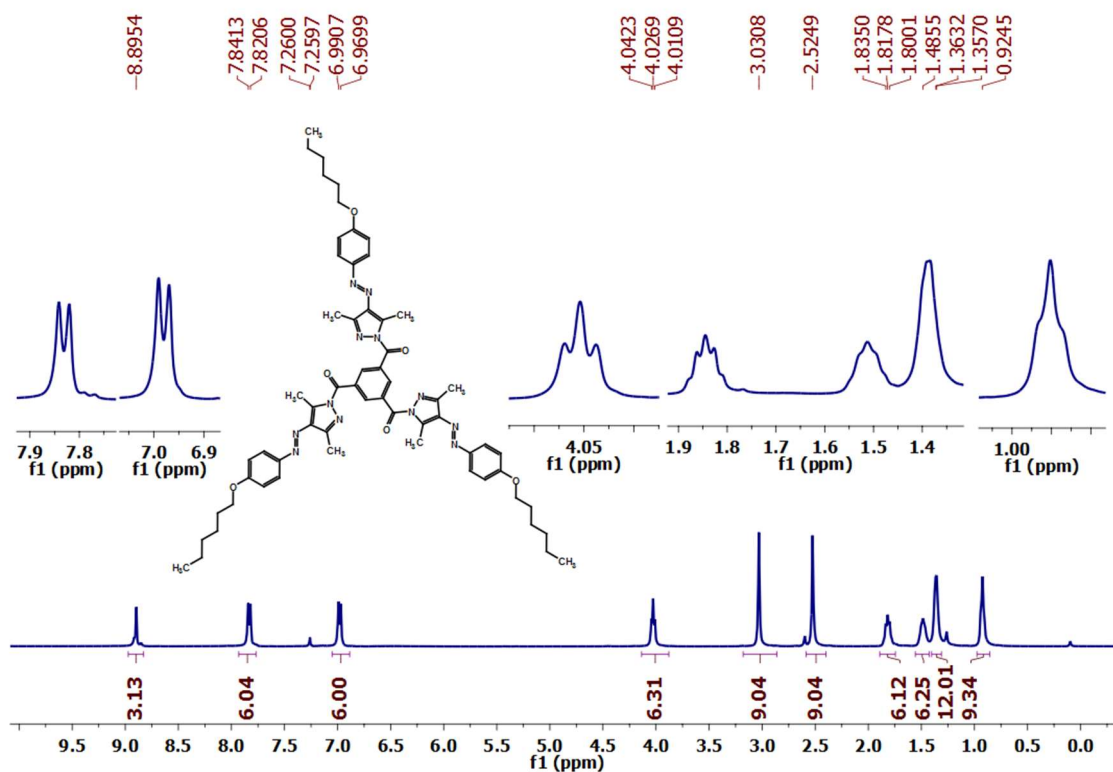


Figure 4C.7. ¹H NMR spectrum of Benzene-1,3,5-triyltris((4-((E)-4-(hexyloxy)phenyl)diazanyl)-3,5-dimethyl-1H-pyrazol-1-yl)methanone) (**7a**)

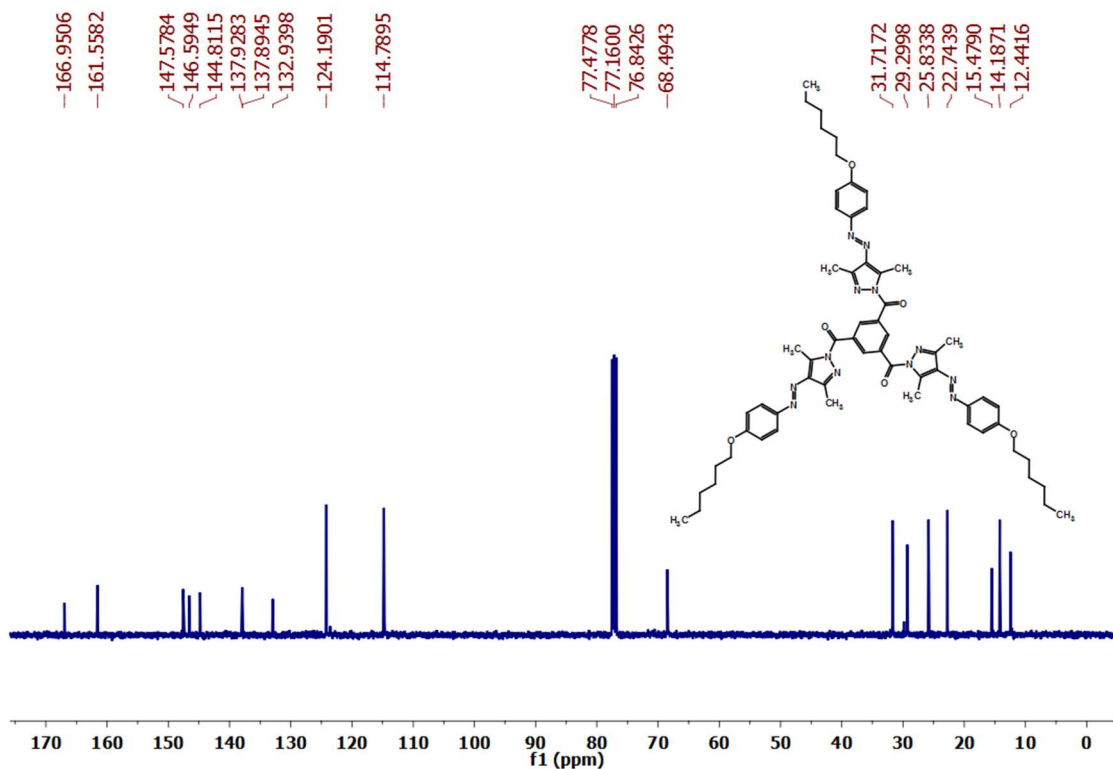


Figure 4C.8. ¹³C NMR spectrum of Benzene-1,3,5-triyltris((4-((E)-4-(hexyloxy)phenyl)diazanyl)-3,5-dimethyl-1H-pyrazol-1-yl)methanone) (**7a**)

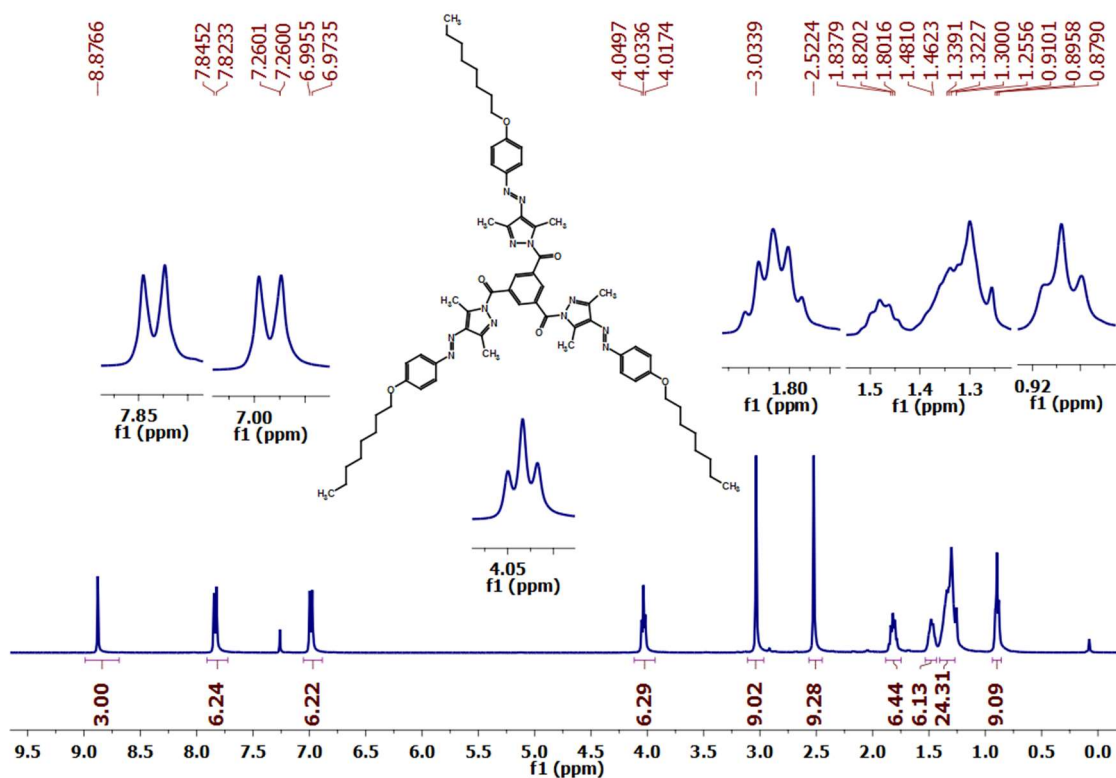


Figure 4C.9. ^1H NMR spectrum of Benzene-1,3,5-triyltris((3,5-dimethyl-4-((*E*)-(4-(octyloxy)phenyl)diazenyl)-1*H*-pyrazol-1-yl)methanone) (**7b**)

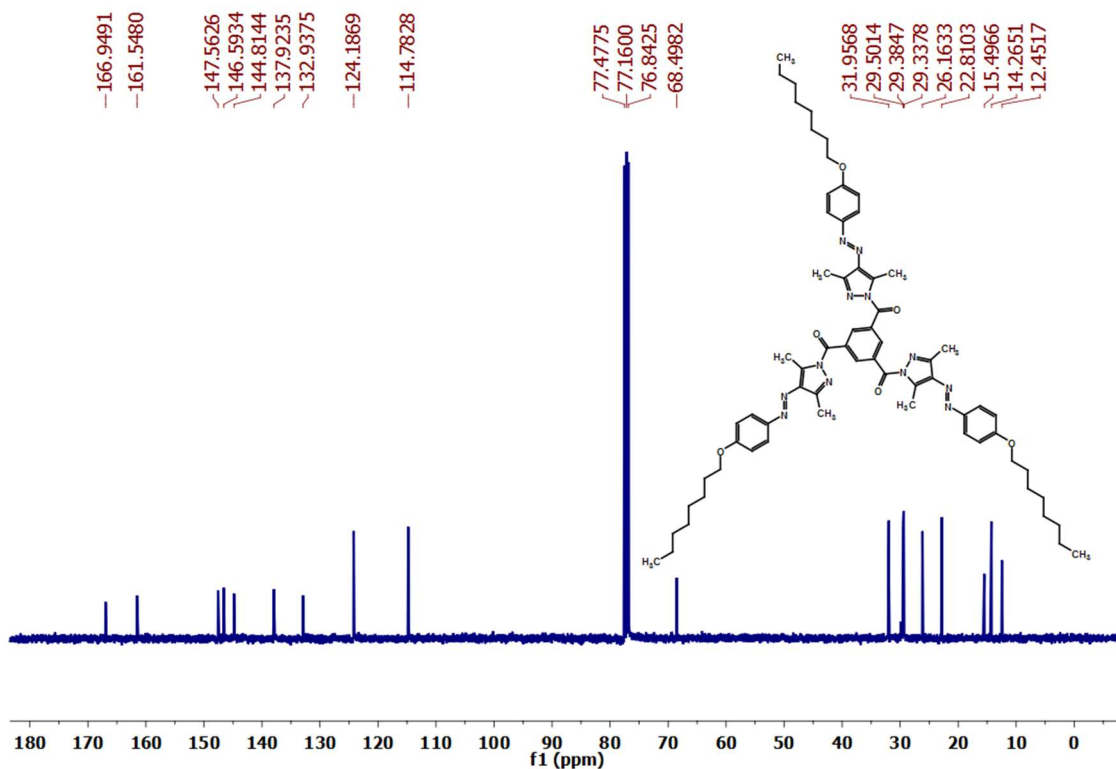


Figure 4C.10. ^{13}C NMR spectrum of Benzene-1,3,5-triyltris((3,5-dimethyl-4-((*E*)-(4-(octyloxy)phenyl)diazenyl)-1*H*-pyrazol-1-yl)methanone) (**7b**)

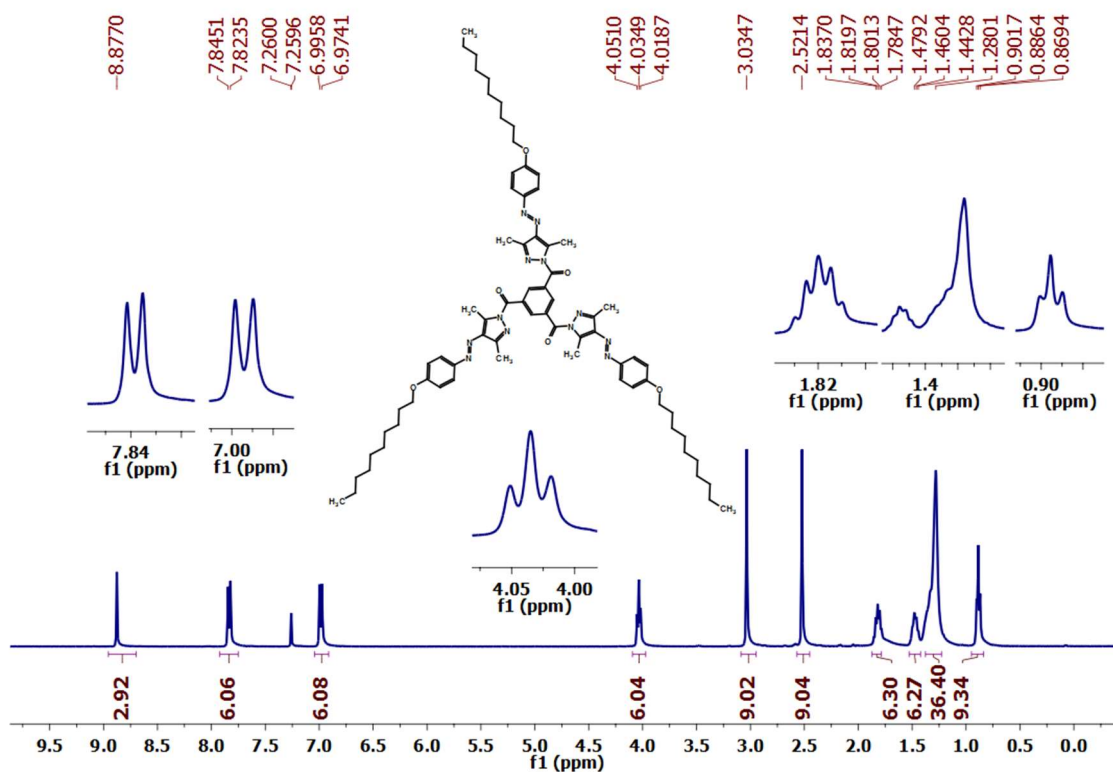


Figure 4C.11. ^1H NMR spectrum of Benzene-1,3,5-triyltris((*E*)-(4-(decyloxy)phenyl) diazenyl)-3,5-dimethyl-1*H*-pyrazol-1-yl)methanone) (**7c**)

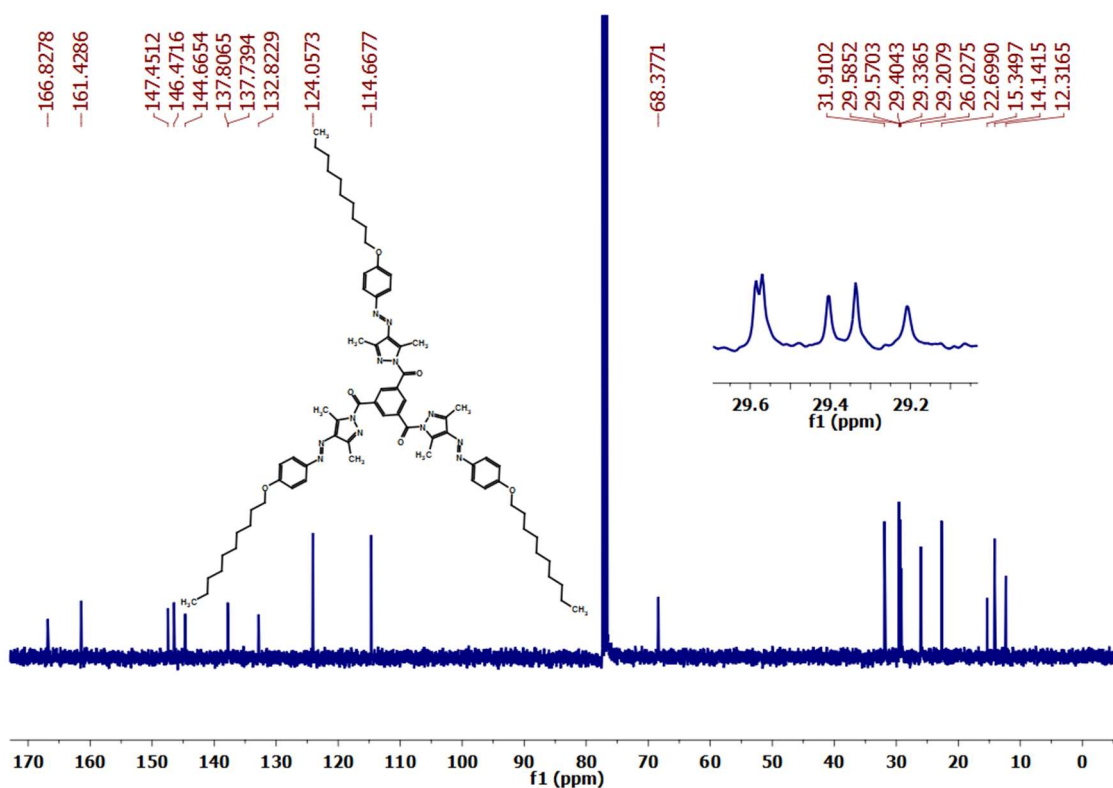


Figure 4C.12. ^{13}C NMR spectrum of Benzene-1,3,5-triyltris((*E*)-(4-(decyloxy)phenyl) diazenyl)-3,5-dimethyl-1*H*-pyrazol-1-yl)methanone) (**7c**)

Appendix 4D

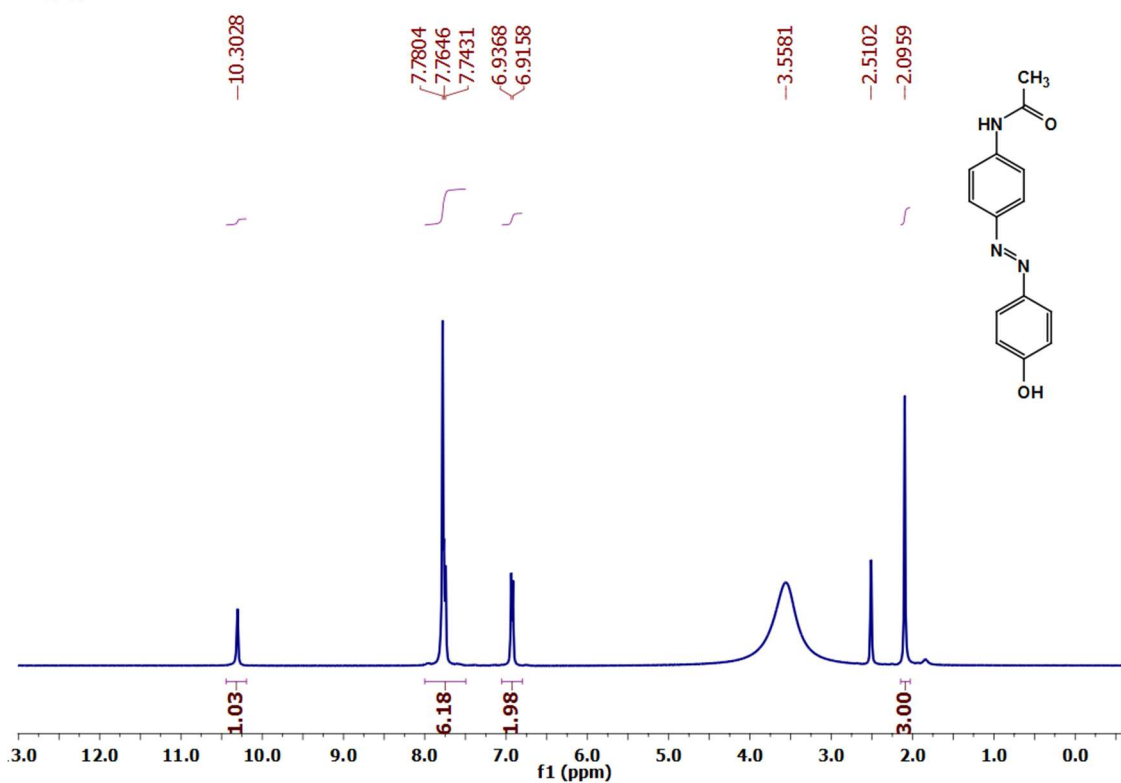


Figure 4D.1. ¹H NMR spectrum of (E)-N-(4-((4-hydroxyphenyl)diazenyl)phenyl)acetamide (10)

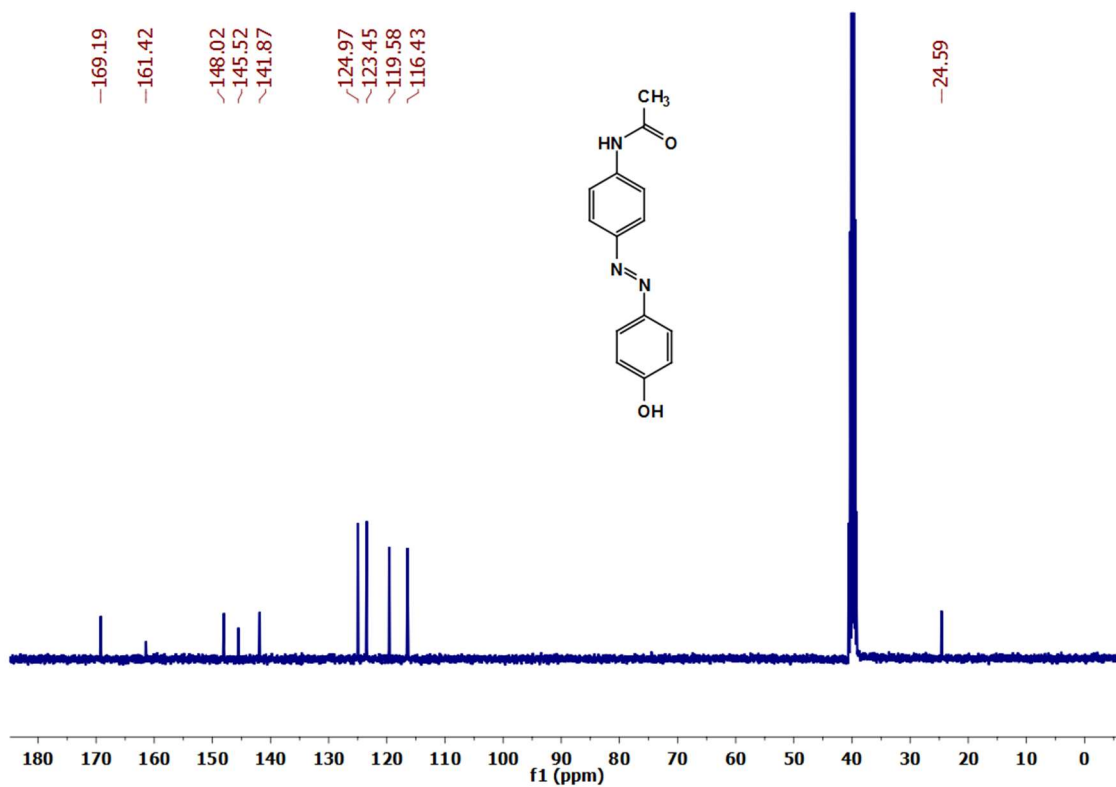


Figure 4D.2. ¹³C NMR spectrum of (E)-N-(4-((4-hydroxyphenyl)diazenyl)phenyl)acetamide (10)

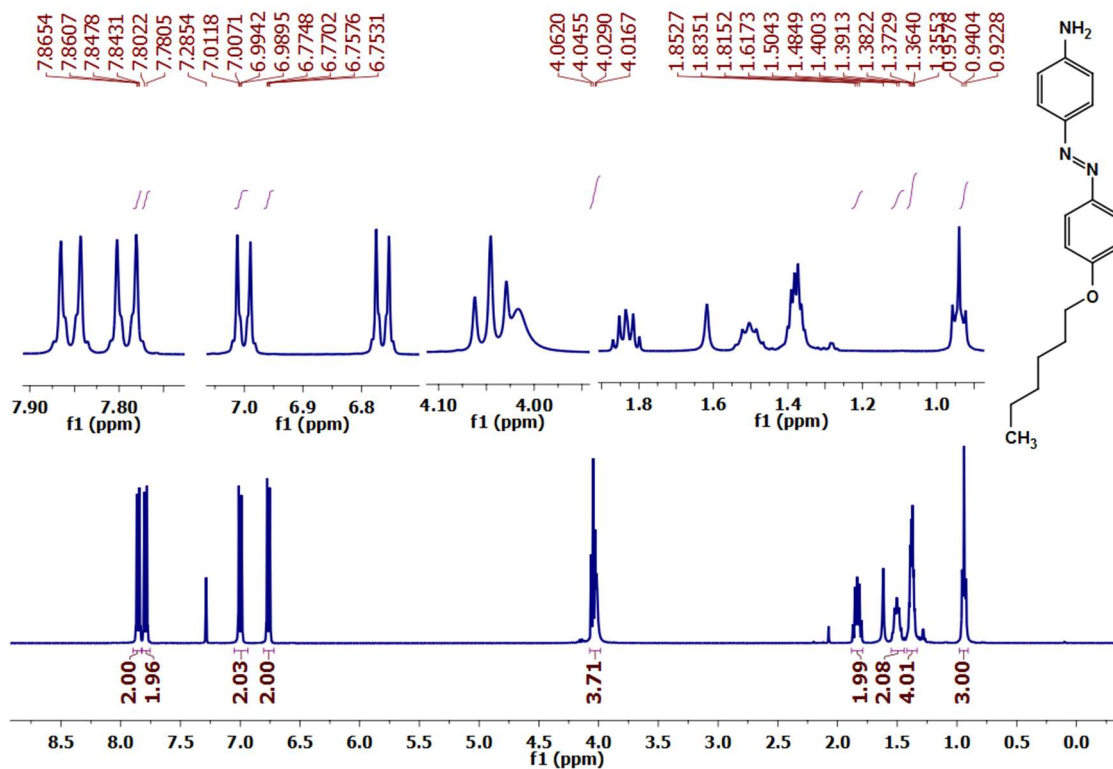


Figure 4D.3. ¹H NMR spectrum of (E)-4-((4-(hexyloxy)phenyl)diazenyl)aniline (**12a**)

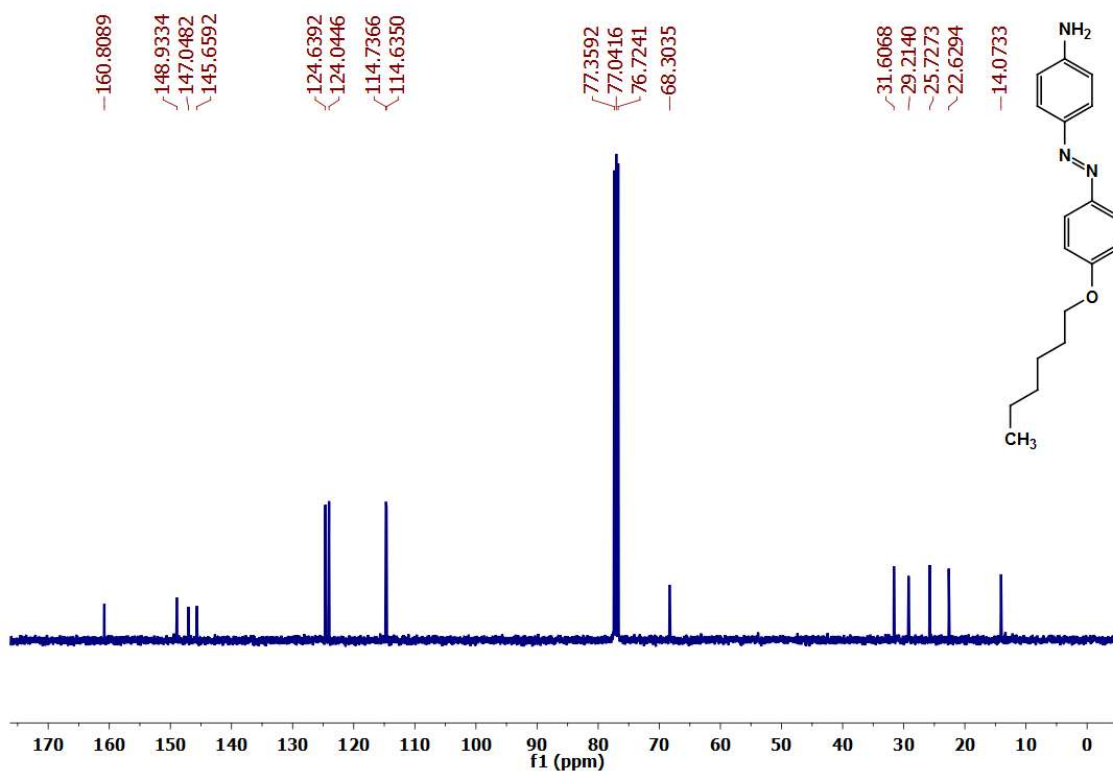


Figure 4D.4. ¹³C NMR spectrum of (E)-4-((4-(hexyloxy)phenyl)diazenyl)aniline (**12a**)

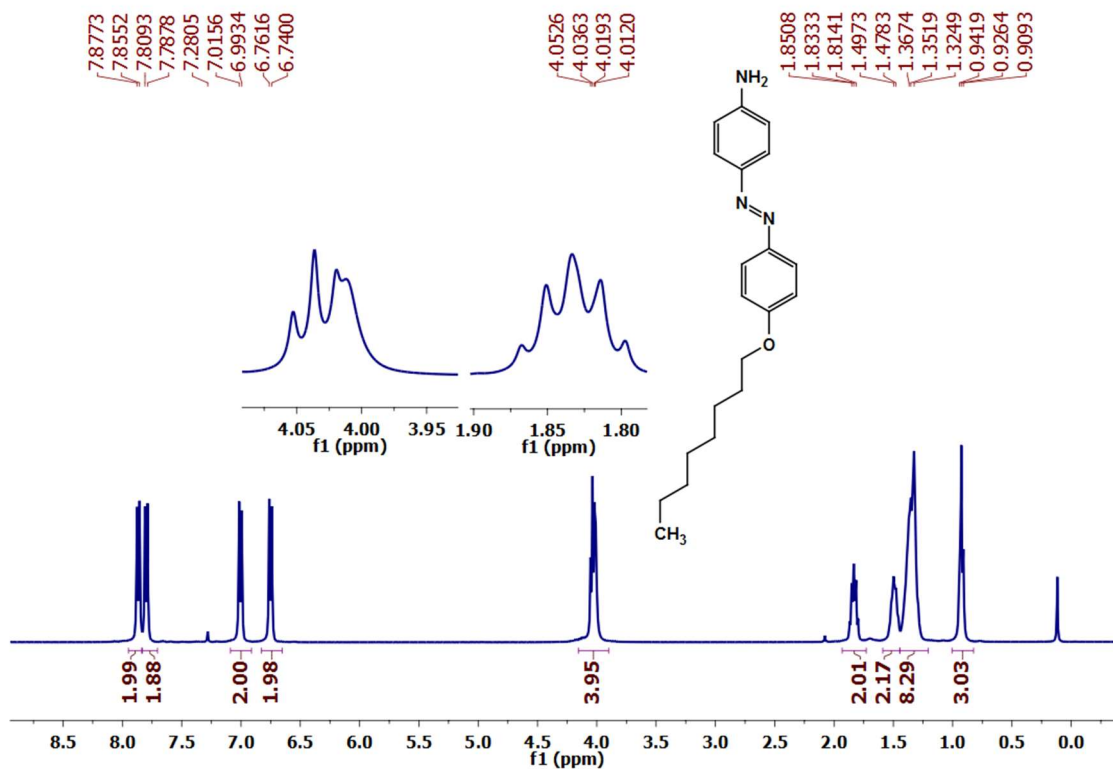


Figure 4D.5. ¹H NMR spectrum of (*E*)-4-((4-(octyloxy)phenyl)diazenyl)aniline (**12b**)

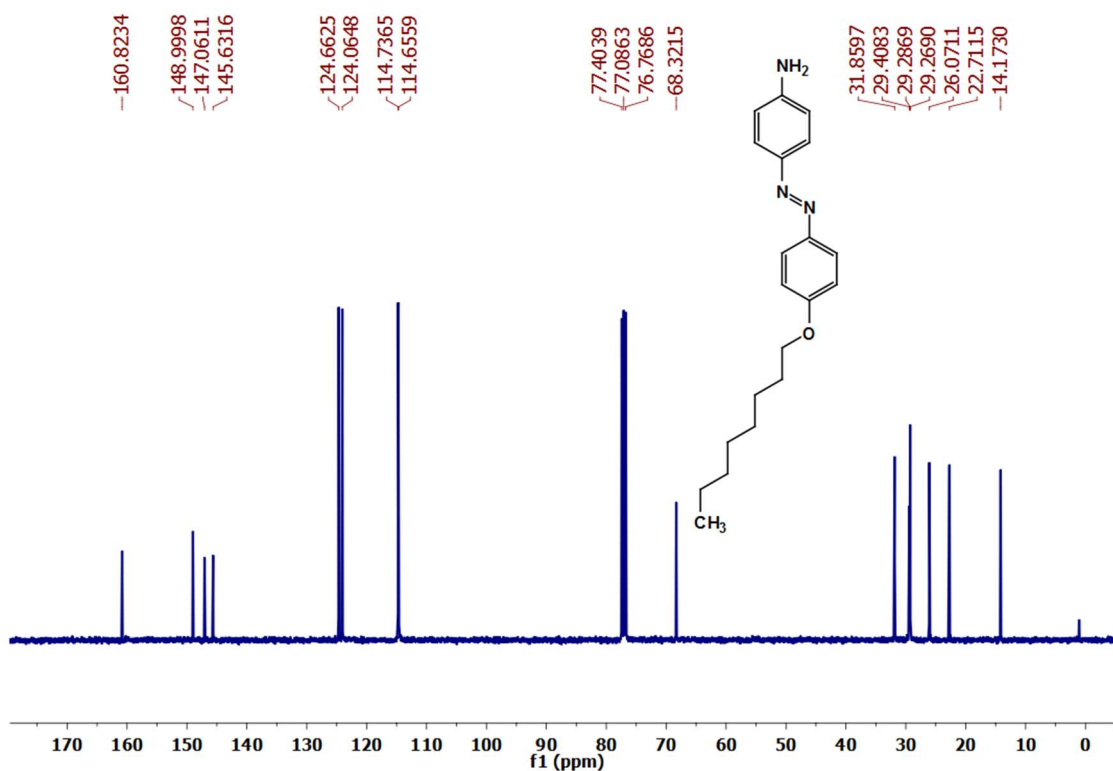
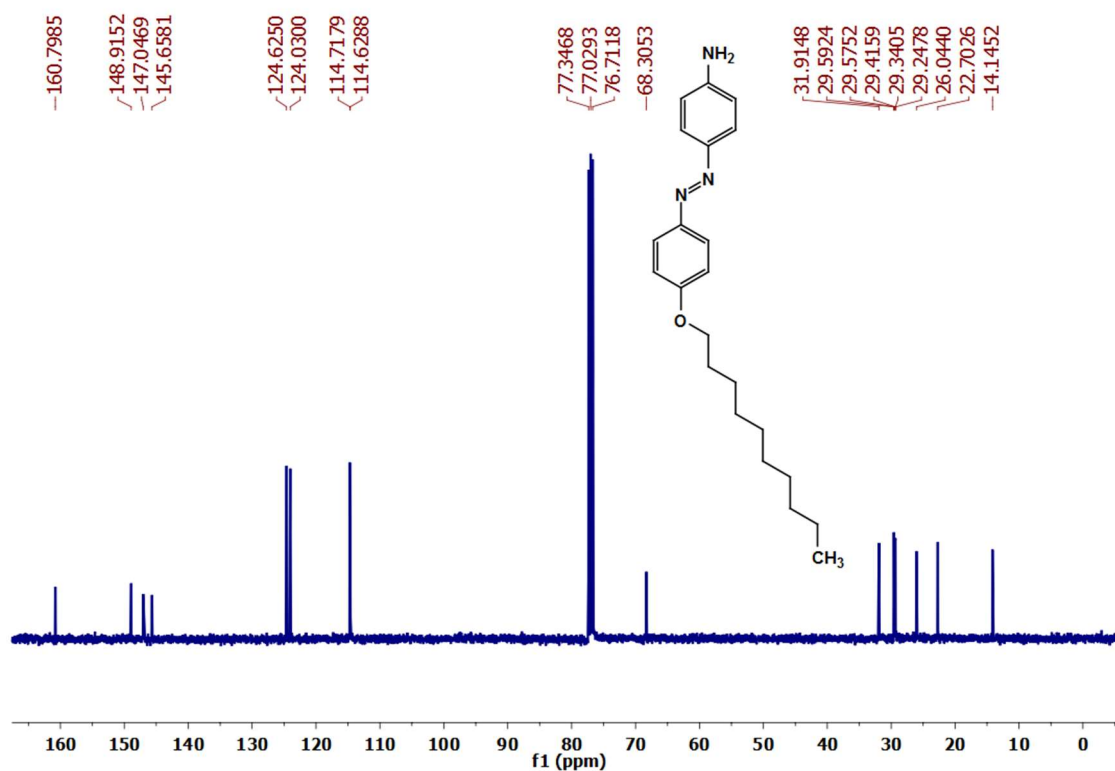
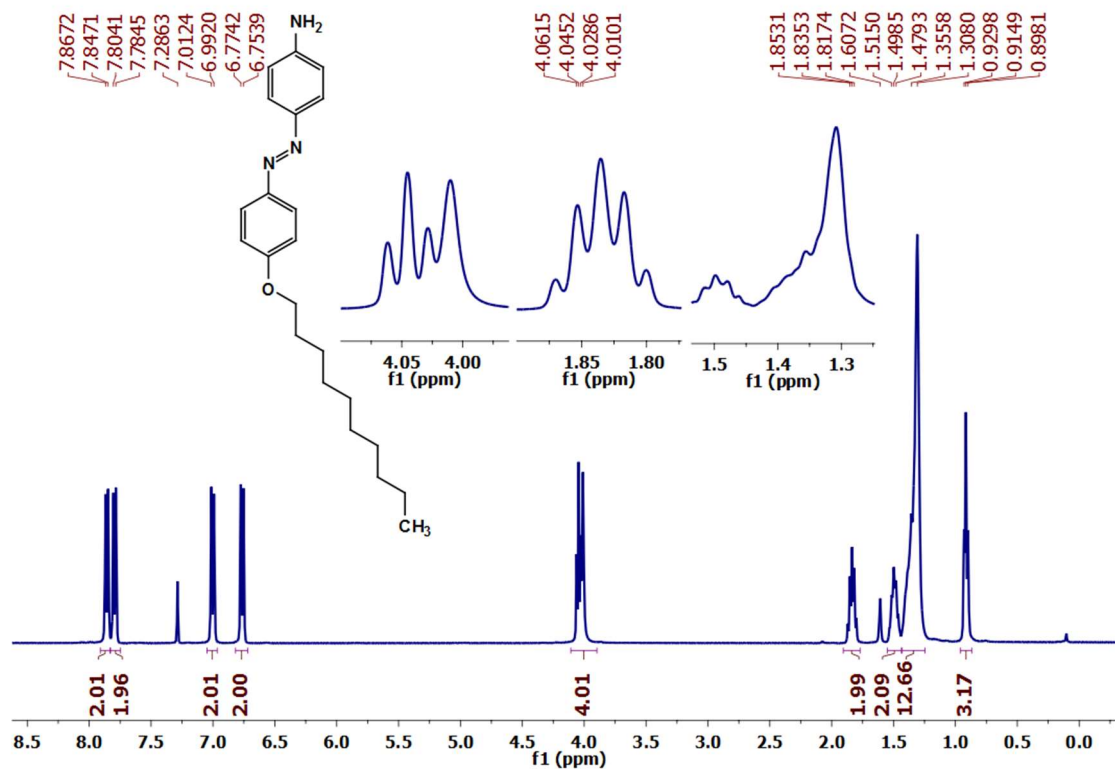


Figure 4D.6. ¹³C NMR spectrum of (*E*)-4-((4-(octyloxy)phenyl)diazenyl)aniline (**12b**)



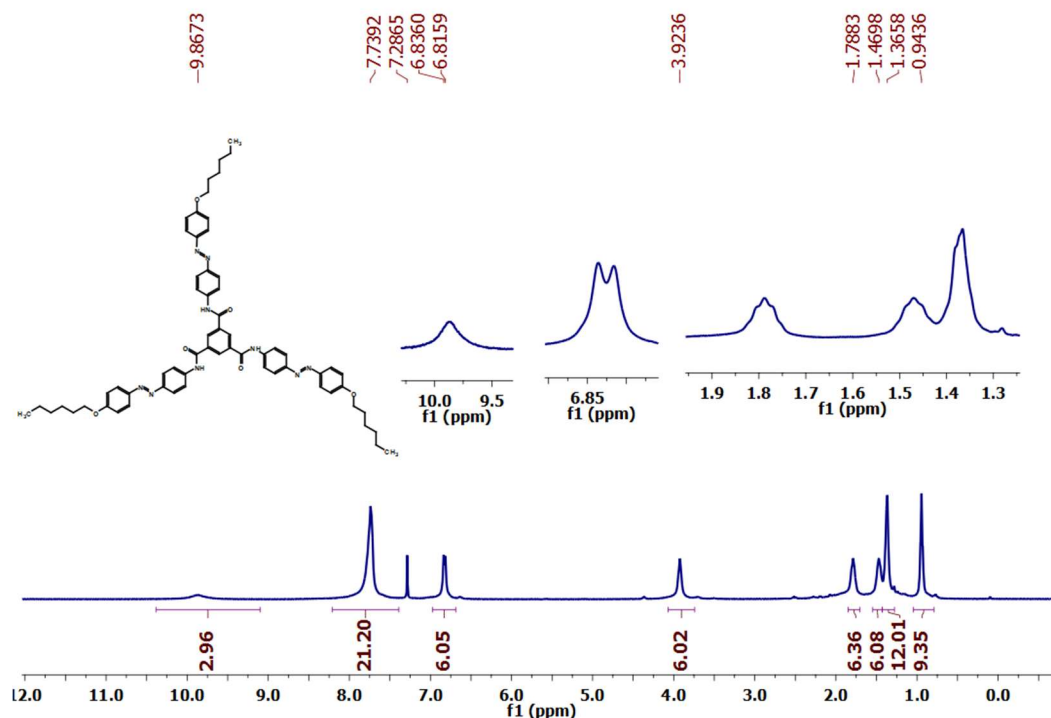


Figure 4D.9. ^1H NMR spectrum of N^1, N^3 -bis(4-((*E*)-(4-(hexyloxy)phenyl)diazenyl)phenyl)- N^5 -(4-((*E*)-(4-((pentyloxy)methyl)phenyl)diazenyl)phenyl)benzene-1,3,5-tricarboxamide (**13a**)

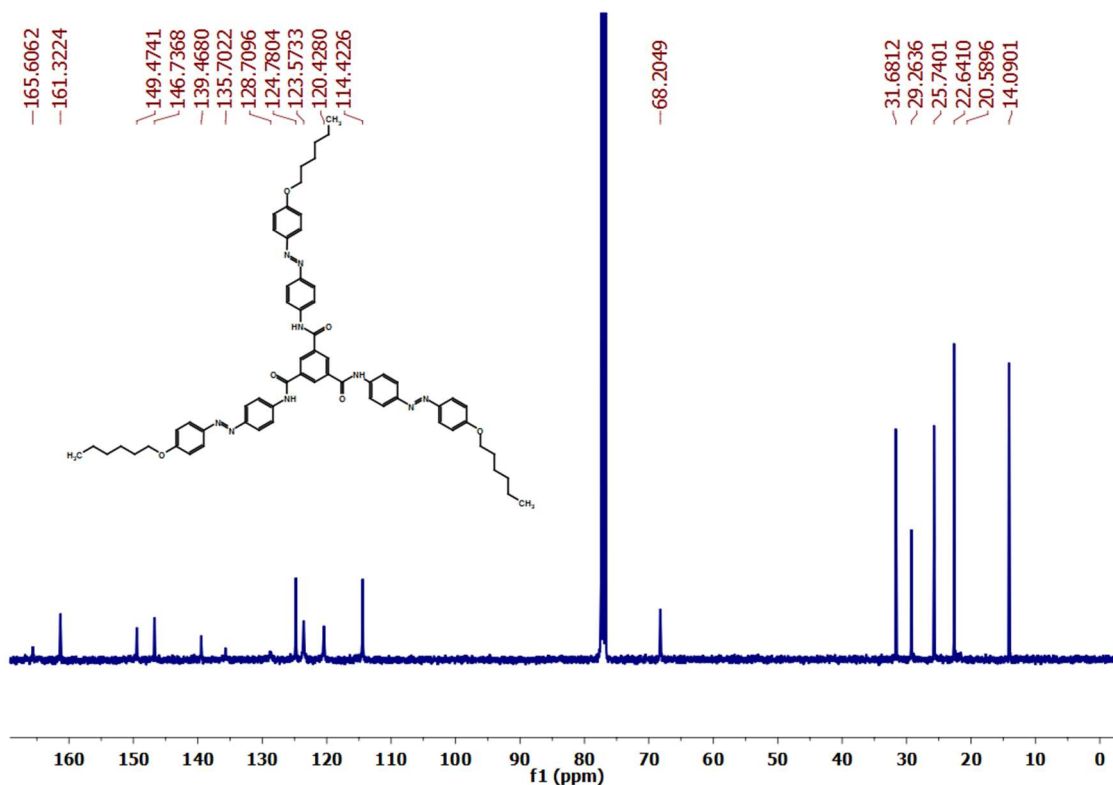


Figure 4D.10. ^{13}C NMR spectrum of N^1, N^3 -bis(4-((*E*)-(4-(hexyloxy)phenyl)diazenyl)phenyl)- N^5 -(4-((*E*)-(4-((pentyloxy)methyl)phenyl)diazenyl)phenyl)benzene-1,3,5-tricarboxamide (**13a**)

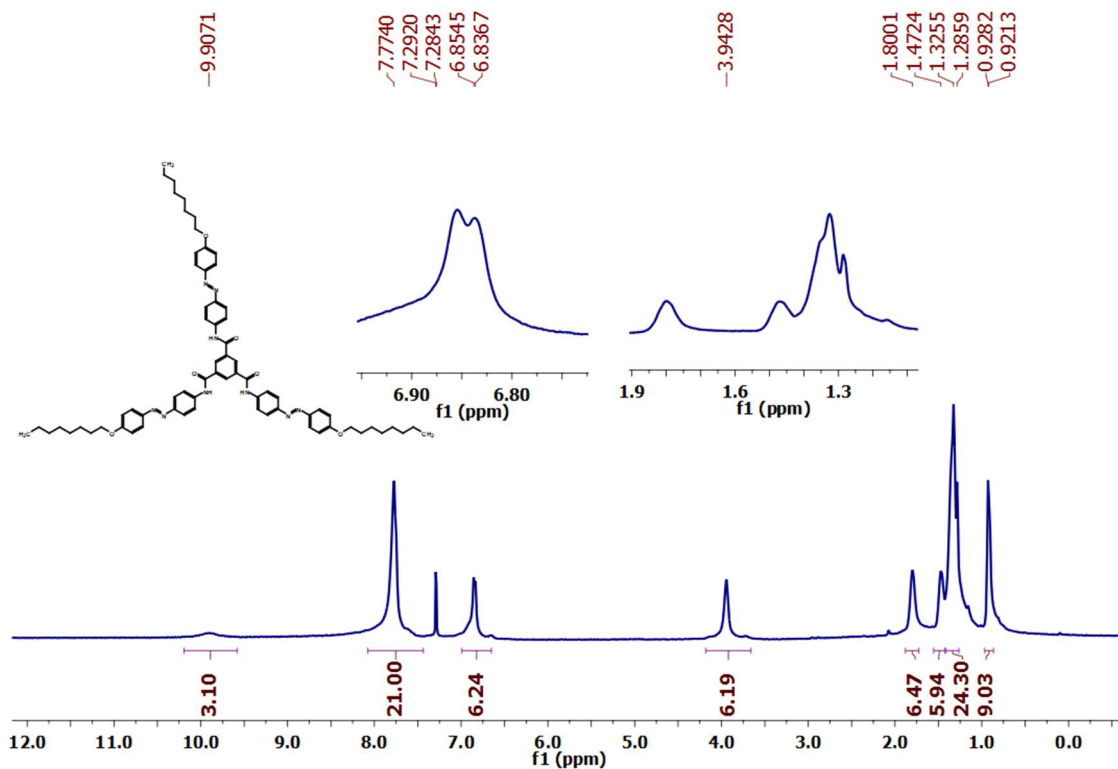


Figure 4D.11. ¹H NMR spectrum of *N*¹,*N*³-bis(4-((*E*)-(4-(octyloxy)phenyl)diazenyl)phenyl)-*N*⁵-(4-((*E*)-(4-((pentyloxy)methyl)phenyl)diazenyl)phenyl)benzene-1,3,5-tricarboxamide (**13b**)

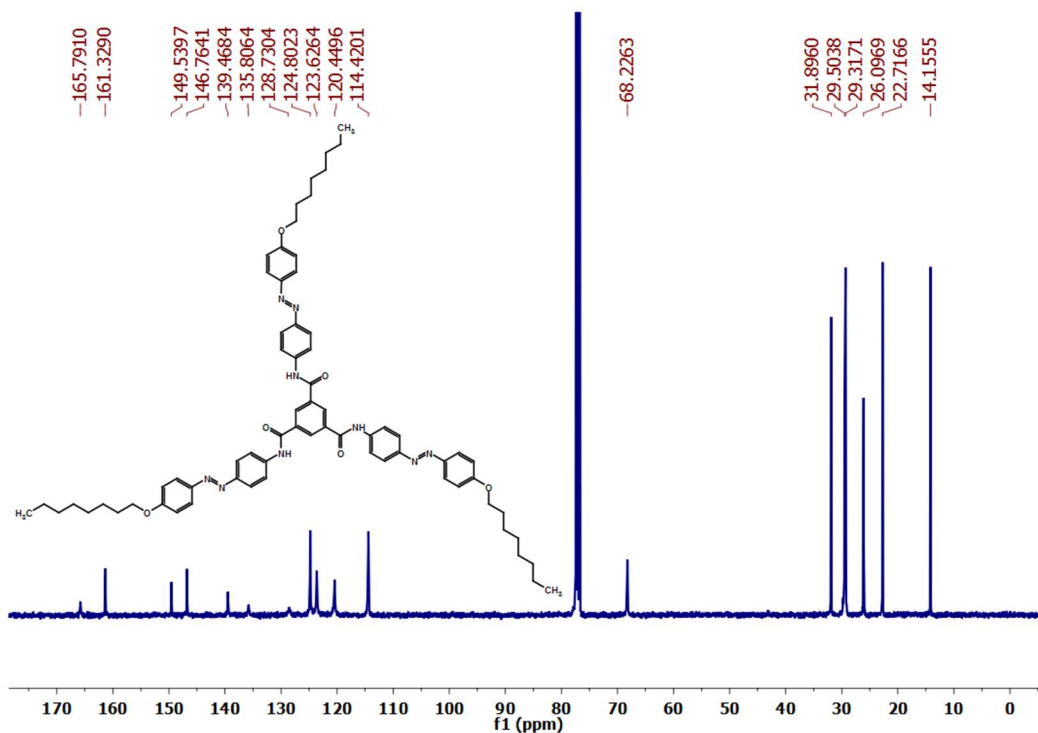


Figure 4D.12. ¹³C NMR spectrum of *N*¹,*N*³-bis(4-((*E*)-(4-(octyloxy)phenyl)diazenyl)phenyl)-*N*⁵-(4-((*E*)-(4-((pentyloxy)methyl)phenyl)diazenyl)phenyl)benzene-1,3,5-tricarboxamide (**13b**)

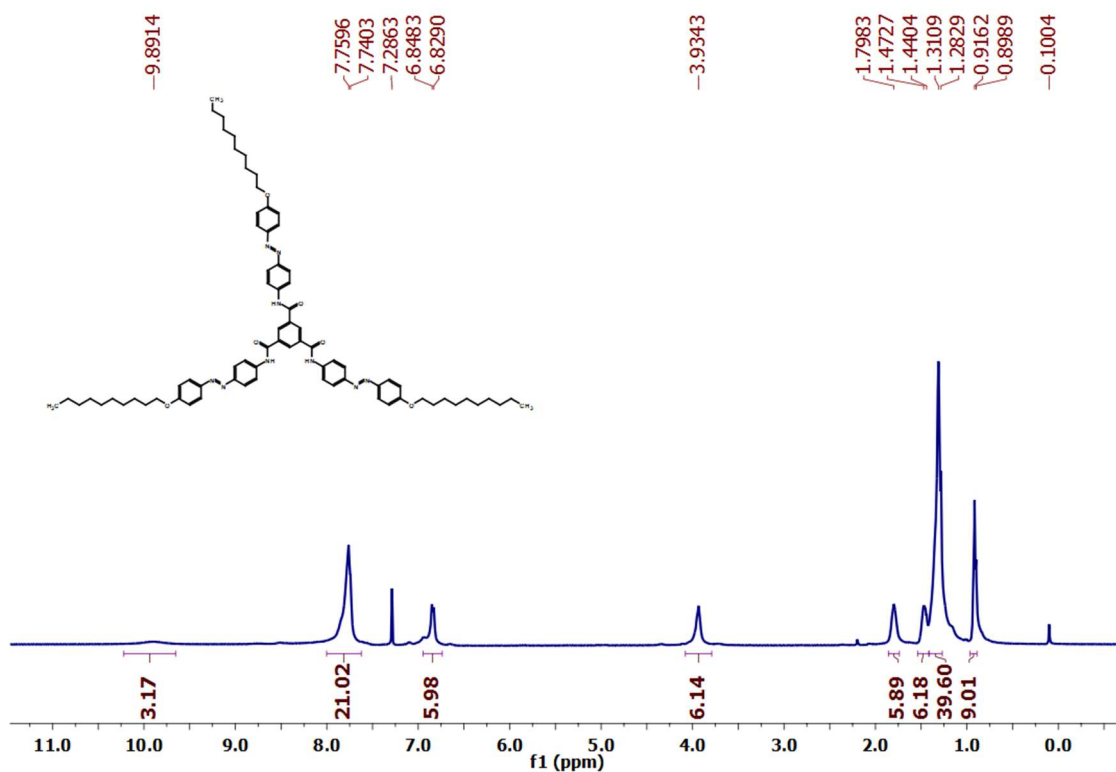


Figure 4D.13. ^1H NMR spectrum of N^1, N^3 -bis(4-((*E*)-(4-(decyloxy)phenyl)diazenyl)phenyl)- N^5 -(4-((*E*)-(4-((pentyloxy)methyl)phenyl)diazenyl)phenyl)benzene-1,3,5-tricarboxamide (13c)

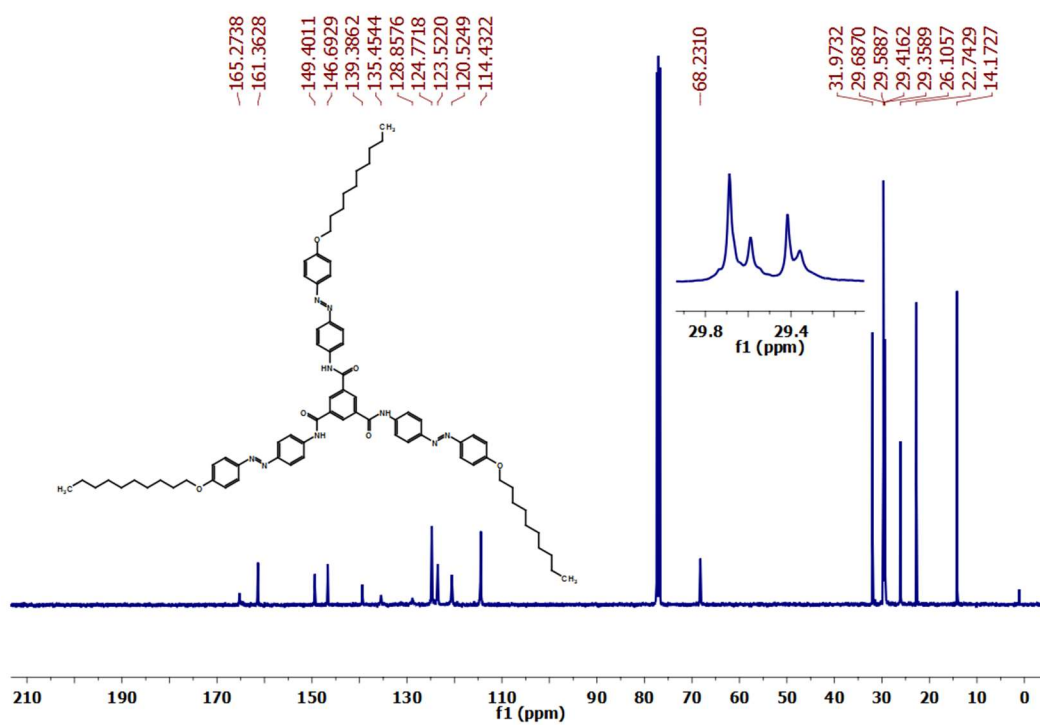


Figure 4D.14. ^{13}C NMR spectrum of N^1, N^3 -bis(4-((*E*)-(4-(octyloxy)phenyl)diazenyl)phenyl)- N^5 -(4-((*E*)-(4-((pentyloxy)methyl)phenyl)diazenyl)phenyl)benzene-1,3,5-tricarboxamide (13c)

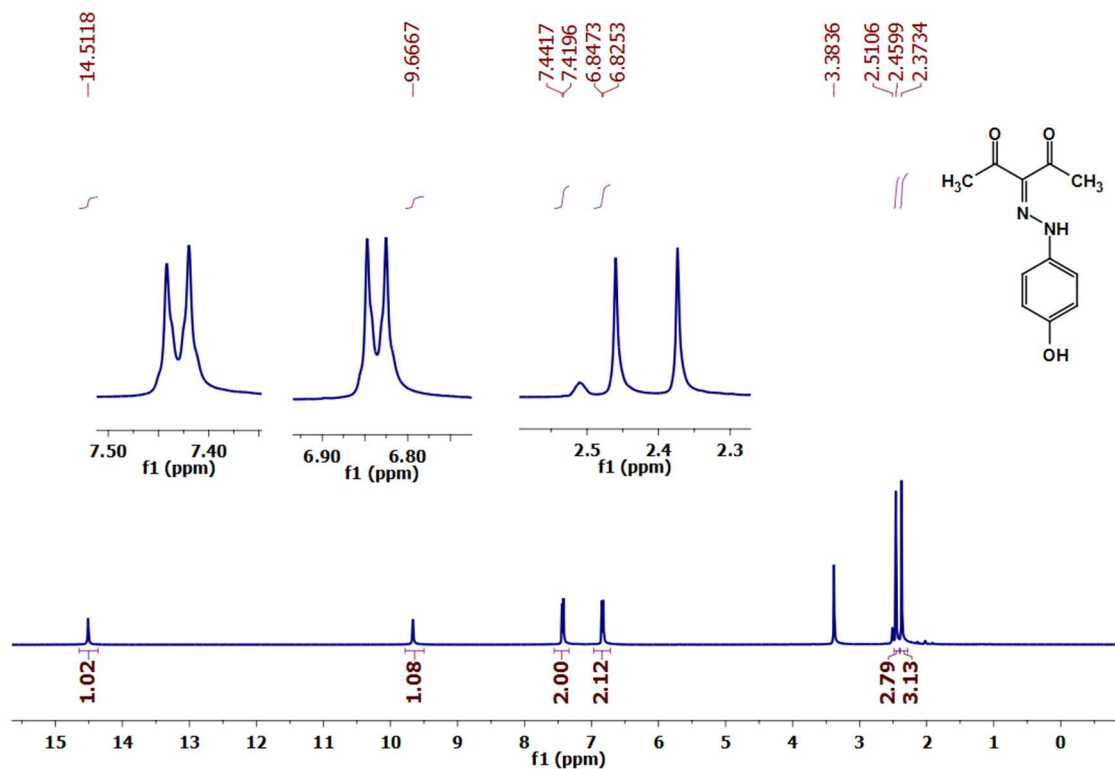


Figure 4D.17. ^1H NMR spectrum of 3-(2-(4-hydroxyphenyl)hydrazono)pentane-2,4-dione(2)

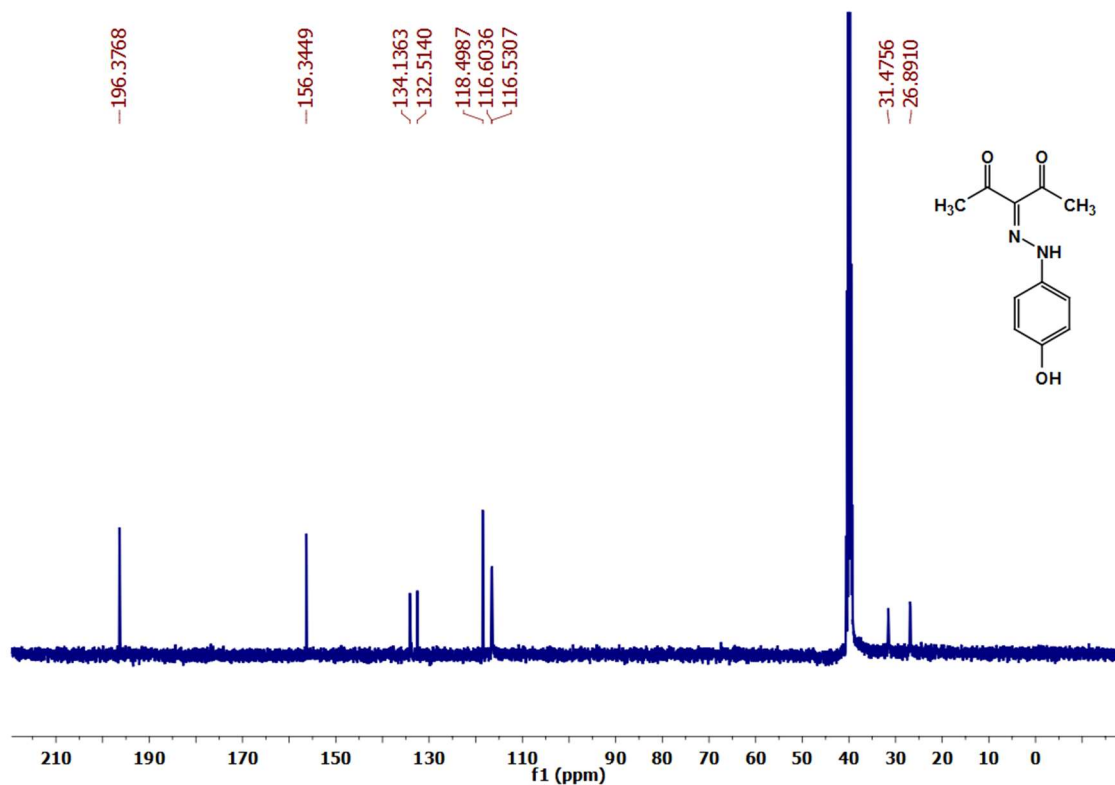


Figure 4D.18. ^{13}C NMR spectrum of 3-(2-(4-hydroxyphenyl)hydrazono)pentane-2,4-dione (2)

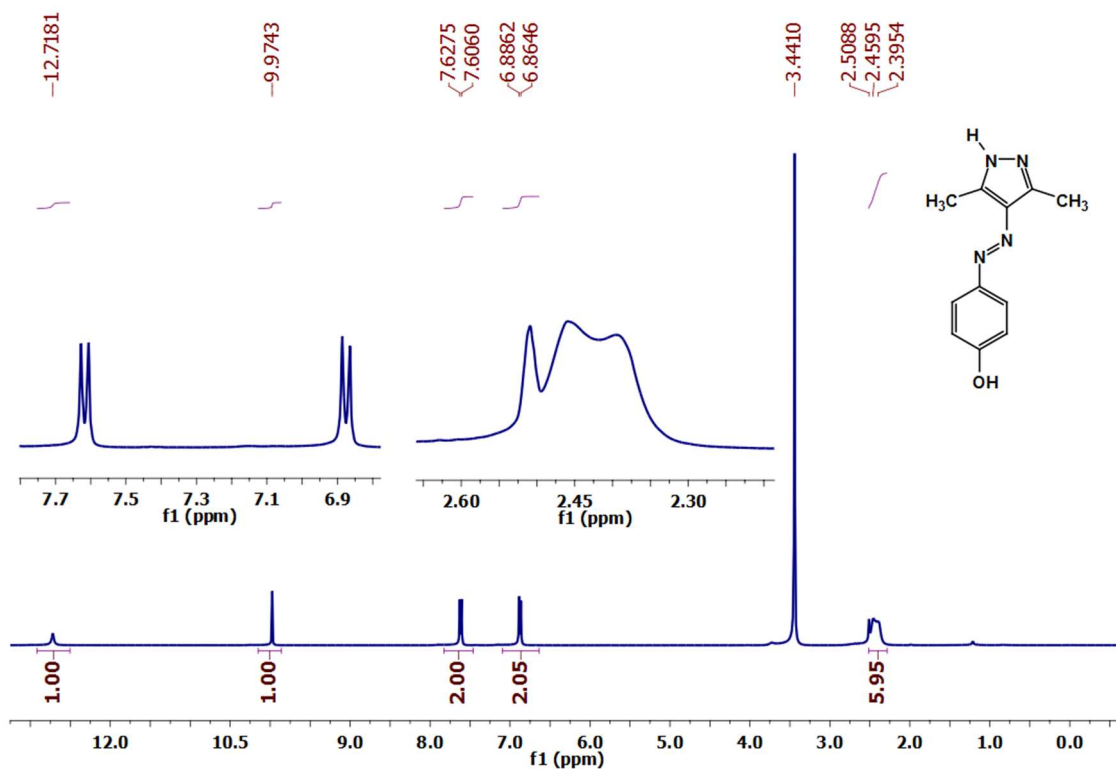


Figure 4D.19. ¹H NMR spectrum of (E)-4-((3,5-dimethyl-1H-pyrazol-4-yl)diazenyl)phenol (3)

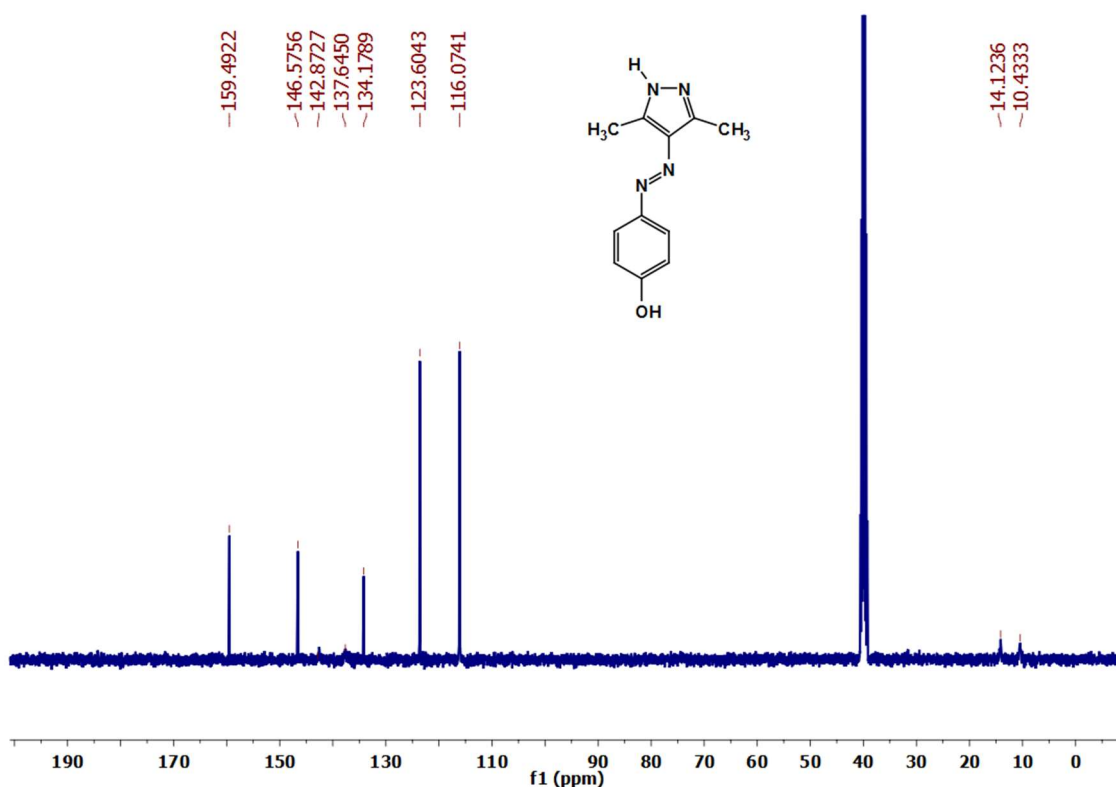
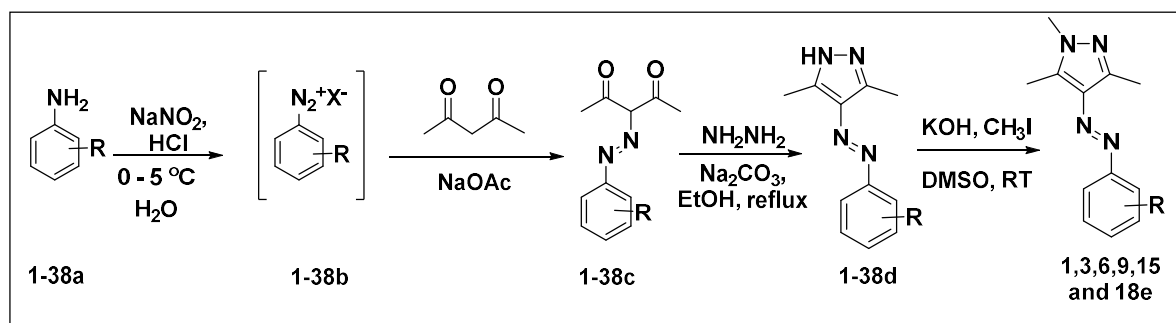


Figure 4D.20. ¹³C NMR spectrum of (E)-4-((3,5-dimethyl-1H-pyrazol-4-yl)diazenyl)phenol (3)

Chapter 5. Conclusions and Perspectives

5.1 Evaluation of substituent effect in *Z*-isomer stability of arylazo-1*H*-3,5-dimethylpyrazoles

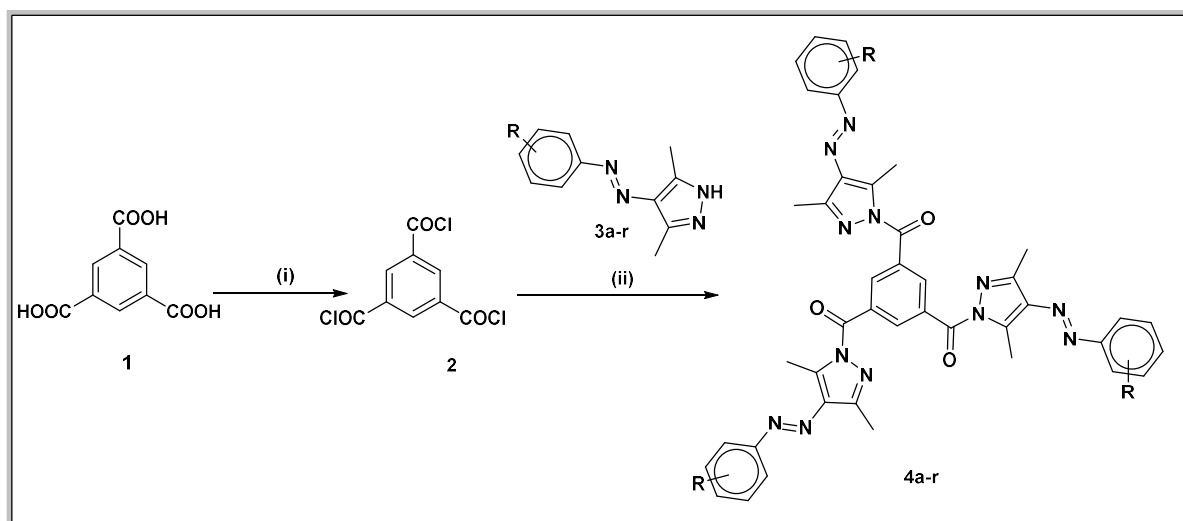
Recently, Fuchter and coworkers reported that *N*-methyl phenylazopyrazoles showed very high stability in *Z*-form, with a half-life of 1000 days. However, if the molecule has methyl groups in the *ortho* position to the azo group, the half-life dropped to 10 days. The same group also modified various heterocycles and tuned the half-life of the heteroazylazobenzenes. So far there is no studies have been carried out with respect to the aryl group substitutions. In this regard, we attempted to understand the electronic and steric effects of the substituents in the phenylazopyrazoles and *N*-methyl phenylazopyrazoles. To follow the reactions conveniently through spectroscopy, we have chosen the system with two methyl groups in the pyrazole unit. A series of 38 substituted derivatives of arylazopyrazole molecules (**1-38d**) with various substitutions at *ortho*-, *meta*- and *para*-positions and six derivatives of *N*-methyl arylazopyrazoles (**1e**) with *meta*-substitutions [**3e (3-F)**, **6e (3-Cl)**, **9e (3-Br)**, **15e (3-CF₃)**, **18e (3-OMe)**] have been synthesized. (**Scheme 5.1**) For all the molecules, photoisomerisation studies, percentage conversion at photostationary states (PSS), and first-order rate constants through kinetics studies of thermal reverse isomerization processes have been performed using UV-Vis spectroscopic techniques. For those derivatives with substitutions at *meta*- and *para*-positions, the above-mentioned studies have been performed using NMR. The rate constants have been computationally deduced using density functional theory (DFT) at B3LYP/6-311G(d,p) level of theory. For understanding the substitution effects, Hammett and Taft plots have been studied using the rate constants computed through all the three methods. Based on the studies, we understood that apart from substantial steric and electronic effects through aryl substitutions, a compelling involvement of hydrogen bonding in determining the rates. To establish the above points, we have utilized the studies on *N*-methyl arylazopyrazoles with *meta*-substitutions, which provided clear support for our hypothesis. Kinetics studies at different concentration, solvent effects and computations have confirmed the decisive role of hydrogen bonding in this regard. Thus, the complex interplay of steric, electronic and hydrogen bonding as factors in dictating the stability of *Z*-isomers in arylazopyrazoles has been demonstrated.



Scheme 5.1. Synthesis of substituted phenylazopyrazoles and *N*-methyl phenylazopyrazoles

5.2 Tripodal arylazo-3,5-dimethylpyrazole derivatives of trimesic acid

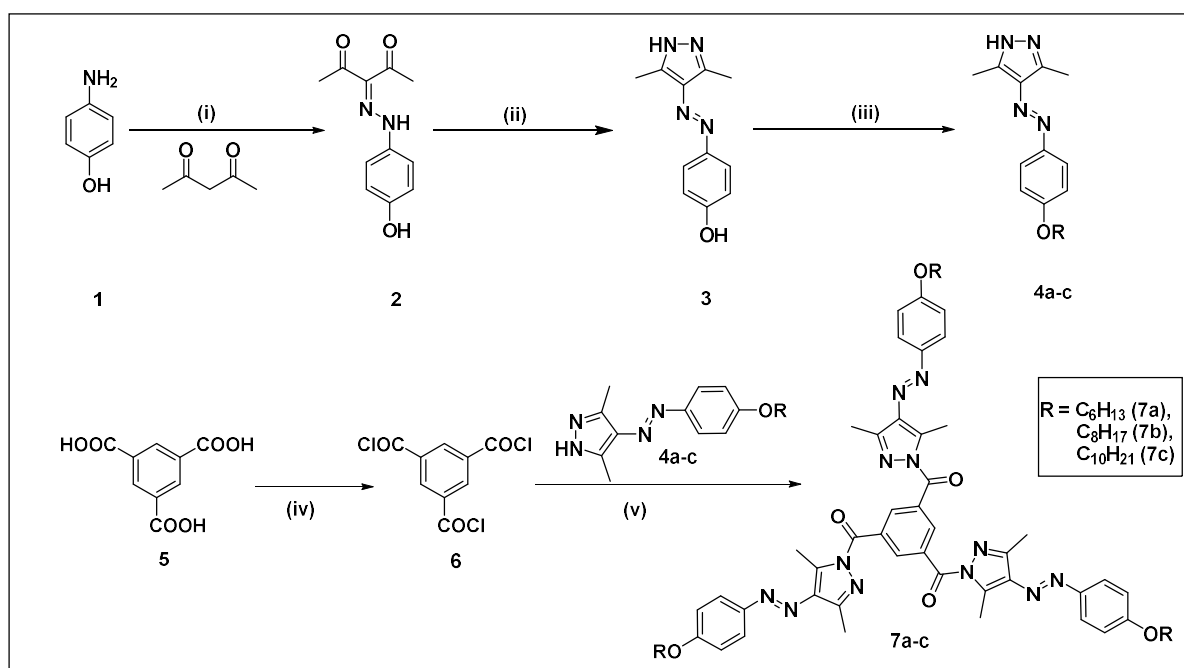
After the understanding of the substituent effects, functionalization strategy of the arylazopyrazoles has been considered. A simple synthetic and purification method has been developed in connecting various aryl-substituted phenylazopyrazoles with trimesic acid through aroylazole linkage at the pyrazole nitrogen. The resulting *tris*(arylazopyrazole) connected 18 derivatives (**4a-r**) are capable of undergoing photoisomerization between *EEE*, *EEZ*, *EZZ* and *ZZZ*-isomers. (**Scheme 5.2**) Through UV-Vis and NMR spectroscopic studies, the multi-state photochromic properties of these molecules have been investigated. Apart from that, these new class of molecules exhibit many interesting properties such as better solubility, higher photoisomerization conversions towards *ZZZ*-isomers, enhanced stability of *ZZZ*-isomers, and long-term switching stability. Above all, these molecules show solid-state reversible photoisomerization as well as colour changes that make them potential candidates for the rewritable imaging applications.



Scheme 5.2. Synthesis of tripodal arylazo-3,5-dimethylpyrazole-1-tricarboxamides **4a-r**.

5.3 Photoswitchable discotic liquid crystals

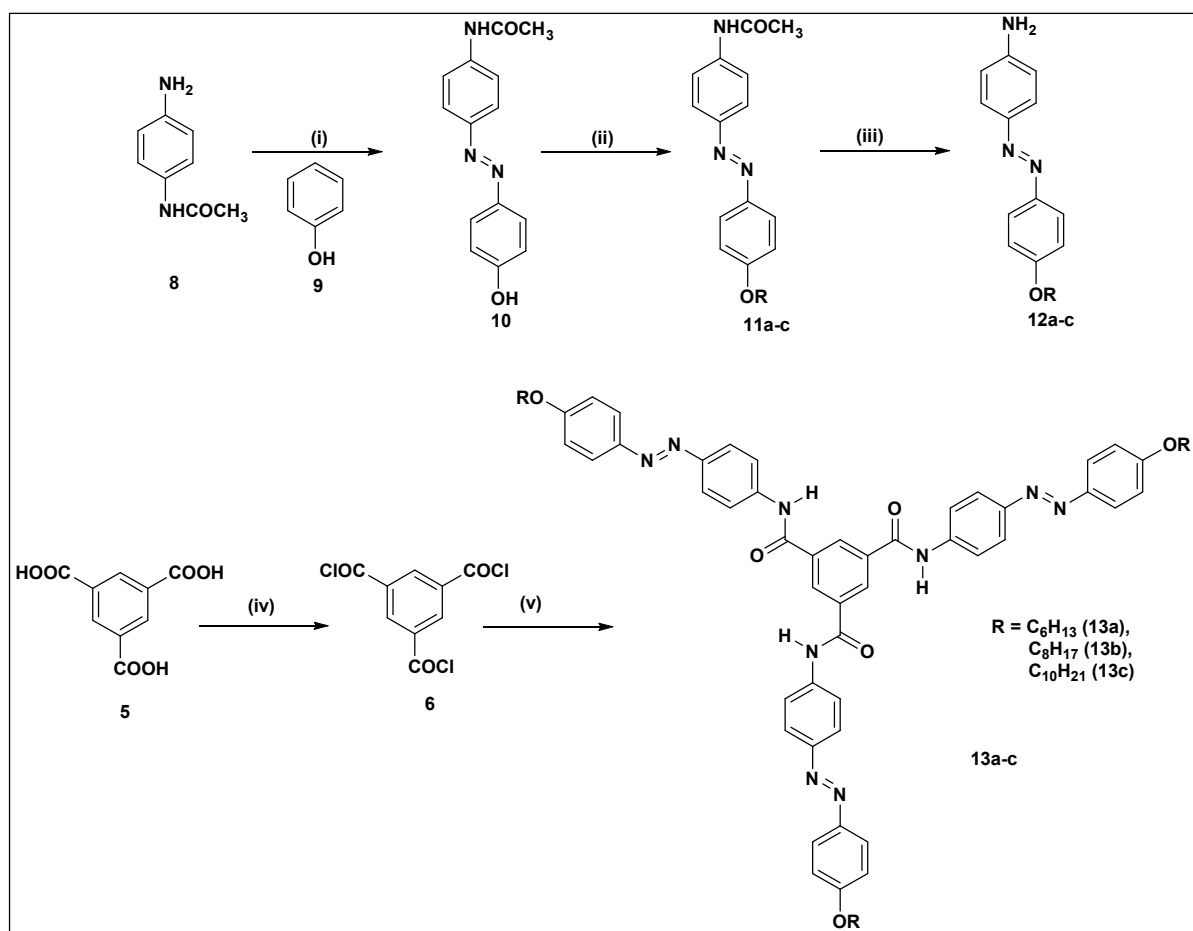
Once the functionalization strategy has been established, we explored the possibility of utilizing azoarenes connected photoswitchable discotic liquid crystals. We have successfully optimized a method for obtaining benzenetricarboxamides functionalized photoswitchable units in good yields. Since these molecules are expected to be planar in all-*trans* geometry, a supramolecular assembly of such molecules can be expected to attain a disc-like structure. If the peripheries of those photoswitchable units are connected with a flexible chain, the resulting molecules may behave like discotic liquid crystals (DLC) that can be tuned by light-induced photoisomerization. With this motivation, long chain alkoxy containing arylazopyrazole with varying chain length C₆, C₈ and C₁₀ have been incorporated into a benzene core through aroylazole linkage. (**Scheme 5.3**) Those molecules showed photoswitching in solution phase, however, they did not show any liquid crystalline properties. Presumably, this can be attributed to the methyl groups present in the pyrazole units, which might prevent the π -stacking. To overcome this issue, we redesigned our strategy and incorporated alkoxy chains (C₆, C₈ and C₁₀) linked aminoazobenzenes have been incorporated into a benzenetricarboxamide core. (**Scheme 5.4**)



Scheme 5.3: Synthesis of tripodal alkoxy chain connected arylazo-3,5-dimethylpyrazole-1-tricarboxamides **7a-c**.

Once again, we have performed the photoswitching studies using UV/Vis and NMR spectroscopic techniques. These molecules exhibit photoswitching behaviour not only in the solution form, but also in the solid (KBr), in thin films and also in the liquid crystalline forms.

Polarized optical microscopic (POM) images and small angle X-ray scattering (SAXS) studies confirmed that all the three derivatives showed DLC properties. Interestingly, the compounds with peripheral C_6 alkyl chain exhibit two different mesophases: namely a columnar rectangular (Col_r) phase at low temperature, and a columnar hexagonal (Col_h) at a higher temperature. In contrast, the other two higher homologues revealed only Col_h phases at all temperature ranges. Despite the molecules showing photoswitching properties in the DLC phase, we could not observe any texture change in the POM images. Thus, we designed, synthesized and demonstrated a photoswitchable DLC molecules.



Scheme 5.4: Synthesis of aminoazobenzene incorporated tripodal molecules **13a-c**.

5.4 Perspectives:

In conclusion of my thesis work, we have done the synthesis of arylazopyrazole, tripodal arylazo-3,5-dimethylpyrazole derivatives of trimesic acid, and aminoazobenzene incorporated benzenetricarboxamides derivatives from readily and cheaply available starting materials such as phenol, aniline and its substituted derivatives. We have obtained good to

excellent yields for the synthesis of intermediates and also the final products. Furthermore, we have investigated the influence of steric effects, electronic effects of substituents, and the influence of hydrogen bonding in the stability of *cis*-isomer. Studies through Taft and Hammett plots revealed the substantial influence of steric and electronic effects, respectively. Apart from that, the hydrogen bonding is equally influential, which can be understood from the solvent effects, and *N*-methylation or functionalization at the pyrazole nitrogen. By synthesizing a new class of tripodal arylazo-3,5-dimethylpyrazole derivatives of trimesic acid, and aminoazobenzene incorporated benzenetricarboxamides derivatives, we have demonstrated the enhancement in the stability of *cis*-isomer. Apart from that, both the classes of such derivatives showed potential applications in the reversible, rewritable imaging and photoswitchable DLCs, respectively. The applications of those molecules can be further explored.

Chapter 6. Materials and Methods

All the reactions have been carried out under argon or nitrogen atmosphere and the glass wares are dried in the oven as well as under vacuum by heating. The reagents (AR grade or LR grade) and solvents were purchased from commercially available sources such as Sigma Aldrich, Merck and TCI etc. Anhydrous solvents for the reactions and for column chromatography have been distilled before use. The NMR spectra have been recorded in Bruker Avance-III 400 MHz spectrometer. ^1H and ^{13}C NMR were recorded at operation frequencies 400 MHz and 100 MHz, respectively. For recording the samples, CDCl_3 and $\text{DMSO-}d_6$ have been used as the solvents. The chemical shift (δ) values are reported in parts per million (ppm) and the coupling constants (J) are reported in Hz. In all the cases the signals due to residual solvents in CDCl_3 (7.26 ppm) and $\text{DMSO-}d_6$ (2.50 ppm) have been used for internal calibration. High-resolution mass spectra have been recorded using Waters Synapt G2-Si Q-TOF mass spectrometer. HRMS were obtained from a TOF mass analyser using electrospray ionization (ESI) in both positive and negative modes. Melting points were recorded on SMP20 melting point apparatus, which are uncorrected. FT-IR spectra were recorded on a Perkin-Elmer ATR spectrometer. Column chromatography was performed over silica gel (100–200 mesh) using EtOAc/hexane as an eluent. Thin layer chromatography was performed on Merck Silica gel 60 F₂₅₄ TLC plates and visualized using UV ($\lambda = 254$ nm) chamber or iodine stain. UV-Vis photoswitching and kinetics studies have been performed either using a Cary 5000 spectrophotometer. For forward photoswitching (*E-Z* isomerization) samples were irradiated at 365 nm using a LED light source either from Applied Photophysics, SX/LED/360 with bandwidth 20 nm or a commercial 9W LED light source. The reverse isomerization has been induced by using either a 35 W CFL lamp. The PSS has been established by irradiating the sample for a prolonged time such that no further spectral change is observed.

CURRICULUM VITAE

SUDHA DEVI

Plot No. 10-A, New Patel Nagar,
Herjendera Nagar, Kanpur, Uttar Pradesh-208007
E-Mail: sudhapatel.knp@gmail.com, sudhadevi@iisermohali.ac.in
Phone No. 9501524730.

● ACADEMIC RECORD

- M.Sc. in Chemistry from C.S.J.M. University, Kanpur in 2009.
- D. Pharmacy from Board of Technical Education, Lucknow, U.P. in 2007.
- B.Sc. in Chemistry and Zoology from C.S.J.M. University, Kanpur in 2005.
- Intermediate from UP Board in 2002.
- Matriculation from UP Board in 2000.

● DOCTORAL DETAIL

- **Thesis Title:** "Tuning, Controlling and Applications of *Cis*-isomer Stability in Azoheteroarenes and Multiple Azoarenes Connected Systems"
- **Supervisor:** Dr. Sugumar Venkataramani, Assistant Professor, IISER Mohali, India

● TEACHING

- July 2009 to January 2012.

● ACHIEVEMENTS

- CSIR-UGC JRF in Dec.-2011 (Rank 86).
- A valid GATE score 2012 (Rank 520).

● EXTRA-CURRICULAR

- Two year worked in National Service Scheme.
- Worked as a Chemist for three months.
- Active participation in Cultural activities.

● TECHNICAL SKILLS

- Instrumentations- NMR, IR, UV/Vis, Fluorescence, HRMS, XRD, and DSC.

SUDHA DEVI